Localisation of the molecular chaperone site of 14-3-3ζ; an intracellular protein associated with toxic neurological protein aggregates

Katy Louise Goodwin

School of Physical Sciences

The University of Adelaide

Supervised by Prof. John A. Carver

and Dr Joanna M. Woodcock

This thesis is submitted to The University of Adelaide

for the degree of *Doctor of Philosophy.*

February, 2015

Abstract

14-3-3 proteins are a family of acidic, dimeric, phospho-serine binding proteins, which are ubiquitously expressed in all mammals. There are 7 known isoforms in mammals (β, γ, ε, ζ, η, τ, σ), which have similar structures and roles. 14-3-3 proteins interact with over 200 target proteins and regulate many roles including apoptosis, protein transportation, mitosis and signal transduction. Due to these diverse roles, 14-3-3 proteins are associated with many diseases, e.g. cancer and neurodegenerative diseases. 14-3-3 is co-located with many neurological protein aggregates; however the role of 14-3-3 in these diseases is unknown. Recently the molecular chaperone action of 14-3-3ζ was described whereby 14-3-3ζ is able to interact with and stabilise aggregating target proteins.

Previous investigations into the regions responsible for chaperone action showed that the C-terminal extension and the polar face of the amphipathic binding groove of 14-3-3ζ are unlikely to be involved in chaperone action. Here, the investigation into the site and mechanism of the molecular chaperone action is extended to target two major hydrophobic regions of 14-3-3ζ: the hydrophobic face of the amphipathic binding groove and the dimer interface.

The hydrophobic face of the amphipathic binding groove is not a critical region for the chaperone action of 14-3-3ζ. This was determined by the mutations of exposed hydrophobic residues, V176, L216, L220 and L227 and assessing the chaperone ability of these proteins compared with WT 14-3-3ζ proteins against the amorphous aggregation of alcohol dehydrogenase and reduced insulin.

The dimer interface was determined to be involved in the chaperone activity of 14-3-3ζ. This region was investigated by targeting hypothesised salt bridging sites in the dimer interface (D21 and E89). Disruption of this region can also be achieved via phosphorylation of S58. The 14-3-3ζ protein, S58D, is a phospho-mimic which exhibits a similar dimer disruption. The disruption caused by these mutations was assessed and the chaperone ability was tested

against amorphous aggregation of alcohol dehydrogenase and reduced insulin and compared to WT 14-3-3ζ. These dimer disrupted proteins exhibited enhanced chaperone ability, implying exposure of the dimer interface is important for the chaperone action of 14-3-3ζ. In addition these 14-3-3ζ mutants also exhibited a shift in the monomer-dimer equilibrium which results in the increased production of monomeric 14-3-3ζ. This shift in the monomer-dimer equilibrium correlates with the enhanced chaperone ability of 14-3-3ζ, suggestive of the 14-3-3ζ monomer being an important chaperone active unit.

To further the investigation of the role of the dimer interface in the chaperone action of 14-3-3ζ the interaction with a physiological lipid mimic was undertaken. The physiological lipid, sphingosine, is known to interact with 14-3-3 and cause disruption to the dimer interface in order to allow phosphorylation of S58. The interaction with a sphingosine mimic caused disruption to the dimer, and the chaperone ability in the presence of this mimic was assessed. There no observed effect on the chaperone activity of 14-3-3ζ as a result of this interaction. However the disruption caused by this interaction is minor and may not be sufficient to cause enough disruption to expose significant region of the dimer interface required for enhanced chaperone ability.

Small angle scattering studies confirmed that the dimer interface is involved in the chaperone action of 14-3-3ζ. Modelling the interaction between aggregating ADH and 14-3-3ζ revealed that ADH interacts with dimeric 14-3-3ζ via a region of the dimer interface. This allows the formation of the dimeric structure which maintains the stability of the ADH-14-3-3 complex. The independent movement of the two interaction regions of the dimer interface makes it possible for one side of the dimer interface to dissociate allowing the interaction with the aggregating target protein. The interactions on the other side of the dimer interface remain intact allowing the dimer to be maintained. This maintains the stability that comes with the dimeric form of 14-3-3ζ whilst still allowing the interaction with aggregating protein via the hydrophobic dimer interface.

This investigation of the chaperone activity of 14-3-3ζ has revealed that 14-3-3 acts as a molecular chaperone via the dimer interface. This interaction occurs when half of the dimer interface dissociates to allow access to amorphously aggregating target proteins. This allows the other side of the dimer interface to maintain salt bridging interactions and retain the dimeric state of the 14-3-3ζ protein with the associated stability. This investigation is the first

instance in which a chaperone protein has been modelled interacting with an aggregating target protein. It also opens up the role of the dimer interface in 14-3-3 function, and clarifies that the monomeric 14-3-3 unit is unlikely to have a role in 14-3-3 pathology due to its inherent reduced stability.

This thesis has provided more in depth knowledge about the chaperone capability of 14-3-3ζ and the potential role of 14-3-3ζ in neurodegenerative disease. The precise function of 14-3-3 proteins in these diseases is not well understood, with 14-3-3 acting as both positive and negative regulator of protein aggregation. The determination of the mechanism of chaperone function of 14-3-3ζ provides important information which can be utilised to further investigate the role of 14-3-3 in these diseases, leading to the development of new therapeutic techniques to overcome these debilitating diseases.

Declaration

Part of the written work in Chapter 1, was written as part of my honours year at the University of Adelaide. With the exception of this, I certify that this work contains no material which has been accepted for the award of any other degree or diploma in my name, in any university or other tertiary institution and, to the best of my knowledge and belief, contains no material previously published or written by another person, except where due reference has been made in the text. In addition, I certify that no part of this work will, in the future, be used in a submission in my name, for any other degree or diploma in any university or other tertiary institution without the prior approval of the University of Adelaide and where applicable, any partner institution responsible for the joint-award of this degree.

I give consent to this copy of my thesis, when deposited in the University Library, being made available for loan and photocopying, subject to the provisions of the Copyright Act 1968.

I also give permission for the digital version of my thesis to be made available on the web, via the University's digital research repository, the Library Search and also through web search engines, unless permission has been granted by the University to restrict access for a period of time.

The small molecule, 41.14, was provided by Dr Joanna Woodcock and the phosphorylation investigations in chapter 6 were undertaken by Carl Coolen. The analysis of data obtained via small angle neutron scattering (chapter 7) was undertaken in collaboration with Dr Agata Rekas (National Deuteration Facility, ANSTO).

_____

Katy Louise Goodwin

Date:

Acknowledgements

"We are so often caught up in our destination that we forget to appreciate the journey, especially the goodness of the people we meet along the way…."

~Unknown

Where else could I start but with thanking my wonderful supervisors, John and Jo. I recently realised how lucky I am to have two supervisors from different disciplines play such active roles in my PhD. I really think that it really rounded out my skills and allowed me insights into both the biological and chemical worlds.

To John, thank you for the guidance and sharing your expertise in such a friendly and welcoming manner. I will always treasure my time being a part of your research group.

To Jo, your enthusiasm about 14-3-3 proteins is so infectious and you make any lab a good place to work. I really don't think I would have made it through the past year without your faith, encouragement and understanding. I will always be grateful for the never-ending support!

To Agata, I can't thank you enough for your help and support whilst undertaking the scattering experiments and analysis. It is not only your help and guidance, but your friendly face that made my visits to ANSTO so memorable.

Many thanks to the Carver group, mainly, Kegg, Yanqin, Nick, Denise, Ran, Manjeet, Danielle and Dave. Thanks for all the laughs and support. You guys have made the lab a fun place to be over the years.

What is science without collaboration, and I have been lucky to work with many different people from around the country. Thank you to Matt Perugini for your time and allowing me to visit your lab to undertake the AUC experiments; Robert Knott and Katy Wood for your technical support whilst undertaking scattering experiments at ANSTO; Emma Parkinson-Lawrence, for getting me set up with the CD; Stephen Polyak, for always being willing to

help with a variety of protein issues; Paul Moretti, for imparting your DNA and site-directed mutagenesis knowledge; and Carl Coolen, for your aid with the phosphorylation work, always with a smile.

Many thanks to my wonderful family and friends for your endless support, understanding and patience over the past few years. You provided a fun place outside of the lab to spend my time, and I appreciate having you all in my life. Mum, I know it's your job, but thanks for listening to all my complaints with a cup of tea and a sympathetic ear. And Dad, you'll be pleased to know I have finished my "book" now.

Finally to Matt..... So many things have changed since I started my PhD, but you have always remained by my side. I could not have asked for a more supportive and awesome partner. I'm really looking forward to sharing many more adventures together.

Table of Contents

List of figures

List of tables

Chapter 1

Introduction

1.1 14-3-3 Proteins

14-3-3 proteins are a family of acidic, phospho-serine binding proteins which are expressed in all eukaryotic cells (1). 14-3-3 proteins undertake many regulatory cellular roles primarily through binding to phospho-serine sites in target proteins. They include the regulation of cell cycle progression, the alteration of the target protein's localization within the cytoplasm and nucleus, and the modulation of the target protein's catalytic activity (2).

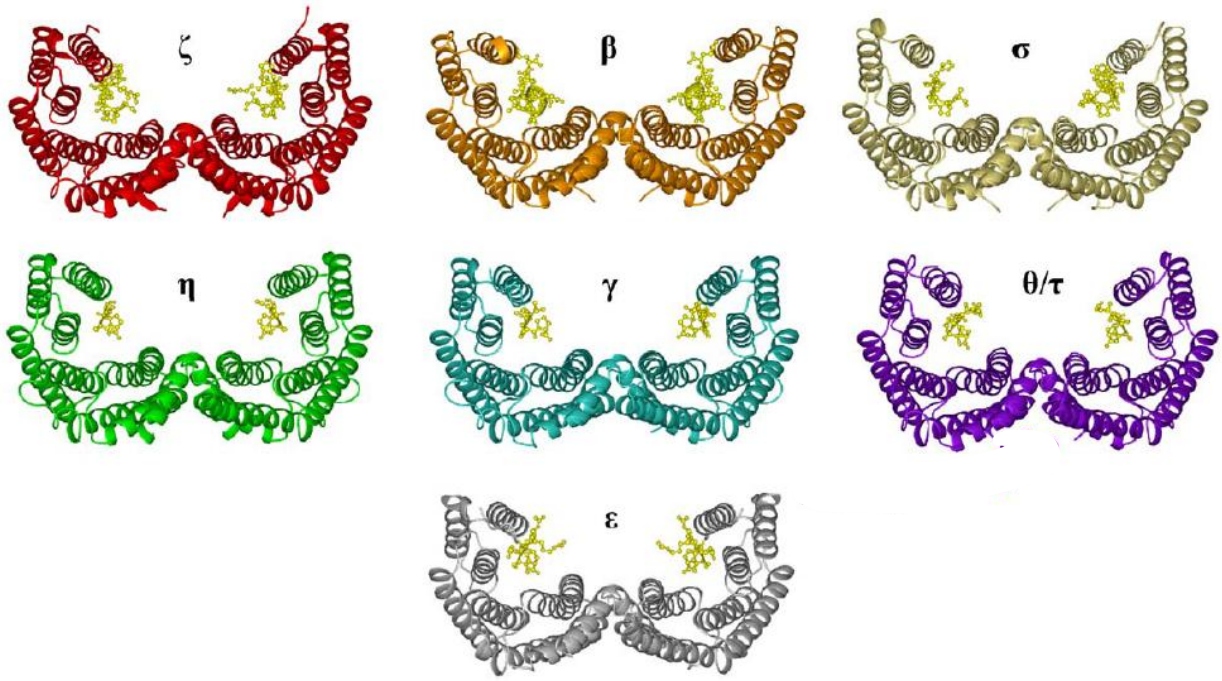

Figure 1.1: Crystal structures of the seven human isoforms of the 14-3-3 dimer when bound to phospho-peptides (yellow); the phospho-peptides are bound in the amphipathic binding groove of the 14-3-3 monomer (taken from (1)).

Each 14-3-3 monomer is approximately 30 kDa in mass (3) and there are seven closely related isoforms (β, γ, η, ζ, τ, ε, σ) in mammals, whose tertiary structures have all been determined via x-ray crystallography (Fig 1.1) (4,5). There are up to 15 isoforms known in plants and two have been identified in yeast (4). The name 14-3-3 was coined based on the elution and migration on two-dimensional DEAE cellulose chromatography of bovine brain homogenates when the protein was first discovered (3). Even though the functions of the protein have expanded greatly from its original identification as a brain protein, the name has been retained (3,4).

1.1.1 Roles of 14-3-3 proteins *in vivo*

14-3-3 proteins interact with more than 200 identified target proteins under constitutive conditions (i.e. non stress conditions) (6), on many different cellular pathways including those associated with metabolism, cell signalling, cell cycle regulation, intracellular protein trafficking and targeting, cytoskeletal structure, apoptosis and transcription (3,4). To demonstrate the variety of roles that 14-3-3 proteins undertakes *in vivo*, the interaction of 14-3-3 with Bad, Raf and cdc25 will be discussed here.

The interaction of 14-3-3 with Bad leads to the prevention of apoptosis. Apoptosis is a highly regulated process of cell death, involving many signalling proteins including the Bcl-2 family of pro- and anti-apoptotic proteins (7). The interaction of Bad with Bcl-2/X_L leads to the initiation of apoptosis. The pro-apoptotic signalling protein, Bad, is known to interact with 14-3-3 in a phospho-serine dependent manner (8). The phosphorylation of Bad, results in binding with 14-3-3ζ. This leads to retention of Bad in the cytoplasm of the cell (Fig. 1.2), preventing the interaction with Bcl_2/X_L, and inhibiting apoptosis (9). In many cases, the initiation of apoptosis results in the interruption of 14-3-3 binding with such apoptotic mediators, demonstrating that 14-3-3 is a major determinate in cell fate determination (9).

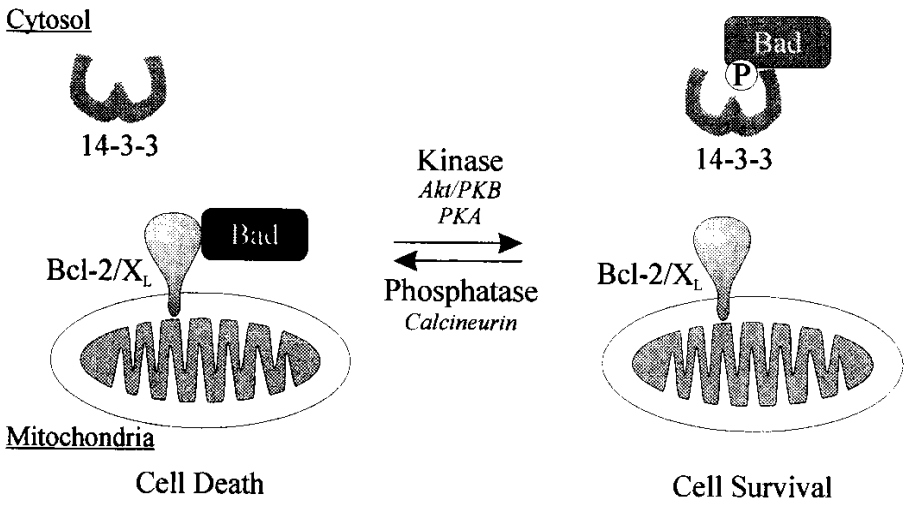

Figure 1.2: The role of 14-3-3 in protection against apoptosis, whereby the phosphorylation of Bad results in binding to 14-3-3 leading to cell survival. This binding of Bad to 14-3-3 prevents its interaction with Bcl-2/X_L, an interaction which leads to apoptosis (taken from (10)).

Conversely, 14-3-3 also has roles in the induction of cell proliferation and survival signalling. 14-3-3 acts as a negative and positive regulator of Raf-1, a kinase which upon activation is responsible for the stimulation of pro-proliferative factors (Fig. 1.3). For example, 14-3-3 mediates signal transduction pathways induced by growth factors, by binding to the kinase Raf-1. This binding of 14-3-3 to Raf-1 results in an inactive form of the kinase. In the presence of mitogenic signals, Raf-1 is recruited to the plasma membrane where 14-3-3 is displaced from the Raf-1 molecule, producing the active form of Raf-1. 14-3-3 binds to this active conformation of Raf-1 to maintain its activity. The maintenance of the active form of Raf-1 leads to the stimulation of pro-apoptotic signals that result in proliferation (10).

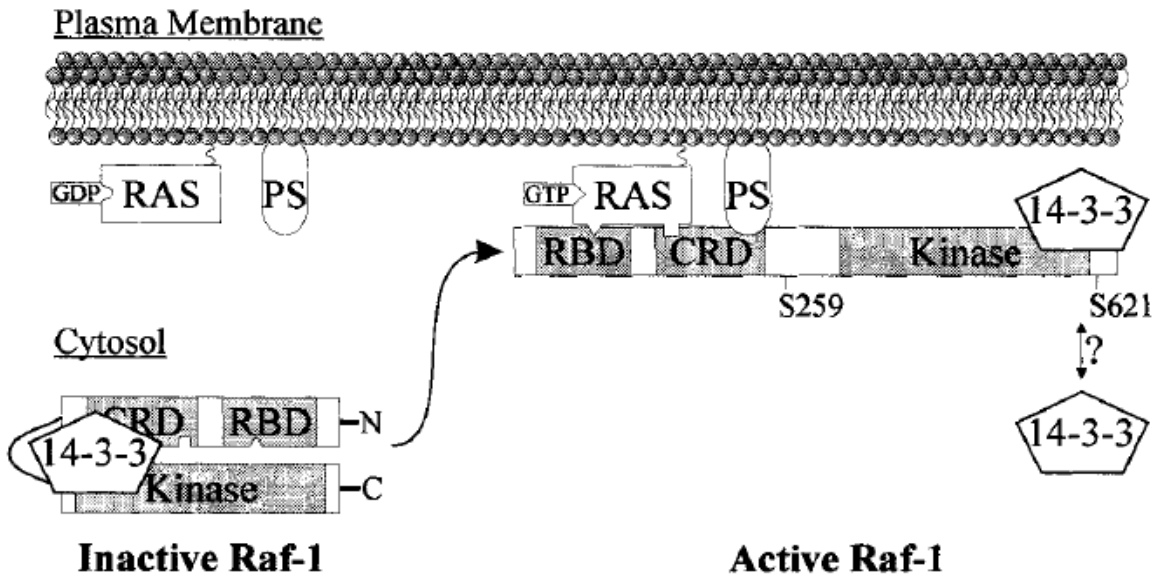

Figure 1.3: The phosphorylation of Raf-1 leads to the binding of 14-3-3, maintaining the inactive form of Raf-1. Upon activation of Ras, Raf-1 is sequestered to the plasma membrane, where 14-3-3 dissociates and allows Raf-1 to adopt its active state. 14-3-3 can bind to this active form to maintain this conformation. The activation of Raf-1 leads to the stimulation of further mechanisms that lead to cell proliferation (taken from (10)).

In connection with this cell proliferative role, 14-3-3 is closely associated with the control of mitosis. The phosphatase, Cdc25 is a highly regulated activator of mitosis. In order to function, it must translocate into the nucleus where it activates the kinase Cdc2, a key mediator of mitosis. The phosphorylation of Cdc25 leads to binding to 14-3-3 and sequestration in the cytoplasm, halting mitosis (Fig. 1.4) (11). Such regulation of mitosis by 14-3-3 proteins is in response to activation signals such as DNA damage (10). Additionally with the onset of DNA damage, there is a major up-regulation in 14-3-3σ, which is responsible for the cytoplasmic localisation of Cdc2 (12).

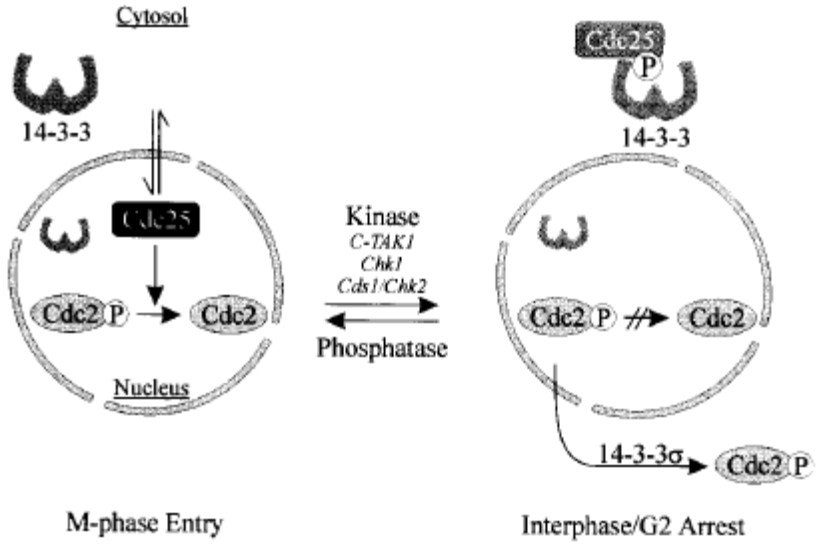

Figure 1.4: When exposed to DNA damage, Cdc25 becomes phosphorylated which leads to the interaction with 14-3-3. This results in Cdc25 being retained in the cytoplasm and prevents its interaction with Cdc2/X_L, preventing the initiation of mitosis. An additional mitosis prevention mechanism is the sequestration of phosphorylation of Cdc2 into the cytoplasm by 14-3-3σ (taken from (10)).

As these examples demonstrate, 14-3-3 proteins have the ability to act as positive regulators which have growth and survival promoting functions and negative regulators which restrain apoptotic factors to prevent cell death (13). Therefore the interaction of 14-3-3 proteins with target proteins is highly regulated. This regulation is primarily phosphorylation-dependent and is usually mediated by the presence of a phosphorylated serine or threonine residue in the target ligand. Thus, the regulation of 14-3-3 activity is dependent on kinases and phosphatases, which phosphorylate the specific residues in the target binding site when the appropriate signals are received (4,14).

1.1.2 Structural organisation of 14-3-3 proteins

14-3-3 is a highly conserved protein family with all isoforms adopting a very similar structure (Fig. 1.1). Each monomer of the 14-3-3 dimer is composed of nine anti-parallel alpha-helices, with mostly short loops between them (Fig. 1.5). Due to a large number of interactions between the alpha-helices, the cup-like structure of 14-3-3 is very rigid (9,15). Binding of phospho-proteins to this rigid dimer can result in conformational changes of the ligand which may alter its stability or catalytic activity (9).

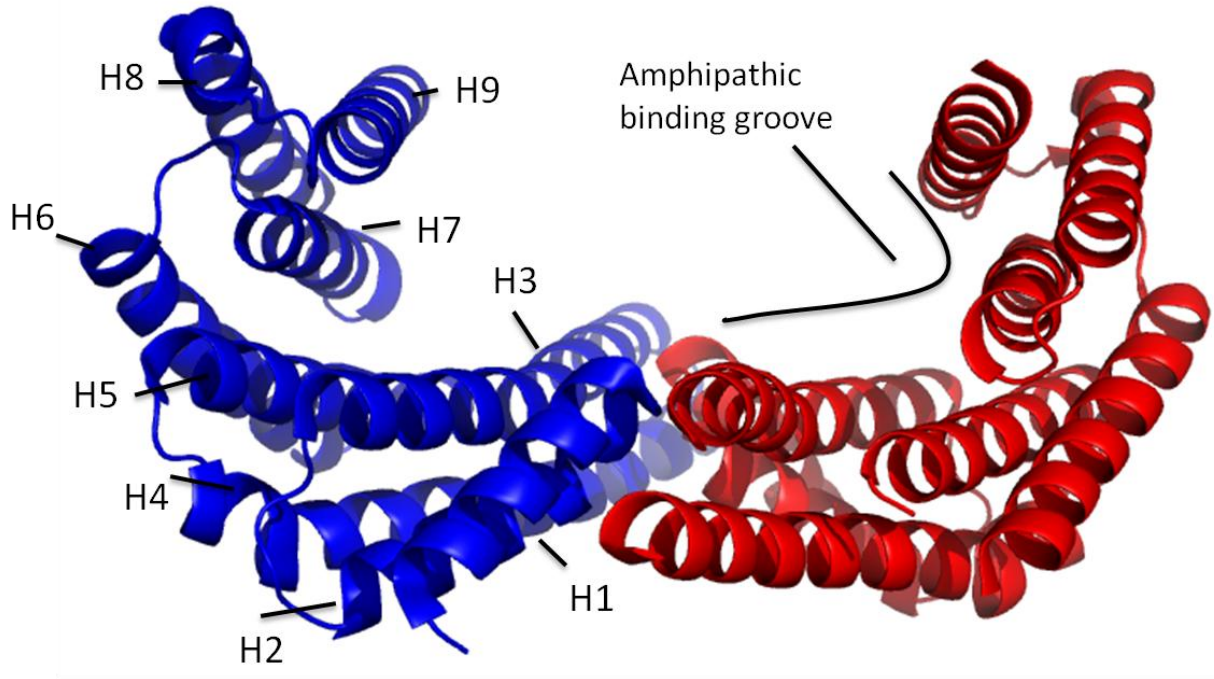

Figure 1.5: The crystal structure of the 14-3-3ζ dimer highlighting the amphipathic binding groove. The individual monomers coloured (red and blue) and the nine alpha helices are numbered. H3, H5, H7 and H9 encompass the amphipathic binding groove (16).

Each 14-3-3 monomer has a conserved inner groove and a more variable outer surface. The inner groove is amphipathic, which is integral to the protein's phospho-serine binding capability (4). The groove is comprised of a basic (positively charged) face and a shydrophobic face and is formed by the four parallel helices H3, H5, H7 and H9 (Fig. 1.5) (17). Phospho-protein binding is dependent on the cluster of these basic and hydrophobic residues comprising the amphipathic binding groove (17). As each dimer contains two binding grooves, 14-3-3 can accommodate the binding of two target proteins or one target protein at two sites (18).

The residues that line the amphipathic groove of the protein are highly conserved across the 14-3-3 isoforms (17). Mutation of key conserved residues in this region results in decreased ligand binding (19). For example, the mutation of lysine 49, in helix 3, to glutamic acid (K49E) in 14-3-3ζ causes significant disruption of the binding of 14-3-3ζ to the kinase Raf-1, which controls growth, transformation and differentiation of cells (6). Additionally K49E 14-3-3ζ has decreased ability to activate ExoS, a protein secreted by the bacterium *Pseudomonas aeruginosa*, which requires 14-3-3 binding in order to function (20). The effect of the point mutation seems to be a result of the charge reversal and does not arise from any structural changes (19). Point mutations of other basic and hydrophobic residues within the binding groove (e.g. R56E, R60E, V176D and L216D) also cause decreased binding of the mutant 14-3-3ζ proteins to ExoS and Raf-1 kinase (20), (21). However the effects are to a much lesser extent than that of the K49E mutation. Thus, it is concluded that there are other basic and hydrophobic residues in the amphipathic groove that are involved in ligand binding but to a lesser degree than lysine 49 (19).

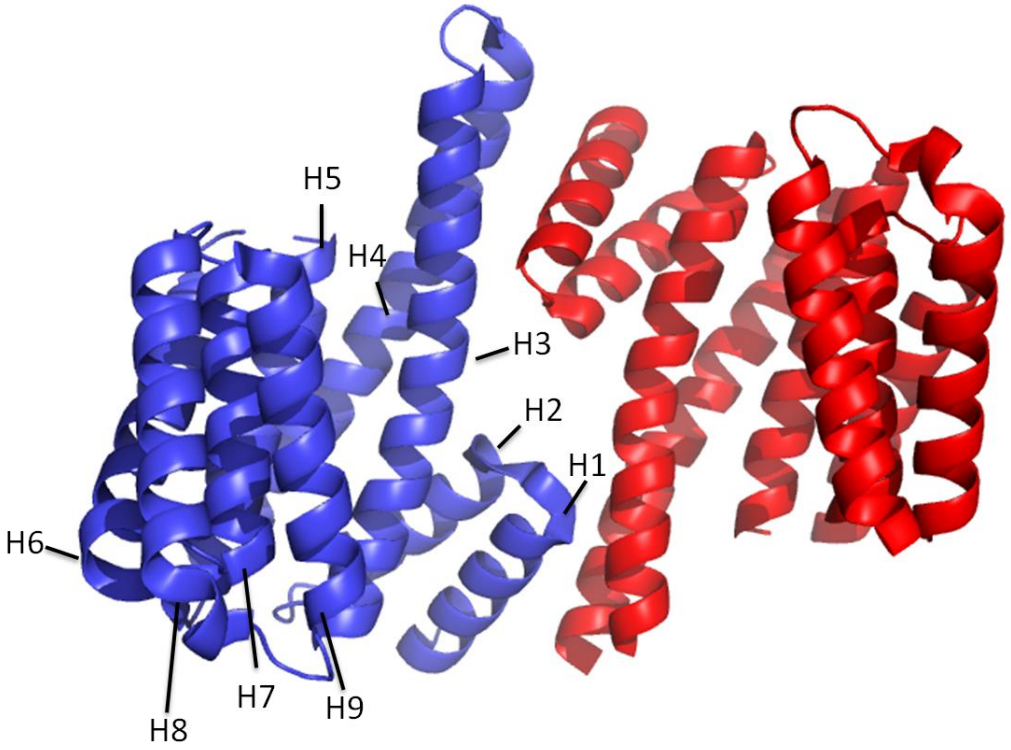

Figure 1.6: The crystal structure of the 14-3-3ζ dimer, aligned to show the nature of the close interaction between the monomers (i.e. the dimer interface) via helices 1, 3 and 4 to form the dimeric structure.

The 14-3-3 proteins can form homo- or hetero-dimers between isoforms (9). A dimer is formed by the interaction between the N-terminal helices of each monomer; specifically the interaction between the helix 1 of monomer A and helices 3 and 4 of monomer B (Fig. 1.6) (16). In 14-3-3ζ, hypothesised salt bridges exist between Arg18-Glu89, Glu5-Lys74, Asp21-Lys85 (1), and Lys9-Glu81 (22) in addition many buried hydrophobic residues (Leu12, Ala16, Ser58, Val62, Ile65 and Tyr82) form hydrophobic interactions (1). Due to the conserved nature of the salt bridging sites across the different 14-3-3 isoforms, hetero-dimer formation occurs readily between the various 14-3-3 isoforms (with the exception of 14-3-3σ, which exclusively forms homo-dimers). However, the physiological role of hetero-dimer formation in 14-3-3 proteins is little understood (5).

Dimeric 14-3-3 is the active form of 14-3-3. There is little to no monomeric form of the protein detected within cells (23). Mutant monomeric forms are degraded at double the rate compared to that of the dimeric protein, potentially preventing unproductive binding of 14-3-3 to target proteins (23). The regulation of 14-3-3 dimerisation can be controlled by the buried residue, Ser58 on helix 3. Phosphorylation of Ser58 in the presence of the physiological lipid sphingosine causes significant disruption to 14-3-3's dimeric structure (24). These disrupted dimers are able to interact with protein targets but are unable to support the target protein's activity (18).

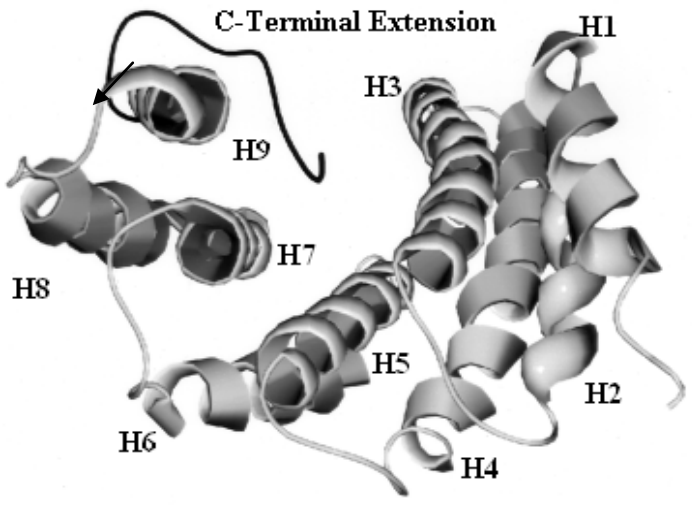

Figure 1.7: The 14-3-3ζ monomer showing the flexible, acidic and unstructured C-terminal extension. The actual position of the C-terminal extension is not defined due to its dynamic nature (taken from (25)).

The C-terminal end of the 14-3-3ζ protein contains a highly flexible region that in 14-3-3ζ consists of the last 15 amino acids, Asp-231 to Asn-245 (inclusive). This region is not resolved in the X-ray crystal structures implying that it is highly mobile (Fig. 1.7) (16). NMR spectroscopy studies confirmed this inherent mobility which is independent of the rest of the protein, whilst also determining that this region is solvent exposed and adopts no ordered secondary structure (26). With a charge of -7 at pH 7.0, the C-terminal extension is very negatively charged due to an abundance of acidic residues (25). The residues in the C-terminal extension are not well conserved across the 14-3-3 family, but are acidic and unstructured in character (Fig. 1.8) (16). The C-terminal extension is important for the overall structural integrity of the protein, and of the resulting complexes which are formed when interacting with target proteins. The removal of the C-terminal extension reduces the stability and solubility of the protein to temperature and denaturant (26).

Structural studies imply that the C-terminal extension interacts with a cluster of basic residues at the top of the amphipathic binding groove (16). Investigations with a C-terminally truncated form of 14-3-3ζ imply that the C-terminal extension interacts with the positively charged region of the amphipathic binding groove and regulates access of target proteins to this binding groove (25,27). Thus, the truncated form of 14-3-3ζ showed an increase in binding affinity to the ligands Raf-1 and Bad, and R18, a synthetic peptide which has high affinity binding to 14-3-3 (25,27).

Figure 1.8: The aligned 14-3-3 C-terminal extensions of the seven human isoforms, with the conserved, acidic residues indicated in bold. As a result of this conservation, this C-terminal extension is highly negatively charged at physiological pH (taken from (25)).

These results suggest that the C-terminal extension acts as a negative regulator of 14-3-3 binding by preventing inappropriate interactions with target proteins. Fluorescence studies suggest that in the absence of a phospho-protein target, the C-terminal extension interacts, in an extended conformation with the amphipathic groove, potentially using its negatively charged residues to increase the interaction between the positively charged face of the amphipathic groove and the acidic C-terminal extension (15). Thus, the C-terminal extension may act as a competitor that blocks the binding of non-phosphorylated proteins. This competition is essential to ensure the correct responses in the cellular environment (25). It is proposed that upon the binding of a ligand, the C-terminal extension is ejected from the amphipathic groove and exists in a flexible and unstructured conformation adjacent to helix 9 of the protein (15). In agreement with this, tryptophan fluorescence studies showed that in the absence of ligand, the C-terminal extension is located in the binding groove and adopts an extended conformation (15). Recent 2D NMR studies have revealed that in the absence of ligand, the C-terminal extension is solvent exposed, unstructured and dynamic, indicating that any interaction with the binding groove is transient (26).

1.1.3 14-3-3 proteins in disease

14-3-3 proteins are highly abundant throughout the body and constitute approximately 1% of the total soluble brain protein (4). Due to this abundance and role diversity, 14-3-3 has been associated with many different diseases including many cancers and neurodegenerative disorders. Neurodegenerative disease is a major health problem in Australia, currently affecting more than 320,000 people. As a result of Australia's aging population, this figure is expected to rise to 900,000 people by 2050 (28). Dementia is a term that refers to a group of diseases which are characterised by the impairment of brain functions occurring as a result of brain degeneration (28). In many cases, brain degeneration is associated with the accumulation of toxic misfolded proteins and peptides (Table 1.1), (29). As shown in table 1.1, each disease is associated with a particular misfolded protein. These proteins are not structurally related and share no common physiological roles, but share the propensity to misfold and aggregate.

14-3-3 proteins are co-localised with pathological protein aggregates in many neurodegenerative diseases e.g. Lewy bodies in Parkinson's disease and plaques and tangles of Alzheimer's disease. Additionally, the presence of 14-3-3 in the cerebral spinal fluid is used as a preliminary diagnostic marker for CJD (30). There has been much speculation about

why 14-3-3 proteins are present in the spinal cerebral fluid of patients with some neurodegenerative diseases. However, the role of 14-3-3 proteins in these deposits and furthermore, their involvement in neurodegenerative disease is unknown (4,13).

Table 1.1: Human neurological diseases associated with the formation of toxic proteinaceous deposits (adapted from Taylor (29), and Chiti and Dobson (31)), and the 14-3-3 isoforms associated with each disease (4,13).

Disease	Protein Deposits	Toxic Protein or peptides	Associated 14-3-3 isoform
Alzheimer's Disease	Extracellular Plaques	Amyloid β	ζ
	Intracellular Tangles	Tau	
Parkinson's Disease	Lewy Bodies	α-synuclein	ε, γ, ζ, θ
Huntington's Disease	Intranuclear and cytoplasmic inclusions	Huntingtin	ζ, γ, β, η
Creutzfeldt-Jacob Disease	Prion Plaque	Prion Protein (PrP)	β, γ, ε, η
Spinocerebellar ataxia type 1	Intranuclear inclusions	Ataxin-1	ε, ζ, η, γ, β

1.2 Protein Folding and Misfolding

Protein folding from the linear polypeptide chain into a functional, structured globular form is a result of the free energy change that occurs with the burial of hydrophobic residues (32). The information needed to fold into a functional form is contained within the primary amino acid sequence (33). Correct folding and its corresponding 3-dimensional structure are essential for the protein's function (34). A protein can go through many cycles of folding and unfolding within its life time for a range of different factors, e.g. during the protein's initial folding, transportation across a membrane, or during exposure to stress conditions such as elevated temperature (34). As a result of this folding/unfolding cycle, there are many opportunities for proteins to incorrectly fold or misfold. Such events occur when exposed hydrophobic regions of the protein associate and form larger, insoluble aggregates (34). Compounding this, the cellular concentration of proteins, which can reach as high as 350mg/mL (35), and the large number of potential interactions between the side chains of different amino acids, make the chance of inappropriate interactions and consequent misfolding between proteins high (36).

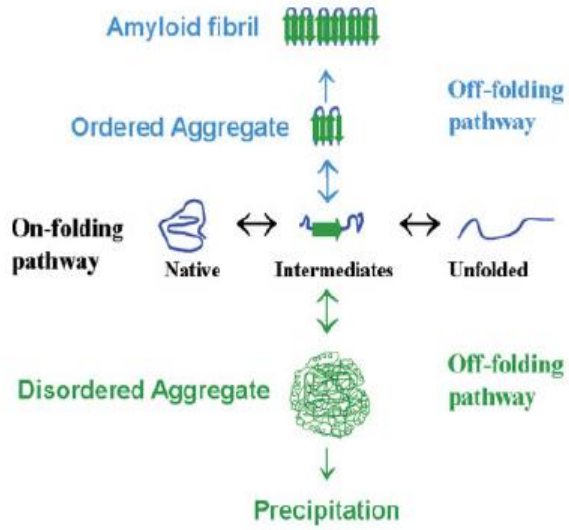

Figure 1.9: The folding of proteins into the native functional state occurs via the production of intermediately folded species on the on-folding pathway in a fast and reversible manner. Under conditions of stress, (e.g. elevated temperature, low pH), protein aggregation can occur via two off-folding pathways which can cause the formation of amorphous (disordered) aggregates or highly ordered amyloid fibrils (taken from (34)).

Misfolding of proteins and their subsequent aggregation can occur via two distinct off-folding pathways (Fig. 1.9): the formation of disordered amorphous aggregates or highly ordered amyloid fibrils. Rapid unfolding, resulting in the exposure of hydrophobic surfaces leads to formation of an amorphous aggregate (37). This can become so large that an insoluble precipitate is eventually formed (34). The kinetics of this process are not well understood (37). Amorphous aggregation is well catered for by the cell under normal conditions, with mechanisms to remove this type of aggregate, such as ubiquitination and degradation of the polypeptide via the proteasome (34).

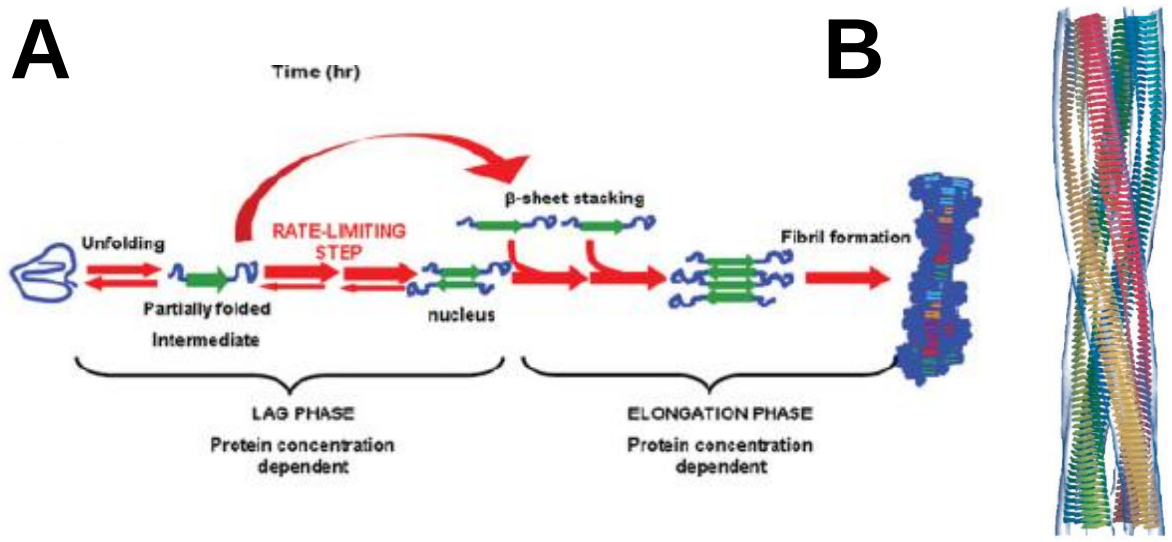

Figure 1.10: (A) The standard nucleation dependent mechanism for amyloid fibril formation starting with the formation of partially folded proteins (taken from (34)). (B) A model of an insulin protofilament, with four individual strands and the arrangement of β-sheets to form the amyloid fibril core (taken from (38)).

In contrast, amyloid fibrils are formed more slowly and exhibit high degrees of ordered structure (Fig. 1.10A). Partially folded regions of a protein interact to form a stable nucleus which can act as a template upon which other intermediately folded proteins are sequestered and extend the oligomer into a protofibril. The addition of more misfolded proteins extends the protofibril into the formation of the beta sheet rich amyloid fibril. The elongation of the fibril is highly dependent on protein concentration (34). Amyloid fibrils are often unbranched, extremely stable and resistant to degradation by proteases and denaturants. This stability is achieved via many intermolecular hydrogen bonds between the backbone amide and carbonyl

groups of amino acids. Mature fibrils can be composed of several protofibrils which can plait together into a rope-like fibre (Fig. 1.10B) (39).

All proteins are potentially capable of forming amyloid fibrils but the amino acid sequence of a protein is a factor that affects its ability to form such structures. The tendency of a protein region to form amyloid fibrils depends on a number of factors, such as the hydrophobicity and net charge of the amino acids (34). Even with the variation in the overall sizes of the fibril forming proteins, the resultant mature amyloid fibrils have comparable structures and dimensions (40). It is thought that in order to remove amyloid fibrils from the cell, the fibril formation is interrupted and the aggregation becomes more amorphous allowing the cell to degrade the polypeptide, i.e. via ubiquitin tagging and proteasomal degradation (34).

The presence of amyloid fibrils in tissues is the hallmark for many neurological diseases (41). Both the mature fibrils and the early soluble oligomers have been shown to have toxic effects on cells (31), (42). The exact mechanism of toxicity within cells is currently unknown, and the cytotoxic species associated with a disease may vary, depending on the fibril-forming protein itself. However various possibilities have been suggested, including the formation of soluble precursors forming a pore like structure in the cell membrane leading to unregulated membrane permeability, or the production of toxic and reactive oxygen species causing damage and cell death (34).

1.2.1 Protein misfolding diseases

Many neurodegenerative disorders are linked to the formation of protein aggregates in the brain. Alzheimer's disease is the most common form of dementia characterised by the presence of amyloid plaques and neurofibrillary tangles (NFTs). Hyperphosphorylated tau is the major protein component of NFTs (43). This phosphorylation is thought to remove the functionality and increase the instability of the Tau protein, enhancing aggregation and neurodegeneration (44,45). 14-3-3 proteins facilitate this Tau phosphorylation, with hyperphosphorylation of Tau prior to the formation of tangles, presumably enhancing the interaction with 14-3-3 proteins (46). Additionally the phosphorylation of Tau in NFTs leads to the interaction with 14-3-3 which would prevent the dephosphorylation of the Tau NFTs and increase the stability of the tangles (47).

Parkinson's disease is a neurodegenerative disease characterised by muscular rigidity, postural instability and muscle tremors (48). Lewy bodies are the characteristic aggregate inclusions which are responsible for the associated neurodegeneration. These Lewy bodies are composed of the protein, α-synuclein in a fibrillar form (49,50). α-Synuclein is widely expressed in neurons and is involved in the regulation of dopamine neurotransmission (4,49). Mutations of α-synuclein result in familial forms of the disease, likely due to an enhanced ability to form amyloid fibrils. 14-3-3 proteins are found co-located with α-synuclein in Lewy body deposits (48,51). The functional significance of the interaction between 14-3-3 and α-synuclein has not been determined. It is currently hypothesised that the over-expression of α-synuclein leads to the sequestration of 14-3-3, preventing the interaction with pro-apoptotic mediators e.g. Bad, leading to cell death.

The polyglutamine class of diseases, including Huntington's disease and spinocerebellar ataxia type-1 (SCA-1) are caused by a CAG expansion encoding glutamine repeats. These polyglutamine expansions increase their tendency to accumulate and aggregate, leading to protein aggregation and neurodegeneration. The length of the CAG repeats correlates to disease severity. Huntington's disease is characterised by the CAG repeats in the protein, huntingtin, and results in early onset dementia. *In vivo* suppression of 14-3-3ζ expression abolishes the aggregate formation of the huntingtin protein, though the mechanism of this interaction is unclear (13).

In SCA-1, there is a polyglutamine expansion in ataxin-1 in a manner similar to Huntington's disease. The physiological function of ataxia is unclear, but is associated with the nuclei of neuronal cells. Toxicity of ataxia-1 is associated with proteins containing a polyglutamine tract (4). The phosphorylation of ataxin-1 leads to an interaction with 14-3-3. This leads to stabilisation of the ataxin protein and slows its normal degradation. This allows the protein to accumulate and aggregate, resulting in neurodegeneration (52).

1.3 Molecular Chaperones

Molecular chaperones are a conserved group of structurally unrelated proteins that are able to assist in the stabilisation and folding of other proteins. These cellular processes include the folding of proteins during and after expression, the refolding of proteins after transportation across membranes, and the association of unfolded proteins to form unstable oligomeric complexes including the degradation and repair of denatured proteins (53). Thus, in neurological diseases associated with protein aggregates, molecular chaperones act to prevent illicit interactions between unfolded proteins that lead to protein aggregation (54), by interacting with and stabilizing partially and unfolded proteins (Fig.. 1.11) (32). Molecular chaperones are not permanent components of these structures, and are not required for the protein's biological function, once the protein has reached the correct conformation (53).

In order to aid the folding of new synthesized polypeptides, amongst other roles, molecular chaperone proteins are expressed constitutively *in vivo* (53). Some molecular chaperone proteins experience greater expression under times of cellular stress (32), such as heat stress. This stress response is ubiquitous and conserved in all organisms and such exposure to stress shifts the protein folding equilibrium, resulting in expression of molecular chaperones being enhanced and directed towards the interaction and stabilisation of misfolded species and preventing aggregation (55). This stress response is thought to be an amplification of the basic chaperone functions that are required by all cells under normal conditions (53). The interaction with misfolded proteins occurs mainly via exposed hydrophobic regions in the chaperone protein (54).

Small heat shock proteins (sHsps) are a major molecular chaperone family over-expressed under heat stress conditions (32). sHsps are also associated with many of the neurological diseases aggregation deposits and are over expressed in patients with Alzheimer's disease and many other protein aggregation diseases (56,57), most likely due to the attempted suppression of toxic aggregates in these tissues.

A member of the sHsps molecular chaperone family is α-crystallin, which exists as a hetero-oligomer of αA- and αB-crystallin (58). Each crystallin component is 20kDa with a predominantly β-sheet structure (59). These crystallin monomers co-associate to form as large, polydisperse oligomers, with some having an average molecular mass of 800kDa (60). At the C-terminal end of the protein, there is a very mobile, acidic, unstructured region which

is responsible for solubilising and stabilising the large sHsps oligomer. The C-terminal extension is essential for the chaperone action of sHsps. It is not directly involved in the chaperoning but is responsible for solubilising the sHsps - aggregate complex (61,62).

sHsps prevent protein aggregation by binding, in an ATP-independent manner, to long-lived intermediates of target proteins to form stable, soluble chaperone-target complexes. sHsps do not have the ability to re-fold a protein back into its native state, but can maintain a misfolded protein's solubility (in a folding-competent state) until conditions have changed in order for it to refold upon its release or when aided by other chaperones (e.g. Hsp70) coupled to ATP hydrolysis (Fig. 1.3) (34,60).

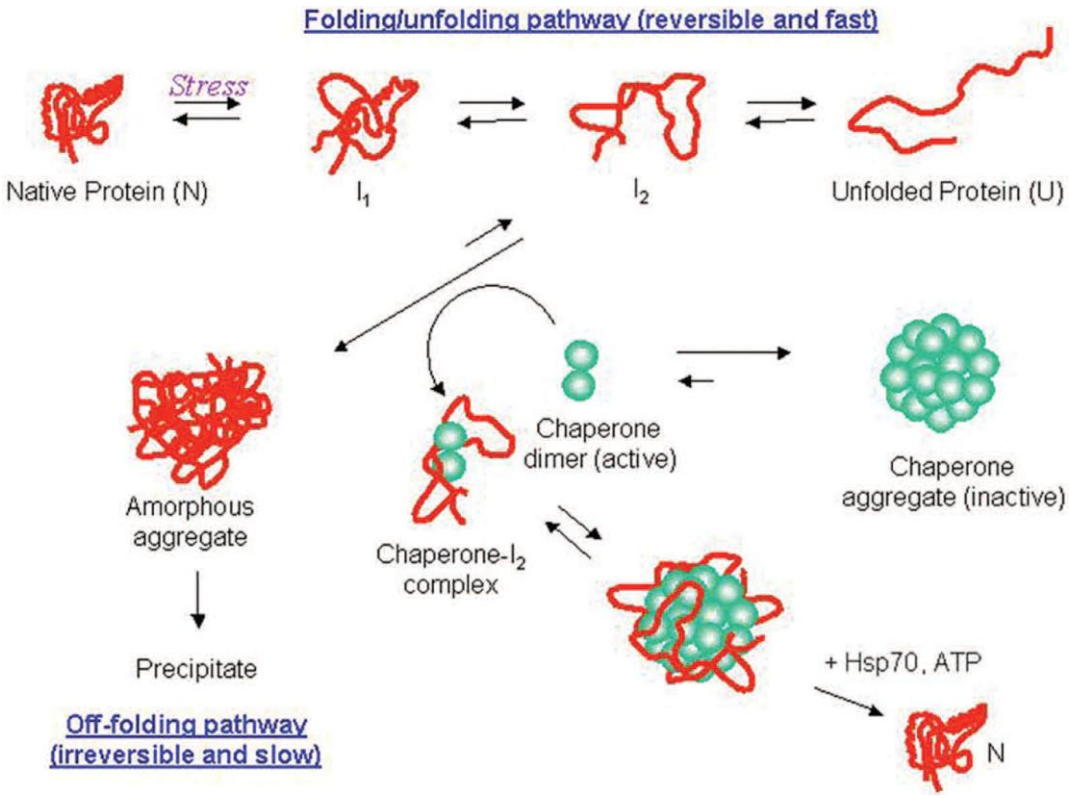

Figure 1.11: A schematic mechanism of the action of the small heat-shock proteins, showing the dissociation of the chaperone active unit from the chaperone oligomer. The dimeric sHsps species is currently hypothesised to be the chaperone active unit. This chaperone active dimer is sequestered to the intermediately folded target proteins (I_2) on the amorphous off-folding pathway via hydrophobic interactions. With the aid of other chaperone proteins (e.g. Hsp70) coupled with ATP hydrolysis, the native conformation of the protein can be recovered (39).

1.3.1 14-3-3ζ as a molecular chaperone

Many different 14-3-3 isoforms are associated with neurodegenerative disorders (Table 1.1). However, with 14-3-3 shown to have neuro-protective and neurodegenerative properties in these diseases, the precise function of these proteins in brain aggregation is unclear.

As mentioned earlier, Yano et al. (14) observed that *Drosophila* 14-3-3ζ is significantly up-regulated by heat stress and depletion of 14-3-3ζ in cells under heat stress resulted in significant amounts of insoluble aggregated mitochondrial precursor protein, apocytochrome c. A soluble form of this protein was produced by the addition of 14-3-3ζ and ATP *in vitro*. This molecular chaperone activity of 14-3-3ζ was replicated *in vitro* with the prevention of heat-induced aggregation of the mitochondrial target protein, citrate synthase, in the presence of 14-3-3ζ. Thus, Yano et al. demonstrated that 14-3-3ζ functions as a heat-stress induced molecular chaperone that can maintain solubility and refold thermally-aggregated proteins. It was hypothesised that 14-3-3ζ action as a chaperone broke down larger aggregates into smaller ones which were then accessible by other chaperones, whereby refolding of target proteins into their native form could be achieved (14). 14-3-3γ has also been shown to be an effective molecular chaperone against the amorphously aggregating protein, rhodonase (63). However the chaperone action of the other 14-3-3 isoforms has not been demonstrated.

The chaperone action of 14-3-3ζ has been further examined by investigating the role of the C-terminal extension and the polar face of the amphipathic groove. The C-terminal extension was investigated using a C-terminally truncated mutant with its last 15 amino acids absent (Δ15C 14-3-3ζ). The investigation of the polar face of the amphipathic binding groove targeted a key residue within the amphipathic groove (K49) (26). Additionally the peptide R18, which has a high binding affinity with 14-3-3 under non stress conditions (27), was utilised to further investigate the role of the amphipathic binding groove. These investigations had little effect on chaperone action, implying these regions of 14-3-3ζ are not critical for the chaperone activity of 14-3-3ζ (26). The site(s) and mechanism of the chaperone action of 14-3-3ζ are currently unknown.

1.4 Aims:

14-3-3 is an abundant protein (10) associated with neurological aggregates (64) and has been identified as a molecular chaperone. 14-3-3ζ has been shown to be an effective molecular chaperone against a number of amorphous and amyloid fibril forming target proteins (14,26,65). Previous investigations have determined that the C-terminal extension and the polar face of the amphipathic binding groove are not critical to the chaperone function of 14-3-3ζ (26). The mechanism and site of the chaperone action of 14-3-3ζ are currently unknown. The overall aim of this thesis is to further characterise and identify the chaperone active site of 14-3-3ζ, in order to further understand the role of 14-3-3 proteins in protein aggregation diseases. As other molecular chaperones are known to interact with target proteins hydrophobically, major hydrophobic regions of the 14-3-3 proteins shall be targeted for investigation. These include the hydrophobic face of the amphipathic binding groove and the dimer interface.

In chapter 3, the investigation of the hydrophobic face of the amphipathic binding groove on the chaperone action of 14-3-3ζ will be undertaken. Exposed hydrophobic residues in this region (V176, L216, L220, and L227) will be mutated. The mutant proteins will be fully characterised by a variety of biophysical and spectroscopic techniques before the analysis of their chaperone function against amorphously aggregating target proteins *in vitro*.

In chapter 4, the investigation of the 14-3-3ζ dimer interface in chaperone action will be examined. Hypothesised salt bridging sites (D21 and E89) in this region and a known phosphorylation site (S58) will be targeted. The initial investigation will determine the role of these sites in dimer formation using various biophysical and spectroscopic techniques. The effects of the potential dimer disruption on the chaperone ability of 14-3-3ζ will be characterised against amorphous aggregating target proteins *in vitro*.

In chapter 5, the monomer-dimer equilibrium of 14-3-3ζ will be further characterised and related to the chaperone function of the protein. The effects of the mutations introduced in chapter 4 will be investigated along with the effects of changing concentration and temperature on the monomer-dimer dynamics of WT 14-3-3ζ.

In chapter 6, to further investigate the dimer interface, the disruption to the dimer of 14-3-3ζ caused by physiological lipid mimics shall be investigated. The disruption shall be

characterised by biophysical techniques before the effects on the chaperone ability of 14-3-3ζ against amorphously aggregating target proteins will be investigated.

In chapter 7, small angle scattering (SAS) techniques shall be implemented to obtain additional information about the complex formed between 14-3-3ζ and an amorphously aggregating target protein, alcohol dehydrogenase. Using small angle X-ray and neutron scattering, real-time structural changes occurring when 14-3-3ζ interacts with aggregating target protein will be monitored. As a result, information on the overall structure of the complex between 14-3-3ζ and its target protein under stress conditions will be obtained, providing detailed information about the mechanism of 14-3-3ζ's chaperone action.

These studies will further our knowledge about the molecular chaperone action of 14-3-3ζ and its interaction with aggregating target proteins. This will enable us to further understand the role that 14-3-3 proteins undertake in protein aggregation diseases.

Chapter 2

Materials and Methods

2.1 Materials

Unless otherwise stated, all materials were of analytical grade and were obtained from Sigma Aldrich (Australia). All solutions were prepared in de-ionised water and were filtered through a 0.22μm membrane (Sartorius) prior to use. The pH of each solution was measured using a FEP20 Five easy plus pH meter (Mettler Toledo, Switzerland), calibrated by 2 point calibration using standard buffers at pH 7.0 and pH 10.0.

The 14-3-3ζ and TEVP proteins were expressed and purified as described in section. 2.2. Amorphous aggregation assays were conducted in clear 96 well plates (Greiner Bio-one, Germany).1,4-Dithiothreitol (DTT) used to induce amorphous aggregation, and isopropyl β-D-1-thiogalactopyranoside (IPTG) used to induce protein expression, were purchased from Astral Scientific. The fluorescent probe, bis-ANS was purchased from Molecular Probes. A stock solution of small molecule 14-3-3ζ inhibitor, #41.14 (2.5mM) was made in DMSO. When used in assays, this stock is diluted into the stated buffer. γ-[^{32}P] labelled ATP was obtained from Perkin Elmer for phosphorylation assays.

All assays were undertaken in 50mM phosphate buffer, 100mM sodium chloride, and 2mM EDTA, pH 7.4, unless otherwise stated.

2.2 Expression and purification of 14-3-3 proteins

2.2.1 14-3-3 Vectors

The WT, D21N, E89Q and S58D 14-3-3ζ-His_6 and Tobacco Etch Virus (TEV) protease-His_7 encoding constructs in the pPROEX HTb vectors obtained from Dr. Joanna Woodcock at SA Pathology.

2.2.2 Generation of 14-3-3 constructs

All the 14-3-3 proteins were generated using a Quickchange Site-directed Mutagenesis kit (QIAGEN Pty Ltd, Australia). The template used for mutagenesis was the WT 14-3-3-His_6 construct in the pPROEX HTb vector (Invitrogen). The combination mutants were generated after 1 and 2 PCR reactions respectively, using the D21N 14-3-3ζ-His_6 construct in the pPROEX HTb vector. The mutagenesis was confirmed by DNA sequencing of miniprep plasmid DNA using oligonucleotides as shown in Table 2.1.

2.2.3 Expression of TEVP and 14-3-3 proteins

All 14-3-3ζ cultures were grown in Luria-Bertani (LB) medium (made in house) with ampicillin (100μg/mL). The inoculation of starter cultures (50mL LB medium) was achieved with a single colony of transformed *E. coli* bacteria and grown overnight (37^{o}C, 200rpm). The starter cultures were diluted into 2L of LB with ampicillin (100μg/mL) and incubated at 37^{o}C until an OD_{600} of 0.6 was reached. Protein expression was induced with IPTG (final concentration = 0.2mM) and the cultures incubated for a further 4 hours (37^{o}C, 200rpm). The cells were harvested after incubation by centrifugation (4^{o}C, 5000rpm, 5mins) using an Avanti JA-301 centrifuge (JLA 10.5 rotor, Beckman Coulter, Australia). The pelleted cells were resuspended in lysis buffer (50mM phosphate buffer, pH7.4, 500mM NaCl, 50mM imidazole, 1mM PMSF), and cells were lysed by incubation with lysozyme (final concentration = 1mg/mL), followed freeze-thawing (three times in dry ice). After lysis, the cell lysate containing the expressed protein was isolated by centrifugation (10,000rpm, 30mins).

Table 2.1: The oligonucleotides utilised to generate the necessary mutation in the 14-3-3 gene, with the mutated bases highlighted in bold. Any restriction sites are highlighted by underlining.

Mutation	Oligonucleotide	Restriction Site
V176D	5'- GCC CTT AAC TTC TCT G**AT** TTC TAT TAT GAG ATC TTG AAC TCC CCA GAG AAA GCC-3'	BglII site added
L216, 220, 227D	5'- GAG TCA TAC AAA GAC AGC ACG **GAT** ATA ATG CAA **GAT** CTG AGA GAC AAC TTG ACA **GAT** TGG ACA TCG GAT ACC CAA GGA GAC G-3'	BglII site added
D21N	5' – GCC GAG CAG GCT GAG CGC TAT GAT **A**AC ATG GCA GCC TGC – 3'	AfeI site added
E89Q	5' – GAG AGA AAA TTG AGA CG**C** AGC TAA GAG A**C**A TCT GCA ATG ATG TAC TG – 3'	EcoRV site is removed
S58A	5' – GTT GTA GGA GCC CGT AGA TCT **GCC** TGG AGG GTC GTC TCA AGT ATT G – 3'	BglII site added
S58D	5' – GTT GTA GGA GCC CGT AGA TCT **GAT** TGG AGG GTC GTC TCA AGT ATT G – 3'	BglII site added

2.2.4 Purification of TEVP

The cellular lysate containing the expressed TEV protease was loaded onto a Ni-Sephrarose column (GE). The column was washed (50mM Sodium phosphate, 500mM Sodium chloride, 50mM imidazole, pH 7.4) to remove unbound proteins before elution with 300mM imidazole in order to collect the purified TEV protease-His_7 protein. The elution was monitored at 280nm. After analysis by SDS-PAGE, the TEV protease-His_7 was concentrated and dialysed into Tris-HCl (50mM, with sodium chloride, EDTA, glycerol, and DTT) and stored at -20^{o}C in 500μL aliquots and used without further purification.

2.2.5 Purification of 14-3-3 proteins

The cellular lysate containing the expressed 14-3-3ζ-His_6 proteins was loaded onto a prepacked Ni-Sephrarose column (GE). The column was washed (50mM Sodium phosphate, 500mM Sodium chloride, 50mM imidazole, pH 7.4), to remove unbound proteins before elution with 300mM imidazole in order to collect the 14-3-3ζ-His_6 proteins. The elution was monitored at 280nm. After analysis by SDS-PAGE, the fractions were combined and diluted to twice the volume (using 50mM Tris, pH8.0, 2mM EDTA and 1mM DTT). In order to produce untagged 14-3-3ζ protein, the 14-3-3ζ-His_6 was incubated with TEVP-His_7 at room temperature overnight. The cleavage reaction was monitored by SDS-PAGE, before purification by Ni-sephrarose chromatography. The untagged 14-3-3ζ proteins were collected in the 50mM imidazole elution buffer. The purified 14-3-3ζ was concentrated and dialysed in 50mM ammonium bicarbonate prior to being lyophilized and stored at -20^{o}C.

2.2.6 Protein concentration determination

The concentrations of the protein solutions were determined using the Beer-Lambert law. The absorbance was measured using a Cary 5000 UV-Vis spectrophotometer (Varian Ltd, Australia). For all the 14-3-3 proteins, the absorbance was measured at 280nm and an extinction coefficient of 23790 M^{-1} cm^{-1} was used. For alcohol dehydrogenase, the absorbance was measured at 280nm and an extinction coefficient of 55000M^{-1} cm^{-1} was used. All concentrations were based upon the monomeric molecular weight of the proteins (Table 2.2).

Table 2.2: The molecular weight (in Daltons) of the 14-3-3ζ proteins, for the calculation of protein concentration.

Protein	Molecular weight (Daltons)
14-3-3 WT	27745
D21N 14-3-3	27744
E89Q 14-3-3	27744
S58D 14-3-3	27773
D21NE89Q 14-3-3	27743
D21NE89QS58A 14-3-3	27727
D21NE89QS58D 14-3-3	27772
V176D 14-3-3	27761
L216, 220, 227D 14-3-3	27751
Alcohol Dehydrogenase	35000
Insulin	5734

2.3 Biophysical Characterisation techniques

2.3.1 Intrinsic tryptophan fluorescence and thermostability of 14-3-3ζ

The intrinsic tryptophan fluorescence of the 14-3-3ζ proteins (7.2μM, 2mL) was measured in a Cary Eclipse fluorescence spectrophotometer equipped with a Peltier temperature controller (Varian, Melbourne, Australia). Protein stability profiles were recorded over a range of 37-80^{o}C at 2^{o}C intervals. All solutions were equilibrated for 2 mins prior to collection. All recordings were taken with an excitation wavelength of 295nm and the fluorescence emission was monitored between 300 and 400nm. The excitation and emission slit-widths were set to 5nm. For WT 14-3-3ζ, the mean melting temperature was 62.66^{o}C with a mean deviation of ± 0.44^{o}C.

2.3.2 Bis ANS assays

A stock solution of bis-ANS was made in 50mM phosphate buffer, pH 7.4 and 100mM NaCl. The concentration was determined by UV absorbance at 395nm, using an extinction coefficient of 23,000M^{-1} cm^{-1} (66).

The 14-3-3ζ proteins (1.4μM, 2mL) were titrated with a stock solution of bis-ANS (2.8mM) over a range of concentrations to give a final concentration of 28μM (20 molar equivalence). The fluorescence of each solution at 37^{o}C was collected via direct excitation at 385nm (emission collected between 400 and 600nm) and via FRET excitation at 295nm (emission collected between 300 and 600nm) on a Cary eclipse fluorescence spectrophotometer with a Peltier temperature controller (Varian, Melbourne, Australia). The excitation and emission slit widths were set to 5nm.

2.3.3 Far UV circular dichroism

The far UV circular dichroism spectra of the 14-3-3ζ proteins (7.2μM, 200μL) were recorded on a J-815 spectropolarimeter (ATA Scientific, NSW, Australia) over a wavelength range of 190-250nm with a scan rate of 50nm/min and a band width of 1nm. All measurements were obtained in 20mM phosphate buffer, pH 7.4 and are represented at the average of 3 accumulations. All high voltage tension records above 600V were discarded and the data was converted to mean residue ellipticity using equation 2.1.

$$mean\ residue\ ellipticity = \frac{CD\ Measurement \times Molecular\ Weight}{Concentration \times pathlength \times Number\ of\ residues} \quad (2.1)$$

Where the units for:

Molecular weight = Da (g mol^{-1})

Concentration = mg/mL

Path length = mm

2.3.4 Cross-linking of 14-3-3ζ proteins with glutaraldehyde

Stock solutions of glutaraldehyde were produced by diluting 100% glutaraldehyde in water. The 14-3-3ζ proteins (250ng, 10µL) was incubated with glutaraldehyde (over a concentration range of 0.001-0.005%) and incubated at 37^{o}C for 15mins. The reaction was terminated using SDS loading buffer. The samples were analysed by SDS-PAGE, Western blotting and immuno-blotting with K19 14-3-3 antibody (Santa-Cruz, SC-629). This was visualised by chemiluminescence on a Las 4000 luminescent image analyser (Berthold, Australia).

2.3.5 Phosphorylation assays

14-3-3ζ proteins (WT, D21N, E89Q and S58D; 0.5µg) were incubated with cetrimonium bromide (CTAB delivered in 0.3% DMSO; 5µM) for 10 minutes at room temperature prior to the addition of 0.25U of PKA in kinase reaction buffer (final concentration; 10mM Tris-HCl pH 7.4, 15mM $MgCl_2$, 0.3mM DTT, 25µM ATP and 333nCi [^{32}P]-ATP). Samples were incubated at 37^{o}C for 20 minutes before terminating the reaction with the addition of SDS-PAGE loading buffer. Reactions were separated by 12.5% SDS-PAGE and Coomassie stained. The phosphorylation of 14-3-3ζ was analysed using a typhoon phospho-imager.

2.3.6 Analytical ultracentrifugation

Prior to analytical ultracentrifugation experiments, all 14-3-3ζ proteins were subjected to size exclusion chromatography using a Superdex 200 column (GE), with fractions collected corresponding to approximately 54kDa. Sedimentation velocity analysis of 14-3-3ζ (WT, D21N, E89Q, S58D and D21N/E89Q/S58A) were performed using a XL-I analytical ultracentrifuge (Beckman-Coulter) with an 8-hole An-50-Ti rotor. Double sector centrifuge cells with quartz windows were loaded with 380µL of protein sample and 400µL of buffer

(20mM Tris-HCl, 150mM NaCl, pH7.4). To determine the optimal wavelength and radial range for the experiments, initial scans were taken at 3000rpm. Two concentrations (9.7μM and 3.2μM) were used, with sedimentation velocity at the lower concentration undertaken at 3 temperatures (4, 20 and 37^{o}C). Absorbance versus radial profiles were obtained using a step size of 0.003cm at a single wavelength (235nm for 9.7μM and 280nm for 3.2μM) every 5 mins. A rotor speed of 40,000rpm was used. The sedimentation velocity data was fitted to a continuous sedimentation coefficient [*c(s)*] distribution model using the program SEDFIT (67,68). The partial specific volume, buffer density and viscosity of the 14-3-3ζ proteins (Table 2.2) were calculated using the program SEDNTERP (69).

2.3.7 Experiments undertaken in the presence of sphingosine mimic #41.14.

A stock solution of #41.14 (2.5mM) was made in 100% DMSO. For all assays, this stock was diluted into the stated buffer. When interacting with 14-3-3ζ, #41.14 was incubated with the protein with a 2 molar excess for 15 minutes prior to the experiment. All experiments included controls for the presence of #41.14.

2.4 Chaperone assays

All assays are undertaken in 20mM phosphate buffer, 150mM sodium chloride and 2mM EDTA, pH 7.4, unless otherwise stated. Amorphous aggregation assays monitored by light scattering, were undertaken in clear 96 well plates (Greiner Bio-One, Baden-Wurttemberg, Germany). Insulin dissolution requires a pH of 2. Insulin was suspended and the pH adjusted to allow dissolution before re-adjustment to pH 7.4.

2.4.1 Chaperone Assays by light scattering

The target proteins, alcohol dehydrogenase (14μM) and insulin (40μM) were incubated separately in the presence and absence of 14-3-3ζ proteins at a 1:0-2 molar ratio of target protein: 14-3-3. The aggregation of insulin was initiated by the addition of DTT (10μM) immediately before incubation at 37^{o}C. Assays using alcohol dehydrogenase were incubated at 42^{o}C. The change in light scattering is monitored at 340nm using a Fluostar Optima plate-reader (BMG Labtechnologies, Australia). Each assay was repeated in triplicate and the data corrected and averaged.

2.4.2 Chaperone assays by intrinsic tryptophan fluorescence

The amorphous aggregation of insulin (10μM, 2mL) was assessed by intrinsic tryptophan fluorescence in the presence and absence of 14-3-3ζ (WT and D21N/E89Q/S58A) at a 1:2 molar ratio of target protein: 14-3-3ζ. The intrinsic tryptophan fluorescence was monitored at 345nm after excitation at 295nm using a Cary eclipse fluorescence spectrophotometer with a Peltier temperature controller (Varian, Melbourne, Australia). The aggregation of insulin was initiated by the addition of DTT (final concentration = 10μM).

2.4.3 Chaperone activity in the presence of 41.14

The target protein alcohol dehydrogenase (14μM, 200μL) was incubated in the presence and absence of 14-3-3(14μM) incubated with #41.14 (28μM). The change in light scattering at 340nm was monitored using a Fluorstar Optima plate reader (BMG Labtechnologies, Australia). Prior to the start of experiments, #41.14 was incubated with the protein at room temperature.

2.4.4 Determining the % protections provided by chaperones

The protection afforded by the 14-3-3 proteins against the amorphous aggregation of alcohol dehydrogenase and reduced insulin, is calculated using Equation 2.2.

$$\%\ Protection = 100\left(\frac{\Delta A - \Delta AChaperone}{\Delta A}\right) \qquad (2.2)$$

Where:

ΔA = the average light scattering at the termination of the assay in the absence of 14-3-3

ΔAchaperone = the average light scattering at the termination of the assay in the presence of 14-3-3

2.5 Small angle scattering Techniques

2.5.1 Sample Preparation

All small angle scattering experiments were undertaken at the Bragg Institute, Australian Nuclear Science and Technology Organisation (ANSTO), Lucas Heights, NSW. Deuterated 14-3-3ζ protein was produced at the National Deuteration Facility by Dr Agata Rekas. The deuterated 14-3-3ζ protein was characterised using the described techniques in sections 2.3 and 2.4 at the University of Adelaide. The ideal scattering conditions were determined using the chaperone assays (in section 2.4) at different temperatures (33^{o}C, 37^{o}C, 42^{o}C). Alcohol dehydrogenase (Sigma Aldrich) was dialysed into 50mM ammonium bicarbonate (pH 7.4) and lyophilised prior to use All experiments were undertaken with alcohol dehydrogenase (28μM) with a 1-3 molar excess of 14-3-3ζ.

2.5.2 Small angle X-ray Scattering

To get an overall picture of stability and sizes of interacting molecules, small angle X-ray scattering data was acquired on a Bruker SAXS NanoSTAR three-pinhole collimation instrument with a rotating anode.

SAXS data was collected of alcohol dehydrogenase (28μM) interacting with 14-3-3ζ at a 1:3 molar equivalence. Scattering was measured in 30minute increments for up to 4 hours.

Radial averaging to produce 1D-scattering intensity profiles of I(q) vs. q for a q range of ~0.02-0.3Å^{-1} was undertaken using the Bruker SAXS data collection software. Detector sensitivity corrections were included in this analysis.

2.5.3 Small angle neutron scattering

The interaction of alcohol dehydrogenase (28μM) with 14-3-3ζ (28 and 56μM) was analysed using small angle neutron scattering, performed at the QUOKKA station at ANSTO (70). Deuterated 14-3-3ζ and a range of D_2O concentrations (0, 40. 70 and 100%) were utilised to obtain contrast variation data series. EDTA was added (with a final concentration of 2mM) to initiate the aggregation of ADH.

Samples were loaded into in-house made demountable quartz samples cells (path-length = 1mm). Two sample detectors distances were used (10 and 1.3m) to cover a q range of 0.001-0.27Å^{-1}. Measurements taken at 10m were obtained over 60mins, and those at 1.3m obtained

over 20mins, guided by the intensity of scattering. All data reduction was performed with IgorPro.

Data analysis and modelling was undertaken by the ATSAS suite of programs available from http://www.embl-Hamburg.de/ExternalInfo/Research/Sax/index.html. Scattering data subtraction, averaging, merging and Guinier analysis was undertaken in PRIMUS. Distance distribution functions were generated in GNOM. Low resolution *ab initio* models were generated using DAMMIF, with molecular envelopes based on the D_{max} for each protein (obtained from GNOM) with averaging of runs for native 14-3-3 and ADH (71).

Chapter 3

Investigation into the functional role of the hydrophobic face of the amphipathic binding groove of 14-3-3ζ

3.1 Introduction:

Yano *et al.* (14) showed that 14-3-3ζ suppresses the thermal-induced aggregation of citrate synthase *in vitro* and is up-regulated in response to heat stress. The presence of a heat shock element in the 14-3-3 gene promoter, results in up-regulation of the protein expression upon binding of a heat shock transcription factor (72). This occurs in a similar manner to that of the structurally unrelated molecular chaperones, small heat shock proteins (sHsps). The C-terminal extension has been demonstrated not to be an important region in the chaperone action of 14-3-3ζ (26). In this chapter, further investigations were undertaken to identify the potential chaperoning sites in 14-3-3ζ.

As described in section 1.4.2, the amphipathic groove is the active binding site of 14-3-3's interaction with primarily phosphorylated target proteins under normal (non-stress) conditions (3). Some proteins have been observed to interact with this region in a phosphorylation-independent manner (17). Thus, regardless of phosphorylation, the current known targets of 14-3-3 predominantly interact with this amphipathic binding groove. The polar face of the amphipathic groove has been previously investigated for its role in chaperone action, using a charge reversal mutant of the well-characterised binding residue, Lys49, and R18, a twenty amino acid, negatively charged peptide known to interact strongly with the amphipathic groove (27). There was no observed effect on chaperone action of 14-3-3ζ, signifying that the polar face of the amphipathic binding groove is not critical for chaperone action of 14-3-3ζ (26).

In the main, molecular chaperones interact with aggregating target protein via hydrophobic interactions (54). As a major region of hydrophobicity, the hydrophobic face of the

amphipathic binding groove is a region potentially involved in the chaperone action of 14-3-3ζ. Hence, exposed hydrophobic residues in this region were targeted for site-directed mutagenesis (Fig. 3.1). After examination of the crystal structure, it was determined that the residues V176, L216, L220 and L227 are exposed hydrophobic residues, that have been previously implicated in the binding of target proteins (21). They are located in helices 7 and 9 and are conserved across human 14-3-3 isoforms (Fig. 3.1).

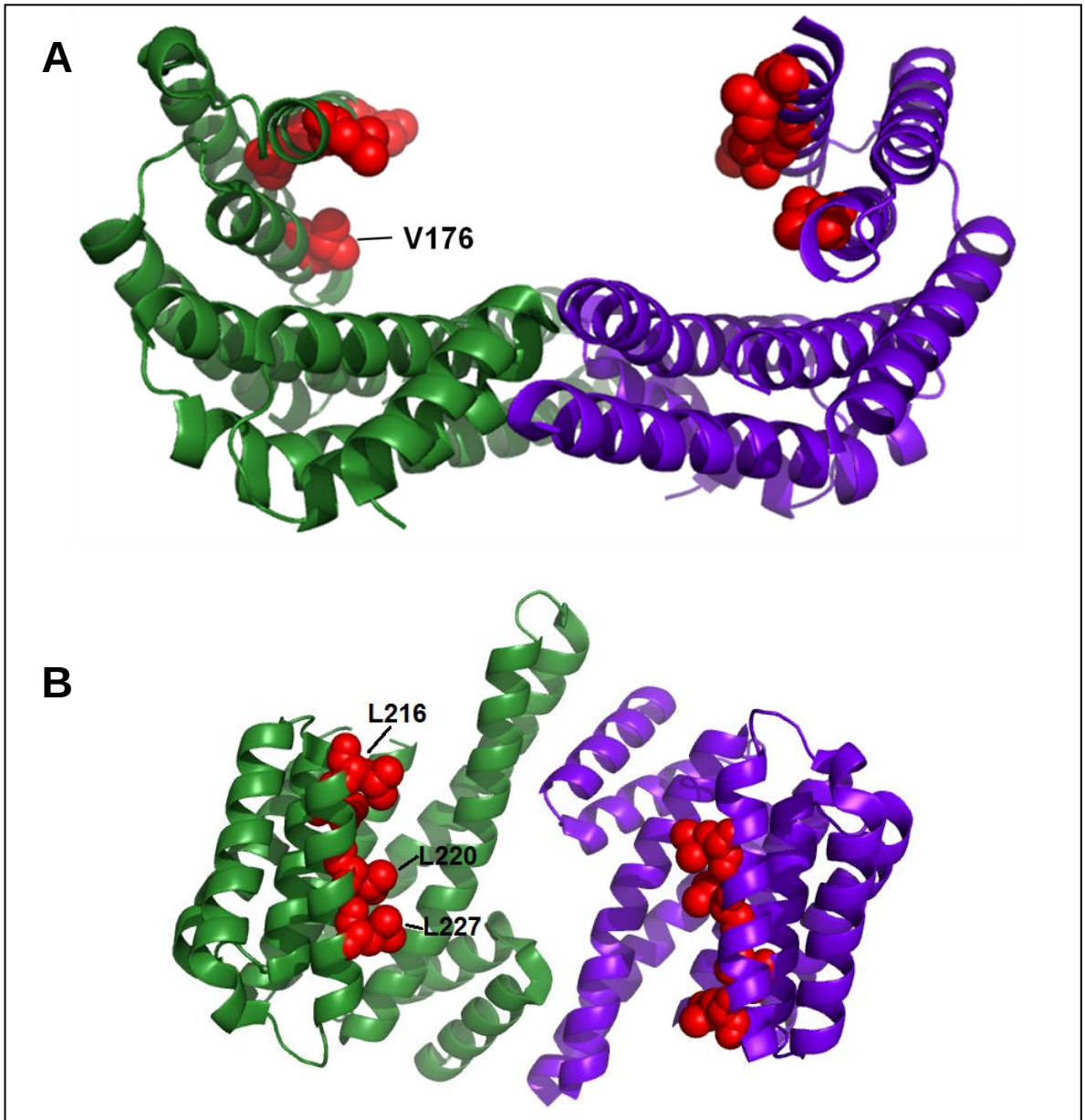

Figure 3.1: The crystal structure of 14-3-3ζ dimer showing the location of the selected hydrophobic residues, V176 (helix 7), L216, L220 and L227 (helix 9), (highlighted in red), which line the hydrophobic face of the amphipathic binding groove looking at the

amphipathic binding groove (A) and down at the dimer interface (B). The individual monomers are coloured green and purple.

In order to test their role in chaperone action, the hydrophobic residues were replaced with the negatively charged residue, aspartic acid (V176D and the triple mutant, L216, 220, 217D), replacing the hydrophobicity with a negative charge, as these mutations have been utilised previously (20). Any structural effects of this conversion were analysed using spectroscopic techniques before the relative chaperone activity of these proteins was assessed and compared to the wild type protein.

3.2 Results: Biophysical characterisation of the 14-3-3 proteins (WT, V176D and L216, 220, 227D)

Mutations were introduced by Quickchange site directed mutagenesis. Mutations were confirmed by sequencing (section 2.2). The 14-3-3ζ proteins were expressed and purified successfully as per Williams et al. (26). All the 14-3-3ζ mutants expressed at a similar level as WT 14-3-3ζ. All the proteins were greater than 95% pure by SDS PAGE analysis.

3.2.1 Native PAGE analysis

Native PAGE gel electrophoresis was undertaken to ensure that the 14-3-3ζ proteins existed primarily in the physiologically relevant dimeric form. The native pI of 14-3-3 proteins is 4-5, meaning they are negatively charged at neutral pH. However, the nature of native-PAGE analysis means that molecular weight cannot be determined. This allows us to analyse the 14-3-3 oligomers by neutral pH native PAGE, whereby the investigation of dimer disrupted mutant proteins of 14-3-3ζ exhibited increased mobility compared to WT 14-3-3ζ, implying a perturbation to the 14-3-3ζ structure (73,74). The analysis of V176D and L216, 220, 227D 14-3-3ζ proteins show that the proteins all migrate as a single band, identical in mobility to the WT 14-3-3ζ protein (Fig. 3.2). The implication is that the 14-3-3 proteins exist as a dimer, indicating no major structural change in quaternary structure has occurred as a result of the mutations.

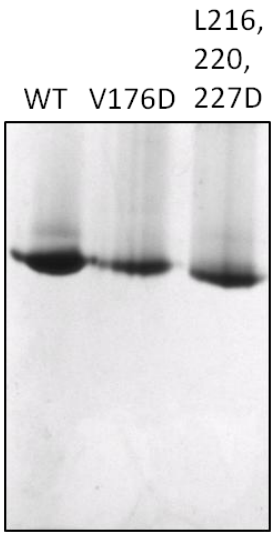

Figure 3.2: Native PAGE analysis of the generated 14-3-3ζ proteins (WT, V176D and L216, 220, 227D) as single bands visualised using Coomassie staining.

3.2.2 Far UV Circular Dichroism

Far UV circular dichroism (as described in appendix A.1) was used to monitor any overall secondary structural changes as a result of the mutations in the hydrophobic face of the amphipathic binding groove. The far-UV CD spectrum of 14-3-3ζ WT was indicative of a protein which is predominantly alpha-helical, and is consistent with previous reports (21).

Compared to WT 14-3-3ζ the 14-3-3ζ mutants exhibited a decrease in the mean residue ellipticity at 208 and 222nm in their CD spectrum, corresponding to a 13% and 26% decrease in the mean residue ellipticity for V176D and L216, 220, 227D 14-3-3ζ proteins respectively (Fig. 3.3). This implies a reduced helical content in both mutant proteins, more so for the triple L216, 220, 227D 14-3-3ζ mutant than for the V176D 14-3-3ζ mutant. All of the selected residues are within a helical environment, and are potentially involved in formation of the helices 7 and 9. Therefore with the introduction of the negatively charged aspartic acid into the helices, there could be some destabilisation to the helical structure resulting in a less-defined helix. Both mutants have very characteristic CD spectra of α-helical proteins, implying that even with a small amount of destabilisation, the remaining regions of the 14-3-3ζ protein remain correctly folded and retain the majority of the characteristic 14-3-3ζ helical structure (Fig. 3.3).

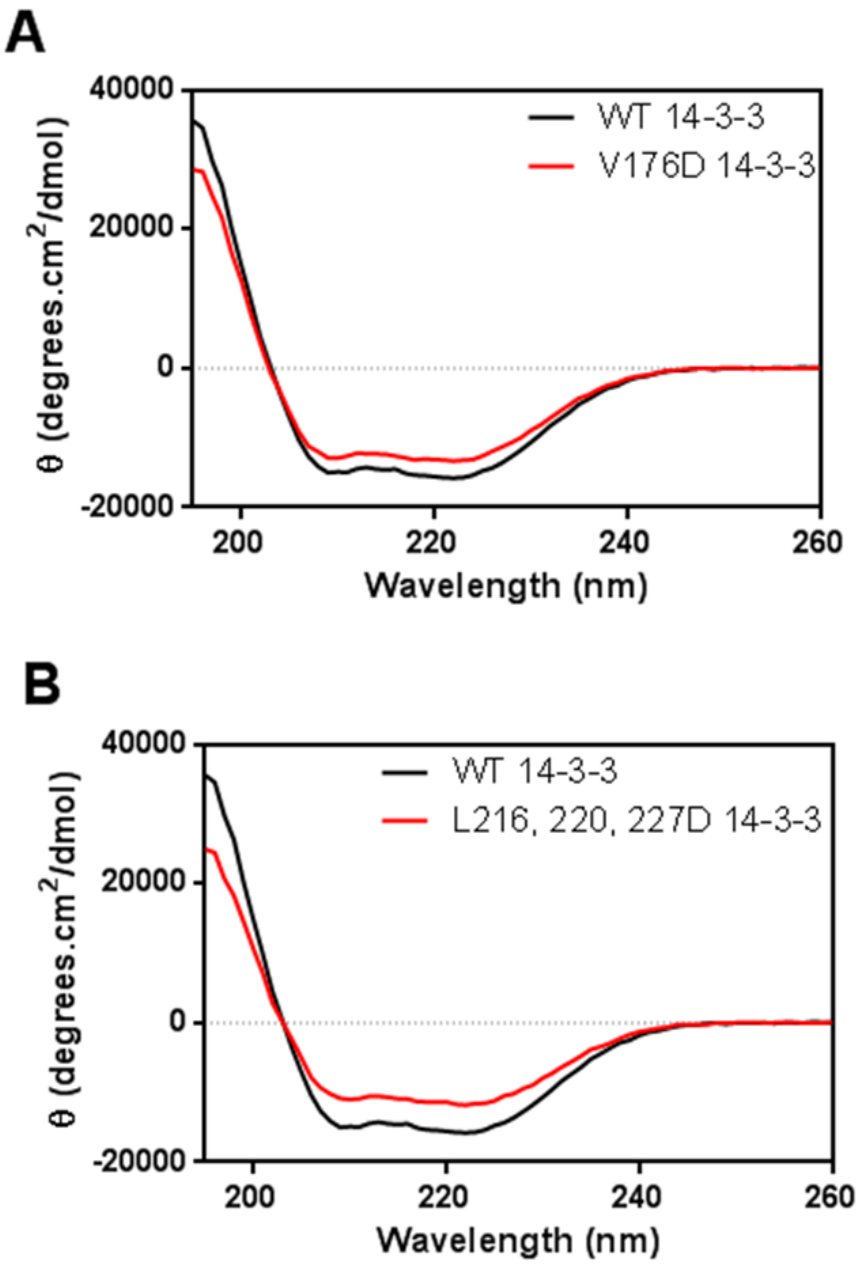

Figure 3.3: The far-UV circular dichroism spectra comparing the WT 14-3-3ζ (7.2uM) profile with that of V176D (A) and L216, 220, 227D (B) 14-3-3ζ (7.2uM) between the wavelengths of 190 and 260nm. The CD spectra were obtained in 20mM phosphate buffer, at pH 7.4 and 20^{o}C.

3.2.3 Intrinsic tryptophan fluorescence

As explained in section Appendix A.2, alterations in the environment of tryptophan residues in 14-3-3ζ as a result of the mutations can be monitored by intrinsic tryptophan fluorescence. 14-3-3ζ has two tryptophan residues, W59 in helix 3 and W228 in helix 9 (75). WT 14-3-3ζ has a fluorescence wavelength maximum of 350nm, i.e. a blue shift compared to free tryptophan (A.2), indicative of the two tryptophan residues being relatively buried within the protein. π-π stacking in 14-3-3γ that occurs between W233 and Y184, W60 is the major contributor to the fluorescence signal. Due to the structure similarity between 14-3-3γ and 14-3-3ζ, it is likely that W59 is the main contributor for the fluorescence signal for 14-3-3ζ.

The intrinsic tryptophan fluorescence of V176D 14-3-3ζ shows a wavelength maximum at 330nm (Fig. 3.4 A), a significant reduction in the maximum wavelength of V176D 14-3-3ζ compared to the WT protein. This blue shift in the V176D mutant is indicative of a structural change most likely resulting in the environment of W59 in the 14-3-3ζ structure becoming less solvent exposed. This enhanced burial of W59 is potentially due to additional interactions within the amphipathic binding groove as a result of introduction of the negatively charged aspartic acid.

The intrinsic fluorescence of L216, 220, 227D 14-3-3ζ shows a wavelength maximum of 350nm (Fig. 3.4 B), comparable with that of WT 14-3-3ζ and the fluorescence emission profiles are near identical. The distance of these mutations from W59 implies that the lack of any shift in the maximum fluorescence wavelength is indicative that there is no major structural change throughout the protein structure. Additionally, the proximity of L277 to W228 and the lack of any change in the tryptophan fluorescence indicate that the π-π stacking interaction between W228 and Y179 has not been interrupted. Hence, this lack of change in the fluorescence wavelength maximum is indicative of no major structural changes in the 14-3-3ζ protein.

In summary, the intrinsic tryptophan fluorescence indicates that the introduction of a charged residue into the core of the amphipathic binding groove in helix 7 of V176D 14-3-3ζ results in some non-native interactions which leads to the changing environment of one or both of the tryptophan residues. In comparison, the introduction of charged residues into helix 9 in L216, 220, 227D, shows little change to the intrinsic tryptophan fluorescence implying a negligible structural change in the vicinity of the two tryptophan residues compared to WT 14-3-3ζ.

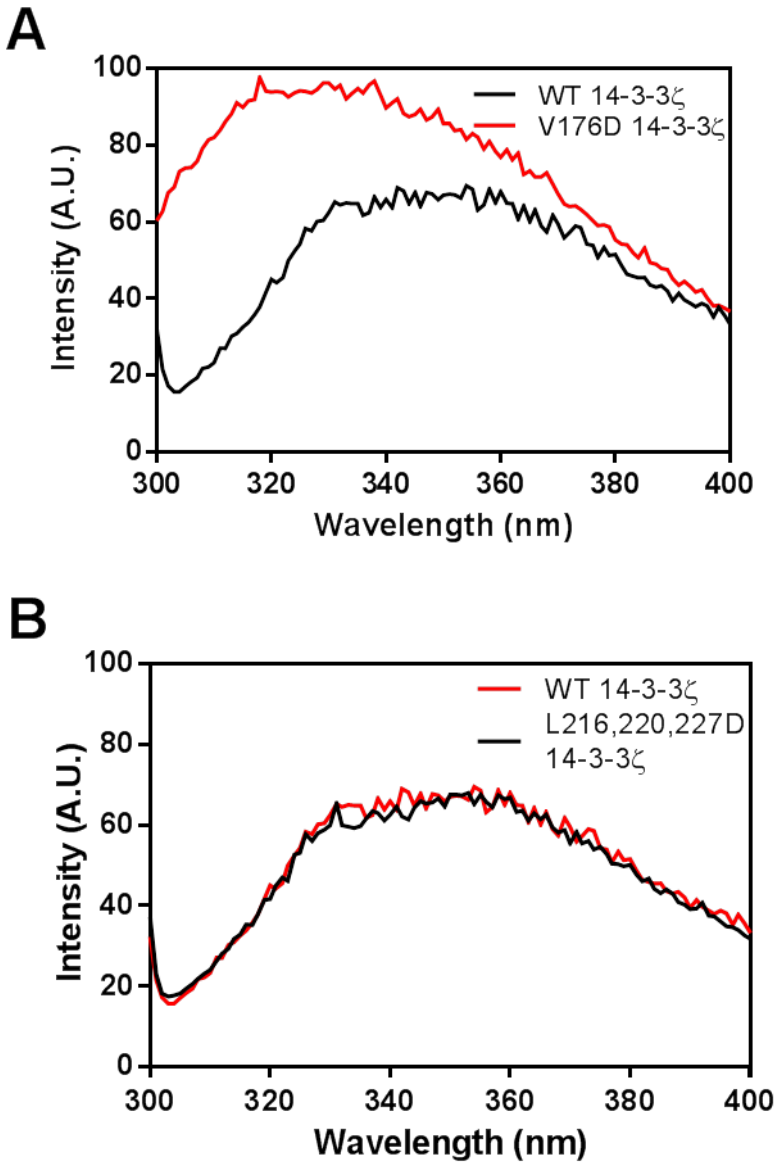

Figure 3.4: The intrinsic fluorescence spectra of WT 14-3-3ζ compared with V176D 14-3-3ζ (A) and L216, 220, 227D 14-3-3ζ (B).The intrinsic tryptophan fluorescence was measured by exciting the 14-3-3ζ proteins (7.2μM, 2mL) at 295nm and acquiring the fluorescence emission between 300 and 400nm at 37^{o}C.

3.2.4 Thermostability, monitored via intrinsic tryptophan fluorescence

The thermostability of each protein was assessed by monitoring the intrinsic tryptophan fluorescence of the 14-3-3ζ proteins between 37 and 80^{o}C. Upon unfolding of the protein, an increase in the fluorescence intensity is observed and the melting temperature can be determined (Appendix A.2). The melting temperature is the temperature at which the percentage of protein unfolding is 50%. With increasing stability, the melting temperature increases. Initially, for all the WT and mutant 14-3-3ζ proteins, there was a small steady decrease in the fluorescence intensity with increasing temperature (Fig. 3.5). Over this range, each protein exhibits a similar rate of quenching, indicating no major structural changes to the proteins.

The thermostability profile of WT 14-3-3ζ (Fig. 3.5) shows an increase in fluorescence intensity at 60^{o}C before stabilising at 66^{o}C. The melting temperature of WT 14-3-3ζ was determined to be 63^{o}C. The thermostability profile for V176D 14-3-3ζ exhibits an increase in fluorescence intensity at 62^{o}C before stabilising at 70^{o}C, giving a melting temperature of 65^{o}C. These thermostability profiles (Fig. 3.5) show that the mutagenesis of Val176 to Asp results in a slight stabilising effect in the protein. This stabilising effect could be a result of a potential interaction of Asp176 with positively charged residue(s) in the amphipathic binding groove, as indicated in the blue shift in the intrinsic tryptophan studies in section 3.2.3.

The thermostability profile for L216, 220, 227D 14-3-3ζ shows an increase in fluorescence intensity at 56^{o}C before stabilising at 60^{o}C. The melting temperature of L216, 220, 227D 14-3-3ζ was determined to be 58^{o}C. In contrast to V176D 14-3-3ζ, the mutagenesis of L216, L220 and L227 to Asp residues appears to have a slight destabilising effect, with a reduction in the melting temperature. As indicated by CD (section 3.2.2), the introduction of negatively charged residues into helix 9 results in the disruption of the helical structure, possibly suggesting a less defined and stable helix.

In summary, V176D 14-3-3ζ is a more thermostable protein than WT 14-3-3ζ, predominantly alpha helical with decreased solvent exposure of Trp59, probably due to increased electrostatic interaction(s) within the protein. In contrast, L216, 220, 227D 14-3-3ζ has a predominantly alpha helical profile, no environmental changes of the tryptophan residues and is less thermally stable than WT 14-3-3ζ, due to the destabilisation of helix 9.

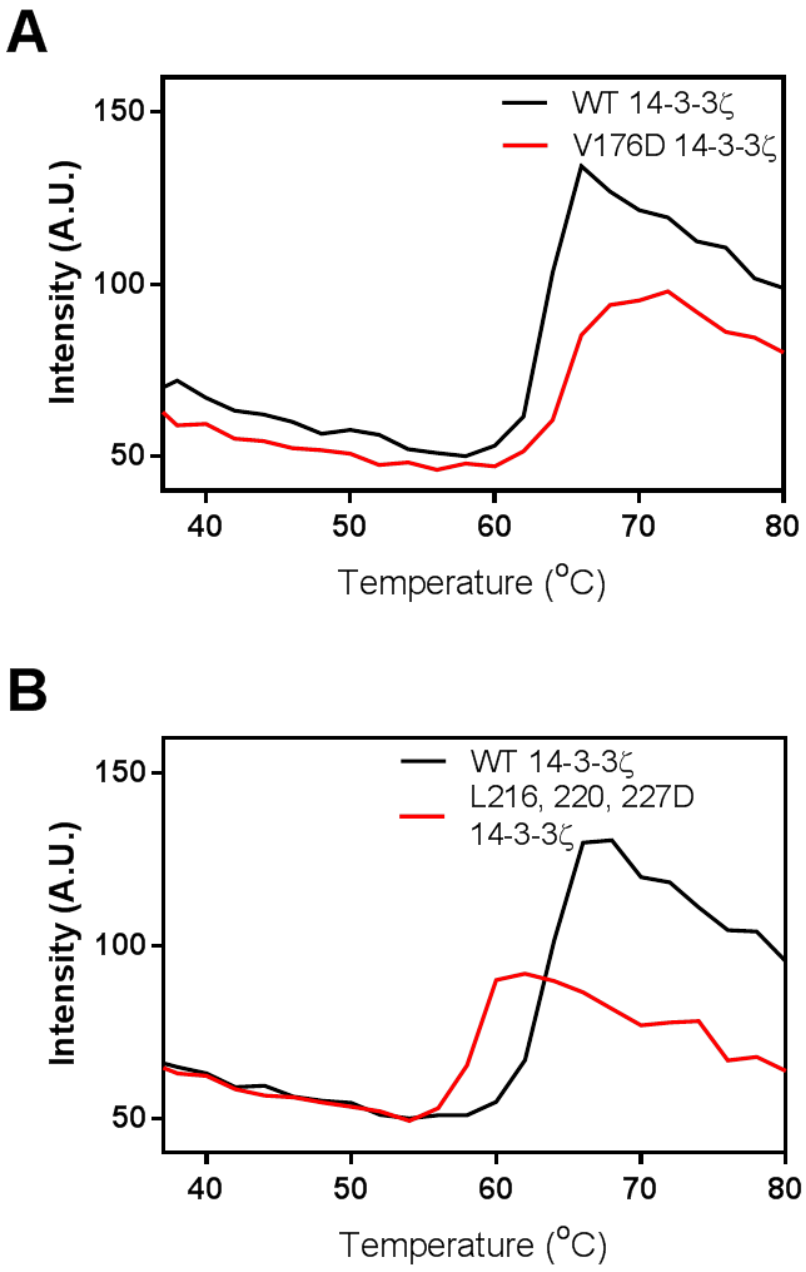

Figure 3.5: The thermostability profiles of WT 14-3-3ζ compared with (A) V176D 14-3-3ζ and (B) L216, 220, 227D 14-3-3ζ with increased temperature, obtained by monitoring the intrinsic fluorescence at 340nm between 37-80°C, in 20mM phosphate buffer at pH 7.4.

3.3 Results: The role of the hydrophobic face of the amphipathic binding groove in the chaperone activity of 14-3-3

The relative chaperone activities of WT, V176D, and L216, 220, 227D 14-3-3ζ were assessed against the amorphous aggregation of reduced insulin and chemically stressed alcohol dehydrogenase (ADH). The target proteins were selected as they are frequently used in many *in vitro* assays to assess the chaperone ability of sHsps (26), and are readily available proteins. Amorphous aggregation was assessed by monitoring the light scattering at 340nm over time. An increase in light scattering is indicative of aggregation, and a decline in light scattering in the presence of the 14-3-3ζ proteins is indicative of the latter's chaperone activity.

3.3.1 Reduction induced amorphous aggregation of insulin

The chaperone activity of WT, V176D and L216, 220, 227D 14-3-3ζ was tested against the amorphous aggregation of reduced bovine insulin. Insulin is comprised of two chains (A and B) linked by two inter-chain disulphide bonds. There is an additional intra-chain bond in chain B. Amorphous aggregation of the B chain is caused by the reduction of these disulphide bonds and separation from the A chain. The A chain does not aggregate as a result of its hydrophilic nature (26). In the absence of 14-3-3ζ, insulin aggregated as observed by an increase in light scattering after 10 mins, before reaching a plateau after 60 mins (Fig. 3.6A, B and C). The WT and the mutated 14-3-3ζ proteins suppressed the aggregation of reduced insulin in a concentration-dependent manner. At a 1:1 molar equivalence of reduced insulin and WT 14-3-3ζ the aggregation is suppressed by 37 ± 5% (Fig. 3.6D).

Similar decreases in light scattering were observed for the mutant 14-3-3ζ proteins, showing that they retain chaperone activity. Thus, the incubation of insulin in the presence of V176D 14-3-3ζ resulted in a decrease in the overall light scattering. At a 1:1 molar equivalence of reduced insulin and 14-3-3ζ, V176D 14-3-3ζ provides a 60% ± 2% protection, i.e. an increased suppression of aggregation compared to WT 14-3-3ζ. On this basis, V176D 14-3-3ζ is a more efficient chaperone against the amorphous aggregation of reduced insulin compared to WT 14-3-3ζ.

The incubation of insulin in the presence of L216, 220, 227D 14-3-3ζ also resulted in a decrease in light scattering. At a 1:1 molar equivalence of reduced insulin and L216, 220,

227D 14-3-3ζ provides a 43 ± 10% protection. Thus, there was no statistical difference between the chaperone abilities of the WT and L216, 220, 227D 14-3-3ζ proteins.

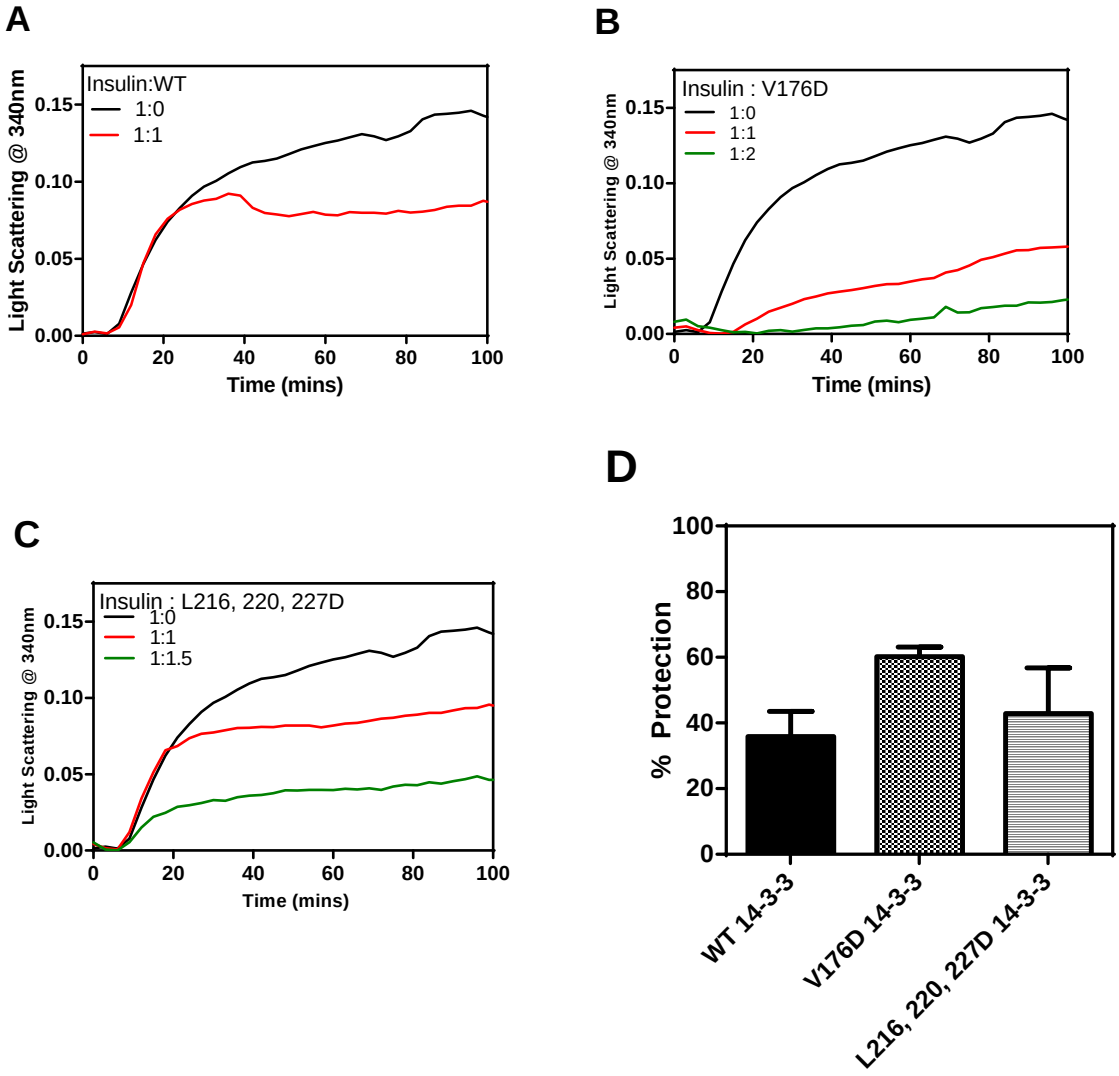

Figure 3.6: The chaperone activity of (A) WT, (B) V176D and (C) L216, 220, 227D 14-3-3ζ against the amorphous aggregation of reduced insulin in 20mM sodium phosphate buffer, pH 7.4, 150mM sodium chloride and 2mM EDTA at 37^{o}C. (D) The percentage protection provided by each 14-3-3ζ protein, at a 1:1 molar equivalence of 14-3-3ζ:ADH. Experiments were done in triplicate and the error bars represent the SEM of the light scattering data.

In summary, V176D 14-3-3ζ exhibited an increased chaperone activity compared to WT 14-3-3ζ against the amorphous aggregation of reduced insulin. However, L216, 220, 227D 14-3-3ζ and WT 14-3-3ζ had comparable chaperone ability against the amorphous aggregation of reduced insulin.

3.3.2 Chemically stressed amorphous aggregation of alcohol dehydrogenase

In a manner similar to section 3.3.1, the chaperone activity of 14-3-3ζ proteins was tested against the amorphous aggregation of ADH. ADH exists as a tetramer with each ADH monomer (35kDa) stabilised by two Zn^{2+} ions. The chelation of Zn^{2+} ions using EDTA leads to the unfolding and subsequent aggregation of ADH when exposed to elevated temperature.

In the absence of 14-3-3ζ, there was an increase in light scattering from 20 mins which resulted in a plateau after 90 mins, indicative of the amorphous aggregation of the target protein. In the presence of 14-3-3ζ, there was an overall decrease in the measured light scattering. Additionally the onset of aggregation was decreased in the presence of 14-3-3ζ. At a 1:1 molar equivalence of ADH and 14-3-3, the aggregation was suppressed 33± 5%.

Compared to WT 14-3-3ζ, a decrease in light scattering was observed with the 14-3-3ζ mutant proteins. When ADH was incubated in the presence of V176D 14-3-3ζ, there was a decrease in the light scattering, suppressing the aggregation by 46 ± 3% at a 1:1 molar equivalence of ADH and 14-3-3ζ. This is an increased suppression of aggregation compared to WT 14-3-3ζ, signifying that V176D 14-3-3ζ is a more efficient chaperone protein than WT 14-3-3ζ, under these conditions. When incubated under these conditions in the presence of L216, 220, 227D 14-3-3ζ, the aggregation is suppressed by 42.5 ± 0.5% at a 1:1 molar equivalence. Thus, L216, 220, 227D 14-3-3ζ exhibits increased suppression of ADH aggregation than the WT protein, implying it is a slightly more efficient chaperone.

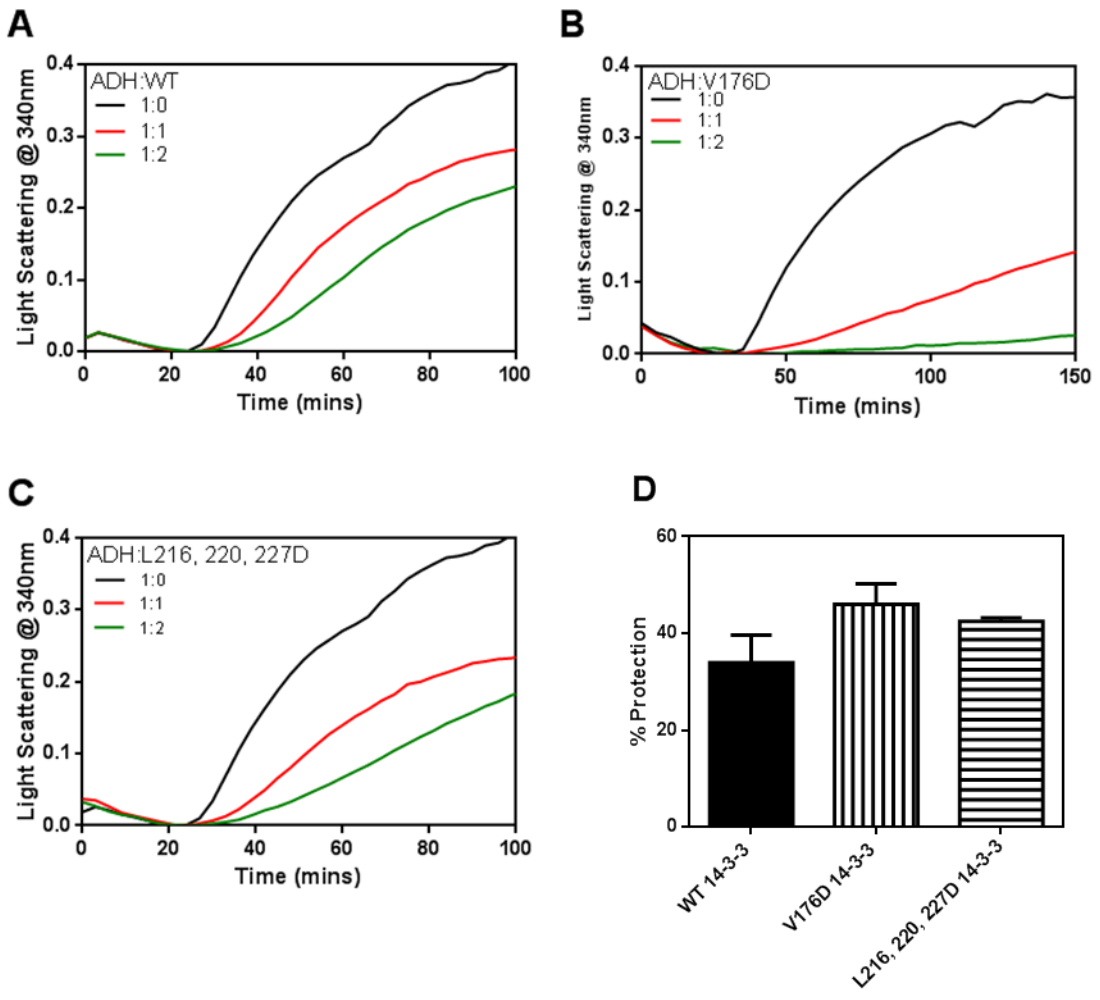

Figure 3.7: The chaperone activity of (A) WT (B) V176D and (C) L216, 220, 227D 14-3-3ζ against the amorphous aggregation of alcohol dehydrogenase at physiological pH.(D) The percent protection provided by each 14-3-3ζ protein at a 1:1 molar equivalence of 14-3-3ζ:ADH. Experiments were repeated in triplicate, and the error bars represent the SEM of the light scattering data.

In summary, both the V176D and L216, 220, 227D (to a lesser extent) 14-3-3ζ proteins show slightly increased chaperone ability against the amorphous aggregation of ADH compared to WT 14-3-3ζ protein.

3.3 Discussion

In order to investigate the role of the hydrophobic face of the amphipathic groove in the chaperone action of 14-3-3ζ, exposed hydrophobic residues (Val176, Leu216, Leu220, and Leu227) in this region were targeted. These residues have been demonstrated via site-directed mutagenesis studies to reduce the binding of 14-3-3ζ to phosphorylated target proteins (21), and were characterised for any structural changes before chaperone ability was tested.

Biophysical characterisation showed that V176D 14-3-3ζ exhibited a dimeric structure, mildly reduced α-helical content, decreased solvent exposure of Trp59, and increased thermostability compared to the WT protein, implying changes to the overall structure of 14-3-3ζ due to this mutation. This increased stability and burial of Trp59 indicates that there are potentially additional interactions occurring between the introduced negatively charged Asp and the exposed, positively charged residues in helix 3 of the amphipathic groove. Due to the proximity within the amphipathic binding groove to Asp176, the most likely interaction is with Arg56, a positively charged residue in helix 3, which has been demonstrated to be involved in binding to phosphorylated target proteins (19). This potential interaction between the Asp at position 176 and Arg56 leads to an additional salt bridge across the amphipathic binding groove, potentially tightening the cup structure (Fig. 3.8). This would account for the further burial of Trp59 in the dimer interface and the slight increased themo-stability of the protein. There is a slight reduction in the alpha helical content of the protein, suggesting that there may be some destabilisation in secondary structure in other regions as a result of the introduction of this charged residue.

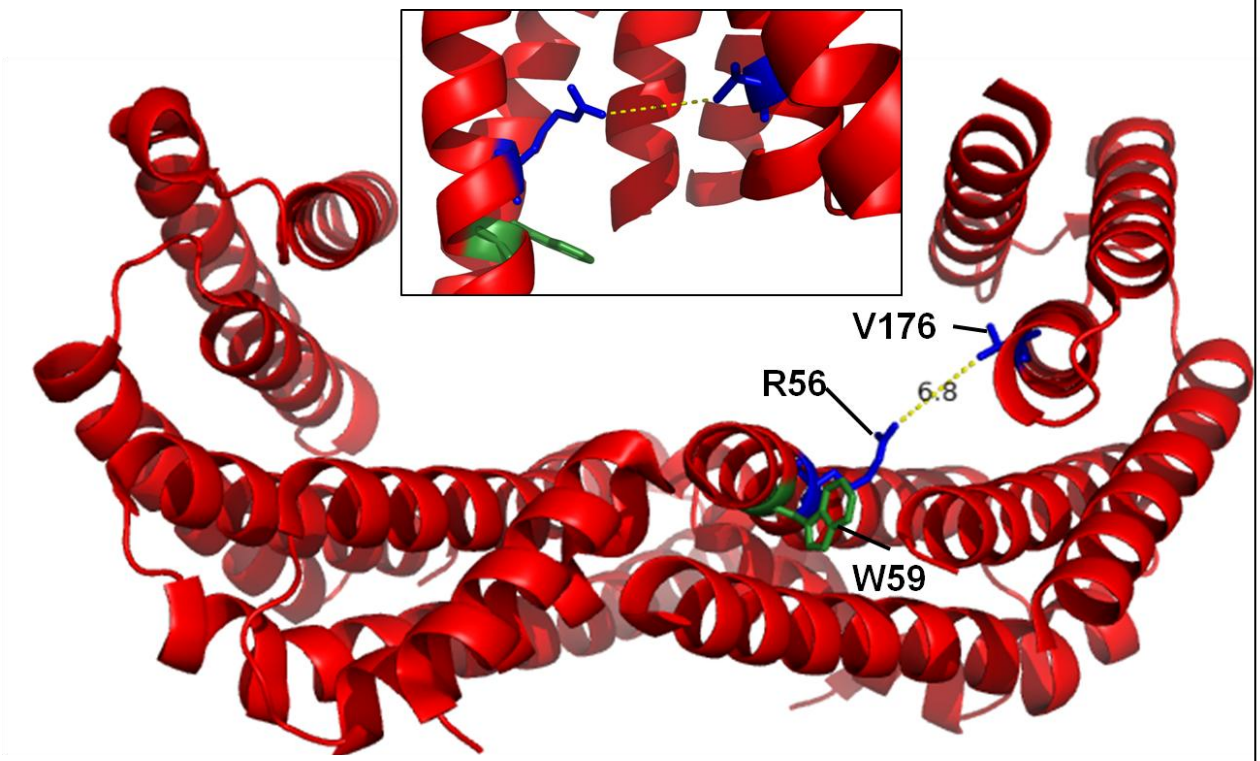

Figure 3.8: The crystal structure of 14-3-3ζ showing the close proximity between Val176 and Arg56, with a distance of 6.8Å. Upon mutation of Val176 to Asp, it is hypothesised that a salt-bridging interaction forms between Asp176 and Arg56 resulting in a conformational change which would cause the additional burial of adjacent Trp59 (green).

The residue Val176 has been previously demonstrated to be involved in the binding of phosphorylated target proteins using the V176D 14-3-3ζ protein (21). However this reduction of binding to target proteins by V176D 14-3-3ζ could potentially be explained by the hypothesised interaction between Arg56 and Asp176. This likely tightens the cup like structure of the binding groove and would reduce the ability of this region to bind target proteins.

The biophysical characterisation of L216, 220, 227D 14-3-3ζ displayed a dimeric structure, with a minor reduction in the alpha helical content and a small reduction in thermostability compared to WT 14-3-3ζ. This suggests that the introduction of the negatively charged aspartic acid residues into helix 9 results in a slightly less stable α-helical structure, making the protein more prone to aggregate with temperature as evidenced by the mutants reduced thermostability compared to WT 14-3-3ζ protein. The mutation of these sites has been undertaken previously to investigate their role in binding to phosphorylated target proteins

(21). In this study, individual specific mutation of each of the leucine residues was executed to give the singly altered mutants and there was no observed destabilisation as measured by CD. However the combination of these mutations in the triple mutated protein appears to have a detrimental effect on helix stability.

The involvement of the hydrophobic face of the amphipathic binding groove in the chaperone action of 14-3-3ζ was explored by examining the chaperone ability of V176D and L216, 220, 227D 14-3-3ζ against amorphously aggregating target proteins. Interestingly, V176D 14-3-3ζ, showed increased chaperone ability against both target proteins compared to WT 14-3-3ζ. The L216, 220, 227D 14-3-3ζ protein had chaperone ability closer to that of WT 14-3-3ζ, with slightly increased chaperone ability against the amorphous aggregation of ADH. As chaperones interact hydrophobically with target proteins, it is unlikely that this increased chaperone ability is as a direct result of the changes to the hydrophobic face of the binding groove. Potentially, the conformational changes associated with the mutations discussed above result in the exposure of other regions which are essential for the chaperone ability of 14-3-3ζ.

Previously the chaperone ability of 14-3-3ζ in the presence of the peptide R18, has been investigated (26). Crystallographic studies have shown that the peptide, R18, interacts with both the polar and hydrophobic faces of the amphipathic binding groove (76). The interaction of this peptide with 14-3-3ζ has little effect on the chaperone action of 14-3-3ζ (26). This further indicates that the hydrophobic face of the amphipathic binding groove is unlikely to be involved directly in the chaperone action of 14-3-3ζ. Therefore, any further investigations, such as x-ray crystallography, to determine any structural changes caused by these mutations were not undertaken.

The polar face of the amphipathic binding groove has also been found not to be involved in the chaperone action of 14-3-3ζ using a charge reversal mutant, K49E (26). With the studies discussed above we can state that the amphipathic binding groove is unlikely to have a functional role in the chaperone ability of 14-3-3ζ. This chaperone function of 14-3-3ζ does not involve interaction with target proteins via the amphipathic binding groove, in contrast to the majority of 14-3-3 target proteins, when interacting under constitutively expressed conditions. This hints to separate functions; 14-3-3ζ as a regulatory protein interacting with phosphorylated target proteins, and 14-3-3ζ as a molecular chaperone, interacting with and

stabilising misfolded proteins under stress conditions and using different regions of the protein structure.

Our studies and others have demonstrated that 14-3-3ζ can act as a negative regulator of aggregation by acting as a phosphorylation-independent molecular chaperone via an unknown region (14,26). In addition to this, 14-3-3ζ has been previously shown to prevent aggregation in a phosphorylation-dependent manner e.g. phosphorylated Tau protein is stabilised by the interaction with 14-3-3 via the amphipathic binding groove (45), i.e. in a manner separate from its chaperone function. In contrast, there have been many instances in which 14-3-3 proteins have been observed to enhance the aggregation of physiological proteins associated with disease, e.g. Huntingtin in Huntington's disease and phosphoataxin-1 in ataxia (4,52). This enhancement (discussed in section 1.4.2) is generally phosphorylation-dependent and occurs via the amphipathic binding groove. Even with the discovery of the molecular chaperone functionality, the roles of 14-3-3 proteins in neurodegenerative disease are complex and remain not well understood, with 14-3-3 able to act as both a positive and negative regulator of physiological protein aggregation.

Chapter 4

An investigation into the functional role of the dimer interface of 14-3-3ζ in chaperone action

4.1 Introduction

As described in chapter 3, 14-3-3ζ acts as a molecular chaperone in suppressing the aggregation of unfolding target proteins (14). The chaperone action has been characterised against several different target proteins and the site of chaperone action is under investigation. These investigations have determined that the C-terminal extension and amphipathic binding groove are not critical factors in the chaperone function of 14-3-3ζ (26). To further extend our characterisation of 14-3-3's chaperone ability, the dimer interface, a region of high relative hydrophobicity, was studied.

The dimer interface is the interaction surface between the two 14-3-3ζ monomers, and is stabilised throughout by hydrophobic and salt bridge interactions (1). Two salt bridges have been proposed at the interface from crystal structure studies (R18-E89 and D21-K85) (1), which are with the exception of 14-3-3ε, conserved across the human isoforms (77) (Fig. 4.1). Additionally the residue S58, buried in the dimer interface (Fig. 4.1), has been shown to be involved in the regulation of 14-3-3 dimerisation. Phosphorylation at this site, in the presence of the physiological lipid sphingosine, results in significant disruption of the dimeric structure (24). This phosphorylation and dissociation of the dimer does not prevent 14-3-3ζ's interaction with phosphorylated target proteins, but the dimeric form of 14-3-3 is necessary to facilitate the structural changes required for the activity of the target protein (78).

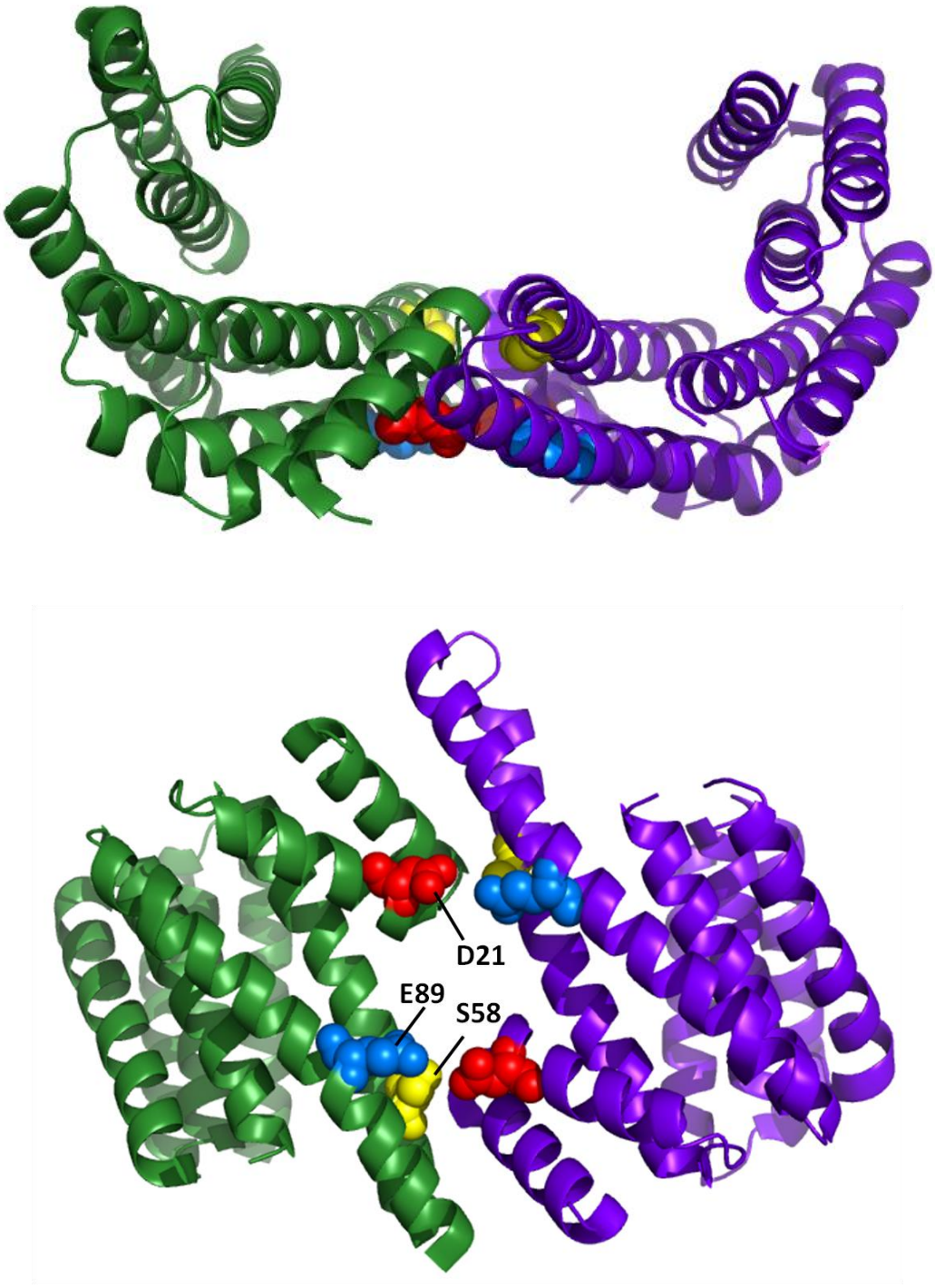

Figure 4.1: The crystal structure (side and bottom views) of 14-3-3ζ (16) showing the location of the potential salt bridging residues D21 (red) and E89 (blue) and phosphorylatable residue, S58 (yellow) in the dimer interface.

In order to investigate the function of the dimer interface in the chaperone action of 14-3-3ζ, we have targeted the hypothesised salt bridge residues (D21 and E89) within the dimer interface, to generate the charge reversal mutants, D21N and E89Q, in addition to producing a phospho-mimic protein (S58D) that causes dimer disruption (22). In order to generate maximum dimer disruption, mutant proteins were also produced exhibiting all of these mutations. The dimer stability of D21N, E89Q, S58D, D21N/E89Q/S58A and D21N/E89Q/S58D 14-3-3ζ proteins were characterised by a variety of spectroscopic and biophysical techniques, before the chaperone ability of each protein was assessed and compared to WT 14-3-3ζ.

4.2 Characterisation of dimer-disrupted 14-3-3ζ proteins

Mutations were introduced by Quickchange site directed mutagenesis. Mutations were confirmed by sequencing. The 14-3-3ζ proteins were expressed and purified successfully as per Williams et al. (26). The mutant proteins expressed at a similar level to WT protein. The proteins used in this chapter were demonstrated to be greater than 95% pure by SDS-PAGE analysis. Expression and purification of D21N/E89Q 14-3-3ζ was attempted but the protein was prone to aggregation. Hence, no further analysis was attempted with this double mutant.

4.2.1 Native PAGE analysis

In order to determine if the mutant proteins showed any major disruption to 14-3-3's quaternary structure, native-PAGE analysis was undertaken (Fig. 4.2B). As discussed previously (section 3.2.1), the acidic pI value of 14-3-3ζ allows for the easy separation and analysis of the 14-3-3ζ proteins by native PAGE. However, native-PAGE does not allow the determination of molecular weight. The D21N and E89Q 14-3-3ζ proteins exhibit a similar mobility compared to WT 14-3-3ζ (Fig. 4.2). The S58D, D21N/E89Q/S58A and D21N/E89Q/S58D 14-3-3ζ proteins had an increased mobility compared to WT 14-3-3ζ protein, more consistent with that of a monomeric form of 14-3-3ζ. These data imply disruption to the dimeric structure of 14-3-3ζ for the mutant 14-3-3ζ proteins. This agrees with previously published data whereby the phosphorylation of S58 causes significant disruption to the dimer, resulting in a high mobility species detected on native-PAGE (24).

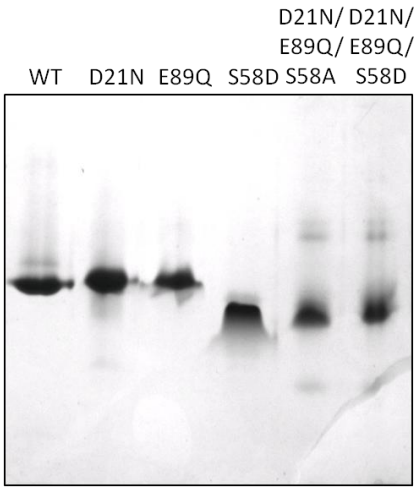

Figure 4.2: Native-PAGE analysis of the mutated 14-3-3ζ proteins visualised by Coomassie blue staining.

4.2.2 Far-UV circular dichroism

Far-UV circular dichroism spectroscopy was used to assess for any major changes of the overall secondary structure of the dimer-disrupted 14-3-3ζ proteins as a result of the mutations. As described in section 3.2.2, the far-UV circular dichroism spectrum of WT 14-3-3ζ protein was indicative of a protein with a predominant alpha-helical structure which is consistent with the crystal structure and with previous reports (21).

The far-UV circular dichroism spectra for all the mutant 14-3-3ζ proteins (Fig. 4.3) showed that they all adopt an alpha-helical structure. However, mutations to the dimer interface resulted, to a varying degree, in a reduction in the mean residue ellipticity at 208 and 222nm for each of the mutant proteins (Fig. 4.3). This reduction in alpha helical content is probably due to the interruption of the salt bridging sites, either as a result of mutation (D21N and E89Q) or the mimicking of phosphorylation (S58D).This effect is exaggerated when the two salt bridging mutations were combined with the phospho-mimic at S58 in the D21N/E89Q/S58D 14-3-3ζ triple mutant (Fig. 4.3E), resulting in a greater reduction in the alpha-helical content of the protein, compared to the other proteins.

This reduction in helical content of the 14-3-3ζ mutants implies that D21 and E89 may be important for the helical structure of 14-3-3ζ. The absence of charge on these residues, potentially removes interaction within helices and between helices of different monomers, resulting in a less-defined helix. However, the predominantly helical profile for all the 14-3-3ζ proteins is indicative that they are mainly folded and exhibit the typical 14-3-3 structure, with the minor destabilisation.

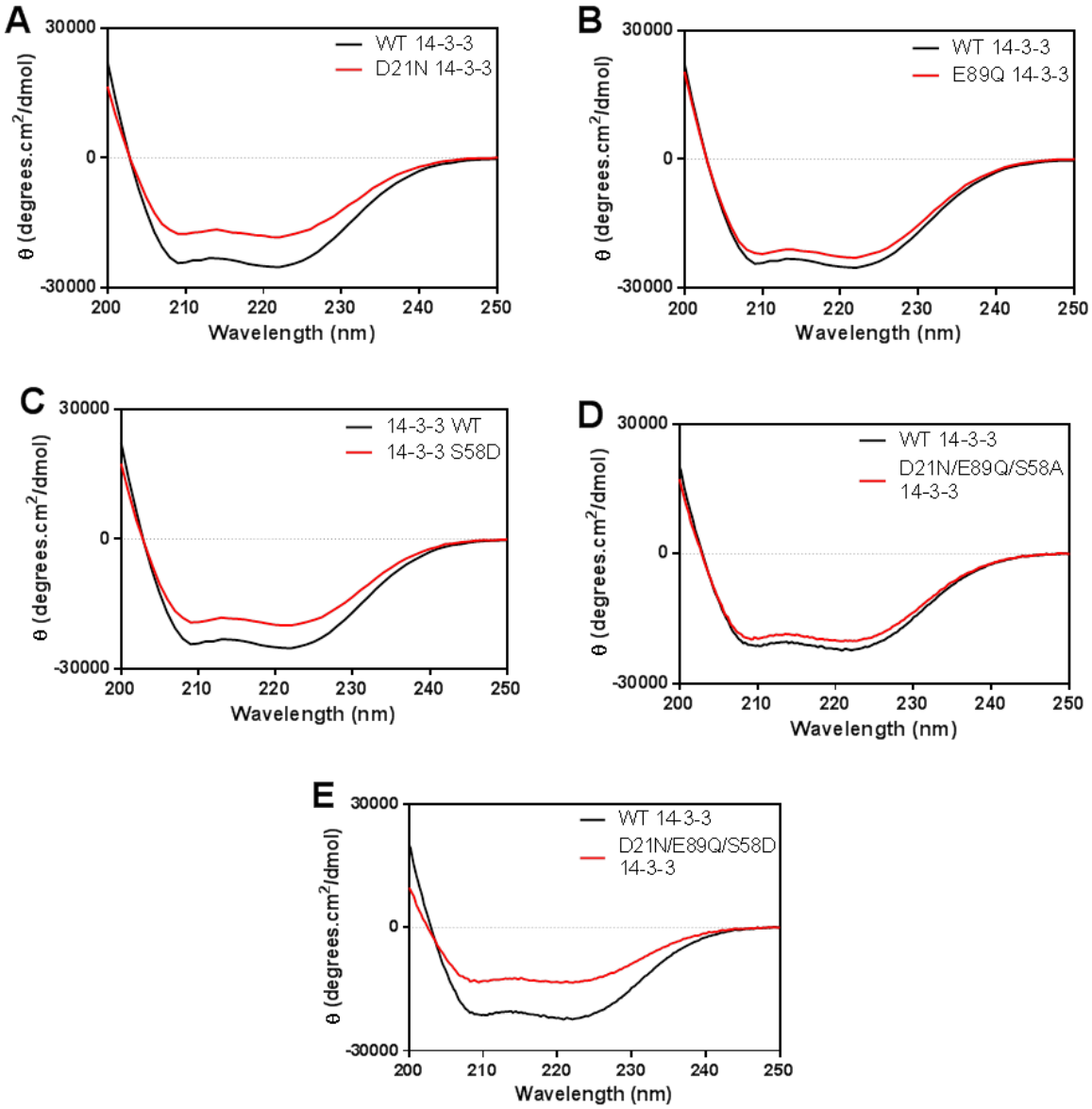

Figure 4.3: The far-UV circular dichroism spectra of WT and (A) D21N, (B) E89Q, (C) S58D, (D) D21N/E89Q/S58A and (E) D21N/E89Q/S58D 14-3-3ζ, acquired between 200 and 250 nm at 20^{o}C, in sodium phosphate buffer at pH 7.4.

4.2.3 Intrinsic tryptophan fluorescence

Environmental changes of tryptophan residues (W59, in helix 3 and W228, in helix 9) in 14-3-3ζ can be monitored by determining the intrinsic tryptophan fluorescence. As described in Appendix A.3, the fluorescence of W59 is the predominant signal in the fluorescence emission of WT 14-3-3ζ, due to quenching of W228 by nearby Y179. Any fluorescence wavelength and intensity shifts of mutant proteins compared to WT 14-3-3ζ provide insight into altered protein conformation in the vicinity of the tryptophan residues. The intrinsic tryptophan fluorescence spectra were acquired by exciting the 14-3-3ζ proteins (7.2μM, 2mL) at 295nm and acquiring the emission between 300 and 400nm (Fig. 4.4), and the maximum emission wavelength were determined (Table 4.1). Similar to section 3.2.3, WT 14-3-3ζ has a wavelength maximum of 345nm when excited at 295nm.

Table 4.1: The maximum emission wavelengths of WT and the mutated 14-3-3ζ proteins at 7.2μM, in 20mM phosphate buffer, pH7.4, and 37^{o}C

14-3-3ζ Protein	Maximum emission wavelength (nm)
WT	345
D21N	347
E89Q	348
S58D	345
D21N/E89Q/S58A	350
D21N/E89Q/S58D	350

The maximum wavelength of D21N, E89Q and S58D 14-3-3ζ do not exhibit any changes in their intrinsic fluorescence compared to WT 14-3-3ζ. E89Q and S58D 14-3-3ζ do experience an increase in fluorescence intensity (Fig. 4.4B and C) compared to WT 14-3-3ζ, suggesting a reduction in quenching indicative of conformational changes. This does not result in any additional solvent exposure to the Trp residues as we observe no significant change in the maximum wavelength, but implies minor conformational change of the proteins. A similar increase in fluorescence intensity is observed in a comparable phospho-mimicking protein S58E (74).

In comparison, the intrinsic tryptophan fluorescence profiles for D21N/E89Q/S58A (Fig. 4.4D), and D21N/E89Q/S58D 14-3-3ζ (Fig. 4.4E) exhibit minor red shifts and intensity increases in their fluorescence emission spectra compared to WT 14-3-3ζ. These red shifts imply greater solvent exposure of W59 (the primary contributor to 14-3-3ζ's fluorescence), due to disruption to the dimer interface of 14-3-3ζ as a result of these mutations.

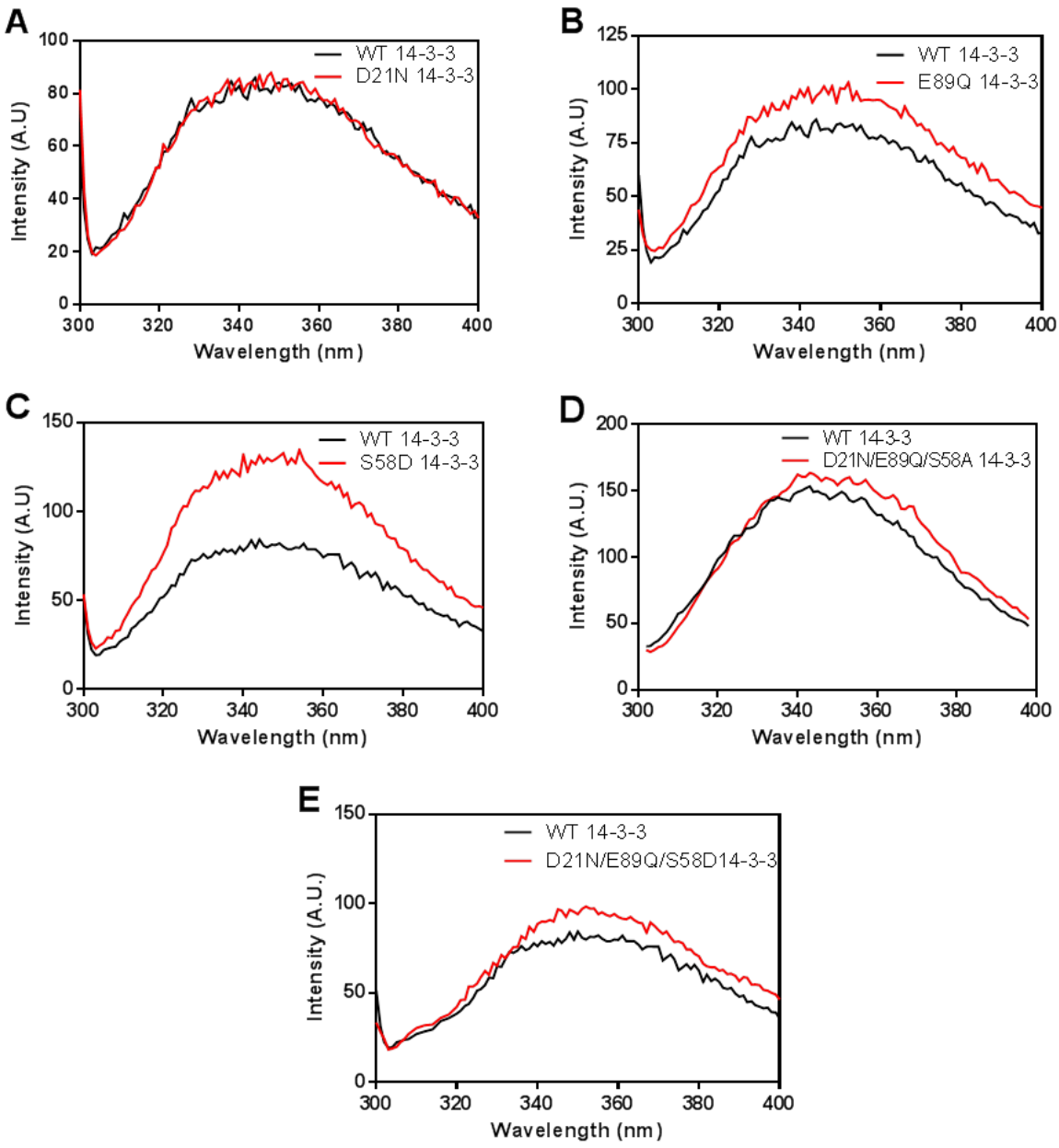

Figure 4.4: The intrinsic tryptophan fluorescence profiles of WT compared with (A) D21N, (B) E89Q, (C) S58D, (D) D21N/E89Q/S58A and (E) D21N/E89Q/S58D 14-3-3ζ, at 7.2μM in 20mM sodium phosphate buffer, pH 7,4 at 37^{o}C. The data was acquired upon excitation at 295nm with the emission collected between 300 and 400nm.

Previously, the dimer dynamics of phospho-mimic S58E 14-3-3ζ were investigated whereby S58E 14-3-3ζ was demonstrated to have a greater monomeric proportion at lower concentration (74). In order to provide greater insight into the changed dynamics of the 14-3-3ζ dimer formation as a result of the changes of the mutations, the intrinsic tryptophan fluorescence was repeated at a lower concentration (1.4μM) (Fig. 4.5). As a result of this concentration reduction, we see a shift in the intrinsic fluorescence profiles produced for the mutated 14-3-3ζ proteins, compared to those obtained at a higher concentration (Fig. 4.4).

Table 4.2: The maximum fluorescence wavelength obtained from the intrinsic fluorescence spectra of the WT and mutated 14-3-3ζ proteins.

14-3-3ζ Protein	Maximum emission wavelength (nm)
WT	345
D21N	360
E89Q	360
S58D	345
D21N/E89Q/S58A	360
D21N/E89Q/S58D	360

All the mutant proteins, with the exception of S58D 14-3-3ζ, exhibit an increase in the maximum fluorescence wavelength (a red shift), indicative of the exposure of W59, which has a close proximity to the dimer interface. In addition, all the mutated 14-3-3ζ proteins have an increased fluorescence intensity compared to WT 14-3-3ζ. The reduction in quenching caused by surrounding protein as a result of disruption of the dimer interface is probably the reason for this, as we would alter the location of peptide bonds which quench the tryptophan signal. This indicates that the 14-3-3ζ proteins have increased dissociation from the dimer at a lower concentration. This is indicative of a shift in the monomer-dimer equilibrium at a low concentration of 14-3-3ζ as a result of these mutations at a low concentration.

Interestingly, by lowering the concentration, the intrinsic fluorescence profile of S58D shows very little alteration. Similarly to the intrinsic fluorescence profile at 7.2μM, there is an increase in fluorescence intensity compared to WT 14-3-3ζ. As S58 is adjacent to W59, the introduced negatively charged Asp residue may shield W59 from solvent exposure. The accumulation of these mutations in D21N/E89Q/S58D 14-3-3ζ may lead to additional destabilisation of the dimer interface which leads to additional exposure of W59, accounting for the wavelength shift observed for this protein.

In summary, the intrinsic fluorescence studies of the mutated 14-3-3ζ proteins indicate that the introduced mutations in the dimer interface result in varying degrees of dimer disruption in the vicinity of W59. A reduction in concentration leads to further disruption at the dimer interface likely due to the dependence of dimer formation on protein concentration as seen previously (74).

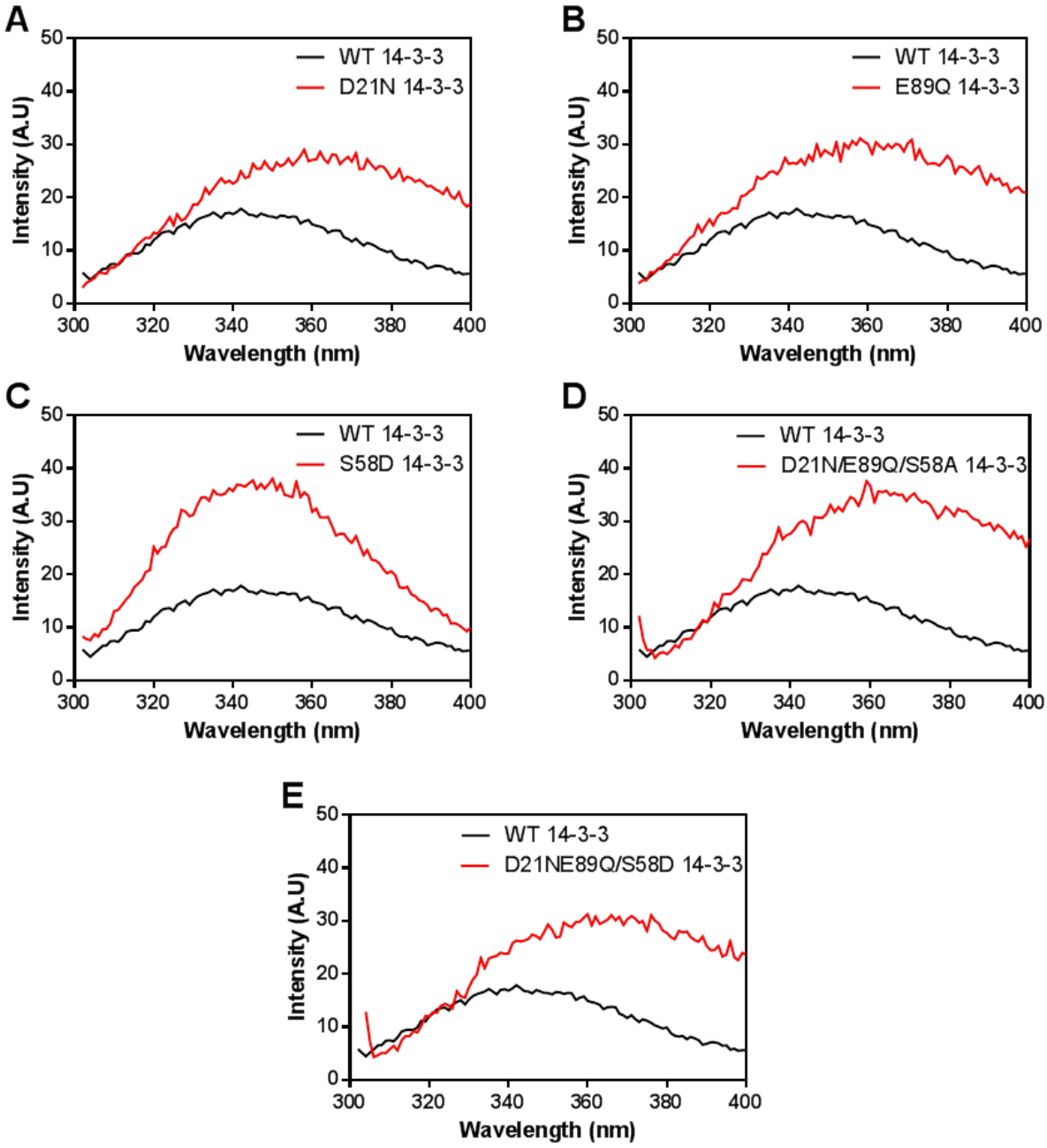

Figure 4.5: The intrinsic tryptophan fluorescence spectra of WT compared with (A) D21N, (B) E89Q, (C) S58D, D) D21NE89QS58A and (E) D21NE89QS58D 14-3-3ζ, at 1.4μM in 20mM sodium phosphate buffer, pH7.4, at 37^{o}C. The data was acquired upon excitation at 295nm with the emission collected between 300 and 400nm.

4.2.4 Thermostability monitored via intrinsic tryptophan fluorescence

The thermostability of each 14-3-3ζ protein was assessed by monitoring the intrinsic tryptophan fluorescence at 345nm over the temperature range of 37-80^{o}C. Unfolding of the protein results in an increase in fluorescence intensity (Fig. 4.6), due to the reduction in the quenching environment surrounding the buried Trp residues. From this, the melting temperature, being the temperature at which a protein is 50% unfolded, of the 14-3-3ζ proteins can be determined (Table 4.3).

Table 4.3: The calculated melting temperatures (^{o}C) of the 14-3-3ζ proteins

14-3-3ζ protein	Melting Temperature (^{o}C)
WT	63
D21N	55
E89Q	56
S58D	58
D21N/E89Q/S58A	56
D21N/E89Q/S58D	57

All of the 14-3-3ζ mutants show a significant decrease in melting temperature compared to WT 14-3-3ζ implying that mutations have a destabilising effect on the protein. The effect of D21N and E89Q mutations show that these residues have an important role in stabilising the dimer interface and the surrounding helical structures. The introduction of the charged residue aspartic acid, into the centre of the dimer interface in the form of phospho-mimic S58D, results in some disruption and destabilisation of this region of the protein. The triple mutants (D21N/E89Q/S58A and D21N/E89Q/S58D) are less stable than WT 14-3-3ζ, but their melting temperature is similar to that of the 14-3-3ζ single mutants, implying that the accumulation of these mutations does not lead to additional thermal instability.

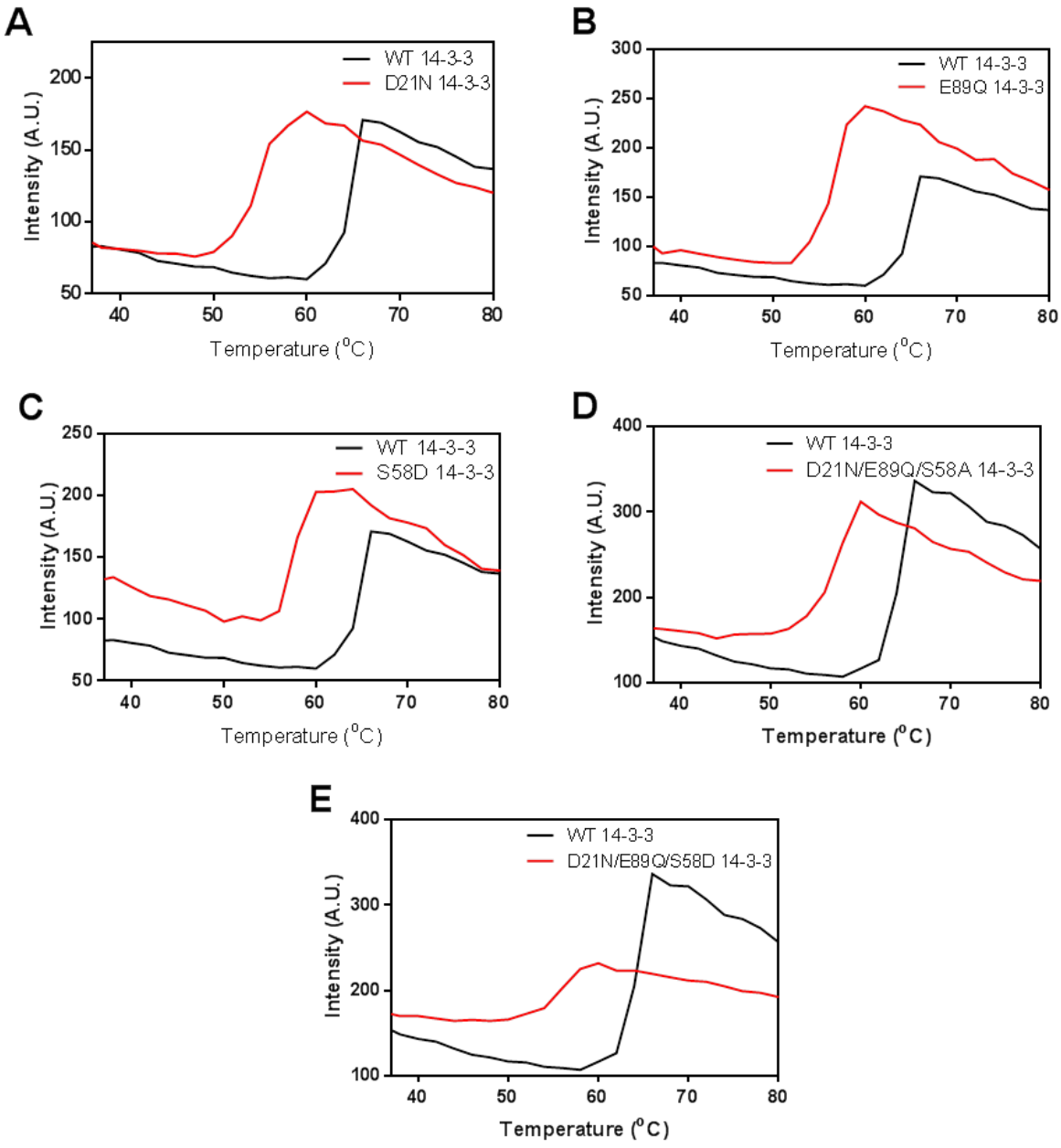

Figure 4.6: The thermostability profiles of WT compared with (A) D21N, (B) E89Q, (C) S58D, (D) D21N/E89Q/S58A and (E) D21N/E89Q/S58A 14-3-3ζ, obtained by monitoring the intrinsic tryptophan fluorescence at the maximum wavelength for each protein between 37-80°C at 7.2μM in 20mM sodium phosphate buffer, pH7.4.

4.2.5 Bis-ANS binding

The disruption of intermolecular interfaces across the dimer interface of 14-3-3ζ leads to the exposure of normally buried hydrophobic surfaces. In order to characterise any changes in hydrophobicity in the 14-3-3ζ mutant proteins, the fluorescent probe, bis-ANS, was utilised. Bis-ANS is a fluorescent molecule which experiences a significant increase in fluorescence intensity when interacting with exposed hydrophobic surfaces (Appendix A.3). In order to obtain bis-ANS fluorescence profiles, bis-ANS is excited at 385nm and the fluorescence emission is acquired between 400 and 600nm. Additional data can be collected via FRET excitation of tryptophan residues at 295nm. In order for FRET excitation to occur, bis-ANS must be interacting with hydrophobic pockets within 20nm of a Trp residue in the 14-3-3ζ structure (79).

The mutated 14-3-3ζ proteins (1.4μM, 2mL) were titrated with bis-ANS (1:0-10, molar ratio of 14-3-3ζ: bis-ANS). The data shown here are from the direct excitation of bis-ANS at 385nm which were comparable to those obtained from FRET excitation (@ 295nm) of tryptophan. The 14-3-3ζ proteins alone when excited at these wavelengths showed no emission between 400 and 600nm (data not shown). All data shown have been corrected for the fluorescence of bis-ANS alone.

The titration of bis-ANS with WT 14-3-3ζ showed a significant increase in fluorescence intensity at 495nm compared to bis-ANS alone (data not shown), implying that bis-ANS interacted with exposed hydrophobic site(s) on the protein. The 14-3-3ζ mutant proteins however showed significantly larger increases in bis-ANS fluorescence intensity compared to WT 14-3-3ζ (Fig. 4.7). With the exception of D21N/E89Q/S58A 14-3-3ζ, all exhibited a similar increase in fluorescence intensity with the binding of bis-ANS, being at least double the fluorescence intensity of WT 14-3-3ζ. D21N/E89Q/S58A 14-3-3ζ exhibited significantly higher fluorescence intensity than all of the other proteins.

These increases in fluorescence intensity are indicative of increased availability of exposed hydrophobic sites for bis-ANS in the mutant proteins. In agreement with section 4.2.3, these data imply that the dimer interface has been disrupted resulting in the exposure of hydrophobic sites that are usually buried in the dimer interface. These data complement previously published accounts for the similar phospho-mimic, S58E 14-3-3ζ, which had increased exposed hydrophobicity compared to WT 14-3-3ζ as monitored by bis-ANS fluorescence (74).

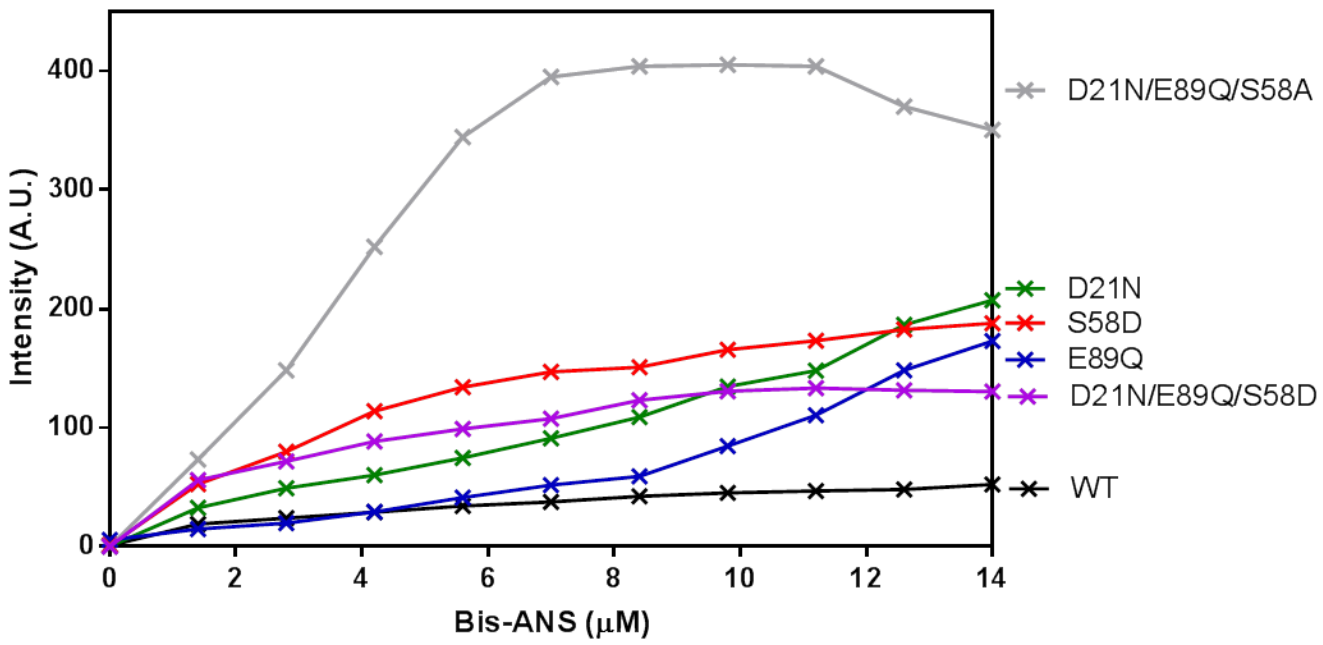

Figure 4.7: The titration of bis-ANS with WT (black), D21N (green), E89Q (blue), S58D (red), D21N/E89Q/S58A (orange) and D21N/E89Q/S58D (purple) 14-3-3ζ proteins (1.4μM). The data were obtained by exciting bis-ANS at 385nm and collecting the emission at 495nm. The data were corrected for the fluorescence of bis-ANS alone.

Native-PAGE analysis (section 4.2.1) indicates a greater mobility of the S58D 14-3-3ζ mutant compared to D21N and E89Q 14-3-3ζ (Fig. 4.2), implying greater dimer disruption compared to the other mutant proteins. Therefore, it would be expected that S58D 14-3-3ζ would provide a greater number of hydrophobic sites for the interaction with bis-ANS compared to D21N and E89Q 14-3-3ζ. However, in both S58D and D21N/E89Q/S58D 14-3-3ζ, there is a similar level of bis-ANS fluorescence regardless of this disruption indicated in the native-PAGE analysis. This could potentially be as a result of the introduction of the negatively charged aspartic acid into the hydrophobic dimer interface, which potentially would affect the interaction of bis-ANS with the surrounding hydrophobic regions, resulting in lower fluorescence intensity.

The D21N/E89Q/S58A 14-3-3ζ mutant has a similar level of disruption by native PAGE analysis as the phosphorylation mimic proteins (S58D and D21N/E89Q/S58D), but is lacking the negatively charged Asp residue, which is replaced instead with the hydrophobic residue, alanine. The interaction of bis-ANS with this mutant is significantly greater than that of all

the other 14-3-3ζ proteins (Fig. 4.7), confirming the increased availability of hydrophobic regions. Therefore, even though these data imply that the phosphorylation-mimicking proteins expose a similar level of hydrophobicity compared to D21N and E89Q 14-3-3ζ, there may a greater level of dimer disruption that cannot be quantified by this method.

4.2.6 Phosphorylation Assays

Phosphorylation of buried residue, S58, results in significant disruption of the 14-3-3ζ dimer (24). This disruption generally prevents the ability of 14-3-3 to act as an effective cellular signalling protein, leading to cell death (80). As S58 is buried in the dimer interface, it is necessary to cause minor disruption to the dimer interface in order to allow access of kinases, such as protein kinase A, to the buried site. Physiological lipids e.g. sphingosine are responsible for this disruption (81).

The characterisation of any existing destabilisation within the dimer interface can be undertaken by assessing the level of Ser58 phosphorylation in the presence and absence of a sphingosine analog. *In vitro* phosphorylation assays using protein kinase A and [γ-^{32}P] ATP, were undertaken in the presence or absence of cetrimonium bromide (also known as CTAB), a sphingosine analogue (Fig. 4.8A), before analysis by SDS-PAGE and Coomassie staining, to confirm equal protein loading, and autoradiography was undertaken.

All the 14-3-3ζ proteins showed high levels of phosphorylation in the presence of CTAB (Fig. 4.8B), with the exception of S58D. As S58 has been mutated to an Asp residue, there is no longer a residue available to be phosphorylated. This lack of phosphorylation also confirms that the phosphorylation of these proteins occurs at S58 and not at another site within the 14-3-3ζ protein. As they have a mutated S58 residue, the D21N/E89Q/S58A and D21N/E89Q/S58D 14-3-3ζ show no phosphorylation in the presence and absence of CTAB (data not shown).

In the absence of CTAB, there is negligible phosphorylation of WT 14-3-3ζ. In contrast, D21N and E89Q 14-3-3ζ show significant phosphorylation of S58 in the absence of CTAB, indicating that Ser58 is accessible to PKA in these mutants independent of sphingosine analogues. This is consistent with the existence of destabilisation of the dimer interface as a result of the mutation, and is consistent with the conclusions in sections 4.2.3 and 4.2.5.

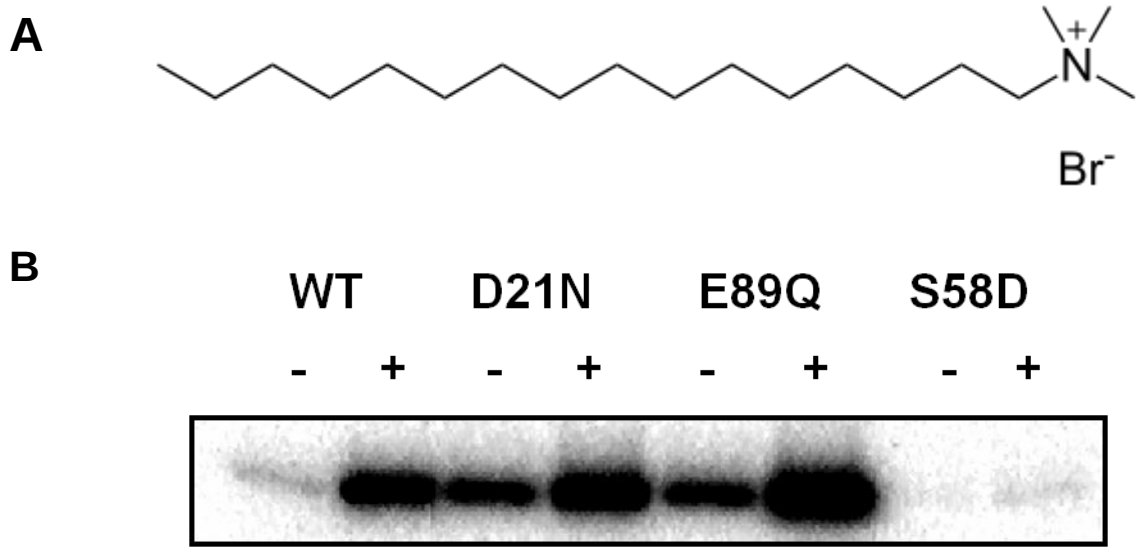

Figure 4.8: (A) The chemical structure of CTAB (B) The phosphorylation of WT, D21N, E89Q and S58D 14-3-3ζ proteins by protein kinase A in the presence and absence of CTAB, and visualised by autoradiography.

In summary, the mutant proteins exhibited a reduced alpha helical content, reduced thermostability, increased exposed hydrophobicity, increased solvent exposure of tryptophan residues at a low concentration and demonstrated dimer disruption by phosphorylation (for D21N and E89Q). Additionally S58D, D21N/E89QS58A and D21N/E89Q/S58D 14-3-3ζ showed increased mobility by native-PAGE. These results indicate that the mutant proteins exhibit dimer disruption to varying degrees, making them good model proteins for investigating the role of the dimer interface in the molecular chaperone action of 14-3-3ζ.

4.3 The role of the dimer interface in the chaperone action of 14-3-3ζ

4.3.1 Chaperone action of dimer disrupted 14-3-3ζ proteins against the amorphous aggregation of alcohol dehydrogenase monitored by light scattering

The chaperone ability of the disrupted dimer 14-3-3ζ proteins was tested against the amorphous aggregation of alcohol dehydrogenase (ADH). As described previously (section 3.3.2), the amorphous aggregation of ADH is initiated by the chelation of intrinsic Zn^{2+} ions by EDTA, leading to unfolding and eventual aggregation of the protein with elevated temperature (42^{o}C) (26). In the absence of 14-3-3ζ, there is an increase in light scattering after 20 mins before reaching a plateau after 80mins. The 14-3-3ζ proteins showed no increase in light scattering over time when incubated alone, indicating that they do not aggregate under these conditions. The increase in light scattering as a result of the aggregation observed is due to aggregating ADH. In the presence of all the 14-3-3ζ proteins there was a decrease in the overall light scattering to varying degrees (Fig. 4.9 and 4.10). This suppression of aggregation was quantified as percent protection as detailed in Section 2.4.4 (Table 4.4).

Table 4.4: The percent protection afforded by the 14-3-3ζ proteins against the amorphous aggregation of ADH at a 1:1 and a 1:2 molar equivalence of ADH: 14-3-3ζ

Protein	Percent Protection (1:1)	Percent Protection (1:2)
WT 14-3-3	30.6 ± 4%	38.6 ± 3.5%
D21N 14-3-3	61.4 ± 1%	89.0 ± 1.0%
E89Q 14-3-3	35.7 ± 1.5%	43.3 ± 5.0%
S58D 14-3-3	20.7 ± 0.5%	54.6 ± 5.5%
D21N/E89Q/S58A 14-3-3	63.7 ± 7.0%	81.1 ± 7.0%
D21N/E89Q/S58D 14-3-3	57.3 ± 4.0%	70.8 ± 7.0%

.

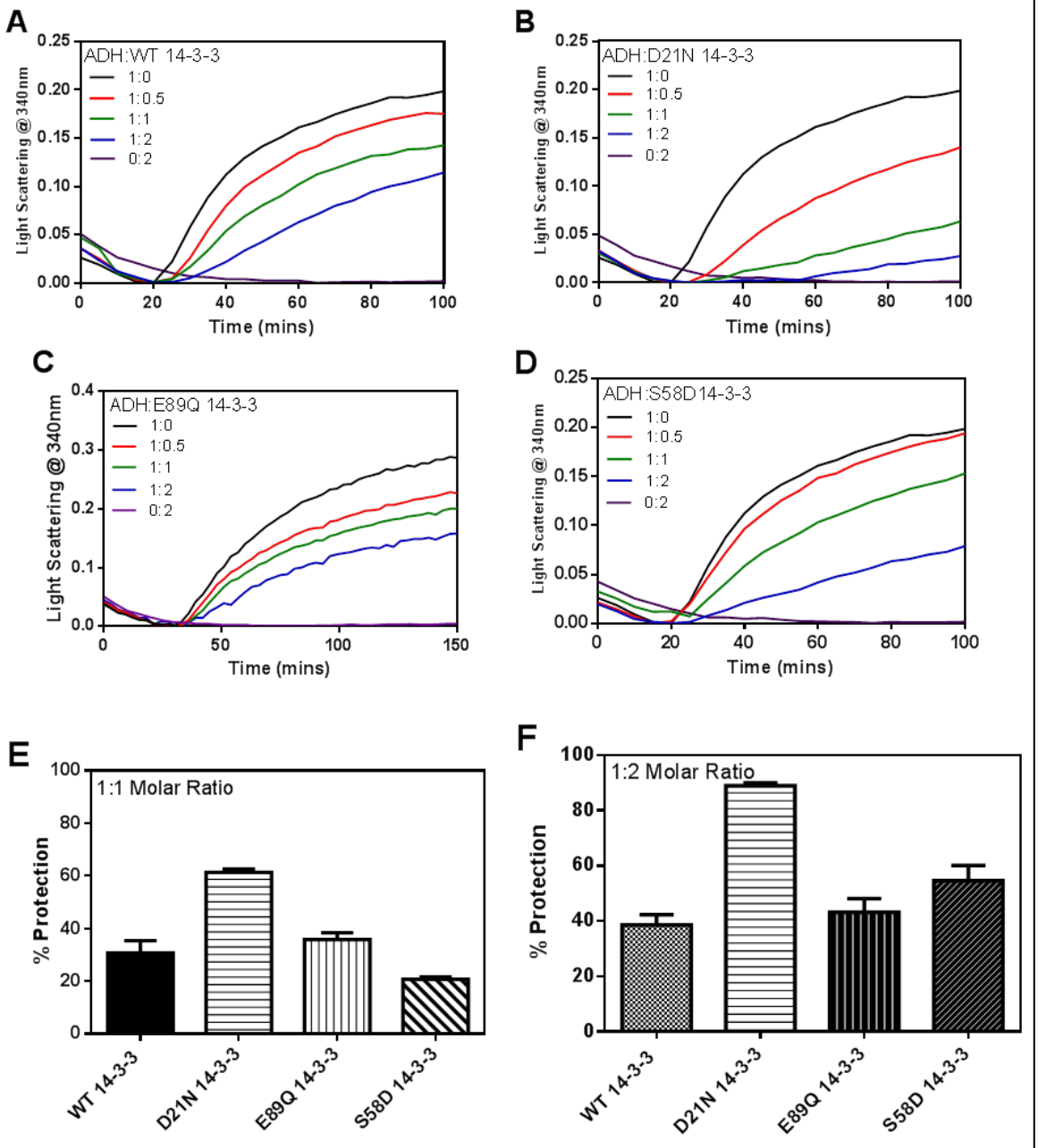

Figure 4.9: The chaperone action of (A) WT, (B) D21N, (C) E89Q and (D) S58D 14-3-3ζ against the amorphous aggregation of ADH at 42^{o}C, and pH 7.4. The percent protection afforded against the amorphous aggregation of ADH at a 1:1 (E) and 1:2 (F) molar equivalence of ADH: 14-3-3ζ, after 100mins. Errors shown represent the SEM of triplicate measurements of the change in light scattering.

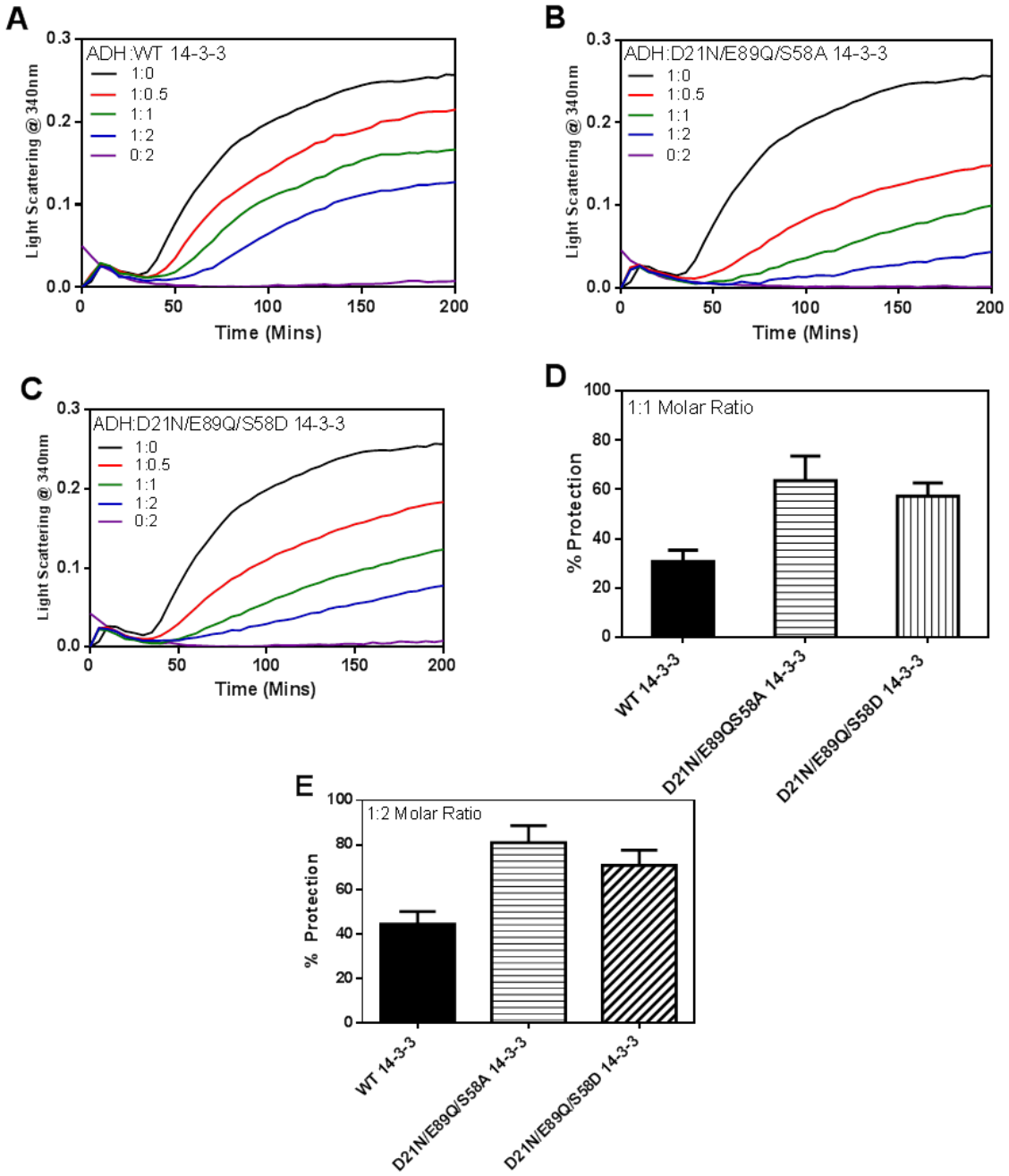

Figure 4.10: The chaperone action of (A) WT, (B) D21N/E89Q/S58A and (C) D21N/E89Q/S58D 14-3-3ζ against the amorphous aggregation of ADH at 42°C. The percent protection afforded against the amorphous aggregation of ADH at a 1:1 (D) and 1:2 (E) molar equivalence after 150mins. Errors shown represent the SEM of triplicate measurements of the change in light scattering.

In summary, exposure of the dimer interface in the D21N, D21N/E89Q/S58A and D21N/E89Q/S58D 14-3-3ζ proteins leads to an enhancement of chaperone activity compared to WT 14-3-3ζ at a 1:1 and a 1:2 molar equivalence. E89Q and S58D 14-3-3ζ has a comparable chaperone action as WT 14-3-3ζ, regardless of the disruption to the dimer interface. This is indicative that the dimer interface has a functional role in the chaperone action of 14-3-3ζ.

4.3.2 Chaperone action of dimer-disrupted proteins against the amorphous aggregation of reduced insulin as monitored by light scattering at 340nm

In section 4.3.1, it was shown that with the exposure of the dimer interface, the chaperone ability of 14-3-3ζ is enhanced. In order to further explore this, the chaperone action of these proteins was tested against the amorphous aggregation of reduced insulin. As described in section 3.3.1, the amorphous aggregation of insulin is initiated by the reduction of disulphide bonds by the incubation with dithiothreitol (26). In the absence of 14-3-3ζ, there is an increase in light scattering after 5 mins, which reached a maximum after 30mins. This is comparable to the aggregation measured in section 3.3.1. The overall light scattering was reduced in the presence of the chaperone proteins, which varied for each mutant protein (Fig. 4.11). The suppression of aggregation was quantified as percent protection as detailed in section 2.4.4 (Table 4.5).

Table 4.5: The percent protection afforded by the 14-3-3ζ proteins against the amorphous aggregation of reduced insulin at a 1:1 and 1:2 molar ratio.

Protein	Percent Protection (1:1)	Percent Protection (1:2)
WT 14-3-3	42.3 ± 2.0%	56.9 ± 0.5%
E89Q 14-3-3	26.1 ± 1.5%	42.9 ± 1.5%
D21N/E89Q/S58A 14-3-3	17.4 ± 1.0%	59.5 ± 3%
D21N/E89Q/S58D 14-3-3	26.0 ± 1.5%	1.7 ± 1.5%

In summary, the dimer disrupted 14-3-3ζ proteins exhibit a decreased chaperone ability compared to WT 14-3-3ζ at a 1:1 molar ratio. At a 1:2 molar ratio, they have a comparable chaperone ability compared to WT 14-3-3ζ with the exception of D21N/E89Q/S58D 14-3-3ζ which was unable to suppress the aggregation of reduced insulin at this molar ratio.

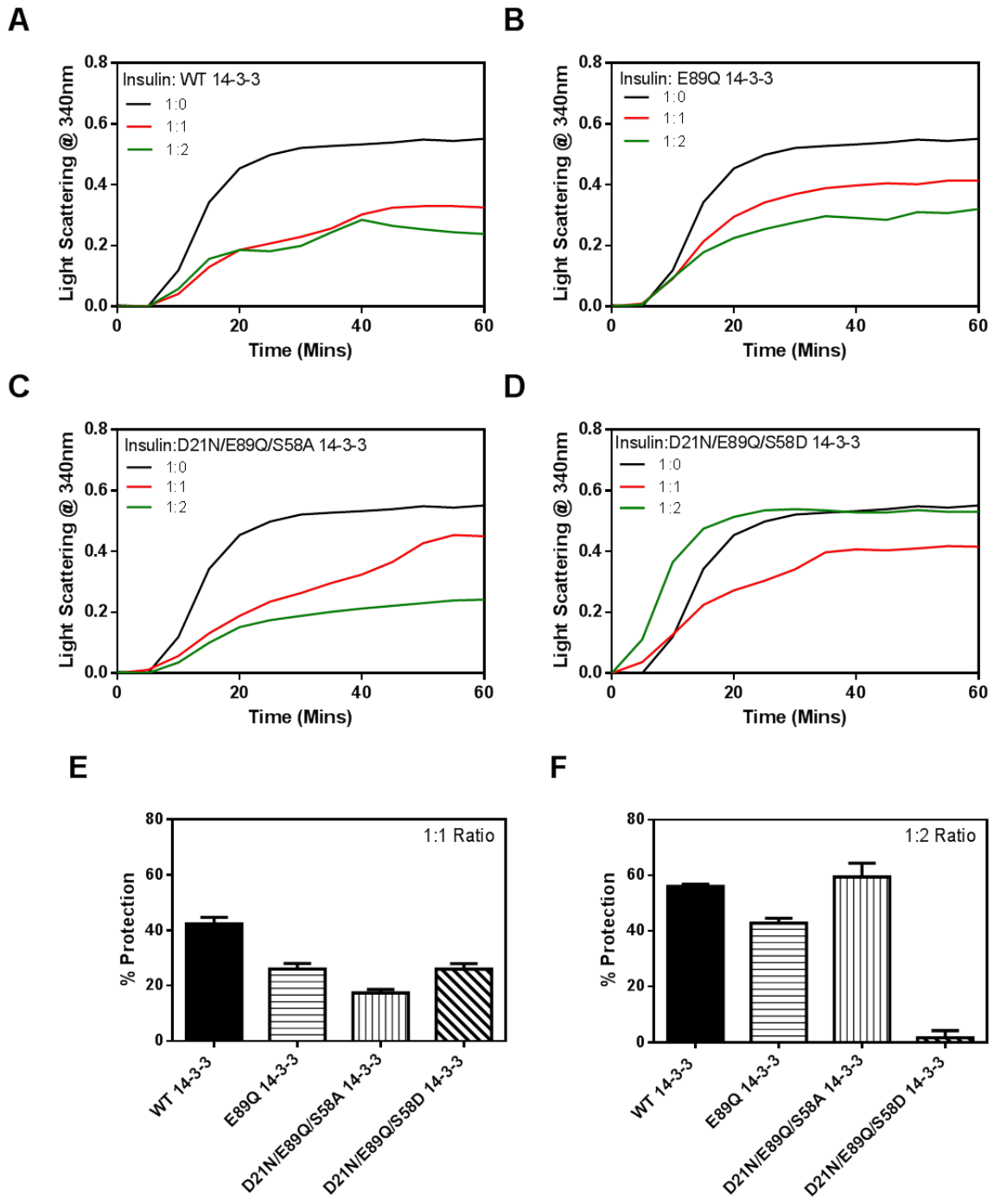

Figure 4.11: The chaperone action of (A) WT, (B) E89Q, (C) D21N/E89Q/S58A and (D) D21N/E89Q/S58D 14-3-3ζ against the amorphous aggregation of reduced insulin. The percent protection afforded against the amorphous aggregation of insulin at a 1:1 (E) and 1:2 (F) molar equivalence after 80mins. Errors shown represent the SEM of triplicate measurements of the change in light scattering.

4.3.3 Chaperone action of dimer disrupted 14-3-3ζ proteins against amorphous aggregation of reduced insulin monitored by fluorescence

In section 4.3.1, it was shown that with the exposure of the dimer interface, the chaperone ability of 14-3-3ζ is enhanced. In order to further explore this result the intrinsic tryptophan fluorescence of 14-3-3ζ was monitored in the presence of the amorphous aggregation of reduced insulin over time. Bovine insulin has no tryptophan residues and therefore will not contribute to the tryptophan emission of a mixture of insulin and 14-3-3ζ. 14-3-3ζ interacts with reduced insulin (section 3.3.2).Two 14-3-3ζ proteins were used for this analysis: WT 14-3-3ζ and the dimer-disrupted D21N/E89Q/S58A 14-3-3ζ, due to its red shifted intrinsic tryptophan fluorescence spectra compared to WT 14-3-3ζ. Due to the presence of W59 in the dimer interface, any changes to the intrinsic tryptophan fluorescence of 14-3-3ζ will provide insight into the interaction of 14-3-3ζ with aggregating insulin B chain.

The intrinsic tryptophan fluorescence of reduced insulin alone has negligible emission, which exhibited little change after the addition of DTT (Fig. 4.12E). In the presence of 14-3-3ζ proteins, we observe the typical emission profile consistent with those obtained previously (sections 3.2.3 and 4.2.3) with WT 14-3-3ζ showing a maximum emission wavelength of 345nm. With the addition of DTT, a 21% quenching of the fluorescence intensity was observed over approximately 10mins, but no major changes in the maximum wavelength occurred (Fig. 4.12A). D21N/E89Q/S58A 14-3-3ζ has a maximum wavelength of 350nm. With the addition of DTT, we again see a quenching of the fluorescence signal corresponding to approximately a 19% reduction in intensity over the first 10 minutes of incubation. There was little change in the maximum wavelength (Fig. 4.12B).

Both 14-3-3ζ proteins in the absence of insulin also experience a quenching of the fluorescence signal when incubated with DTT, corresponding to approximately a 12% and 14% reduction in fluorescence intensity for WT and D21N/E89Q/S58A 14-3-3ζ proteins respectively (Fig. 4.12C and D). Therefore some of this fluorescence quenching is likely due to the incubation with DTT. However the amount of quenching is greater when the 14-3-3ζ proteins are incubated with insulin. This implies that there may be minor conformational changes of the 14-3-3ζ structure upon the interaction with the aggregating insulin B chain.

The absence of a major wavelength shift whilst chaperoning reveals no major environmental changes of the tryptophan residues (W59 and W228) in 14-3-3ζ during chaperone action with reduced insulin. Even though we see little change, this does not prove that the dimer interface

is not involved in the chaperone action of 14-3-3ζ. It implies that if this region is critical for chaperone action, the interaction between 14-3-3ζ and the insulin B chain is a transient one, which does not permanently affect the environment of W59.

Similar experiments have been undertaken with the molecular chaperone α-crystallin, part of the sHsps family, interacting with the target protein, reduced insulin. Similarly to the results discussed here, a quenching of the tryptophan fluorescence was observed upon the addition of DTT, with a minimal red shift in the fluorescence emission spectra. This quenching was greater when incubated with the aggregating B chain of insulin (82).

In summary, there is a quenching of the tryptophan signal of 14-3-3ζ when interacting with reduced insulin. This is likely due to the interaction of 14-3-3ζ with reduced insulin, increasing the quantity of fluorescence quenching residues surrounding W59. No major environmental changes of W59 occurred whilst interacting with reduced insulin.

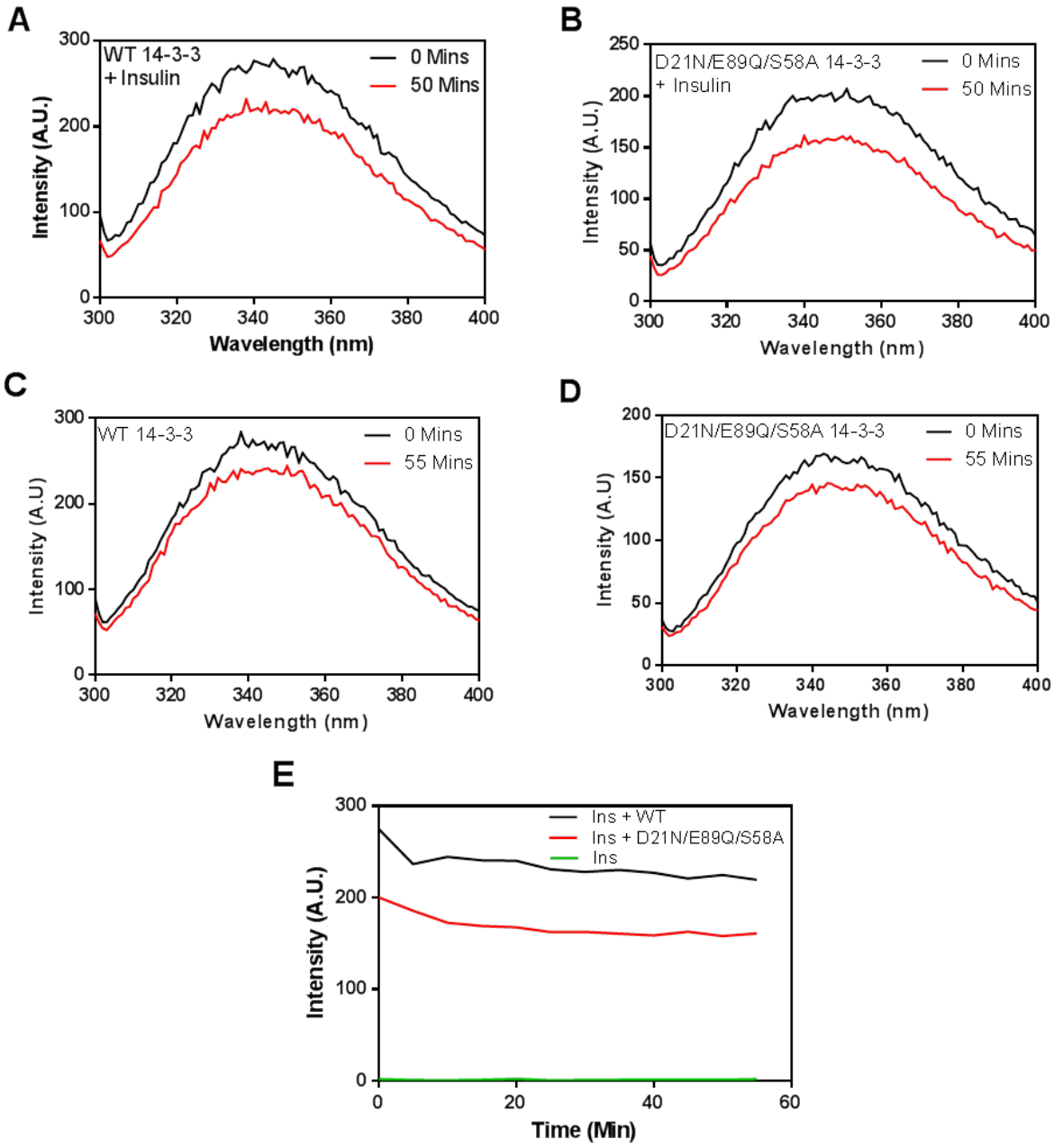

Figure 4.12: Monitoring the intrinsic fluorescence of the (A) WT and (B) D21N/E89Q/S58A 14-3-3ζ whilst interacting with the amorphously aggregating reduced insulin (2mg/mL) at 0 (black) and 50mins (red) at a 1:2 molar ratio of reduced insulin:14-3-3ζ. (E) The change in fluorescence intensity with time, of reduced insulin and WT 14-3-3 (black), reduced insulin and D21N/E89Q/S58A 14-3-3ζ (red) and reduced insulin alone (green) at 345nm and 350nm for each protein respectively. DTT was added at time = 0 mins.

4.4 Discussion

In order to investigate the role of the dimer interface in chaperone action, interactions within this region were investigated. Any conformational changes as a result of these mutations was analysed using various spectroscopic and biophysical techniques. X-ray crystal structures of these mutated 14-3-3ζ proteins could not be obtained due to their dynamic nature.

It has been previously described that the phosphorylation of buried residue, S58, compromises the integrity of the dimer (24,73,83). A known mimic of the phosphorylated protein is S58D 14-3-3ζ. We have characterised this 14-3-3ζ mutant by various biophysical techniques and have shown that it is has a higher proportion of monomeric species by native PAGE, reduced alpha-helical content, increased fluorescence intensity, decreased thermostability and increased exposed hydrophobicity. This introduction of a negative charge into the predominantly hydrophobic region results in the disruption of dimeric structure, leading to an overall less stable structure. These results are comparable with previous reports for this phospho-mimic (24). An alternative phospho-mimic protein, S58E 14-3-3ζ, has been previously characterised in a similar manner (74), and exhibits dimer disruption comparable with that observed for S58D 14-3-3ζ.

D21 and E89 are hypothesised salt bridging sites which were predicted from 14-3-3ζ crystal structure (1,5). These residues are conserved in all human isoforms except 14-3-3ε, which lacks E89 (1). In order to determine if these sites are involved in dimer formation, biophysical characterisation of mutants (D21N and E89Q) was undertaken. D21N and E89Q 14-3-3ζ exhibit a reduced alpha-helical content, reduced thermostability, increased exposed hydrophobicity and demonstrated dimer disruption as assessed by phosphorylation. Thus, these sites lead to a clear disruption of the dimeric structure and are likely to be salt bridging sites in the dimer interface. In these mutants however, dimer disruption does not lead to the complete dissociation of the dimer, as shown in the native PAGE analysis. Other interactions in the dimer interface allow a dimer to form even with the mutation of either of these sites.

In order to obtain species potentially with a greater disruption of the dimer, the D21N/E89Q/S58A and D21N/E89Q/S58D 14-3-3ζ proteins were generated. The compounding of these mutations in the two triple mutants of 14-3-3ζ, leads to greater disruption of the dimer, as observed by native PAGE and intrinsic fluorescence. The major difference between these proteins is the measured level of exposed hydrophobicity. As

discussed in section 4.2.5, this difference may be due to the introduction of the negatively charged Asp residue at position 58, which affects the interaction of bis-ANS with hydrophobic pockets in this region. All the other characterisation shows that D21N/E89Q/S58D 14-3-3ζ has a comparable level of disruption compared to D21N/E89Q/S58A 14-3-3ζ. The compounding of the salt bridging sites with the phospho-mimic at S58 would be predicted to exhibit the greatest level of disruption of all of the mutant proteins.

The involvement of the dimer interface in the chaperone activity of 14-3-3ζ was investigated using the characterised dimer disrupted mutants against the amorphously aggregating target proteins. The chaperone activities of the dimer-disrupted proteins was determined (section 4.4.1), and it is shown that, with the exception of E89Q and S58D 14-3-3ζ, they have enhanced chaperone ability compared to WT 14-3-3ζ against the amorphous aggregation of ADH, implying that this dimer interface is implicated in the chaperone action of 14-3-3ζ. In comparison, the dimer disrupted proteins showed no chaperone enhancement against the amorphous aggregation of reduced insulin. The fluorescence studies of the interaction of 14-3-3ζ and reduced insulin imply that this chaperone interaction is transient one, which does not affect the environment of W5, and causes no major conformational changes of 14-3-3ζ.

The chaperone ability of the 14-3-3ζ mutants was very different against the amorphous aggregation of ADH and reduced insulin, with the mutant proteins showing little change in chaperone ability against reduced insulin. In the case of D21N/E89E/S58D there was a minor enhancement of insulin aggregation at high molar ratios. This discrepancy between the chaperone ability of the dimer disrupted 14-3-3ζ proteins against different target proteins can be rationalised. The rapid aggregation of insulin may account for this discrepancy. Even with their enhanced chaperone ability, these mutant proteins are more unstable. With the rapid aggregation of reduced insulin, 14-3-3ζ struggles to prevent the major aggregation of insulin. The interaction of these mutant proteins with the very rapid aggregation of insulin, results in the 14-3-3 proteins being unable to prevent this aggregation. 14-3-3 still tries to chaperone but its instability may lead to the incorporation of these proteins into the rapidly forming aggregate and in some cases an enhancement of aggregation is observed.

Potentially the enhancement of the chaperone action of the dimer disrupted proteins against the amorphous aggregation of ADH is a result of the increased exposed hydrophobicity. However if an increase in exposed hydrophobicity is all that is required for enhanced

chaperone activity, all of mutant proteins should have exhibited an increased chaperone ability, which was not the case. Unlike all of the other mutant proteins, E89Q and S58D 14-3-3ζ exhibited little significant change in its chaperone ability, even with the demonstrated dimer disruption and increased exposed hydrophobicity (section 4.2). Given the proximity of E89 to D21, any disruption to either would presumably expose similar regions of the dimer interface, implying that they would exhibit similar chaperone abilities. Examining the crystal structure of WT 14-3-3ζ reveals the potential of R18 (the salt bridging partner of E89) to interact with the hydroxyl group of Y82 (Fig. 4.13). This opportunist interaction could reduce the dissociation from the dimer and therefore lead to a reduced exposure of this region of the dimer interface. This may account for the observed chaperone ability. However this interaction of R18 with Y82 is less stabilising than the native salt bridge (R18-E89) resulting in reduced overall stability of the protein.

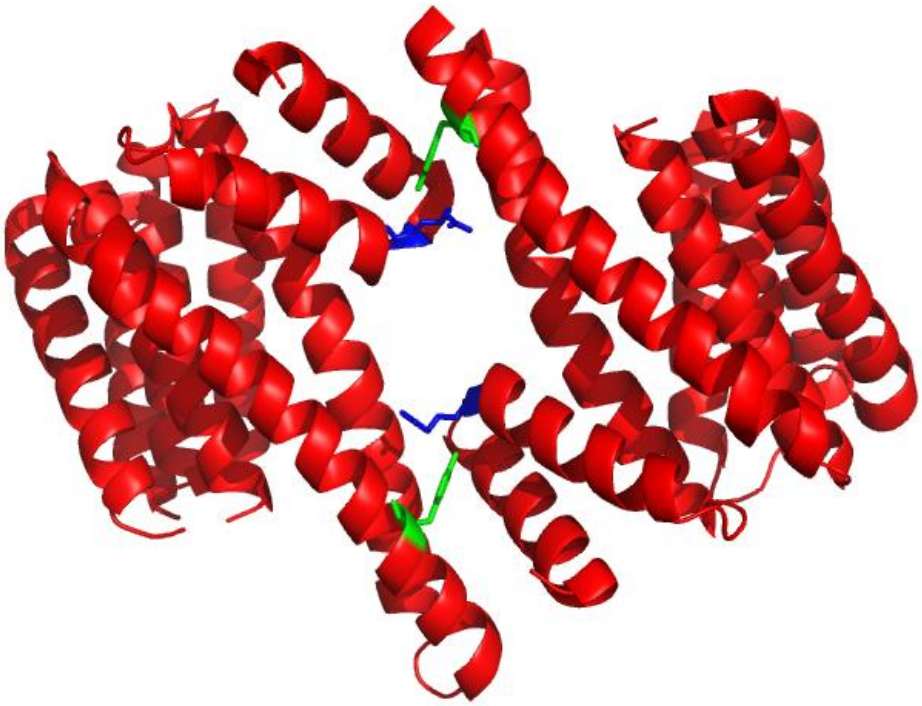

Figure 4.13: The arrangement of R18 (blue) and Y82 (green) within the dimer interface. With the mutation of E89 to Q, there is no salt bridging partner for R18. With a rotation of R18, there could be a potential interaction with the hydroxyl group on Y82, which reduces the dimer dissociation available with this mutant 14-3-3 protein.

The phospho-mimicking protein, S58D 14-3-3ζ, exhibited little change in chaperone activity compared to WT 14-3-3ζ against the amorphous aggregation of ADH, and exhibited a reduced chaperone ability compared to D21N, D21N/E89Q/S58A and D21N/E89Q/S58D 14-3-3ζ proteins. S58D 14-3-3ζ demonstrates disruption of the dimer, which is comparable to the other mutant proteins. The introduction of the negatively charged aspartic acid residue potentially changes the hydrophobic properties of the dimer interface, making it less able to interact with misfolded target proteins. This effect is observed when comparing the chaperone abilities of D21N/E89Q/S58D and D21N/E89Q/S58A 14-3-3ζ. The mutation of S58 to alanine produces a marginally better chaperone than the D21N/E89Q/S58D 14-3-3ζ mutant, implying some negative effects on the chaperone action with the presence of the negatively charged Asp at position 58 residue.

The chaperone ability of a monomeric form of 14-3-3ζ has been recently investigated (78) and the results correlate with these herein. This mutant protein (L12Q/A13Q/E14R) has been characterised and shown to be a monomer at 3mg/mL by SEC-MALLS, with increased exposed hydrophobicity present. This 14-3-3ζ protein was found to be a more effective molecular chaperone than WT 14-3-3ζ against various model target proteins including ADH and reduced insulin (78), (84).

All of this is suggestive that the dimer interface of 14-3-3ζ is implicated in the chaperone action of 14-3-3ζ. Thus, dissociation of the dimer to its monomeric form, or at least the shift in equilibrium to this species, may be the crucial step in the chaperone action of 14-3-3ζ. We hypothesise that under stress conditions, the equilibrium shifts (e.g. as a result of increased temperature) to produce a greater proportion of monomeric 14-3-3ζ, which can then interact with stressed proteins. This potential dissociation is akin to the function of molecular chaperone family, sHsps. Whilst chaperoning, sHsps dissociate from a large oligomer into a chaperone active dimeric form in order to interact with aggregated target proteins (85).

Chapter 5

Characterisation of the dimer-monomer equilibrium of 14-3-3ζ, by cross-linking and analytical ultracentrifugation

5.1 Introduction

It was demonstrated in chapter 4 that dimer-disrupted 14-3-3ζ proteins have enhanced chaperone ability, which may result from greater exposure of the dimer interface. The implication is that the dimer interface is important for the chaperone action of 14-3-3ζ. Dissociation of a dimer into its component monomeric species is possibly the simplest way to expose this region to aggregating target proteins. The native 14-3-3 proteins exist in an equilibrium between both monomeric and dimeric states (5). However, 14-3-3 monomer-dimer exchange has not been examined to any significant extent.

In particular, the monomer-dimer equilibrium of 14-3-3ζ has had little characterisation. Previous studies show that exchange between 14-3-3 subunits is relatively slow due to the stability of the 14-3-3 dimer (86). This study predominantly focused on the formation of hetero-dimers from pure homo-dimeric proteins (5). The effects of dimer disruption, changes in temperature and concentration on this equilibrium are currently unknown.

This monomer-dimer equilibrium is akin to the subunit exchange in small heat shock proteins (sHsps). In sHsps, increased temperature leads to enhanced subunit exchange (87). However changing concentrations had little effect on the subunit exchange of αA-crystallin (88). The chaperone ability of αA-crystallin is proposed to be related to this equilibrium whereby dissociation from the oligomer to the dimer produces the chaperone-active unit (85).

In this chapter, it was investigated if the chaperone action of 14-3-3ζ is similarly related to the monomer-dimer equilibrium. In chapter 4, it was determined that the generation of D21N, E89Q, S58D, D21N/E89Q/S58A and D21N/E89Q/S58D 14-3-3ζ proteins causes dimer disruption. Here, the effect of dimer disruption on the monomer-dimer equilibrium was explored using cross-linking and analytical ultracentrifugation studies. Consequently, the potential role of the monomer-dimer equilibrium in the chaperone ability of 14-3-3ζ was assessed. In addition, the dependence of this equilibrium on temperature and concentration was determined.

5.2 Results: The monomer-dimer equilibrium of the dimer disrupted 14-3-3ζ mutant proteins.

The mutant proteins were expressed and purified successfully as previously described in chapter 4. The proteins used in this chapter were demonstrated to be greater than 95% pure by SDS-PAGE analysis.

5.2.1 Cross-linking with Glutaraldehyde

To further investigate the dimeric nature of 14-3-3ζ with the stated mutations, cross-linking using glutaraldehyde was undertaken. Glutaraldehyde is highly reactive towards amine groups at a neutral pH, forming chemically stable cross-links. Glutaraldehyde has the ability to cross-link with several functional groups of amino acids. However the ε-amino group of lysine is the most reactive at neutral pH (89). It has previously been demonstrated that glutaraldehyde has the ability to crosslink the two monomers of 14-3-3ζ, preventing dissociation from the dimer (90). This cross-linking can then be analysed via SDS-PAGE. In order to further characterise the effects of the stated mutations on the monomer-dimer dynamics of the protein, cross-linking with glutaraldehyde over a concentration range (0.001-0.005%) was undertaken, and analysed by SDS-PAGE and immuno-blotting. The overall intensity of each band was quantified using Molecular Dynamics ImageQuest 2.0 software and the percentage of monomer and dimer for each concentration of glutaraldehyde was determined.

The cross-linking of WT 14-3-3ζ with glutaraldehyde shows two species with different mobility by SDS-PAGE (Fig. 5.1). The species with slower mobility corresponds to a dimeric form of 14-3-3ζ, confirming that the 14-3-3ζ dimer can be cross-linked with glutaraldehyde (Fig. 5.1A). With increasing concentrations of glutaraldehyde, there is an observable increase in the dimeric content of WT 14-3-3ζ, indicating increased cross-linking of the 14-3-3ζ dimer. With this increase in cross-linking efficiency, there is a corresponding decrease in faster migrating species.

Increases in the dimeric content of 14-3-3 with increasing concentrations of glutaraldehyde are also observed for D21N and E89Q 14-3-3ζ (Fig. 5.1). E89Q 14-3-3ζ shows comparable cross-linking compared to WT 14-3-3ζ. However D21N 14-3-3ζ exhibits a different profile compared to WT and E89Q 14-3-3ζ, with a small quantity of cross-linked dimeric protein even at higher glutaraldehyde concentrations. However with S58D 14-3-3ζ there is little or no

cross-linking across the glutaraldehyde concentration range, implying that the distance between monomers is increased in this mutant due to significant dimer disruption. Consistent with this cross-linking analysis, previous analysis indicated that the introduction of the negatively charged Asp residue at position 58 in 14-3-3ζ disrupts the dimeric structure (22,74).

Thus, the introduction of Asp into the dimer interface leads to significantly reduced cross-linking compared to D21N and E89Q 14-3-3ζ, with a greater shift in the monomer-dimer equilibrium towards the monomeric form in S58D 14-3-3ζ. There is little change in the dimer dissociation with E89Q 14-3-3ζ compared to the WT protein. D21N 14-3-3ζ exhibits a propensity to be less dimeric at higher glutaraldehyde concentrations (Fig. 5.1B). Phosphorylation assays show dimer disruption but the proteins can still be cross-linked by glutaraldehyde, as the existing interactions present in the dimer interface allow the dimer to form but with reduced stability.

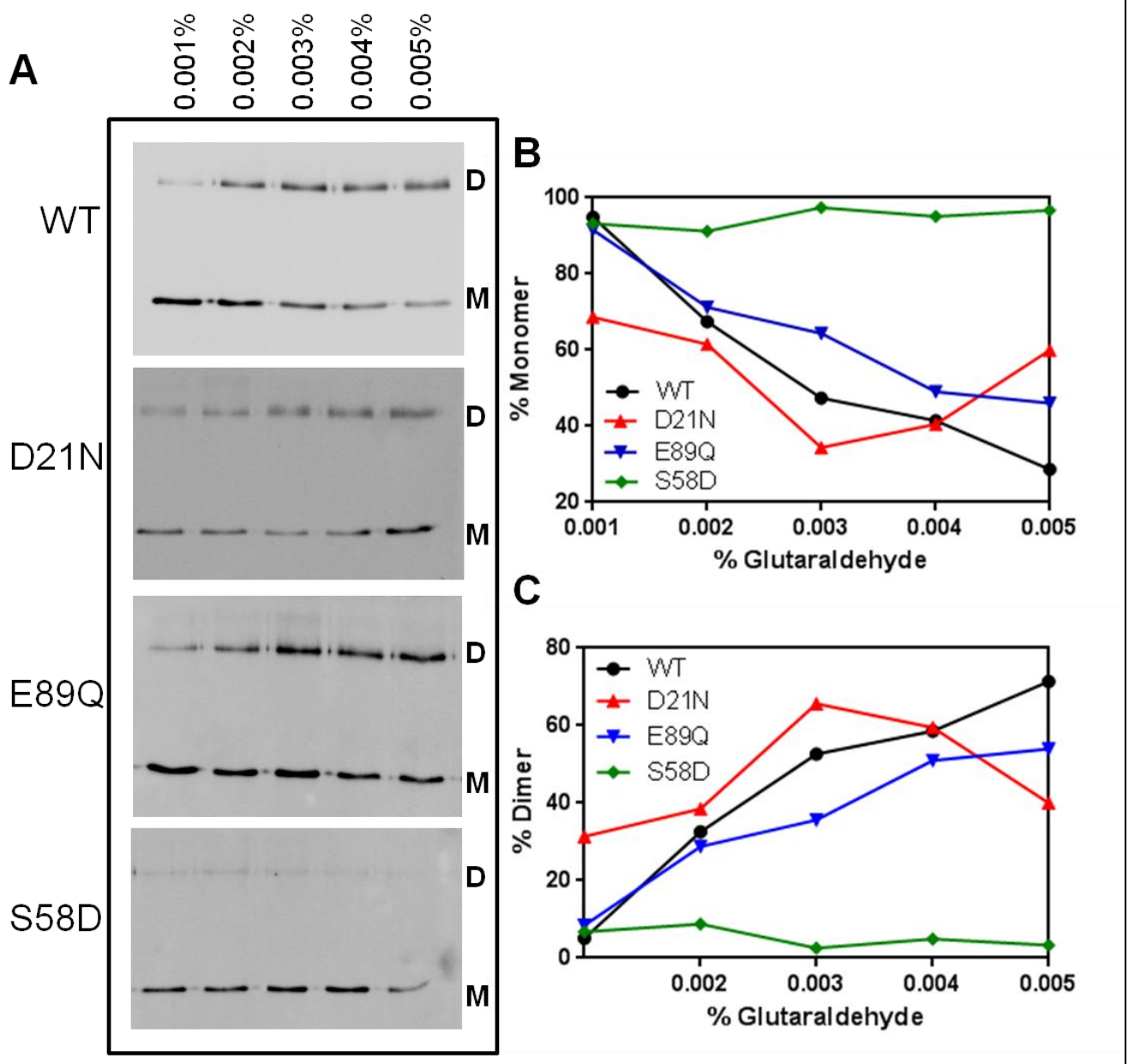

Figure 5.1: The cross-linking of 14-3-3ζ proteins by glutaraldehyde; (A) Cross-linking of WT, D21N, E89Q and S58D 14-3-3ζ by glutaraldehyde (0.001-0.005%) was analysed by immuno-blotting for 14-3-3 after SDS-PAGE. The presence of dimeric or monomeric protein is denoted with a D or M respectively. The calculated percentage of (B) monomeric and (C) dimeric 14-3-3ζ for each mutant protein, relative to the total protein, at each glutaraldehyde concentration (0.001-0.005%) is shown.

5.2.2 Analytical Ultracentrifugation

Since the early 20th century, analytical ultracentrifugation (AUC) has been used to study the behaviour of macromolecules in solution (91). AUC allows the determination of hydrodynamic properties of macromolecules without the interaction with a matrix or surface (92). There are two basic types of AUC experiments: sedimentation velocity, which allows estimation of sedimentation coefficients and molecular weights, and sedimentation equilibrium, which can provide association constants for many interacting systems (92).

Sedimentation velocity experiments measure the movement of an initially uniform protein solution with the application of angular velocity, in order to determine particle size (67). The centrifugal force causes the protein to be rapidly sedimented towards the bottom of the cell. This results in a depletion of the protein at the meniscus (top of the cell), with a concentration boundary that moves towards the bottom of the cell (Fig. 5.2). This migration in a gravitational field is dependent on the size of the macromolecule (92),(68).

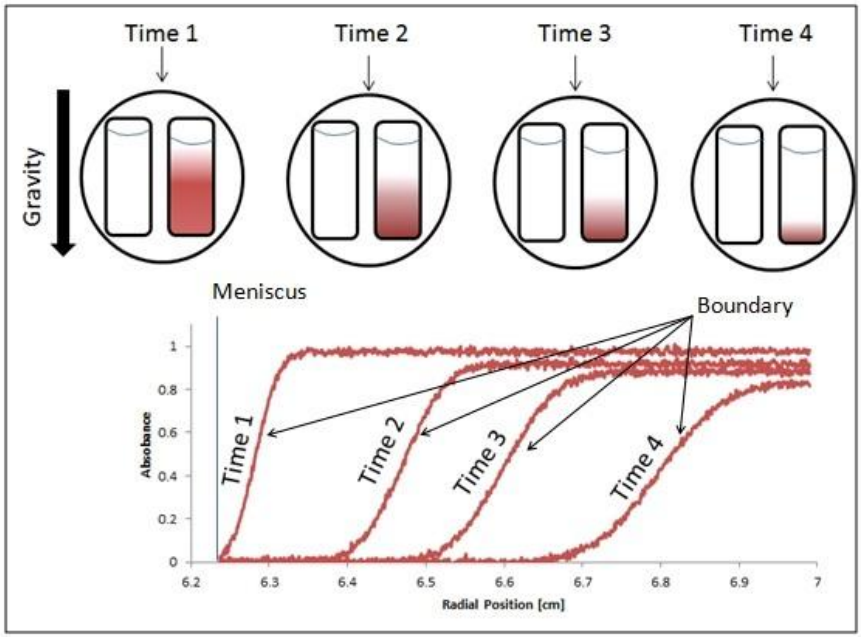

Figure 5.2: The principle of sedimentation velocity experiments showing how sedimentation of a protein produces a concentration boundary (taken from (93)).

The time-dependent movement of the boundary can be analysed using various techniques and used to determine the sedimentation coefficient for the species. All data collected here were analysed using the SEDFIT program, which was developed by Schuck et al. (67), (68). The goodness of the model fit can be assessed by the residuals; i.e. the difference between each experimental point and the corresponding point on the calculated curve. A good fit is indicated by the random distribution of points around zero with a low standard deviation (94).

To obtain accurate sedimentation coefficients from velocity experiments, a number of factors must be known: the rotor speed, temperature, elapsed time, viscosity and buoyancy. Temperature and buffer changes can lead to changes in the viscosity of the aqueous environment. Therefore observed sedimentation coefficients must be corrected to the standard conditions (pure water and 20^{o}C), referred to as the $S_{20,W}$ (69). All the data presented here have been corrected to the $S_{20,W}$. Sedimentation velocity experiments have been previously used to assess changes to the monomer-dimer dynamics of 14-3-3ζ (74).

In order to assess the dimer disruption in the 14-3-3ζ mutants, sedimentation velocity experiments were undertaken at 0.09mg/mL and 0.27mg/mL, at different temperatures (4, 20 and 37^{o}C). All the 14-3-3ζ proteins were subjected to size exclusion chromatography prior to use to ensure protein purity. All experiments were undertaken at 40,000rpm, with the data collected continuously. After analysis, all data were corrected to $S_{20,W}$.

Initial AUC experiments were undertaken at 0.27mg/mL. Sedimentation velocity analysis of WT 14-3-3ζ yielded standardised sedimentation coefficients of 3.75S and 6.20S (Fig. 5.3A). The residuals show a good fit for these data (Fig. 5.3B). All future analysed data show similar residual plots indicative of good fits. The [*c(M)*] distribution was obtained and gave molecular masses of ~54kDa and 108kDa for the two species present. These values correspond to the mass of dimeric and tetrameric 14-3-3ζ species. By far the predominant species is dimeric with approximately 1% of the total protein existing as a tetramer. A tetrameric form of 14-3-3ζ has not been reported previously.

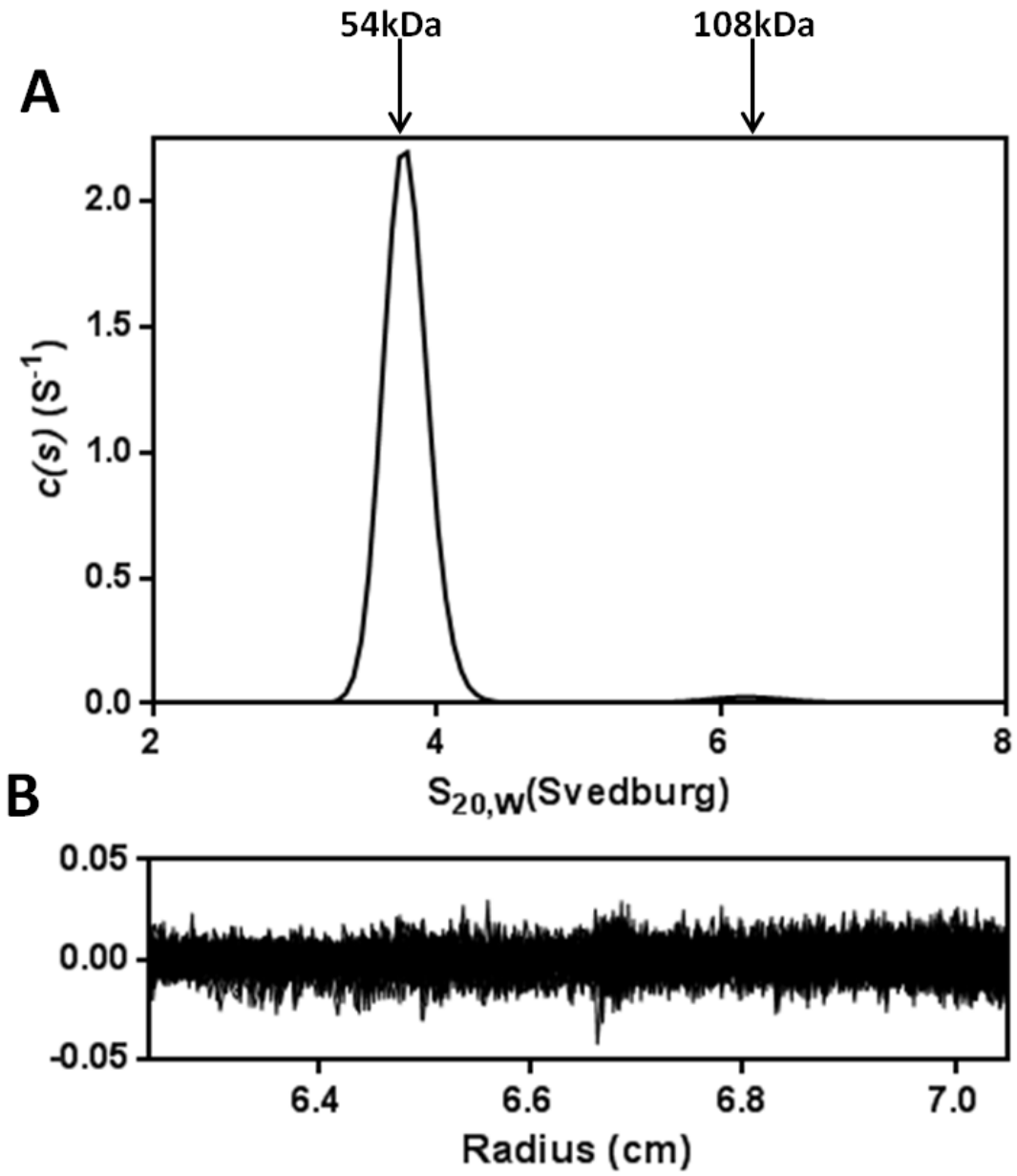

Figure 5.3: (A) The continuous sedimentation coefficient (*c(s)*) distribution of WT 14-3-3ζ at 20^{o}C plotted as a function of sedimentation coefficient ($s_{20,w}$). Two peaks are observed, corresponding to the dimeric (54kDa) and tetrameric (108kDa) forms of 14-3-3ζ. (B) Residuals resulting from the c(s) distribution best fits are shown as a function of radius of the cell.

Sedimentation velocity analysis of the dimer-disrupted 14-3-3ζ mutants was undertaken at 0.27mg/mL and compared to WT 14-3-3ζ (Fig. 5.4). All of the dimer disrupted proteins showed an overall reduction in $S_{20,W}$ for the major peak compared to WT 14-3-3ζ (Table 5.1), which may be indicative of altered structure. For some mutants, particularly the triply mutated protein, there is an additional peak present at ~ 2.4S which corresponds to a protein of approximately 27 kDa in mass i.e. a monomeric 14-3-3ζ species. The degree of monomer content varies for each protein with D21N and E89Q 14-3-3ζ possessing a small amount of monomer (1.5% and 2.5% respectively) and S58D and D21N/E89Q/S58A 14-3-3ζ showing a greater monomer content (10.8 and 60.4% respectively). All the 14-3-3ζ proteins exhibited a very minor tetrameric species (at ~6S) at 0.27mg/mL to a similar level (not shown). D21N/E89Q/S58A 14-3-3ζ showed an additional minor peak at ~5S, corresponding to a trimeric state of 14-3-3ζ, which was not observed for the other 14-3-3ζ proteins.

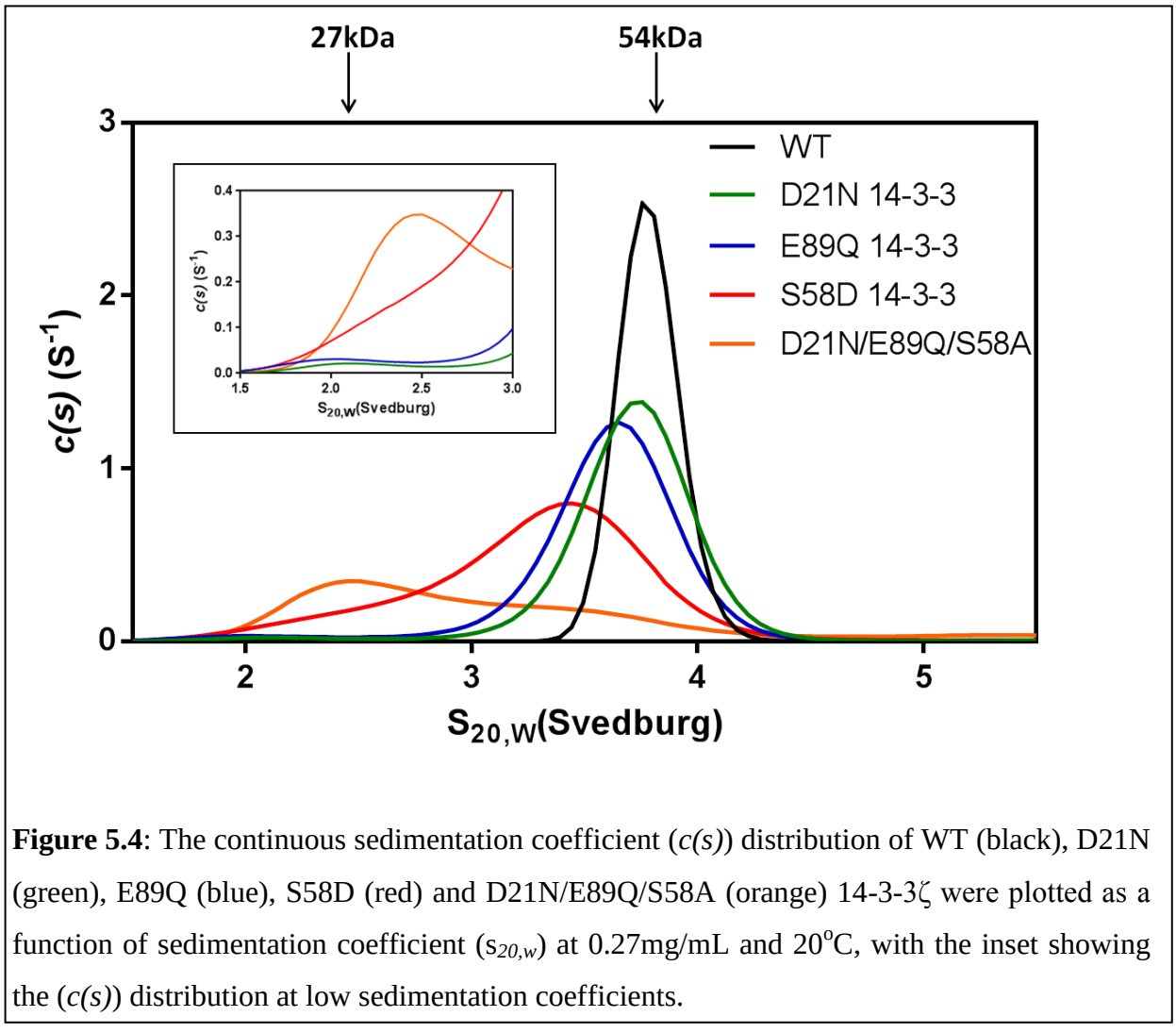

Figure 5.4: The continuous sedimentation coefficient (*c(s)*) distribution of WT (black), D21N (green), E89Q (blue), S58D (red) and D21N/E89Q/S58A (orange) 14-3-3ζ were plotted as a function of sedimentation coefficient ($s_{20,w}$) at 0.27mg/mL and 20°C, with the inset showing the (*c(s)*) distribution at low sedimentation coefficients.

In D21N and E89Q 14-3-3ζ, there is a minor disruption causing an increase in monomeric content compared to WT 14-3-3ζ as a result of removal of the salt bridges at the dimer interface. S58D 14-3-3ζ is more disrupted than D21 and E89Q, leading to significant increase in the relative monomer content. However D21N/E89Q/S58A 14-3-3ζ, with the removal of both salt bridges, has significant disruption to the dimer and a resultant greater proportion of monomer present. In summary, the sedimentation velocity experiments show that there is a dramatic perturbation to the monomer-dimer equilibrium as a result of the introduction of these mutations (Fig. 5.4).

The effect of varying the concentration on the monomer-dimer distribution of 14-3-3ζ was analysed (Fig. 5.5). The standardised sedimentation coefficients were obtained for all the 14-3-3ζ proteins at 0.09mg/mL and 20°C and are summarised in Table 5.1. All the 14-3-3ζ proteins (with the exception of D21N/E89Q/S58A 14-3-3ζ) have a decrease in $S_{20,w}$ value as a result of this concentration reduction. This is indicative of some perturbation to the monomer-dimer equilibrium, on the reduction of protein concentration.

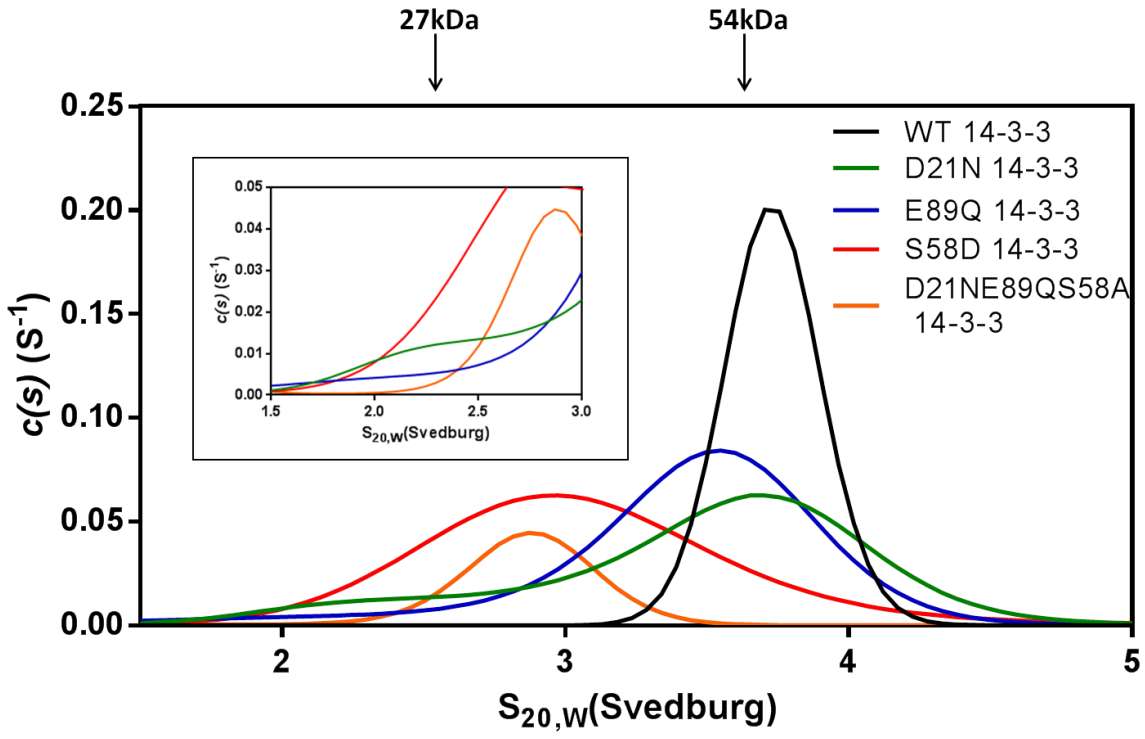

Figure 5.5: The continuous sedimentation coefficient (*c(s)*) distribution of WT (black), D21N (green), E89Q (blue), S58D (red) and D21N/E89Q/S58A (orange) 14-3-3ζ at 0.09mg/mL and 20°C with the inset showing the (*c(s)*) distribution at low sedimentation coefficients.

By analysing the *c(s)* distributions at 0.09mg/mL (Fig. 5.5), it is apparent that there is an increase in the monomer content for the dimer-disrupted 14-3-3ζ mutants compared to the WT protein. The broad peak for E89Q 14-3-3ζ indicates a rapid equilibrium between the monomer and dimer species. D21N 14-3-3ζ also shows a broad peak with a greater quantity of monomeric species presence compared to E89Q 14-3-3ζ (Fig. 5.5inset). Even though D21N 14-3-3ζ has a higher $S_{20,w}$ value compared to E89Q 14-3-3ζ, this greater amount of monomeric species for the D21N protein is indicative that D21N 14-3-3ζ exhibits a similar, if not greater, disruption to the monomer-dimer equilibrium. Both S58D and D21N/E89Q/S58A 14-3-3ζ exhibit only one broad peak in the profile, with a significantly reduced sedimentation coefficient compared to WT 14-3-3ζ and a calculated mass of ~35kDa. This is indicative of a rapid equilibrium between the monomeric and dimeric species, and a significant shift in the monomer-dimer equilibrium of these proteins towards the monomer. No tetrameric species was observed at 0.09mg/mL for any of the proteins, implying that these species form at higher concentrations. The increase in the presence of the monomeric species in the dimer disrupted mutants with decreasing protein concentration is indicative that decreasing the protein concentration causes a shift in the monomer-dimer equilibrium of 14-3-3ζ towards the monomer.

Table 5.1: The standardised sedimentation coefficients ($S_{20,w}$) of WT, D21N, E89Q, S58D and D21N/E89Q/S58A 14-3-3ζ at 0.27mg/mL and 0.09mg/mL, with the difference between the concentrations ($\Delta_{S20,w}$) stated.

Protein	**0.27mg/mL**	**0.09mg/mL**	**$\Delta_{S20,w}$**
WT 14-3-3	3.75	3.70	-0.05
D21N 14-3-3	3.70	3.65	-0.05
E89Q 14-3-3	3.60	3.54	-0.06
S58D 14-3-3	3.45	2.90	-0.55
D21N/E89Q/S58A 14-3-3	2.45	2.85	+0.40

Finally the effect of temperature on the monomer-dimer equilibrium was analysed. By observing WT 14-3-3ζ (0.09mg/mL) at three different temperatures (4, 20 and 37^{o}C), the standardised sedimentation coefficients were obtained (Fig. 5.6; Table 5.2). There is a small decrease in *S20,w* with increasing temperature (3% over the temperature range), implying a minor shift in the monomer-dimer equilibrium, towards the monomeric form at higher temperatures. This most likely arises due to increased exchange of subunits with increasing temperature. A similar trend was also observed for the 14-3-3ζ mutants at 37^{o}C (Table 5.2). At lower temperatures (4^{o}C), there was no increase in sedimentation coefficient as seen with WT 14-3-3ζ, indicating that the lower temperature does not result in a shift in the monomer-dimer equilibrium with a push towards the dimer at lower temperatures for the mutants. With alteration of temperature there was no tetramer observed for any of the 14-3-3ζ proteins (0.09mg/mL), implying that this concentration is too low for the self-association of 14-3-3ζ.

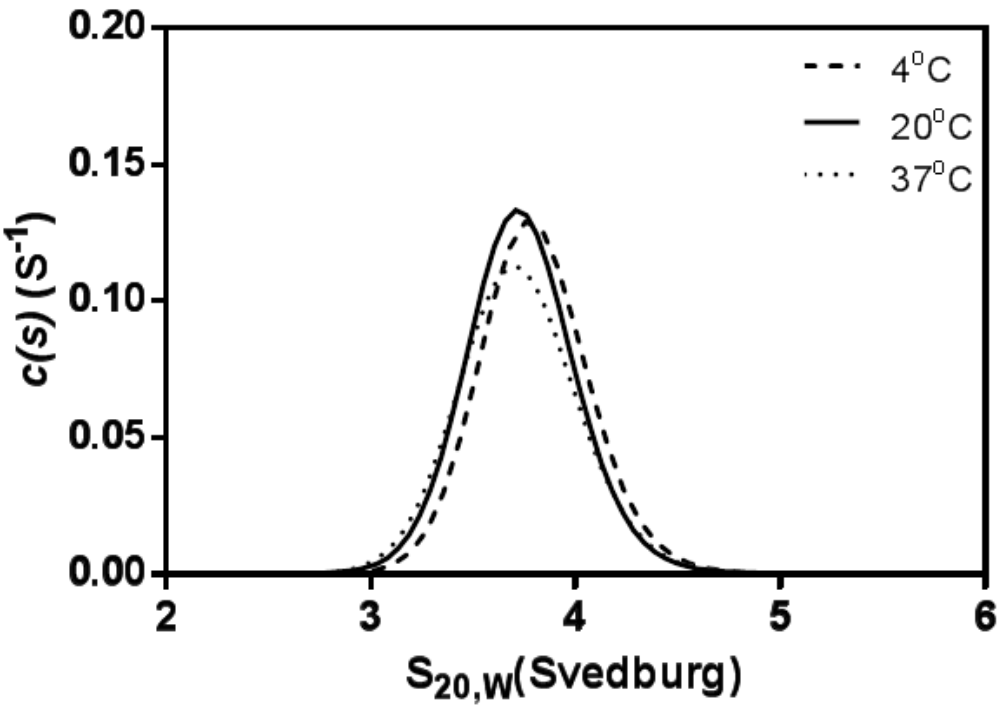

Figure 5.6: The continuous sedimentation coefficient (*c(s)*) distribution of WT 14-3-3ζ at 4^{o}C (dashed line), 20^{o}C (solid line) and 37^{o}C (dotted line) at 0.09mg/mL.

Table 5.2: The standardised sedimentation coefficients ($S_{20,W}$) determined for WT, D21N, E89Q, S58D and D21N/E89Q/S58A 14-3-3ζ proteins at 4, 20 and 37°C and 0.09mg/mL.

Temperature (°C)	WT	D21N	E89Q	S58D	D21N/E89Q/S58A
4°C	3.75	3.61	3.38	2.95	2.71
20°C	3.70	3.65	3.54	2.90	2.85
37°C	3.64	2.84	3.10	2.91	2.51

In summary, the sedimentation velocity analysis of the 14-3-3ζ proteins shows that the introduced mutations lead to a shift in the monomer-dimer equilibrium of 14-3-3ζ and result in a greater amount of the monomer protein. Additionally, varying concentration and temperature also leads to a shift in the monomer-dimer equilibrium of 14-3-3ζ. Thus higher 14-3-3ζ concentrations (for WT and the mutant proteins) favour the dimeric form.

5.3 Discussion

The monomer-dimer equilibrium of 14-3-3ζ has not been well characterised previously with most analyses aimed towards the further understanding of the interactions between different isoforms of 14-3-3ζ. Hetero-dimers are able to form *in vitro* which is indicative of a monomer-dimer equilibrium in cells and the ability of subunit exchange to occur between 14-3-3 proteins (5). There has been little previous analysis into the monomer-dimer equilibrium of 14-3-3 proteins, with studies focussing on the formation of hetero-dimers from pure homo-dimers by mass spectrometry. This subunit exchange of 14-3-3 is relatively slow due to the stability of the dimer (5).

In chapter 4, it was demonstrated that the removal of salt bridges from the dimer interface of 14-3-3ζ and a phospho-mimicking protein led to the disruption of this region (section 4.2). Here, the effects of these mutations, specifically on the monomer-dimer exchange of 14-3-3ζ, were examined further. It was concluded that the introduction of these mutations into 14-3-3ζ results in a perturbation of the monomer-dimer equilibrium to varying degrees for each mutant. S58D 14-3-3ζ exhibited significant changes in the monomer-dimer equilibrium by cross-linking and AUC, the latter indicating a shift more toward the monomer. The combination of all these mutations in D21N/E89Q/S58A 14-3-3ζ shows significant perturbation to the monomer-dimer equilibrium, resulting in a predominantly monomeric species. By AUC, the D21N/E89Q/S58A 14-3-3ζ protein exhibits a greater shift in the monomer-dimer equilibrium towards the monomer compared to all the other 14-3-3ζ proteins.

The above analysis indicates that the removal of the salt bridging sites is sufficient to cause significant disruption of the protein. The removal of one salt bridging site in the D21N and E89Q 14-3-3ζ still allows the formation of the dimer, though it is less stable than the WT 14-3-3ζ dimer. The removal of the two salt bridges in D21N/E89Q/S58A 14-3-3ζ leads to significant destabilisation, which is amplified with the removal of both, indicating the importance of these residues in the formation of a stable 14-3-3ζ dimer.

Cross-linking and hydrogen-deuterium exchange studies of S58D 14-3-3ζ show that this protein exists as a monomer (22). The data presented herein demonstrates that S58D 14-3-3ζ7, although significantly disrupted, is able to and does exist as a dimer, with the AUC studies showing a predominantly dimeric protein at 0.27mg/mL. Thus, even with the disruption caused by the introduction of the negatively charged Asp, there is the ability to

form interactions within the dimer interface (the salt bridge interactions; D21-K85 and R18-E89 (1)) to generate a dimer. However the introduction of this disrupting negative charge into a predominantly hydrophobic region causes significant disruption, causes this dimer to be short lived and too transient a species to be cross-linked.

AUC analysis of WT 14-3-3ζ revealed the presence to a minor extent of a tetrameric form of 14-3-3ζ at higher concentrations. This 14-3-3ζ tetramer has not been reported before and is most likely a result of the high protein concentration. However this self-association is reminiscent with the behaviour of molecular chaperones, sHsps, which associate to form large oligomers in order to enhance stability, with the C-terminal extension playing a functional role in solubilising the oligomers (61). The self-association of 14-3-3ζ could also act in a similar manner, as a method of stabilising the protein at higher concentrations. The arrangement of the 14-3-3ζ dimers to form this tetrameric structure is unknown.

In addition, AUC experiments confirm that the monomer-dimer equilibrium of 14-3-3ζ is affected by varying concentration and temperature. A reduction in concentration and an increase in temperature lead to a shift in the monomer-dimer equilibrium, to generate more of the monomeric species. Investigations into the subunit exchange of αA-crystallin (a member of the sHsps family) demonstrate a similar dependence on alteration in temperature, whereby an increase in temperature leads to increased subunit exchange (87). However changes of concentration have little effect on subunit exchange of αA-crystallin (88).

The increase in monomeric content for the disrupted 14-3-3ζ proteins correlates well with the enhanced chaperone action of these proteins, and may also provide insight into the discrepancy of the chaperone abilities of D21N and E89Q 14-3-3ζ. Both proteins exhibit dimer disruption as a result of their mutations, with a shift in the monomer-dimer equilibrium towards the 14-3-3ζ monomer. However, D21N 14-3-3ζ shows increased monomeric species and a more significant reduction in sedimentation coefficient at elevated temperatures compared to E89Q 14-3-3ζ (Fig. 5.5; Table 5.2). E89Q 14-3-3ζ is more dimeric at 0.09mg/mL compared to D21N 14-3-3ζ, potentially due to additional interactions, wherein R18 (the salt bridging partner of E89) could interact with other residues within the dimer interface (as previously discussed in chapter 4), which would not occur in D21N 14-3-3ζ,. The availability of more monomeric D21N 14-3-3ζ may be necessary for the chaperone ability of 14-3-3ζ, and results in its enhanced chaperone ability.

The data presented here implies that the monomer-dimer equilibrium of 14-3-3ζ investigated here may play a crucial role in the chaperone action of 14-3-3ζ. Stress conditions (e.g. elevated temperature) promote the shift in the monomer-dimer equilibrium towards the monomer. The dissociation from the dimer leads to enhanced chaperone ability with the interaction of aggregating target proteins occurring via the hydrophobic face in the dimer interface (Fig. 5.8). As discussed previously, this has parallels with the chaperone action of sHsps, which depends on the dissociation of the sHsps oligomer into the chaperone active dimer for chaperone function (85).

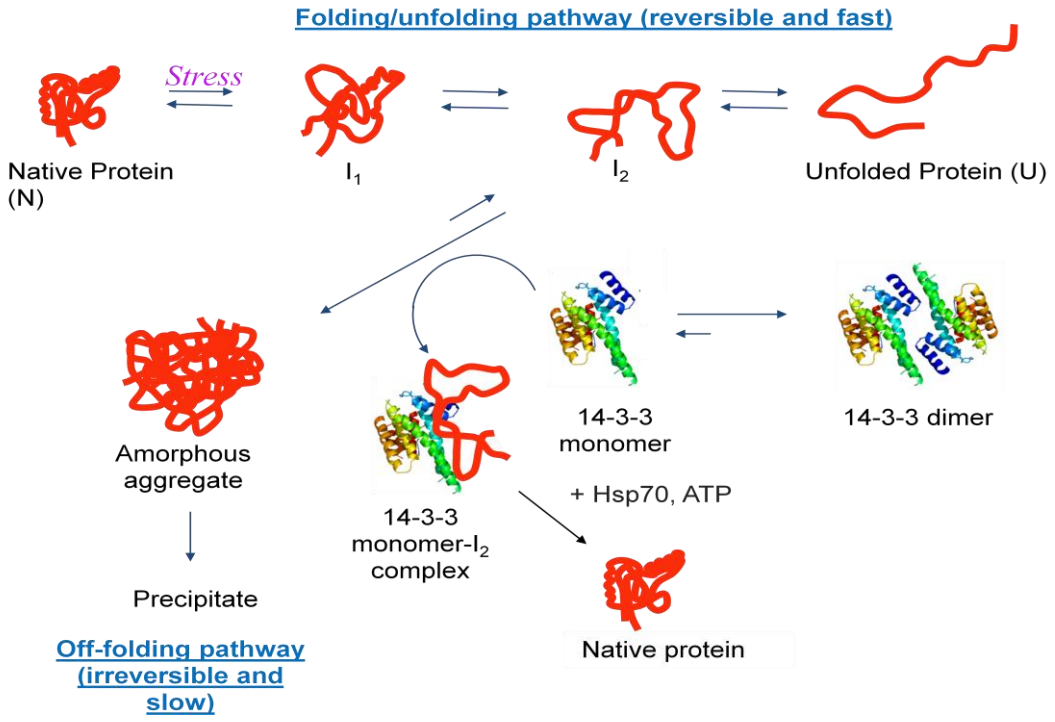

Figure 5.7: The hypothesised mechanism of the chaperone action of 14-3-3ζ against amorphously aggregating target proteins, whereby under stress conditions, 14-3-3ζ dissociates from the dimer, in order to interact with and stabilise aggregating target proteins. The native form of the protein can be recovered with the aid of other chaperone proteins (Hsp70) coupled with ATP hydrolysis (adapted from Carver et al., which outlines the mechanism for sHsps chaperone action (39)).

Chapter 6

A structural and functional investigation into the chaperone ability of 14-3-3ζ in the presence of physiological lipid mimetics

6.1 Introduction

It was observed in chapter 4 (section 4.3.1), that dimer disrupted 14-3-3ζ proteins have enhanced chaperone ability. Although there is no clear evidence for the presence of 14-3-3ζ monomers under normal physiological conditions, it is known that *in vitro* monomers can exchange (5), suggesting that 14-3-3 dimers are in a dynamic equilibrium. Under stress conditions, accumulation of lipids e.g. sphingosine within cells, due to the breakdown of sphingomyelin in cell membranes (95). These cellular lipids are implicated in many cellular roles, including apoptosis, mitosis and cell differentiation (96). Sphingosine (Fig. 6.1) accumulation within cells leads to apoptosis, leading to the general consensus that it may be an apoptotic mediator. However, the precise mechanism of sphingosine-induced apoptosis has not been determined (81). The regulation of 14-3-3 proteins has been identified as a potential mechanism by which sphingosine can induce cell death. As described in chapter 4 (section 4.2.6), sphingosine interacts with 14-3-3ζ, causing disruption of the dimer interface and allowing access of kinases to the buried S58 phosphorylation site (81). This dimer disruption reduces 14-3-3 proteins interaction with phosphorylated target proteins resulting in cell death. The conformational changes of 14-3-3ζ upon interaction with sphingosine have not been extensively characterised. The phosphorylation of the residue S58 results in major dimer disruption of 14-3-3ζ (24), as paralleled with the phospho-mimic S58D 14-3-3ζ (section 4.2) (22). This dimer disruption is thought to be a regulation mechanism for 14-3-3 proteins, with each 14-3-3ζ monomer having the ability to bind target proteins, but a reduced capability of supporting the function of the interacting target protein (80). This

leads to the inability of 14-3-3ζ to suppress pro-apoptotic mediators causing the induction of apoptosis in cells.

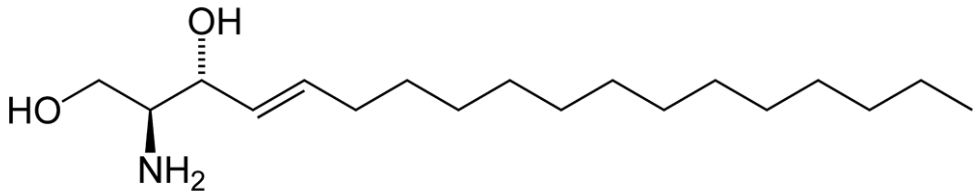

Figure 6.1: The chemical structure of sphingosine, the physiological lipid that disrupt the dimer interface of WT 14-3-3ζ (81).

Based on sphingosine, mimics have been identified which share the ability to allow the phosphorylation of 14-3-3ζ at S58 (81). As with sphingosine, the precise conformational changes undergone by 14-3-3ζ within the dimer interface upon interaction with these small molecules are unknown. In order to extend the investigation of the chaperone ability of the dimer interface of 14-3-3ζ, the effect of a sphingosine mimic was assessed. Due to confidentially restraints, the structure of the sphingosine mimic will not be revealed and the molecule shall be referred to as #41.14. The dimer disruption caused by the interaction between #41.14 and WT 14-3-3ζ was characterised here followed by determination of the chaperone ability of 14-3-3ζ in the presence of #41.14.

6.2 Results: Characterisation of the interaction between 14-3-3ζ and sphingosine mimic, 41.14.

WT 14-3-3ζ was expressed, purified and demonstrated to be greater than 95% pure by SDS-PAGE analysis. Due to solubility difficulties, a stock solution of #41.14 (2.5mM) was generated in DMSO. For use in assays the stock solution of #41.14 was diluted in the stated buffer. The maximum DMSO concentration was 0.5% v/v, which did not affect the structure and function of 14-3-3ζ (Urmi Dhagat, personal correspondence).

6.2.1 Phosphorylation assays

As discussed previously (section 4.2.6), phosphorylation of 14-3-3ζ at the buried residue, S58, results in significant disruption of the dimer (24). The phosphorylation only occurs in the presence of physiological lipid, sphingosine or analogues (81). In order to demonstrate that the sphingosine mimic, #41.14 is able to disrupt the dimeric structure and allow the phosphorylation of 14-3-3ζ, phosphorylation assays were undertaken in the presence and absence of #41.14. Phosphorylation was accomplished by protein kinase A (PKA). Coomassie staining showed equal loading of protein before the phosphorylation was visualised by autoradiography.

In the absence of #41.14, there is minimal observable phosphorylation of 14-3-3ζ, consistent with previous studies (Fig. 6.2) (81). This confirms that in the absence of the sphingosine mimic, there is no phosphorylation of S58. In the presence of #41.14, however, there is a detectable phosphorylation of 14-3-3ζ (Fig. 6.2). This phosphorylation in the presence of #41.14 suggests disruption of the dimer interface, in order to allow access of the kinase to the site, in a manner similar to sphingosine. Furthermore, #41.14 behaves in a similar manner to sphingosine itself, including the apoptosis of cells (Joanna Woodcock, personal correspondence).

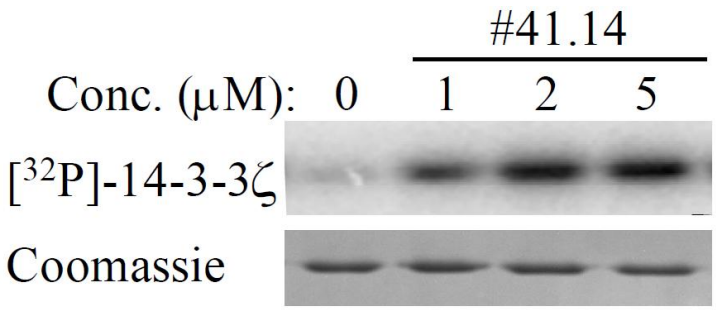

Figure 6.2: The phosphorylation of WT 14-3-3ζ by PKA in the presence and absence of various concentrations of #41.14, as analysed by SDS-PAGE and visualised by autoradiography. Visualisation of the protein loading was undertaken via Coomassie blue staining.

6.2.2 Intrinsic fluorescence of WT 14-3-3ζ in the presence of 41.14

The environment of the tryptophan residues of 14-3-3ζ was monitored in the presence and absence of the sphingosine mimic, #41.14. Upon excitation at 295nm, #41.14 exhibits strong fluorescence emission (Fig. 6.3A). All spectra presented here were corrected for the emission due to the presence of #41.14 on its own.

The addition of #41.14 to 14-3-3ζ exhibits little change in the intrinsic fluorescence profile of 14-3-3ζ (Fig. 6.3B) and no significant shifts in the maximum wavelength, implying little change to the tryptophan environment. In section 6.2.1, it was demonstrated that there is disruption to the 14-3-3ζ dimer interface upon interaction with #41.14, allowing the phosphorylation of Ser58. This fluorescence emission implies that dimer disruption does not result in the exposure of major regions of the dimer interface, leading to changes in the environment of W59.

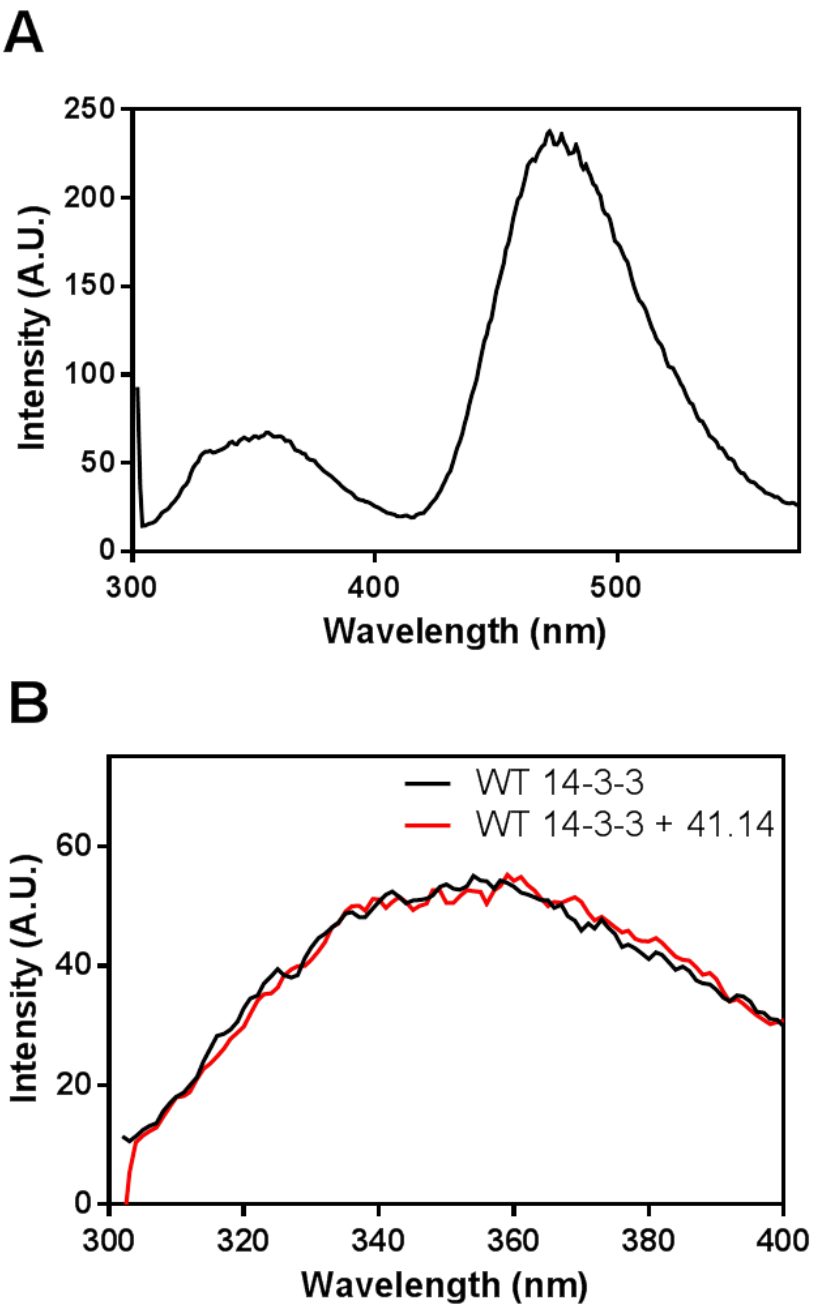

Figure 6.3: (A) The fluorescence spectrum of sphingosine mimic, #41.14 alone (14.4μM) upon excitation at 295nm, with the emission acquired between 300 and 600nm, in sodium phosphate buffer, pH 7.4, and 37^{o}C. (B) The intrinsic fluorescence profile of WT 14-3-3ζ (1.4μM) in the presence and absence of the small molecule, #41.14 (2.8μM). The spectrum was obtained by exciting the protein at 295nm and acquiring the emission between 300 and 400nm, in sodium phosphate buffer, pH 7.4, at 37^{o}C. The fluorescence profile was corrected for the presence of #41.14 alone.

6.2.3 Thermostability of 14-3-3ζ in the presence of 41.14

The thermostability of 14-3-3ζ in the presence and absence of #41.14 was assessed by monitoring the change in intrinsic fluorescence with temperature (over the range of 37-80^{o}C). Upon unfolding, a fluorescence intensity increase is observed, and from this the melting temperature can be determined.

The thermostability profile for WT 14-3-3ζ (7.2μM, 2mL) shows an increase in fluorescence after 60^{o}C before stabilising at 68^{o}C (Fig. 6.4). The melting temperature was determined to be 64^{o}C. In the presence of the small molecule #41.14, there was an increase in fluorescence at 63^{o}C before stabilising at 68^{o}C. The melting temperature was determined to be 65.5^{o}C. Thus, in the presence of #41.14, there is little change in the melting temperature indicating that the interaction between 14-3-3ζ and #41.14, although allowing dimer interface phosphorylation, does not alter the 14-3-3ζ structure in a manner comparable to the salt bridging mutants.

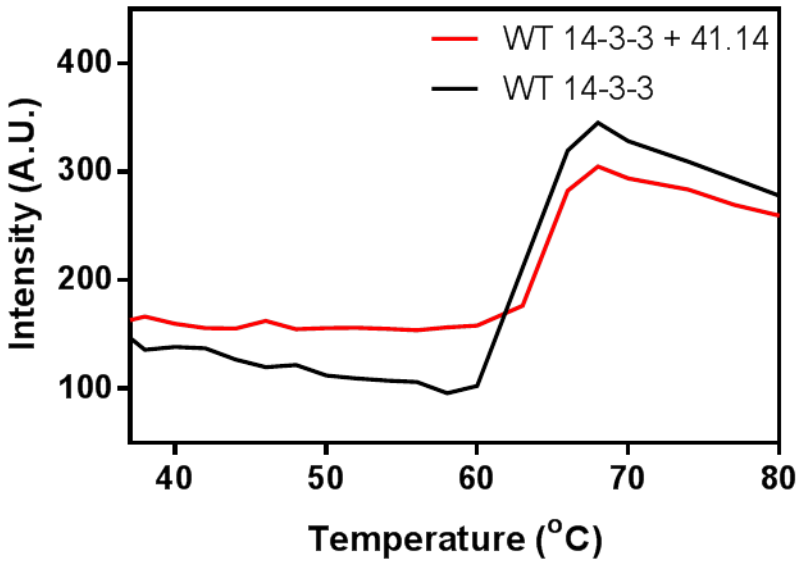

Figure 6.4: The thermostability profile of WT 14-3-3ζ (7.2μM) in the presence and absence of #41.14 (14.4μM), obtained by monitoring the intrinsic tryptophan fluorescence emission at 345nm between 37-80^{o}C, in sodium phosphate buffer at pH7.4. The fluorescence data have been corrected for the presence of #41.14.

6.2.4 The binding of bis-ANS to WT 14-3-3ζ in the presence of 41.14

The disruption of 14-3-3ζ's dimer interface exposes regions of normally buried hydrophobic surfaces as seen in section 4.2.5 with dimer-disrupted 14-3-3ζ mutant proteins. In order to characterise any changes in hydrophobicity in the presence of #41.14, the fluorescent probe bis-ANS was used. Upon interaction with hydrophobic regions, bis-ANS experiences a major increase in fluorescence intensity when excited (97).

WT 14-3-3ζ (1.4μM) in the presence and absence of #41.14 (2.8μM), was titrated with bis-ANS (1:0-20 molar ratio of WT 14-3-3ζ: bis-ANS), (Fig. 6.5). The fluorescence of bis-ANS was measured via two methods; direct excitation at 385nm and via FRET excitation of tryptophan at 295nm. The fluorescence emission was acquired between 400 and 600nm. The results obtained by direct excitation and via FRET excitation were comparable and therefore only the data from direct excitation of bis-ANS are presented (at 385nm). All data were corrected for the fluorescence of bis-ANS and #41.14 alone.

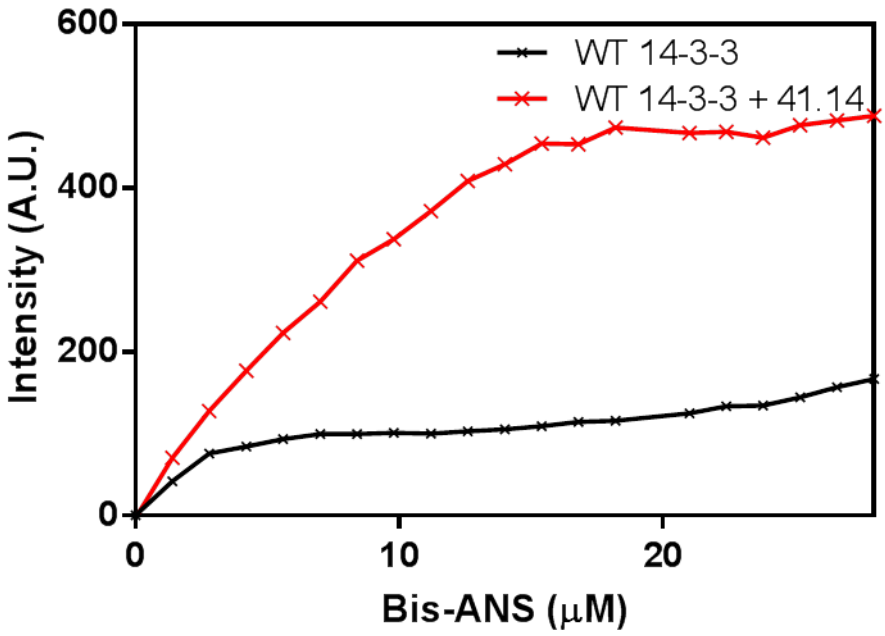

Figure 6.5: The titration of bis-ANS (μM) with WT 14-3-3ζ (1.4μM) in the presence and absence of #41.14 (2.8μM). The data were obtained by exciting at 385nm and acquiring the emission at 495nm.

The titration of bis-ANS into WT 14-3-3ζ showed an increase in fluorescence intensity at 495nm compared to bis-ANS alone, implying interactions of bis-ANS with exposed hydrophobic sites on the surface of 14-3-3ζ. In the presence of #41.14, there was a significant (400%) increase in the fluorescence intensity compared to WT 14-3-3ζ alone (Fig. 6.5). This is indicative of increased exposed hydrophobicity as a result of the interaction between WT 14-3-3ζ and #41.14, presumably within the dimer interface. This supports the conclusions drawn from the phosphorylation assays (section 6.2.1), that #41.14 interacts with WT 14-3-3ζ and disrupts the dimer interface leading to the exposure of normally buried hydrophobic sites.

By way of a control, to ensure this major increase in fluorescence is due to the interaction between 14-3-3ζ and #41.14, the interaction of #41.14 with bis-ANS was assessed (Fig. 6.6). Upon addition of bis-ANS, there was a major increase in fluorescence implying there is an interaction between the two molecules. However, this fluorescence is quickly saturated (at 2μM of bis-ANS) and the fluorescence of bis-ANS at higher concentrations is quenched. The fluorescence intensity of #41.14 incubated with bis-ANS never reaches that of 14-3-3ζ (which experiences five times the fluorescence intensity when incubated with bis-ANS). Thus, this interaction between bis-ANS and #41.14, does not account for the large increase in fluorescence observed when 14-3-3ζ is incubated with #41.14. Even with the quenching effect of #41.14, there is a significant increase in fluorescence intensity when 14-3-3ζ is interacting with #41.14. Therefore, any interactions between #41.14 and bis-ANS are not responsible for the observed changes in fluorescence. Additionally, bis-ANS assays were undertaken using related small molecules with similar structures and fluorescence properties as #41.14 (data not shown). When titrated with bis-ANS, there was little difference in the observed fluorescence intensity of 14-3-3ζ in the presence or absence of these molecules. Therefore it is concluded that the observed increase in fluorescence seen in Fig. 6.7A is due to the interaction between 14-3-3ζ and #41.14 and is not as a result of potential hydrophobic interactions between #41.14 and bis-ANS.

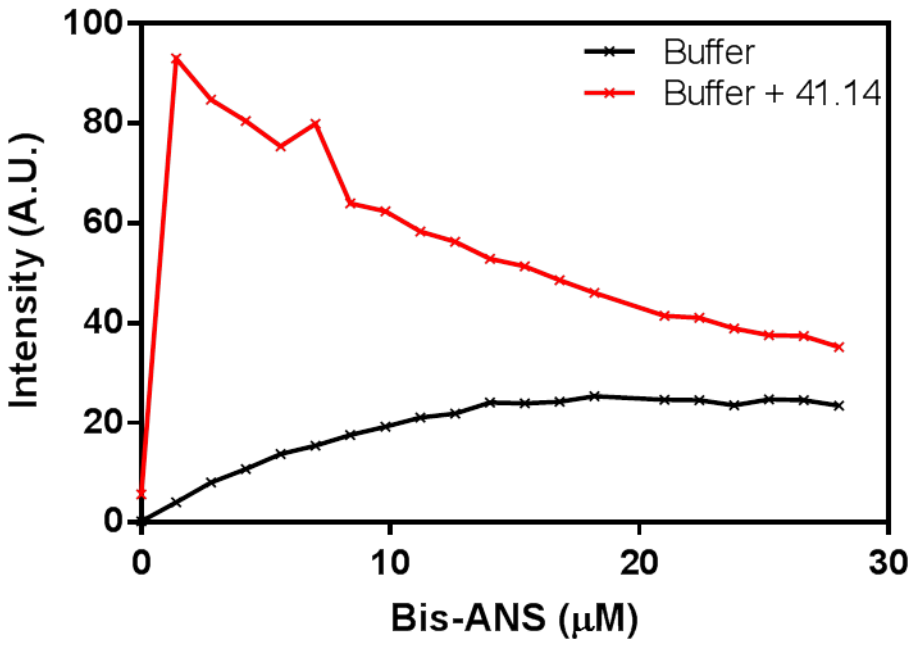

Figure 6.6: The interaction of bis-ANS (μM) with sphingosine mimic, #41.14 (2.8μM). The data were obtained by excitation at 385nm and acquiring the emission at 495nm. All experiments were corrected for the fluorescence of free bis-ANS and #41.14.

6.3 Chaperone action of WT 14-3-3ζ in the presence of sphingosine mimetics

The relative chaperone ability of WT 14-3-3ζ in the presence and absence of the sphingosine mimic, #41.14, was assessed against the amorphous aggregation of the thermally stressed target protein, alcohol dehydrogenase (ADH). As previously described the amorphous aggregation of ADH is induced after chelating the stabilising Zn^{2+} ions. The incubation of ADH with increased temperature ($42^{o}C$), leads to unfolding and eventual aggregation.

When ADH (14μM) is incubated alone, there is an observed increase in light scattering after 40 mins before reaching a plateau at 100 mins (Fig. 6.7A). The incubation of #41.14 (28μM) with stressed ADH, results in a shorter lag time, with the aggregation of ADH starting after 30mins, before reaching a plateau after 80 mins. Additionally the presence of #41.14, results in increased levels of the overall aggregation of ADH (Fig. 6.7B).

In the presence of WT 14-3-3ζ (14μM), there is an overall decrease in the measured light scattering, with a small delay in the onset of aggregation. At a 1:1 molar equivalence of ADH and WT 14-3-3ζ, the aggregation is suppressed by 53.7 ± 6.0% (Fig. 6.7C). The chaperone activity of WT 14-3-3ζ in the presence of #41.14 was assessed. WT 14-3-3ζ was incubated with #41.14 prior to the addition to stressed ADH. In this case, there was a delay in the onset of the aggregation of ADH with an increase in light scattering at 40 mins before reaching a plateau after 120 mins. The aggregation of ADH in the presence of WT 14-3-3ζ and #41.14 resulted in an overall decrease in the light scattering. At a 1:1 molar equivalence, the aggregation is suppressed by 55.4 ± 1.0% (Fig. 6.7C).

In summary, the incubation of ADH with #41.14 increases the overall aggregation of ADH. In the presence and absence of #41.14, WT 14-3-3ζ exhibits similar chaperone ability against the amorphous aggregation of ADH.

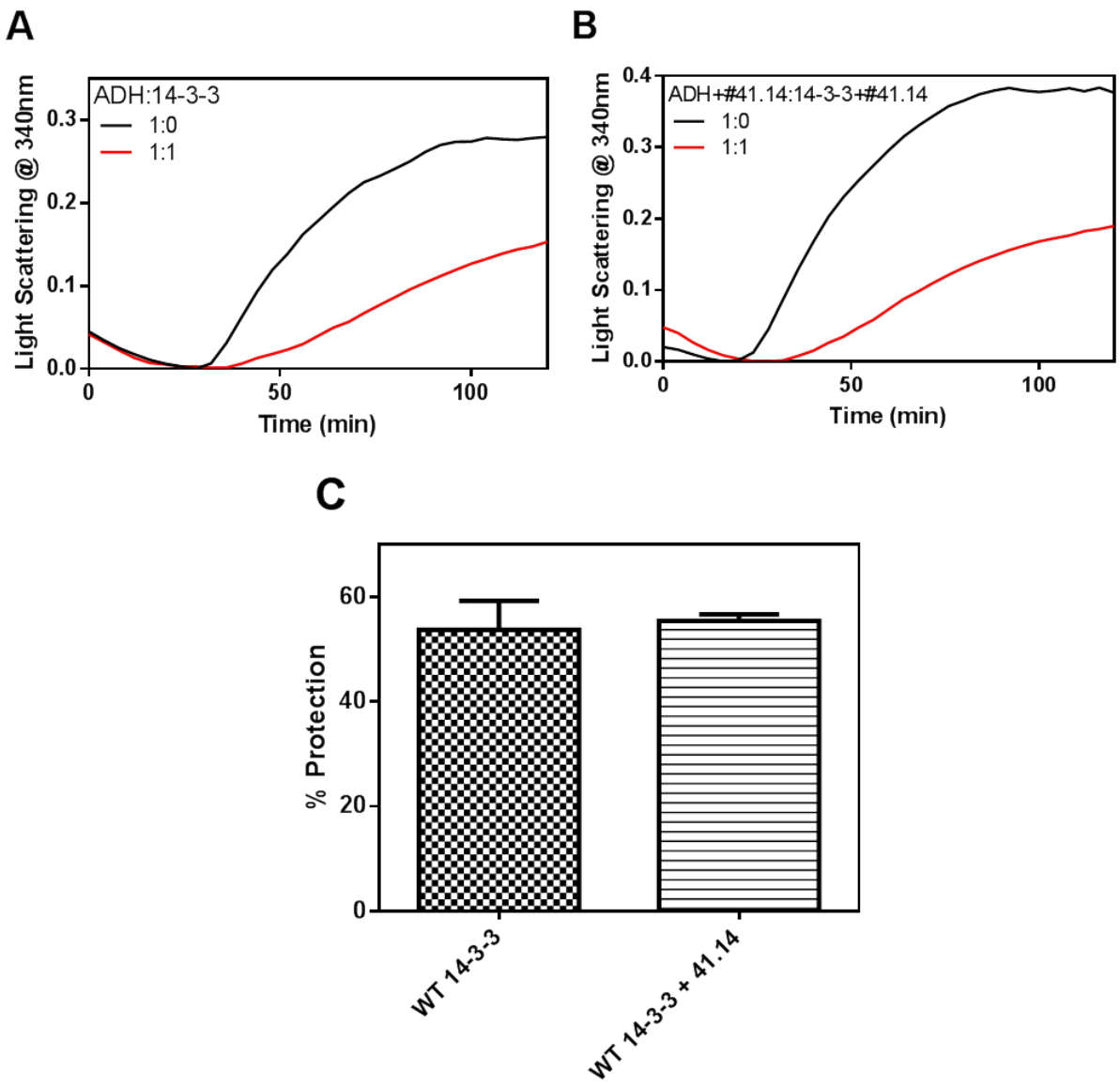

Figure 6.7: The chaperone action of WT 14-3-3ζ (14μM) in the (A) absence and (B) presence of the small molecule #41.14 (28μM) against the amorphous aggregation of ADH (14μM), in sodium phosphate buffer, pH 7.4, at 37^{o}C. (C) The percent protection afforded by WT 14-3-3ζ in the absence and presence of small molecule #41.14, against the amorphous aggregation of ADH at a 1:1 molar ratio of ADH: 14-3-3ζ. Experiments were repeated in triplicate and errors represented are the SEM of the light scattering data.

6.4 Discussion

Disruption of the 14-3-3ζ dimer can be achieved by the phosphorylation of S58. This phosphorylation is dependent on the physiological lipid, sphingosine (81). The incubation with sphingosine leads to the perturbation of 14-3-3ζ's dimer interface which allows kinases to access the buried S58 site. Furthermore, small molecule mimics of sphingosine have been identified. More recently it has been demonstrated that sphingosine mimics are also capable of allowing kinases to phosphorylate S58 (81). The destabilisation caused by the interaction between 14-3-3ζ and sphingosine mimics has not been fully characterised. Here, the characterisation of the interaction between 14-3-3ζ and the sphingosine mimic, #41.14, was undertaken.

It has been demonstrated here, that the incubation of 14-3-3ζ and #41.14 has little effect on the intrinsic tryptophan fluorescence of 14-3-3ζ, and 14-3-3ζ's thermostability. However, a concentration-dependent phosphorylation and increased exposed hydrophobicity (as measured by the binding of bis-ANS) was observed when 14-3-3ζ is incubated with #41.14, confirming that there is disruption of the 14-3-3ζ dimer in the presence of #41.14, which is comparable with the removal of salt-bridging sites in the dimer interface (Chapter 4). However, this interaction between 14-3-3ζ with #41.14 is less destabilising than that caused by the removal of the salt bridges. There is little change in the thermostability and intrinsic fluorescence of 14-3-3ζ and #41.14 implying that the interaction of the two species is transient which does not result in any permanent major structural changes of 14-3-3ζ. Upon dissociation of #41.14 from 14-3-3ζ, the protein is able to reform its native, stable dimeric structure as none of the interactions between monomers have been altered.

Even with this transient interaction between #41.14 and 14-3-3ζ, there is significant disruption which facilitates phosphorylation of 14-3-3ζ. Additionally, a major increase in bis-ANS fluorescence was observed: the minor disruption of the 14-3-3ζ protein caused by incubation with #41.14 allows the interaction of bis-ANS with exposed hydrophobic surfaces. Interestingly, dissociation of #41.14 from 14-3-3ζ, this does not affect the binding of bis-ANS to the protein. The interaction of bis-ANS with 14-3-3ζ may also lead to additional destabilisation allowing more bis-ANS molecules to interact. This increase in bis-ANS binding observed when 14-3-3ζ is incubated with #41.14, is comparable to changes observed in section 4.2.5, whereby the disruption of the dimer leads to increased exposed hydrophobicity, upon mutagenesis to remove inter-subunit salt-bridge interactions. In

summary, there is small structural destabilisation caused by the interaction of 14-3-3ζ and #41.14. The destabilisation most likely occurs in the dimer interface, enabling the phosphorylation of S58 by PKA.

In order to further investigate the role of the dimer interface in the chaperone action of 14-3-3ζ, the sphingosine mimic, #41.14, was employed. The chaperone action of WT 14-3-3ζ in the presence and absence of #41.14 was monitored against the amorphous aggregation of alcohol dehydrogenase. Despite the minor structural disruption caused by the incubation with #41.14, WT 14-3-3ζ has comparable chaperone activity in the presence or absence of #41.14.

It was previously shown that dimer disruption via mutagenesis of inter-subunit residues leads to an enhancement of chaperone action of 14-3-3ζ (Chapter 4). However no such enhancement is observed in the presence of #41.14. Previously, the effect of sphingosine on the chaperone action of 14-3-3ζ was investigated. Similarly, no enhancement to chaperone action was observed (98). Sphingosine is found to be elevated under cellular stresses and is significantly elevated in the brains of Alzheimer's patients (99). FTY720 is a FDA approved drug that was primarily used for the treatment of multiple sclerosis (100), and has been identified as a sphingosine mimetic with the ability to allow phosphorylation of S58 by PKA (81). In more recent years, it has become identified as possessing neuro-protective properties (100). In a Huntington disease mouse model, there was an observed reduction in the huntingtin protein aggregates after treatment with FTY720. However the mechanism by which FTY720 could provide such protective actions against protein aggregation was not determined. In light of the results presented here, it is feasible to postulate that the interaction of FTY720 leads to the modification of 14-3-3 (e.g. phosphorylation) which leads to the "activation" of 14-3-3 as a molecular chaperone. This would in turn prevent the interaction of 14-3-3 with its binding partners involved in cellular signalling. The characterisations undertaken with sphingosine mimic, #41.14, shows that the sole presence of #41.14 is not enough to enhance the chaperone activity. However the conformational change caused by the interaction of 14-3-3ζ and #41.14 could lead to further modification of the protein *in vivo* which could lead to significant dimer disruption.

It is concluded that the disruption caused by #41.14 is minor and the dimer interface has limited exposure to aggregating target proteins before dissociation of #41.14. In order for the chaperone capabilities of 14-3-3ζ to benefit from dimer disruption, the disruption probably requires the permanent introduction of a destabilising effect e.g. phosphorylation or removal

of a stabilising salt bridge, which would cause a shift in the monomer-dimer equilibrium of 14-3-3ζ, which may occur in an *in vivo* environment.

Chapter 7

The characterisation of the molecular chaperone action of 14-3-3ζ by small angle scattering techniques

7.1 Introduction

Recently, small angle scattering (SAS) studies using X-rays or neutrons have been widely used to investigate the structures of biological macromolecules under physiological conditions (101). Scattering studies make it possible to investigate intermolecular interactions such as assembly and arrangement of complexes and large-scale conformational changes (71). They have many advantages over x-ray crystallography studies. For example, obtaining crystals of multi-subunit assemblies can be difficult and cannot be achieved for all systems (102), with flexible and dynamic behaviours in protein complexes resistant to crystallisation (103). SAS has the ability to provide information at low resolution about the structures of assemblies and their interactions in solution (102). As the scattering data are information-poor, the best results are obtained when information yielded from scattering techniques are combined with structural data, e.g. from crystallography studies or NMR spectroscopy (102). The interaction of a molecular chaperone with an aggregating target protein is a very dynamic process, resulting in difficulty obtaining crystals of their complex. Potentially, therefore scattering techniques can provide low resolution information about the interaction between the molecular chaperone 14-3-3ζ and an aggregating target protein that cannot be obtained by other means.

In order for a scattering signal of a macromolecule to be visualised, its scattering length density must be different from that of its solvent environment (103,104). Small angle X-ray scattering (SAXS) requires contrast in electron density which is proportional to the atomic mass. As a result, the X-ray scattering for proteins in aqueous solution is rather low as a result of the similarities between the scattering cross-sections of a protein and its solvent, which are both composed of mainly light elements (102). The minor electron cloud surrounding

hydrogen atoms makes them particularly difficult to visualise via SAXS. Neutrons, however, interact with the atomic nuclei, therefore small angle neutron scattering (SANS) contrast requires a more complex nuclear parameter, the neutron scattering length density. In particular, the large difference in the scattering length density of hydrogen versus deuterium is very advantageous for the studies of biological systems (102). Although scattering length densities of different proteins are very similar, the contrast can be varied by introducing deuteration into the protein and/or solvent to study protein-protein interactions by neutron scattering techniques. This contrast variation allows the observation of the conformational changes to either component individually, without the scattering being affected by the presence of the other molecule. It has been utilised in many studies of biological macromolecules in solution or lipid phases (105-110). As shown in figure 7.1, the scattering length density of hydrogenated proteins is significantly different to that of deuterated proteins. This scattering length density of each component varies with differing D_2O concentrations. At a specific D_2O concentration whereby the scattering length density of the solvent is the same as the protein, the protein is indistinguishable from the background. This is known as the match point. Therefore, after subtraction of the scattering of the buffer, the scattering pattern only shows the other (non-D_2O matched) component. Therefore, deuterium labelling of one of the components and contrast variation allows visualisation of each individual component in a protein complex, allowing the extraction of shape and size information of each component (111).

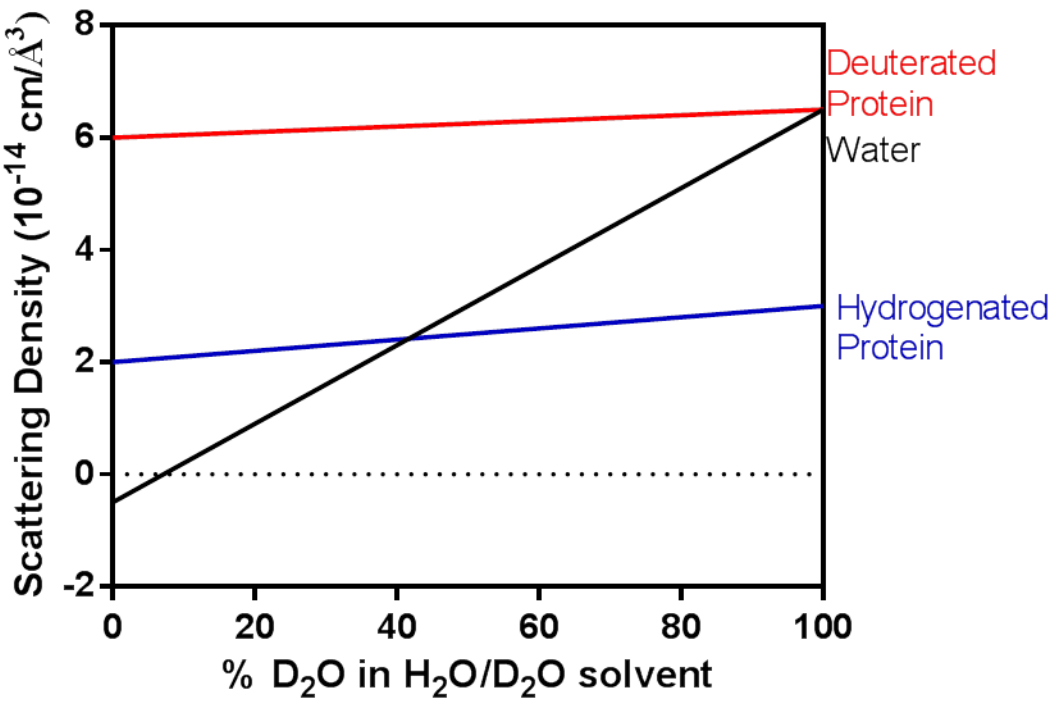

Figure 7.1: The scattering length density of protonated (blue) and deuterated (red) proteins and water (black), as a function of the D_2O/H_2O ratio of the solvent, adapted from (104). The match point is the D_2O concentration at which the scattering density of the protein is equal to that of water. For hydrogenated protein that is approximately 40%.

Solution scattering has advantages and disadvantages over high resolution techniques, such as crystallography or NMR, and is best used as a complementary structural technique. Unlike crystallography, small amounts of protein are required for solution scattering techniques. However, scattering data from 3-dimensional objects are information poor due to phase averaging of scattering signal, yielding a one-dimensional scattering pattern. In order to derive shape and structural information from the scattering data, pair distance distributions functions, p(r), are calculated as the inverse Fourier transformation of the normalised scattering intensity, I(q), which reflects the distribution of interatomic distances within a particle (Fig. 7.2). P(r) distributions are characteristic of molecular shapes e.g. globular proteins generally have bell shaped p(r) functions (Fig. 7.2). From a p(r) distribution of a protein, *ab initio* modelling, can then be undertaken to generate low resolution models of the protein's conformation in solution. *Ab initio* modelling of the scattering data, especially when combined with other known information about the molecules, leads to reliable shape and structure determination.

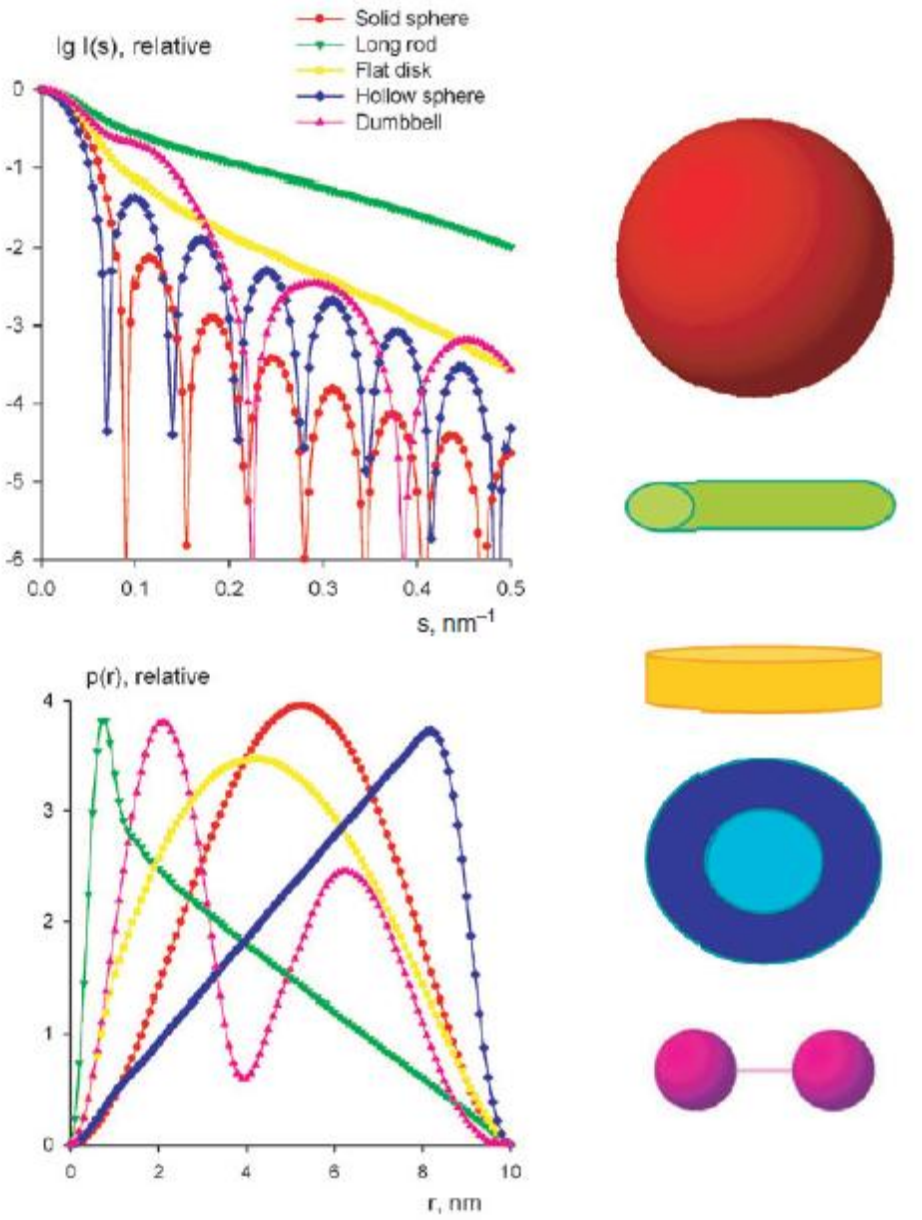

Figure 7.2: The scattering intensities and pair distance distribution plots for different geometric bodies (taken from (71)).

In order to characterise the interaction between the molecular chaperone 14-3-3ζ and aggregating target protein, small angle neutron scattering (SANS) experiments were undertaken. Alcohol dehydrogenase (ADH) was selected as the target protein, which has been well established to aggregate consistently upon removal of its constituent zinc ions via chelation by EDTA and with the ability of 14-3-3ζ to chaperone it (26). Contrast variation was utilised, so that the conformational changes of each protein during chaperone interaction could be observed.

7.2 Results: Determination of the best conditions for scattering experiments

Prior to commencing the scattering experiments to characterise the chaperone action of 14-3-3ζ, the optimal aggregation conditions needed to be determined. Major aggregation can obscure the interactions between two proteins due to excess scattering which would dominate the scattering pattern of the solution. In order to visualise the complex formed between the two proteins, the conditions were needed whereby the aggregation of the target protein is not excessive. However, the chaperone effect of 14-3-3ζ is most evident against slowly aggregating target proteins (65), in time-frames exceeding practical experimental duration within the allocated SANS beam-time. By reducing the incubation temperature of ADH, the initial lag period increases but the aggregation is better able to be controlled. The aggregation of ADH and the chaperone action of 14-3-3ζ was tested at 3 different temperatures, 42^{o}C, 37^{o}C and 33^{o}C (Fig. 7.3).

At 42^{o}C, there is an increase in light scattering of ADH after 30mins following the addition of EDTA, which reaches a plateau after 150mins (Fig.7.3A). The light scattering is suppressed by the presence of 14-3-3ζ by 46 ± 4% at a 1:2 molar equivalence. At 37^{o}C, there is an increase in light scattering after 40mins which reaches a plateau at 150mins (Fig. 7.3B). The aggregation is suppressed by the presence of 14-3-3ζ by 70 ± 1% at a 1:2 molar equivalence. At 33^{o}C, there is an increase in light scattering after 60mins, which reaches a plateau after 200mins (Fig. 7.3C). The light scattering is suppressed in the presence of 14-3-3ζ by 86 ± 2% at a 1:2 molar equivalence of ADH:14-3-3ζ.

The chaperone assay results show an increased lag time of aggregation of ADH with a decrease in temperature (Fig. 7.3D). It is likely that the 14-3-3ζ chaperone interacts with the unfolding ADH during this lag time, before visible aggregation commences. This is also consistent with a lower magnitude of the final light scattering at lower temperature. Thus, the slower aggregation of ADH allows 14-3-3ζ to act as a more effective chaperone (as discussed in chapter 4), resulting in almost complete suppression of aggregation at 33^{o}C. The difference in suppression between 2 and 3 molar equivalence of 14-3-3ζ at 33^{o}C is minimal and it is likely that the suppression of aggregation seen at 33^{o}C is the maximum level of suppression of aggregation that 14-3-3ζ is able to provide. Therefore, it was concluded that the optimal conditions for the scattering experiments were at 33^{o}C and a 1:3 molar ratio of ADH: 14-3-3ζ.

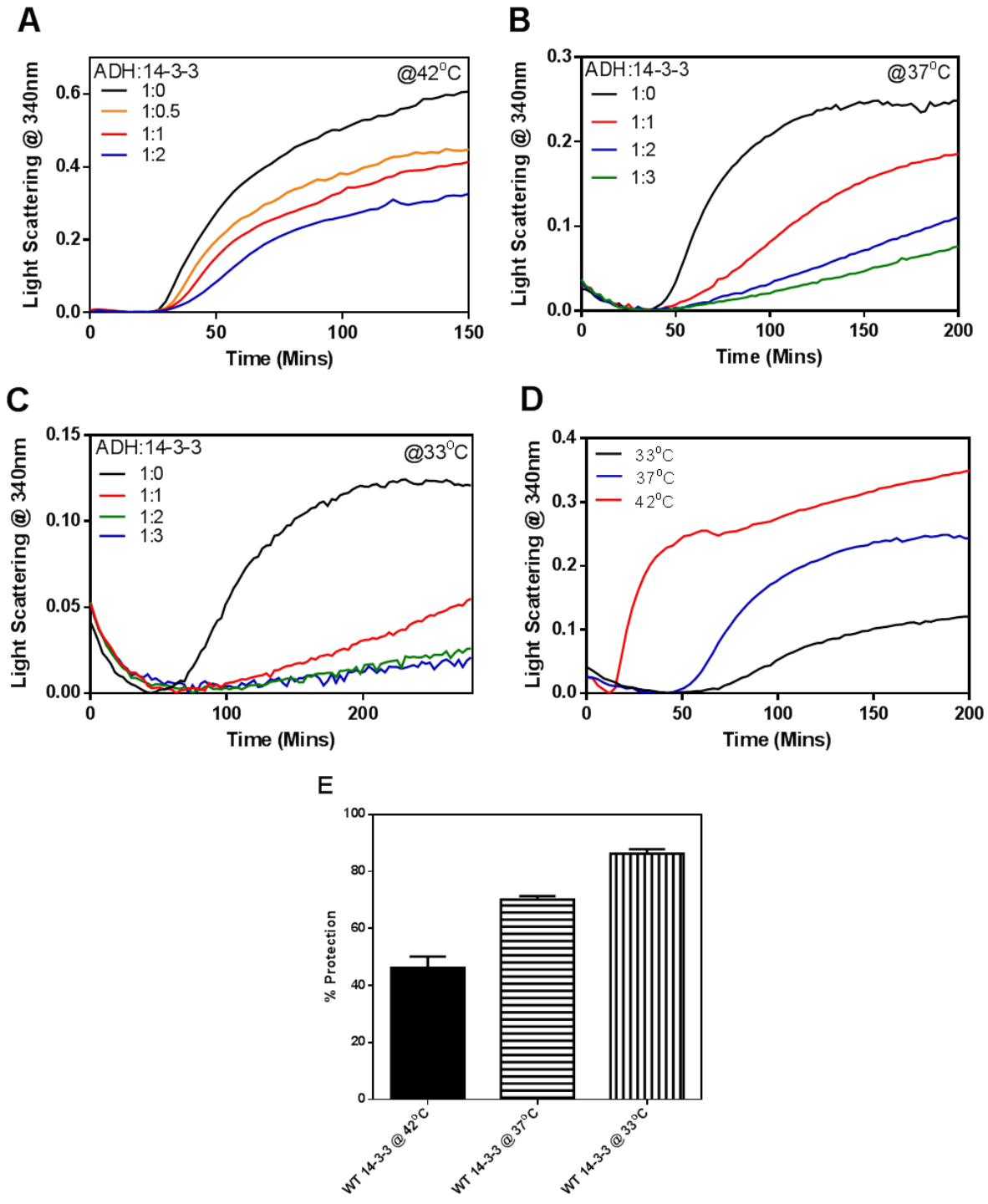

Figure 7.3: The chaperone activity of 14-3-3ζ against the amorphous aggregation of ADH (28μM) upon addition of EDTA (2mM) at (A) 42°C, (B) 37°C and (C) 33°C. (D) The aggregation of ADH at 33°C, 37°C and 42°C (E) The percent protection of WT 14-3-3ζ at a 1:2 molar equivalence of ADH:14-3-3 at 42°C, 37°C and 33°C. Assays were performed in triplicate and errors shown are the SEM of the light scattering data.

7.3 Results: Small angle x-ray scattering

Small angle X-ray scattering (SAXS) experiments were undertaken to monitor the chaperone activity of 14-3-3ζ when interacting with misfolded target protein, alcohol dehydrogenase (ADH). In order to prevent any scattering caused by excess aggregation, the best conditions for the SAXS experiments were pre-determined to be 33^{o}C with a 1:3 molar ratio between ADH and 14-3-3 (section 7.2.1).

The data was collected every 30 mins over four hours and analysed via the ATSAS suite of programs (from http://www.embl-Hamburg.de/ExternalInfo/Research/Sax/index.html) (112). If no change in scattering was observed over the measurement period, the scattering data were averaged. The buffer signal was subtracted to give a final scattering trace of the proteins. Native ADH, 14-3-3ζ and the ADH:14-3-3ζ complex had no change in scattering over the four hours of measurement. Misfolded ADH (after incubation with EDTA) showed minor changes to its scattering profile and its individual data sets were therefore treated differently.

To obtain shape and size data, p(r) functions were calculated for native ADH (in the absence of EDTA) and 14-3-3ζ (Fig. 7.4A and B). This gives information on the D_{max} (the maximum length of the species) and the shape envelope of the protein molecule. Native ADH has a symmetrical bell-curve distribution, which implies a globular protein with a slightly elliptical shape (Fig. 7.4A). 14-3-3ζ has a slightly elongated bell-curve distribution, again implying a globular protein with a elongated shape (Fig. 7.4B). Both distributions correlate well with the known crystal structures for both proteins.

Ab initio modelling was generated and compared with the crystal structures of the proteins (Fig. 7.4C and D). There is a good correlation between the *ab initio* models and the crystal structures.

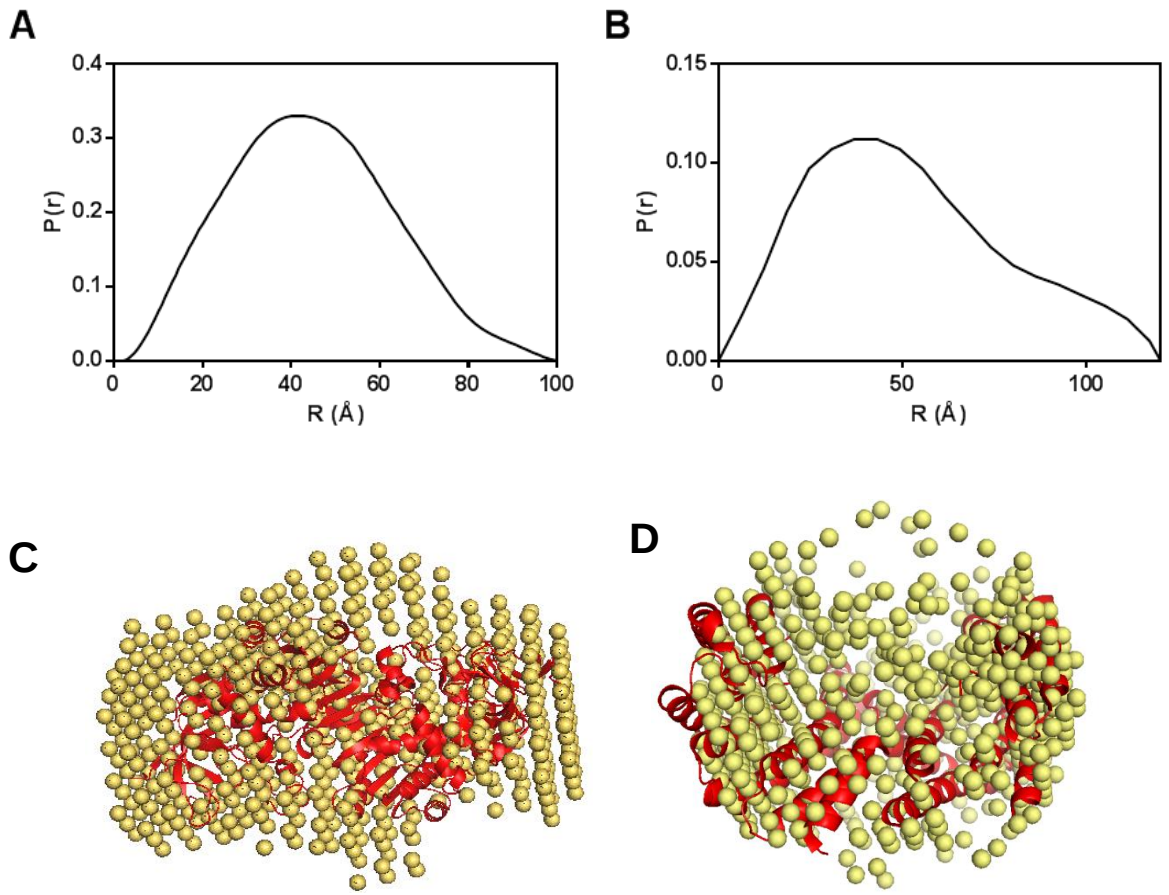

Figure 7.4: The P(r) distributions of (A) native ADH and (B) 14-3-3ζ. The ab initio modelling of the scattering data overlaid with the crystal structures of (C) native ADH and (D) 14-3-3ζ as determined using the Dammin software from the ATSAS suite (113).

The misfolding of alcohol dehydrogenase was examined and p(r) distribution functions were calculated. A significant increase in the D_{max} was observed due to destabilisation of the protein resulting in the removal of its constituent zinc ions. There is still retention of some globular structure, represented by the peak at 50Å (Fig. 7.5A). This implies that partial unfolding and elongation of the protein, occurs with a significant proportion of the protein retaining a relatively native-like globular fold. The D_{max} increases with time to a maximum of 800Å after four hours (240mins) of incubation. The slow increase in D_{max} is consistent with previous light scattering studies under these conditions (33^{o}C and low ADH concentration), whereby slow unfolding of the protein rather than rapid aggregation occurs (Fig. 7.3C).

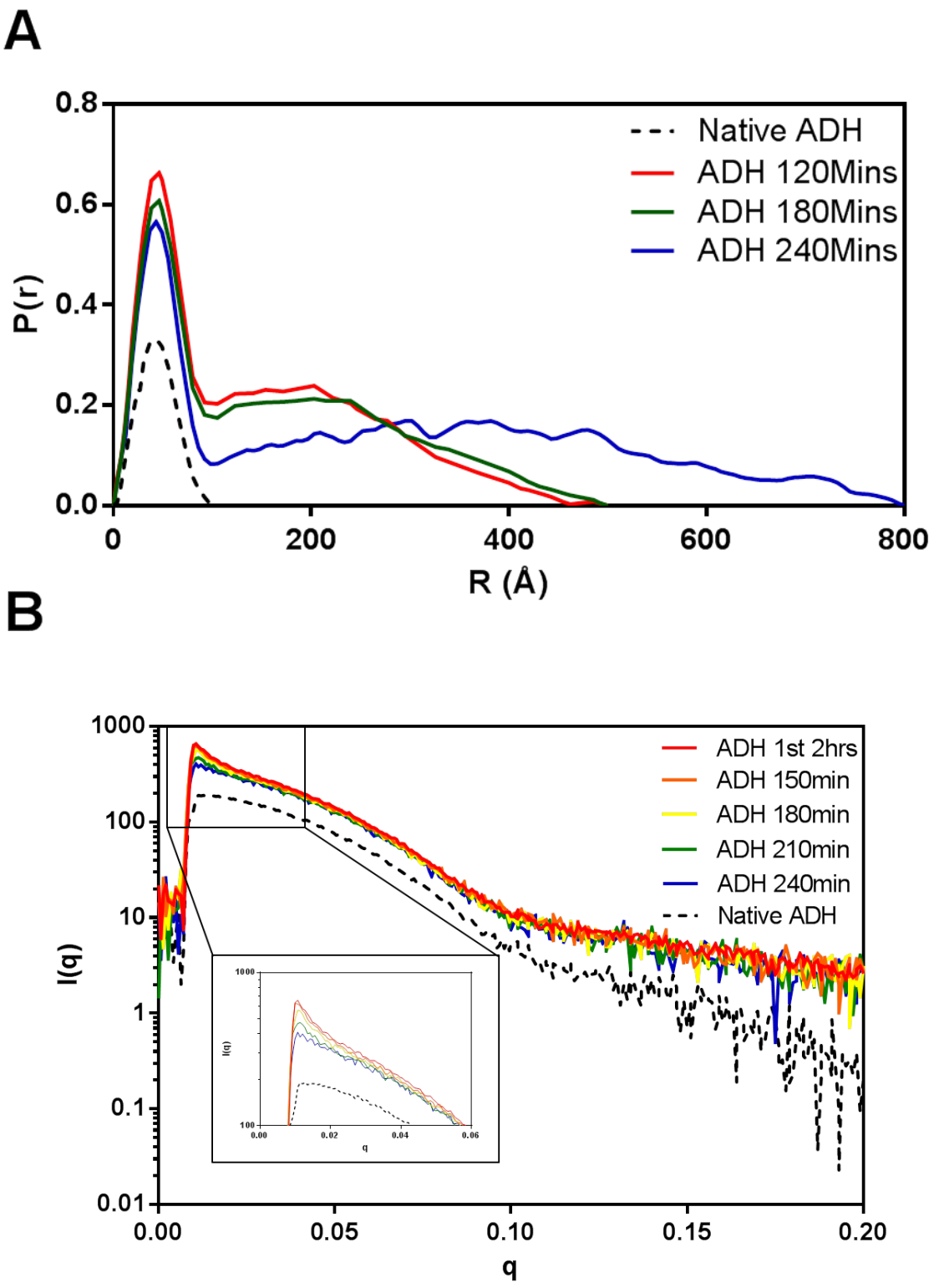

Figure 7.5: (A) The P(r) distributions of amorphously aggregating ADH with time. (B) The scattering profiles of aggregating ADH with time, showing a reduction in the overall intensity (inset) of the scattering at low q with time.

Major aggregation of ADH was not detected in the SAXS data. Rather than a progressive increase, a reduction in the scattering intensity at low q was observed in scattering profiles of misfolded ADH (Fig. 7.5B). Large aggregates were visually detected in the sample after the measurements were taken. This implies that as the protein misfolds and elongates the larger protein aggregates exceed the SAXS length scale and eventually fall out of solution.

Misfolding ADH in the presence of 14-3-3 produces a P(r) distribution with a D_{max} of 350Å after four hours (Fig. 7.6). This reduction of the D_{max} confirms that there is an interaction between the two proteins. This D_{max} is comparable with the early unfolded species of ADH observed after the addition of EDTA. This implies that 14-3-3ζ interacts with ADH early to prevent major aggregation. Thus, 14-3-3ζ interacts with a partially unfolded, intermediate state of ADH.

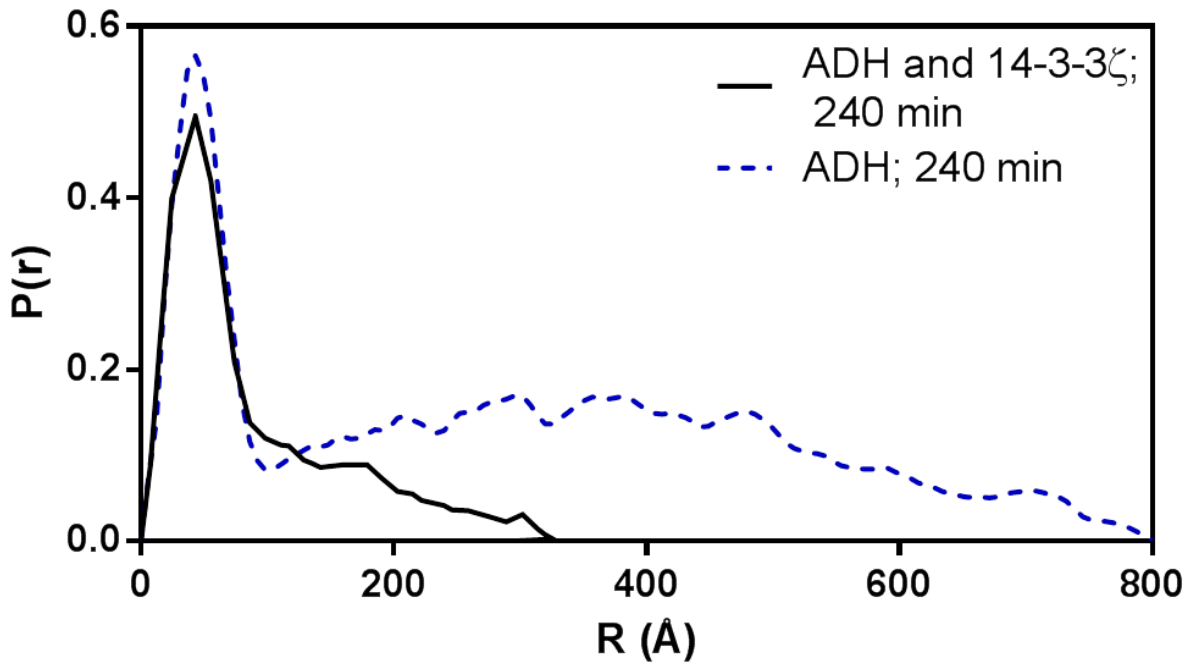

Figure 7.6: The P(r) distribution of aggregating ADH (28μM) in the presence (black) and absence (blue) of 14-3-3ζ (at a 3x molar equivalence) at 240 minutes.

In conclusion, the SAXS data show that when stressed, by chelation and removal of its constituent zinc, ADH misfolds to form an extended structure, but with significant retention of globular native-like conformation. The molecular chaperone 14-3-3ζ interacts with ADH in its partially folded molten globule state to prevent the formation of the large aggregates. The SAXS data shows that there is an interaction between 14-3-3ζ and misfolding ADH which is established very swiftly as we see no change in the scattering after 30 minutes of measurement. These data are supported by the previous light scattering data (Chapters 3 and 4). However, specific details about the conformational changes of 14-3-3ζ or how it interacts with ADH cannot be determined from the SAXS data alone.

The X-ray scattering measurements indicate that a viable protocol has been developed to study the interaction of 14-3-3ζ with ADH, by small angle neutron scattering (SANS). In order to determine the nature of the interaction between misfolding ADH and 14-3-3ζ and to monitor any conformational changes undergone by 14-3-3ζ whilst chaperoning, contrast-variation SANS experiments were undertaken using deuterated 14-3-3ζ.

7.4 Results: Small angle neutron scattering

Small angle neutron scattering (SANS) experiments were undertaken to monitor the chaperone action of 14-3-3ζ whilst interacting with the amorphously aggregating ADH, in a manner similar to the collection of SAXS data. Using contrast variation, we are able to monitor the conformational changes of 14-3-3ζ and ADH separately when interacting with each other. Contrast variation was possible using deuterated 14-3-3ζ.

7.4.1 Biophysical characterisation and chaperone activity assays of deuterated 14-3-3ζ

Deuterated 14-3-3ζ (d14-3-3ζ) was expressed and purified at the national deuteration facility at ANSTO, Lucas Heights, NSW, by Dr Agata Rekas. To determine if the deuteration has altered the structure and function of 14-3-3ζ, biophysical characterisation and chaperone assays were undertaken.

The circular dichroism spectrum of d14-3-3ζ was obtained and compared to that of hydrogenated 14-3-3ζ (h14-3-3ζ) (Fig. 7.7A). d14-3-3ζ has a similar alpha helical profile compared to h14-3-3ζ. There was a minor reduction of the mean residue ellipticity for d14-3-3ζ implying a small reduction in the helical content, which could indicate slight destabilisation of the protein.

The intrinsic tryptophan fluorescence spectrum of d14-3-3ζ was obtained and compared with h14-3-3ζ (Fig. 7.7B). There is a minor decrease in the maximum wavelength and a significant increase in the fluorescence intensity for deuterated 14-3-3ζ compared to h14-3-3ζ. The quenching of the tryptophan signal in proteins is predominantly a result of the surrounding peptide bonds (97). The quenching by NH_2 groups, has been demonstrated to be less effective when the hydrogens are replaced with deuterium (114). Therefore this fluorescence intensity increase is most likely a result of the incorporation of deuterium into the protein rather than any major protein conformational changes.

The thermostability of d14-3-3ζ was determined by monitoring the intrinsic tryptophan fluorescence with increasing temperature (over the range of 37-80^{o}C) (Fig. 7.7C). The melting temperature of d14-3-3ζ was determined to be 60^{o}C. This is marginally lower than the melting temperature for h14-3-3ζ, which is 63^{o}C. Similar results have been illustrated with other proteins (115) and it implies that the minor destabilisation of 14-3-3ζ is a result of deuteration.

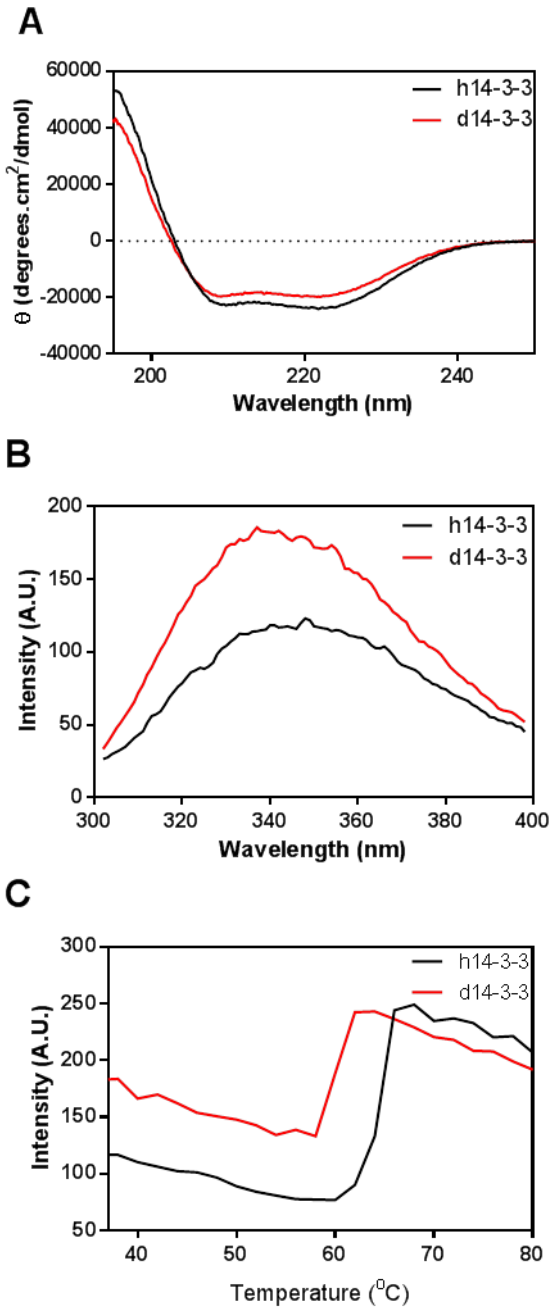

Figure 7.7: (A) The circular dichroism spectra of hydrogenated 14-3-3ζ (black) compared with deuterated 14-3-3ζ (red) between 195 and 250nm represented as the average of three accumulations. (B) The intrinsic fluorescence spectrum of hydrogenated 14-3-3ζ (black) compared with deuterated 14-3-3 (red) after excitation at 295nm with the emission acquired between 300 and 400nm. (C) The thermostability profile of hydrogenated 14-3-3ζ (black) compared with deuterated 14-3-3ζ (red) obtained by monitoring the intrinsic tryptophan fluorescence at 340nm between 37-80^{o}C.

The chaperone activity of d14-3-3ζ was tested and compared to h14-3-3ζ against the amorphous aggregation of ADH (Fig. 7.8). The protection afforded by hydrogenated 14-3-3ζ at a 1:1 molar equivalence of ADH:14-3-3ζ is 32 ± 2%. The protection afforded by deuterated 14-3-3ζ at a 1:1 molar equivalence of ADH: 14-3-3ζ is 35 ± 6%. Thus, deuteration of 14-3-3ζ does not affect its function, with a comparable percent protection afforded against the amorphous aggregation of ADH.

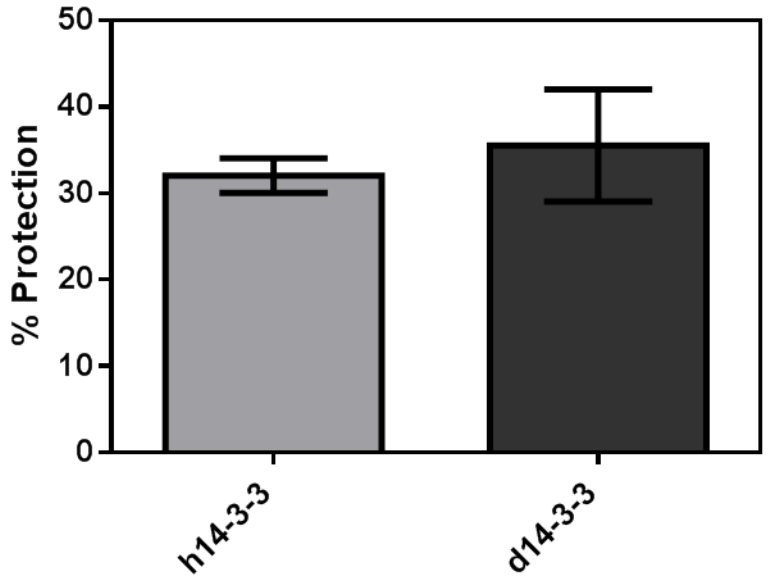

Figure 7.8: The percent protection provided by h14-3-3ζ (grey) and d14-3-3ζ (black) against the amorphous aggregation of ADH (28μM) at a 1:1 molar equivalence of ADH: 14-3-3ζ at 42^{o}C in 50mM sodium phosphate buffer, pH 7.4. The experiments were repeated in triplicate and the errors represent the SEM of the light scattering data.

In summary, the biophysical and chaperone characterisation of d14-3-3ζ shows that the introduction of deuterium into 14-3-3ζ leads to some minor structural alteration. However, this does not prevent the protein from maintaining the appropriate conformation and acting as an effective molecular chaperone. Therefore, the use of d14-3-3ζ in the scattering experiments should provide an effective model for observing any conformational changes of 14-3-3ζ whilst acting as a molecular chaperone.

7.4.2 Small angle neutron scattering of native 14-3-3ζ and ADH

The SANS experiments were undertaken to monitor the chaperone activity of 14-3-3ζ when interacting with the misfolded target protein, ADH. The conditions utilised were 33^{o}C with a 1:1 and a 1:2 molar ratio of ADH and 14-3-3ζ. The ratio of 14-3-3ζ is reduced from the SAXS experiments. This is to ensure that the maximum amount of 14-3-3ζ is interacting with the aggregating protein and not existing in the non-chaperoning state, enabling any conformational changes undergone by 14-3-3ζ to be characterised via SANS. The unfolding of ADH was initiated with the addition of EDTA to a final concentration of 2mM, as described in chapters 3 and 4. The contrast match points of ADH and deuterated 14-3-3ζ were calculated using the online algorithm (http://research.mmb.usyd.edu.au/NCVWeb):

14-3-3ζ, deuteration level 0.67; 97.1% D_2O match point

Alcohol dehydrogenase, hydrogenated; 41.9% D_2O match point

In order to visualise each protein component, different D_2O concentrations were used (0%, 40% and 100%) for samples with both protein species present. The SANS data were collected over a wide q range (utilising 10m and 1.3m sample detector distance settings). The scattering of native samples was collected for 30 min at each detector setting. After the initiation of ADH unfolding, the samples were measured four times over a period of 12 hours at both detector settings. The accumulated data were analysed using the ATSAS suite of programs available from http://www.embl-Hamburg.de/ExternalInfo/Research/Sax/index.html. The data collected from both sample-detector distance settings, were merged and time averaged if there was no change in scattering over the measurement period. The buffer was subtracted to provide a final scattering trace.

Firstly, the radius of gyration (R_g) and p(r) were determined for native ADH (Fig. 7.9) and d14-3-3ζ (Fig. 7.10), as described in section 7.3, in 100% and 40% D_2O respectively. The p(r) distributions compared well with those obtained by SAXS (section 7.3). The deuteration of 14-3-3ζ and the dissolution at varying D_2O concentrations did not significantly change the shape and structure of the two proteins.

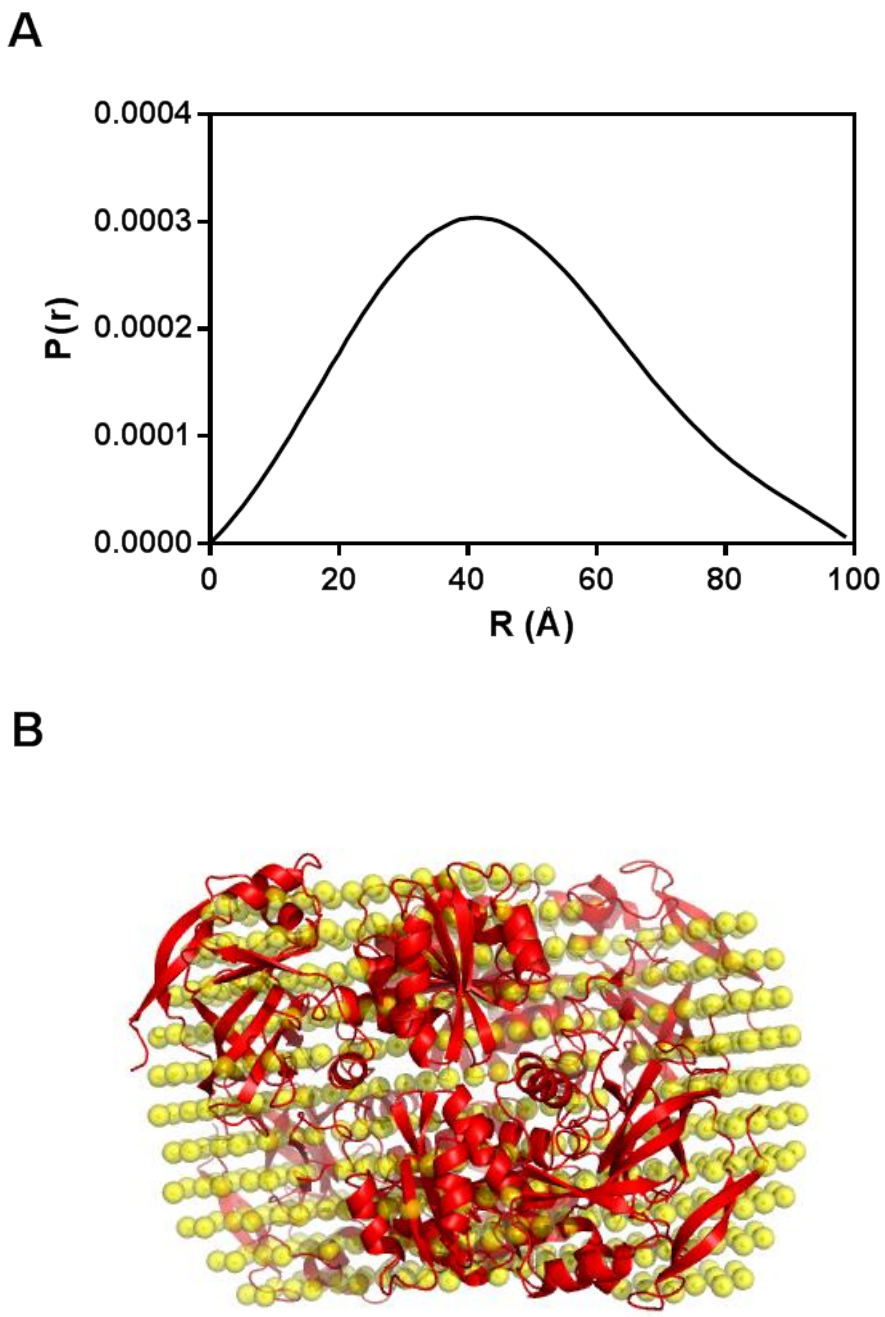

Figure 7.9: (A) The pair distance distribution (p(r)) of native ADH at 100% D_2O. (B) The low resolution ab initio model of native ADH tetramer overlayed with the X-ray crystal structure.

The p(r) of 14-3-3ζ reveals a larger molecule than predicted from crystal structures. Oligomer analysis (ATSAS component program) indicates the presence of a tetrameric 14-3-3ζ component, comprising of approximately a quarter of the total protein volume. The tetrameric form of 14-3-3ζ used in the analysis has stacking between the bottoms of the 14-3-3ζ dimers with the arrangement shown in Figure 7.10B (which was obtained from x-ray

crystal structures). This Oligomer analysis provides some insight into the alignment of the dimers to form this tetrameric structure. The presence of the tetrameric form of 14-3-3ζ results in a polydisperse solution. This polydispersity makes the modelling of these species problematic, due to the averaging of the scattering signal. Therefore, models generated using the entire q range data represent an average of the dimeric and tetrameric 14-3-3ζ structures present in the sample.

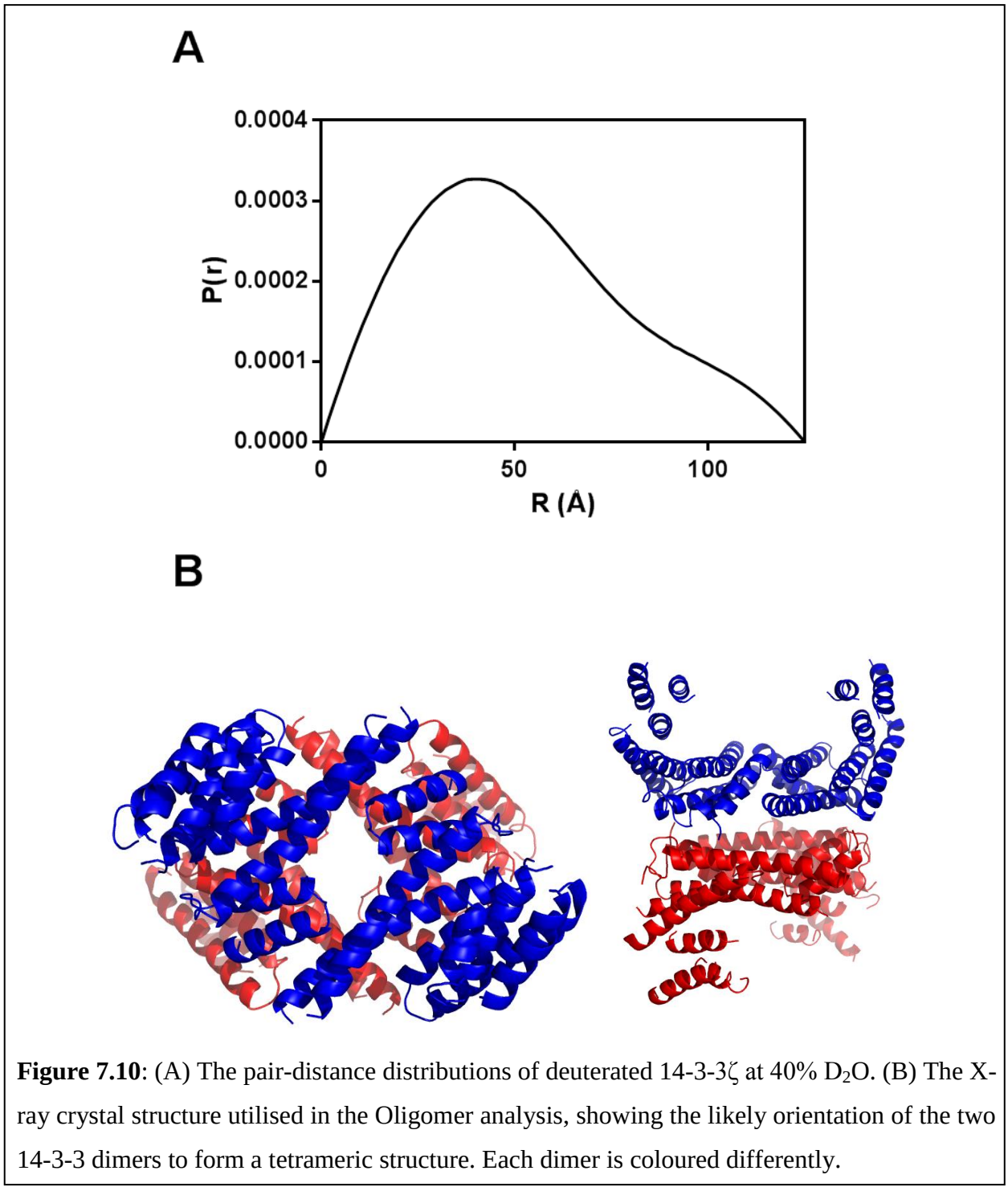

Figure 7.10: (A) The pair-distance distributions of deuterated 14-3-3ζ at 40% D_2O. (B) The X-ray crystal structure utilised in the Oligomer analysis, showing the likely orientation of the two 14-3-3 dimers to form a tetrameric structure. Each dimer is coloured differently.

7.4.3 Monitoring the aggregation of ADH by SANS

The aggregation of ADH was monitored by SANS at 100% D_2O and 33^oC. In order to measure the approximate size of each protein species and detect any size changes, the radius of gyration (R_g) was estimated using Guinier analysis. The R_g values of ADH following addition of EDTA exhibit an increase in size over time (Table 7.1), implying an unfolding and expansion of ADH. In examining the change of R_g values with time, a very rapid increase in R_g that reaches a plateau after an hour, before the apparent size decreases after 12 hours. This reduction is most likely a result of the larger aggregates exceeding the SANS length scale as they accumulate and precipitate. The scattering profile confirms this as it shows a minor increase in intensity with time, before a subsequent decrease after 12 hours (Fig. 7.11A). Additionally, large precipitates were observed visually in the samples after the scattering measurements had been acquired.

Table 7.1: A table showing the radius of gyration (R_g) values of native and unfolding ADH in 100% D_2O over time, as estimated by Guinier analysis.

Protein Species	**R_g(Å)**
Native ADH	**38.0**
ADH + EDTA (after 1hr)	**59.4**
ADH + EDTA (after 3 hr)	**58.9**
ADH + EDTA (after 5 hr)	**59.3**
ADH + EDTA (After 12hrs)	**45.8**

P(r) distributions were also determined (Fig. 7.11B), which showed a significant increase in the size of ADH as it unfolds and aggregates. Similarly to the SAXS studies (section 7.3) there is some retention of the globular protein. With time, there is a decrease in the globular protein content, with the development of a long, unstructured polypeptide chain. However, the elongation of the protein does not occur to the same extent as observed via SAXS, with the protein size stabilising with a D_{max} of 550Å (compared to 800Å observed via SAXS). After overnight incubation, there was an overall decrease in both the P(r) and scattering intensities. This corresponds to the precipitation of the larger aggregate species which are too large for the SANS length scale. Aggregation was visually observed in the sample during removal.

The presence of D_2O does affect the ability of ADH to aggregate, with a reduction in the overall size of the elongated protein at 100% D_2O (Fig. 7.11B), compared to that at 0% D_2O, obtained via SAXS (Fig. 7.7A). Additionally, the scattering profiles have less alteration in intensity with the initiation of aggregation, implying slower aggregation of ADH when incubated in D_2O-based buffer.

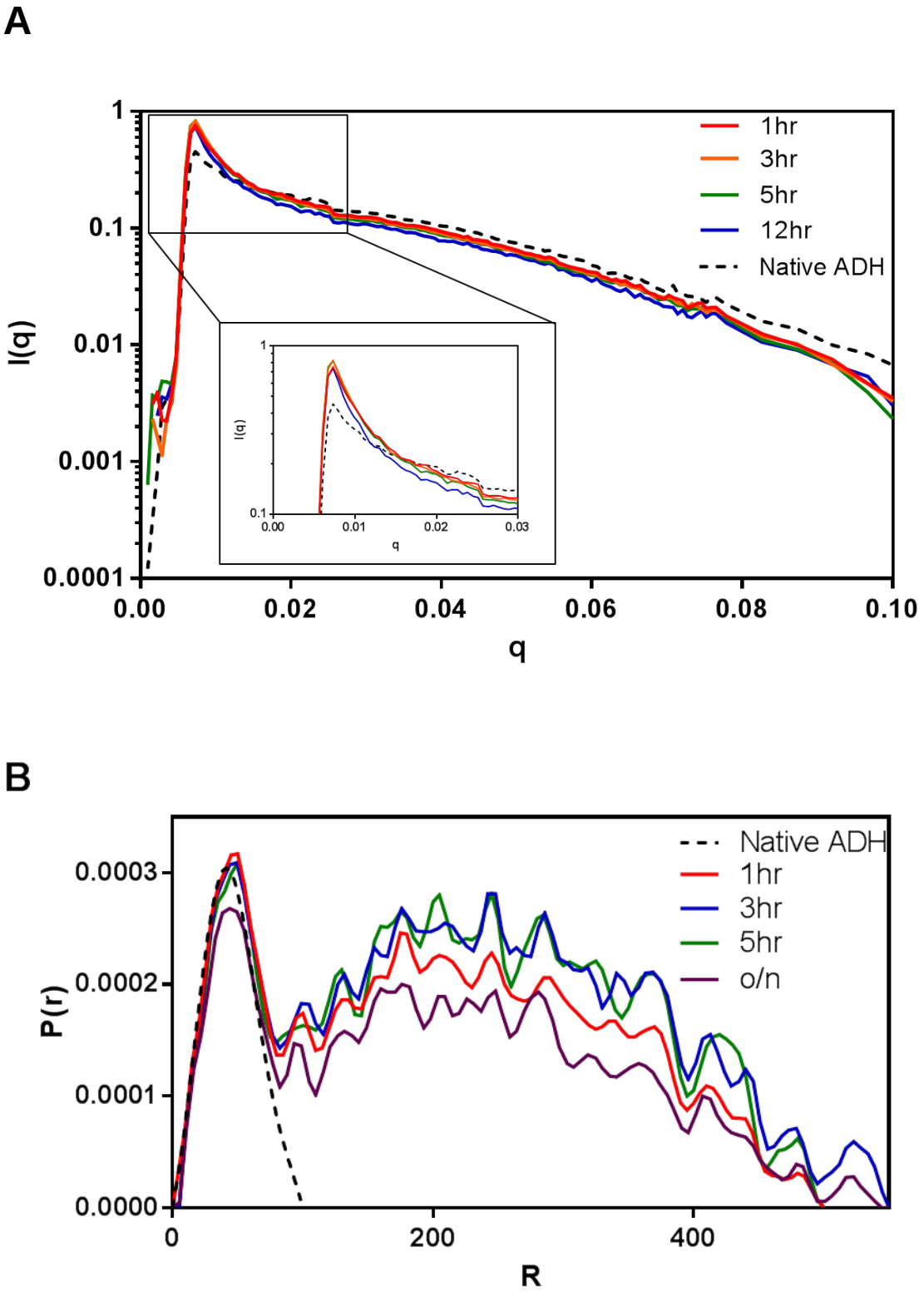

Figure 7.11: (A) The scattering profiles of aggregating ADH with time, showing the decrease in scattering intensity as ADH precipitates out of solution. (B) The pair-distance distribution of aggregating alcohol dehydrogenase with time at 100% D_2O.

7.4.4 Monitoring the interaction between aggregating ADH and 14-3-3ζ by SANS

The interaction between the 14-3-3ζ and ADH was monitored by SANS. Unlike SAXS, the changes of each individual component can be monitored using contrast variation. ADH was monitored at 100% D_2O and deuterated 14-3-3ζ at 40% D_2O.

The mixture of both proteins was monitored by SANS prior to the addition of EDTA, to ensure no prior interaction between the two protein species (Fig. 7.12). From their p(r) distributions (Fig. 7.12), the native components were of a similar size and shape compared to the native proteins alone (Fig. 7.9 and 7.10), indicating no interaction and/or aggregation prior to the addition of EDTA. Consequently, there does not appear to be any interaction occurring between 14-3-3ζ and ADH that results in structural changes of either species under native conditions (Fig. 7.12).

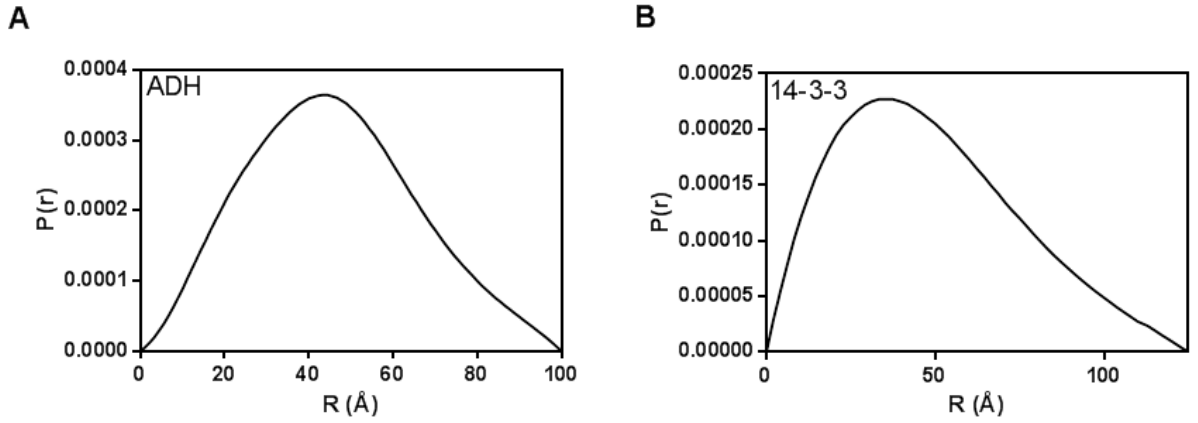

Figure 7.12: The p(r) distributions of the protein mixture at (A) 100% and (B) 40% D_2O, representing ADH and 14-3-3ζ respectively, prior to the addition of EDTA to the mixture of both proteins (at a 1:1 molar ratio).

The aggregation of ADH in the presence of 14-3-3ζ was monitored at 100% D_2O, at a 1:1 and a 1:2 molar ratio of ADH:14-3-3ζ for 3 hours upon addition of EDTA. The R_g and p(r) distributions were determined (Fig. 7.13). At both ratios of ADH:14-3-3ζ, an increase in protein size was observed compared to that of native ADH alone. However, the D_{max} of the system was significantly lower than that of aggregating ADH in the absence of 14-3-3ζ, with a D_{max} value of 150Å after 4 hours. This indicates that there is an interaction with 14-3-3ζ which

results in a reduction in the size of ADH. Due to the significant relative reduction in the protein size, it is likely that 14-3-3ζ interacts early along the off-folding pathway of ADH, preventing the formation of large amorphous ADH aggregates (as observed in section 7.3).

At a 1:1 ratio of ADH:14-3-3ζ, the D_{max} of the system did not change with time. However there was a minor reduction in the globular ADH protein component observed with time (Fig. 7.13A). This is indicative that even though 14-3-3ζ is acting as a chaperone, it is insufficient to fully prevent unfolding of ADH as observed in the light scattering assays (Fig. 7.3).

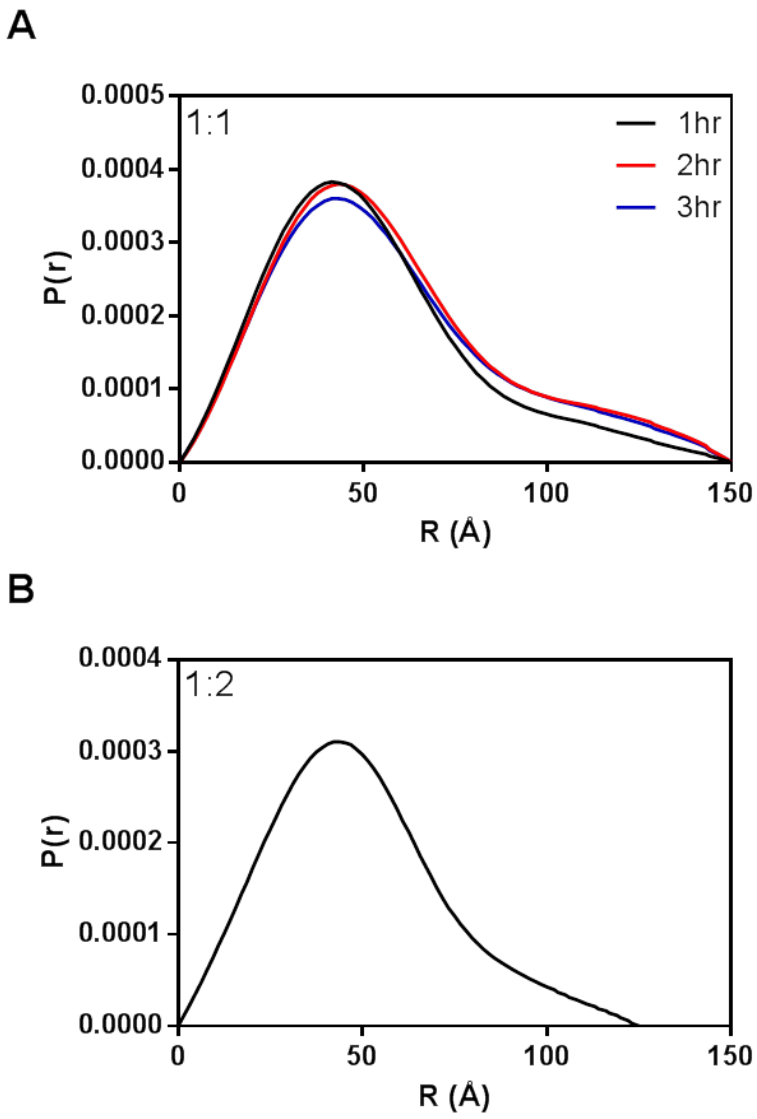

Figure 7.13: The p(r) distributions of destabilised ADH in the presence of the molecular chaperone 14-3-3ζ at a 1:1 (A) and a 1:2 (B) molar ratio of ADH:14-3-3ζ at 100% D_2O with time.

By increasing the quantity of 14-3-3ζ (i.e. using a 1:2 molar ratio of ADH:14-3-3ζ) and repeating the experiment, the chaperone was more effective, leading to less unfolding of ADH, with a D_{max} of 120Å. There was no change in the scattering intensity and the p(r) distributions over time, illustrating that the increased molar ratio of 14-3-3ζ is more efficient at preventing the aggregation of ADH. This further confirms that there is an interaction between 14-3-3ζ and ADH, which results in the prevention and stabilisation of the unfolded ADH protein. Low resolution *ab initio* model of the intermediately folded state of ADH was obtained (Fig. 7.14), which shows unfolding and elongation of a region of the protein with the remainder in the native globular state.

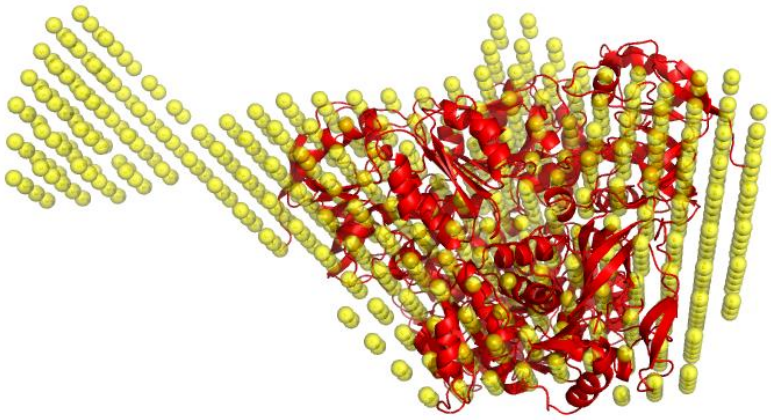

Figure 7.14: The low resolution model of ADH at 100% D_2O, in the presence of a molar equivalence of 14-3-3ζ. The crystal structure of native ADH is for the comparison to show the overall elongation of the intermediately folded state of ADH.

Conformational changes of 14-3-3ζ whilst chaperoning were monitored by SANS at 40% D_2O. The R_g and p(r) values were obtained. The p(r) distribution at a 1:1 molar equivalence of ADH:14-3-3ζ (Fig. 7.15A) shows little change in the size and shape, with the p(r) distribution similar to that of 14-3-3ζ alone. There is an initial decrease in the intensity, likely due to the addition of EDTA, which results in a minor dilution of the protein solution. As described earlier, native 14-3-3ζ is shown to possess a tetrameric component. Oligomer analysis was utilised, indicating that there was a greater tetrameric component present with the higher molar ratio of 14-3-3ζ (Fig. 7.15C). No monomeric 14-3-3ζ was detected in the scattering profiles when 14-3-3ζ was interacting in a chaperone manner with the aggregating ADH.

A

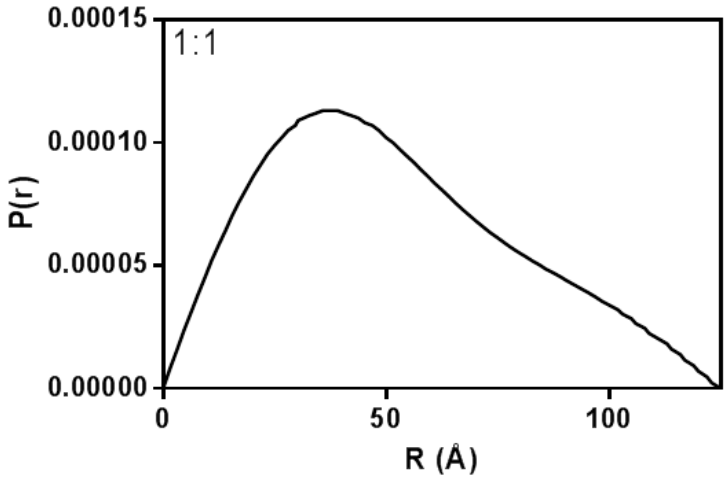

B

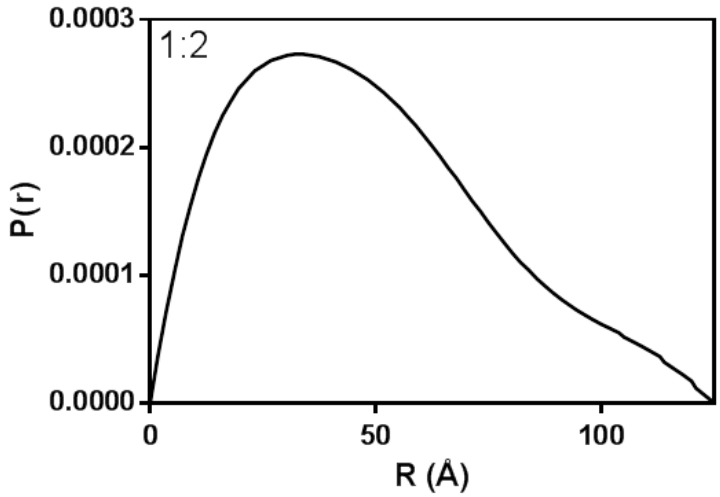

C

Ratio of ADH:14-3-3	R_g (Å)	% Dimer	% Tetramer
1:1	28.9	71.4	28.6
1:2	29.5	48.3	50.7

Figure 7.15: The p(r) distributions for the 14-3-3ζ in the presence of destabilised ADH at a (A) 1:1 and (B) 1:2 molar ratio of ADH:14-3-3ζ at 40% D_2O. (C) Summary of R_g values and volume % of dimer and tetramer from Oligomer analysis of the 14-3-3ζ data at 40% D_2O in the presence of ADH.

Modelling of the interaction between unfolding ADH and 14-3-3ζ was undertaken, using MONSA (a component program of the ATSAS suite). MONSA analysis allows the prediction of the most likely arrangement of unfolded ADH and 14-3-3ζ to form a complex (Figs. 7.16 and 7.17). This analysis indicates that the intermediately folded, molten globule state of ADH interacts with the dimer interface of 14-3-3ζ, but with the retention of the dimeric structure. The unfolded extension of the ADH molecule interacts asymmetrically with 14-3-3ζ i.e. interacts with half of the dimer interface. Studying the crystal structure of 14-3-3ζ, the dimer interface exists as two interaction interfaces separated by an aperture. The MONSA model shows the interaction of elongated ADH into one region of the dimer interface (Fig. 7.17). This may indicate that one side of the dimer interface dissociates and allows the interaction with elongated ADH, without the complete dissociation of the 14-3-3ζ dimer.

In summary, small angle neutron scattering experiments were undertaken in order to observe the interaction between the molecular chaperone 14-3-3ζ and the aggregating target protein, alcohol dehydrogenase (ADH). Contrast variation allows us to characterise the intermediately folded state of the aggregating ADH when interacting with a molecular chaperone protein. There was little change to the overall size and shape of 14-3-3ζ whilst chaperoning amorphously aggregating target proteins. MONSA analysis indicates that the intermediately folded state of ADH interacts with 14-3-3ζ via one side of the dimer interface, with 14-3-3ζ retaining its dimeric state.

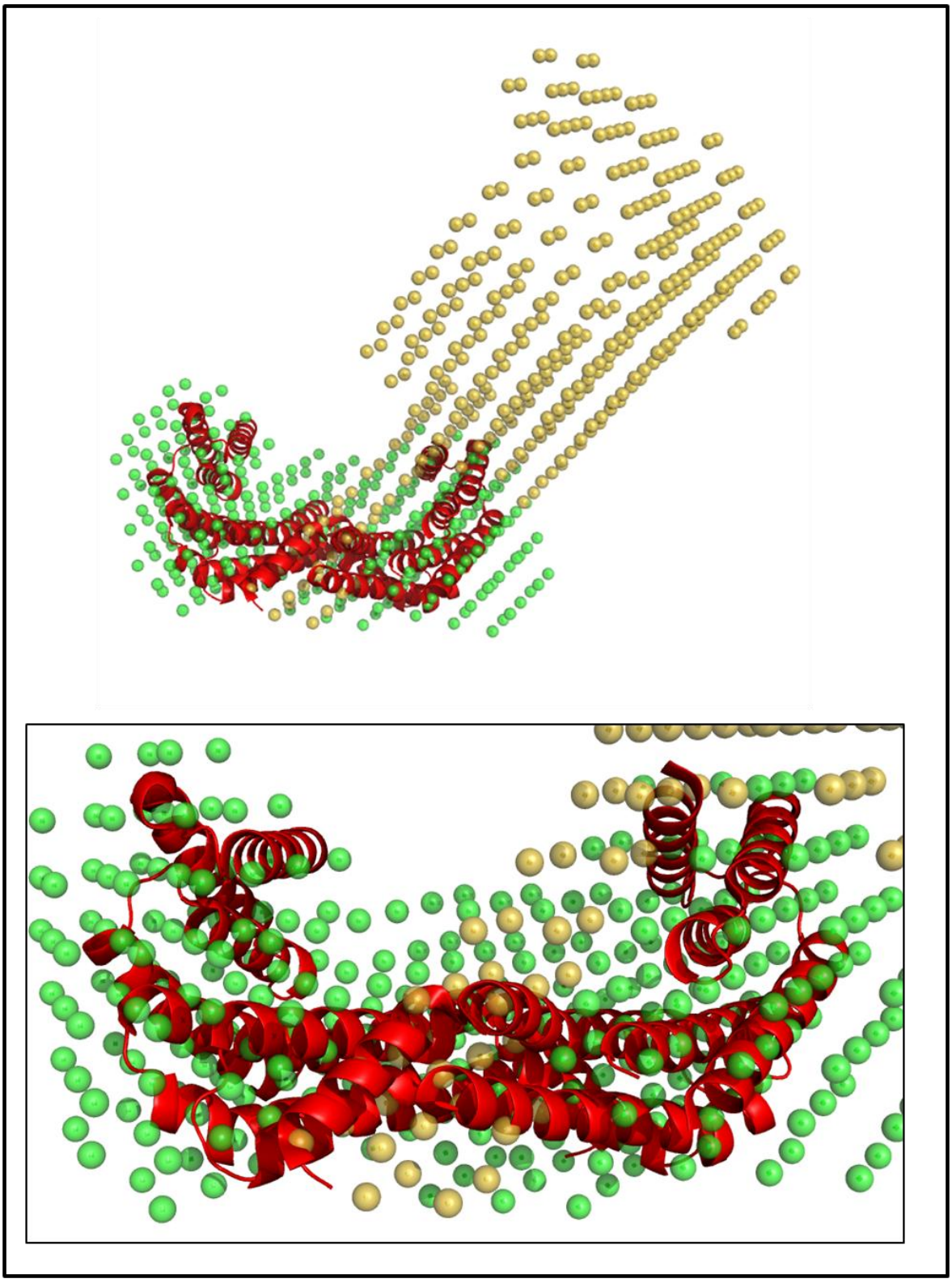

Figure 7.16: Modelling (obtained using the MONSA component program from the ATSAS suite), showing the most likely interaction between 14-3-3ζ (green) and the intermediately folded state of ADH (yellow), with the X-ray crystal structure of 14-3-3ζ (red) overlaid showing the amphipathic binding groove.

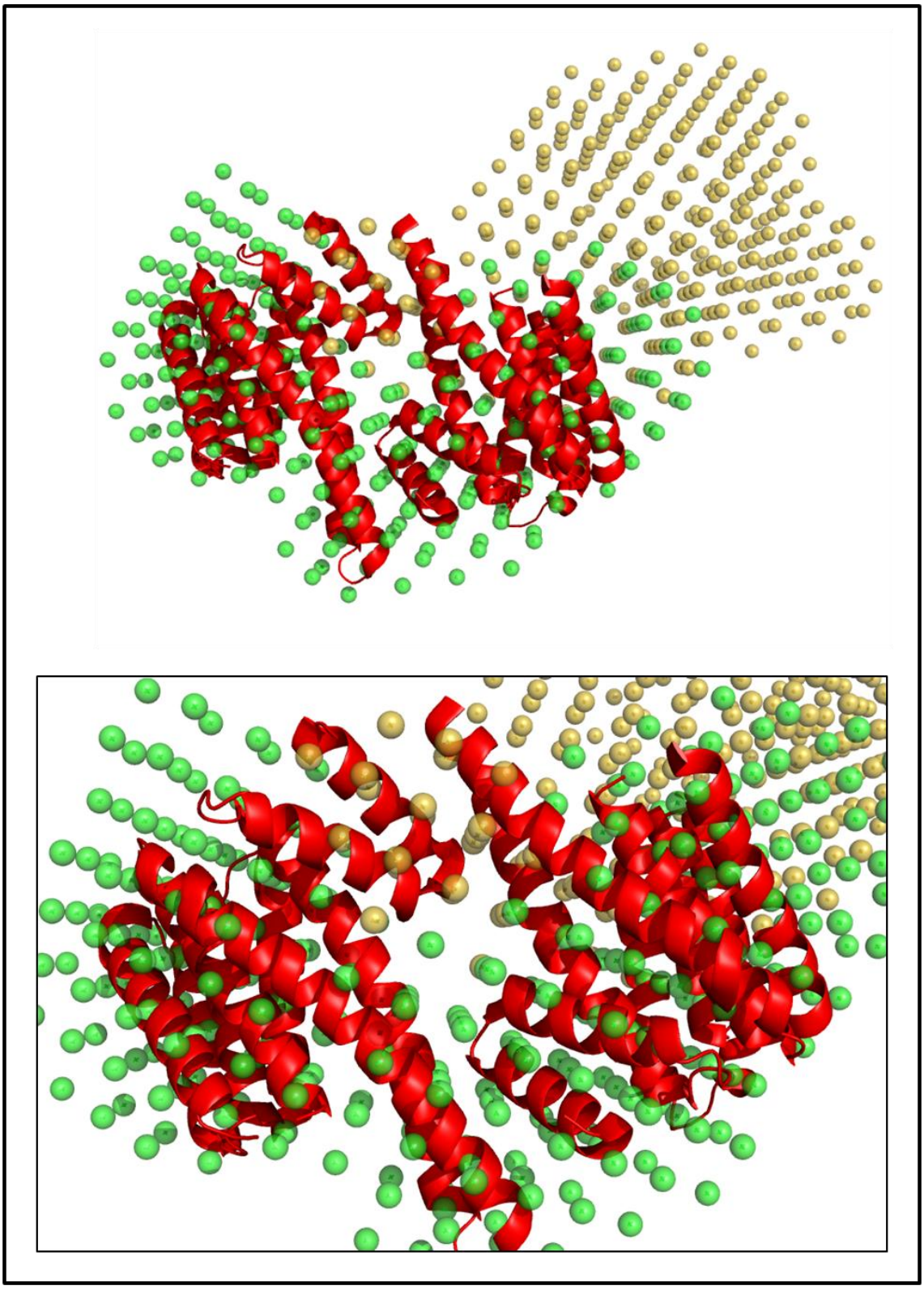

Figure 7.17: Modelling (obtained using the MONSA component program from the ATSAS suite), showing the most likely interaction between 14-3-3ζ (green) and the intermediately folded state of ADH (yellow), with the X-ray crystal structure of 14-3-3ζ (red) overlaid showing the dimer interface interaction regions joined by an aperture.

7.5 Discussion

Small angle scattering (SAS) techniques were employed in order to monitor the interaction between the molecular chaperone 14-3-3ζ and the aggregating target protein, ADH. SAS techniques provide low-resolution information about the size and shape of a macromolecule in solution (101). Previous studies (chapter 4) have demonstrated that changing the monomer-dimer dynamics of 14-3-3ζ leads to enhancement of chaperone action. However, this work did not enable the examination of any conformational changes undergone by 14-3-3ζ whilst chaperoning. Due to the dynamic nature of the chaperone interaction between 14-3-3ζ and its target protein, ADH, a crystal structure of the two species interacting is unlikely to be obtained; one of the best means to extract structural data for such a system is via SAS techniques.

ADH was selected as a target protein due its reproducible amorphous aggregation over a relatively short timeframe. To obtain a good scattering signal for the target protein, the aggregation must be controlled by the chaperone protein 14-3-3ζ. It has been previously demonstrated that 14-3-3ζ acts more effectively in a chaperone manner against slowly aggregating proteins (65) (as discussed in chapter 4). Conditions were optimised for SAS by lowering the incubation temperature, to reduce the level of aggregation of ADH and increase lag time. This allowed 14-3-3ζ to more efficiently interact with ADH, providing near complete suppression against the amorphous aggregation of this target protein at 33^{o}C at a 1:2 molar ratio of ADH:14-3-3ζ.

In order to confirm that these aggregation conditions were appropriate for a scattering system, SAXS experiments were conducted. These experiments showed strong scattering with the complex formed between the aggregating ADH target protein and 14-3-3ζ which was not overwhelmed by excessive aggregation. Additionally, the aggregation of ADH was monitored. The SAXS results confirmed that a scattering signal of the complex formed between a chaperone and aggregating protein could be obtained, without excess scattering obscuring the signal. However, SAXS studies are unable to elucidate any conformational changes undergone by ADH and 14-3-3ζ individually upon interaction. Therefore, SANS combined with contrast variation was used to monitor any changes to 14-3-3ζ whilst chaperoning. In order to utilise contrast variation, deuteration of 14-3-3ζ was undertaken.

Deuteration of 14-3-3ζ resulted in some minor structural change in the protein, which has been previously observed for other proteins (116). C-D bonds have a shorter length than C-H bonds and as a consequence have reduced hydrophobicity (115). As protein folding is driven primarily by hydrophobic interactions, d14-3-3ζ is expected to be slightly less stable than its hydrogenated counterpart, with destabilisation common amongst deuterated proteins (117). However, this effect is lessened when deuterated proteins are incubated in D_2O. As the majority of the SANS experiments utilising 14-3-3ζ were undertaken in 40% D_2O, with 14-3-3ζ retaining its ability to function as a molecular chaperone, this destabilisation is unlikely to detrimentally affect the interpretation of the SANS data.

The *ab initio* shape models of the molecular chaperone 14-3-3ζ protein and non-aggregating target protein ADH were obtained by SANS. The SAS-derived native conformation of ADH correlates well with the crystal structure. The size and shape of 14-3-3ζ when incubated alone was obtained and generated a D_{max} value larger than that indicated by the crystal structure. Further analysis revealed that the presence of a tetrameric species is responsible for shifting the size of 14-3-3ζ towards larger particles. Analytical ultracentrifugation analysis (as described in chapter 5) first indicated that 14-3-3ζ is able to form a tetrameric species. However, these studies were not undertaken at conditions utilised for scattering experiments. The precise arrangement between the two dimers could not be determined via this technique. Scattering analysis has enabled the resolution of the overall arrangement of the two 14-3-3ζ dimers. This arrangement was obtained from x-ray crystal structures. However, due to the association of two highly negatively charged regions of 14-3-3ζ required to form this arrangement, it may be more likely that the dimers stack in a different manner with a similar associated size and shape. The most likely arrangement would be the dimers stacking with the hydrophobic regions of the amphipathic binding groove interacting. As described in chapter 5, this self-association is likely to be an artefact of high protein concentrations, such as those used in the SANS experiments and is seen in the obtained crystal structures for 14-3-3ζ (16). However, the presence of this tetrameric species results in polydisperse solution, which hinders modelling of the 14-3-3ζ species. Previous SAS studies of the 14-3-3 structure have only been conducted on 14-3-3σ (118). The native structure of 14-3-3σ is comparable to that obtained of 14-3-3ζ, though no larger self-associated species were reported potentially indicating that different isoforms of 14-3-3ζ have distinct capabilities to self-associate.

The unfolding and amorphous aggregation of ADH has been monitored by light scattering previously (26). However, the mechanism for the formation of amorphous aggregates has been poorly explored, with light scattering incapable of elucidating any conformational changes in the protein. The SAXS and SANS studies both confirmed the presence of an initial, relatively small unfolded species immediately after addition of EDTA to the native protein. Additionally these studies showed that there is an initial unfolding of a region of the protein with the retention of the globular protein core. It is thought that these smaller species have the ability to accumulate and form large aggregates. This aggregation has been shown to be affected by the D_2O concentration. ADH in 0% and 100% D_2O showed significantly different scattering profiles by SAXS, implying that incubation in D_2O leads to reduced aggregation. As stated previously, the replacement of hydrogen with deuterium leads to a reduction in hydrophobicity of chemical bonds (115). Protein aggregation is driven by the exposure of hydrophobic regions in proteins. The incubation of misfolding ADH in D_2O, leads to a reduction in the overall hydrophobicity due to altered interaction with D_2O, which likely accounts for the reduced size of the unfolding ADH.

The intermediately folded conformational states of ADH were characterised in the presence of the molecular chaperone 14-3-3ζ. Light scattering experiments determined that in the presence of 14-3-3ζ, the aggregation of ADH was reduced in a concentration-dependent manner (26). The SANS results revealed that increasing concentrations of 14-3-3ζ led to a reduction in the size of intermediately folded ADH, with a 1:2 molar ratio of ADH:14-3-3ζ resulting in less elongation of ADH than a 1:1 ratio. This is indicative of 14-3-3ζ interacting with ADH early along its unfolding pathway to prevent the formation of large-scale aggregate ADH species. Further increases in the concentration of 14-3-3ζ may prevent any elongation of ADH when incubated with EDTA. This characterisation reveals the intermediately folded, molten globule state of ADH. This is the first instance where the overall shape and characteristics of an unfolding protein (ADH) has been defined whilst interacting with a molecular chaperone protein.

Previously, the molecular chaperone action of 14-3-3ζ has been studied via light scattering (as demonstrated in chapters 3, 4 and 6). The use of protein deuteration and contrast variation in SANS experiments allows us to monitor 14-3-3ζ individually whilst chaperoning. There was little change to the overall size and shape when 14-3-3ζ was interacting with amorphously aggregating target proteins. The modelling of the two protein components interacting using MONSA analysis, provides some insight into the interaction between the two proteins. This

modelling indicates that the misfolded ADH interacts via half of the dimer interface, whilst the dimeric 14-3-3ζ structure is retained. This SANS modelling indicates that the dimer is essential for the chaperone action, at least by stabilising the bound partly unfolded target protein. Examining the crystal structure reveals that the dimer interface has two interaction regions separated by an aperture (Fig. 7.18). The most likely mechanism of action is the partial dissociation of one of these interaction regions within the dimer interface, resulting in exposure of the hydrophobic chaperone face and allowing the interaction with aggregating target proteins without complete dissociation from the dimer. The maintenance of the dimeric structure increases the stability of the chaperone-aggregating protein complex. Alternatively, this interaction with the dimer interface could be due to the sequestration of the unfolding target protein by monomeric 14-3-3ζ before the rapid reformation of the dimer. The dissociation would be so rapid that this cannot be detected by SANS. However, with the inherent instability of the monomeric unit, as demonstrated using dimer disrupted proteins in chapter 4, it is unlikely that this unit would be able to maintain its own stability, especially when interacting with aggregating target proteins.

The involvement of the dimer interface in the chaperone action of 14-3-3ζ parallels with results previously obtained showing that a shift of the monomer-dimer dynamics of 14-3-3ζ, towards the monomer, leads to enhanced chaperone ability (chapters 4 and 5). This shift would lead to increased dissociation of each of the interaction regions in the dimer interface allowing the interaction of target proteins with this hydrophobic region.

D21N 14-3-3ζ experienced the greatest enhancement in chaperone action; greater even than other mutant proteins which exhibit greater dimer disruption than D21N 14-3-3ζ. The increased dimer disruption of S58D, D21N/E89Q/S58A and D21N/E89Q/S58A 14-3-3ζ mutant proteins results in a more significant shift in the monomer-dimer equilibrium towards the monomeric species, compared to D21N 14-3-3ζ. However these mutant proteins do not experience greater chaperone ability than D21N 14-3-3ζ. As the modelling from the SANS indicates, the dimer is likely to be essential for the interaction with and stability of the aggregating target proteins- chaperone complex. The instability of these proteins, and the overall reduction of dimeric species compared to D21N 14-3-3ζ, may result detrimentally on their chaperone abilities.

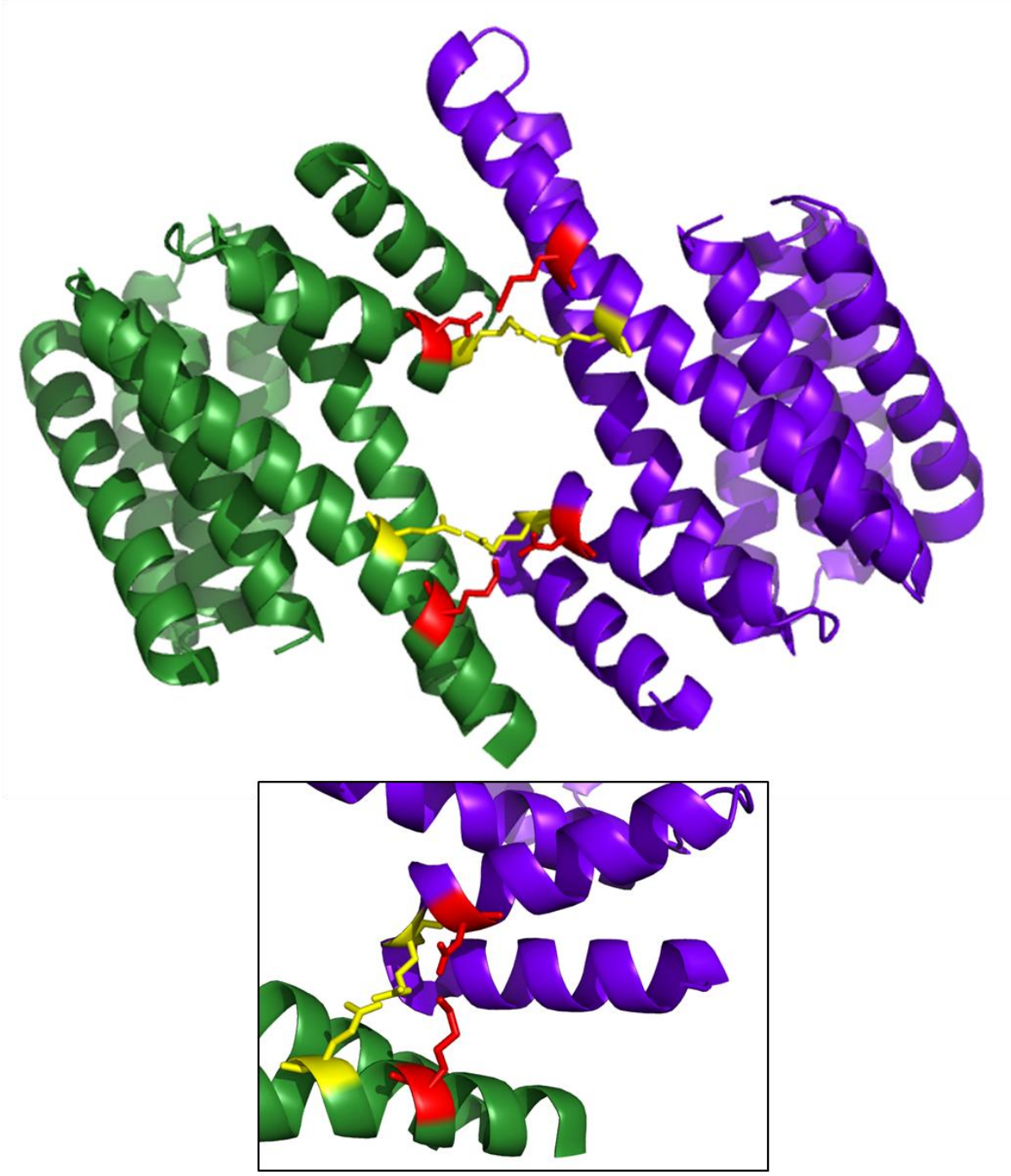

Figure 7.18: The alignment of the helices in the dimer interface of 14-3-3ζ highlighting the two interaction regions separated by an aperture. The stabilising salt bridging interactions are highlighted (D21-K85 in red and R18-E89 in yellow).

The models (Fig. 7.16 and 7.17) indicate that in the timeframe of SANS experiments the elongated ADH species interacts with 14-3-3ζ down into the dimer interface. This interaction also occurs passing by amphipathic binding groove. In chapter 3, it was demonstrated that this region was unlikely to be critical in the chaperone function of 14-3-3ζ. It is possible that this interaction near the amphipathic binding groove prevents the interaction of 14-3-3ζ with phospho-serine target proteins involved in cellular signalling (19) whilst acting as a molecular chaperone protein.

Neutron scattering experiments have been previously used to determine how chaperone proteins interact with aggregating target proteins (119,120). This scattering analysis is the first instance where the interaction of a chaperone protein with an aggregating target protein has been characterised. The use of contrast variation has allowed the characterisation of the partially folded, molten globule state of ADH, any conformational changes undergone by the chaperone protein whilst interacting, along with generating a model showing the interaction interface between the two species. The low resolution data does not provide information about the precise interactions between the two proteins. However it has allowed the determination of the approximate interaction region of the protein and the potential mechanism of action which will direct future studies into the chaperone action of 14-3-3ζ.

Chapter 8

Conclusions and Future Directions

14-3-3 proteins are a family of dimeric, acidic, phospho-serine binding proteins. There are 7 isoforms in mammals (β, γ, ε, σ, τ, η, ζ) with comparable structures and functions, and are mostly expressed ubiquitously (1,3). Each monomer is 30kDa and is composed of 9 anti-parallel alpha helices. The interaction between 2 monomers occurs in the N-terminal region (between helices 3 and 4 of one monomer and helix 1 of another). The arrangement of the alpha helices creates a cup-like amphipathic binding groove, which is the primary region of binding to phospho-target proteins. 14-3-3 proteins are known to interact with over 200 targets, and regulate many roles within the cell, including mitosis, apoptosis, signal transduction and protein transportation. This involvement in many cellular signalling roles has implicated 14-3-3 proteins in many disease states e.g. cancers and neurological diseases.

Neurodegenerative diseases are caused by the irreversible and toxic unfolding and aggregation of cellular proteins as protein plaques. 14-3-3 proteins are co-located in many of these protein plaques and lesions. As 14-3-3 has been shown in different cases to act as either a positive or negative regulator of protein aggregation, the function of 14-3-3 proteins in these diseases is currently unknown. 14-3-3ζ was demonstrated to act as a molecular chaperone, with the ability to interact with and stabilise aggregating target proteins via hydrophobic interactions (14). Previously, the C-terminal extension and the polar face of the amphipathic binding groove of 14-3-3ζ were investigated for their role in chaperone action and were found to not be involved. The site and mechanism of the molecular chaperone action of 14-3-3ζ are unknown and was investigated here, primarily targeting regions of major hydrophobicity.

8.1 Conclusions

The first site explored for chaperone action of 14-3-3ζ was the hydrophobic face of the amphipathic binding groove. In chapter 3, exposed hydrophobic residues in this region were targeted, mutated and characterised. The removal of hydrophobicity in the region using V176D and L216, 220, 227D 14-3-3ζ proteins lead to some minor destabilisation of the 14-3-3ζ protein structure. This did not inhibit the chaperone ability of 14-3-3ζ, implying that this region is not critical for its chaperone function. The polar face of the amphipathic binding groove has previously been investigated via site directed mutagenesis (26). Together, this indicates that the interaction of 14-3-3ζ with aggregating target proteins is unlikely to occur via the amphipathic binding groove.

This amphipathic binding groove is the primary region of interaction with phosphorylated target proteins for cellular signalling purposes, under normal physiological conditions. In addition to this, there have been several instances in which 14-3-3 proteins have been observed to enhance the aggregation of physiological proteins associated with pathology of disease, e.g. Huntingtin in Huntington's disease and phosphoataxin-1 in ataxia (4,52). This enhancement (discussed in section 1.4.2) is generally phosphorylation-dependent and occurs via the amphipathic binding groove. In contrast, the molecular chaperone action of 14-3-3ζ is phosphorylation and amphipathic binding groove independent. This indicates that this chaperone function is a separate functional role of 14-3-3ζ from its cellular signalling functions.

After determining that 14-3-3ζ's interaction with aggregating target proteins is unlikely to occur via the amphipathic binding groove, other regions of hydrophobicity were investigated. A major region of hydrophobicity is the dimer interface. This region is stabilised by many salt bridging and hydrophobic interactions. In chapter 4, hypothesised salt bridges (D21 and E89) were targeted and a phospho-mimic of S58 was generated. These proteins (D21N, E89Q, S58D, D21N/E89Q/S58A and D21N/E89Q/S58D 14-3-3ζ) all exhibited dimer disruption with increased exposed hydrophobicity as exhibited by bis-ANS binding. Further analysis was undertaken by AUC and cross linking studies, showing that they exhibit a shift in the monomer-dimer equilibrium towards monomeric 14-3-3ζ to varying degrees for each mutant. This was influenced by alteration of temperature and concentration.

The chaperone ability of these dimer disrupted 14-3-3ζ proteins were tested and, with the exception of E89Q 14-3-3ζ, was shown to possess an enhanced chaperone action. With the observed shift in the monomer-dimer equilibrium associated with these mutant proteins, it was hypothesised that the monomeric unit of 14-3-3ζ was the chaperone active species which interacts with aggregating target proteins under stress conditions, in a manner comparable to the chaperone functions of sHsps (39).

To further explore the role of the dimer interface in chaperone action, the effect of the interaction of a sphingosine mimic (#41.14) on the chaperone action of 14-3-3ζ was undertaken. This sphingosine mimic interacts with the dimer interface allowing phosphorylation at the buried S58 site in a manner similar to the physiological lipid sphingosine. This interaction was characterised and generates increased exposed hydrophobicity by bis-ANS binding. However this interaction was unable to enhance the chaperone ability of WT 14-3-3ζ, presumably due to a transient interaction which doesn't provide significant disruption to fully expose the potential chaperone surface within the dimer interface. The lack of chaperone enhancement of 14-3-3ζ *in vitro*, does not fully preclude sphingosine from having a role in the chaperone ability of 14-3-3ζ. A related molecule FTY720, has been demonstrated to reduce the aggregation in the brains of a mouse model, displaying Huntington's pathology (100). Sphingosine is also elevated in the brains of patients with Alzheimer's disease. This may indicate that in the presence of sphingosine, there is further modification to 14-3-3's dimeric structure, which may lead to the enhancement of the chaperone activity.

Finally, any conformational changes undergone by 14-3-3ζ whilst acting as a molecular chaperone were characterised via small angle scattering experiments. These scattering studies confirm that 14-3-3ζ interacts with the aggregating target protein, ADH, resulting in a reduction in the overall aggregation. The intermediately folded, molten globule state of ADH was characterised here for the first time. Modelling of the ADH-14-3-3ζ complex revealed that this interaction likely occurs within the dimer interface via the 14-3-3ζ dimer. This analysis is the first instance where the interaction between a chaperone protein and an aggregating target protein has been modelled. ADH interacts via one side of the dimer interface. The interactions on the other side of the dimer interface can thus maintain the dimeric state of 14-3-3ζ. Further analysis did not indicate the presence of any monomer 14-3-3ζ species whilst interacting with aggregating ADH. This indicates that either the monomer

does not have any role in the chaperone action of 14-3-3ζ or the dimer is rapidly reformed after the interaction, which cannot be visualised by SANS. Due to the inherent instability of the monomeric species it is likely that if involved in chaperone activity, it is a transient species, with the unstable monomer likely enhancing the aggregation of any target proteins.

The investigations undertaken here determined that the molecular chaperone 14-3-3ζ interact with aggregating target proteins via the hydrophobic dimer interface. Under stress conditions such as elevated temperature, protein misfolding events increase. Under the same conditions 14-3-3ζ experiences a shift in the monomer-dimer equilibrium which promotes the partial dissociation of the dimer interface, allowing the interaction with intermediately folded target proteins. Thus 14-3-3ζ has the potential to reduce the accumulation of disease causing aggregates.

Previous attempts to understand the molecular chaperone action of 14-3-3ζ have targeted the polar face of the amphipathic groove and the C-terminal extension (26). The dimer interface has also been investigated (78,84). Sluchanko *et al*. have shown that a "monomeric" 14-3-3ζ mutant protein has enhanced chaperone ability (78). This analysis was undertaken using a triply mutated protein based on a previously described dimer deficient protein generated by Tzivion et al., (18). The original dimer deficient mutant incorporated E5K, L12Q, A13Q, E14R, Y82Q, K85N and E87Q mutations (18) and was used to determine the importance of the dimeric structure on 14-3-3's ability to bind to target proteins. These residues were targeted due to their reported proximity to the dimer interface and this combination mutant was predicted to cause dimer dissociation, but this was not characterised in this study (18). Upon inspection of the crystal structure, the residues targeted for mutation do not all lie within the dimer interface, with the side chain of E14 and E87 pointing away from the interface region. This combination mutation may lead to additional and unnecessary destabilisation of regions not involved in dimer formation.

More recently however, studies have been undertaken to more fully characterise the dimer deficient mutant protein of Tzivion (18). The fully mutated protein could not be purified from bacteria due to aggregation issues (121). Therefore Sluchanko *et al.* separated the original dimer deficient mutant into different segments to more fully assess the effect on dimer formation (E5K, L12Q/A13Q/E14R and Y82Q/K85N/E87Q mutant proteins) (121). The monomeric status of L12Q/A13Q/E14R 14-3-3ζ was confirmed by SEC-MALLS and cross-linking and the protein was shown to be monomeric over a range of concentrations (0.5-

6.0mg/mL). The chaperone ability of Sluchanko's triple mutant (78,84) was explored and found to exhibit enhanced chaperone ability in a manner similar to that demonstrated here (section 4.3.1), which supports our hypothesis that the dimer interface is involved in the chaperone ability of 14-3-3ζ. However, none of the dimer disrupted proteins presented in this thesis (chapters 4 and 5), demonstrate a pure monomeric component, even at very low concentrations (0.09mg/mL) (section 5.2.2). The removal of salt bridging interactions has produced mutant proteins which maintain the hydrophobicity of the dimer interface, making these proteins a better physiological model for the determination of the chaperone regions in 14-3-3ζ. The ability of the L12Q/A13Q/E14R triple mutant protein used by Sluchanko to exist as a monomer (with no dimer present) suggests disruption beyond intermolecular interactions in the dimer interface.

The role of the dimer interface in the chaperone ability of 14-3-3 has also been explored by another study. The interaction of 14-3-3β with Prion protein (PrP) was undertaken by Han *et al*. (122), and also demonstrated that the interaction is likely to occur in the dimer interface. However the hypothesised residues of interest were D22 and D23, with the latter being a conserved salt bridge residue important for the stabilisation of the 14-3-3 dimer in a manner similar to that of D21 in 14-3-3ζ. The mutagenesis of these sites led to a reduced affinity of 14-3-3β with PrP. However, it seems unlikely that D22 and D23 are responsible for chaperoning PrP as they carry a negative charge. As described earlier, molecular chaperone proteins commonly interact with aggregating targets via hydrophobic interactions. The authors also proposed that the presence of full length PrP enhances the dimeric status of 14-3-3β, with the lack of PrP resulting in a monomeric species (122). The results indicated in this thesis show that the generation of a monomeric protein leads to destabilisation of the overall structure, and is not the native structure. The WT 14-3-3β protein used by Han *et al.* showed a significant level of monomeric protein natively, which leads to some speculation about the folding status of the proteins used in this study, leading to the possibility that the interactions indicated between the prion protein and 14-3-3β are simply due to the inherent instability of the 14-3-3β proteins utilised.

The molecular chaperone protein function of 14-3-3ζ that has been characterised in this thesis and previously by others, describes the preventative action of 14-3-3ζ against intracellular protein aggregation and the resultant neurodegeneration, likely via the dimer interface. Compared to other specialised molecular chaperones e.g. sHsps, 14-3-3 is less efficient at

suppressing aggregation, with the inability to function efficiently against very rapid aggregation or against fibril forming targets (65). As these fibrillar species are the pre-dominant toxic species associated with neurodegenerative disease, the physiological importance of this molecular chaperone action of 14-3-3ζ is queried.

Importantly, some molecular chaperone proteins, in addition to stabilising the unfolding target protein, can divert the unfolding and formation of a pre-fibrillar species to a more amorphous aggregation like species. It is likely that 14-3-3 is sequestered to interact with these amorphous species, allowing specialised chaperone proteins to continue interacting with toxic pre-fibrillar species, without being overwhelmed by the resultant amorphous aggregates. Additionally due to the abundance of 14-3-3 proteins in cells, especially in the brain, it is also likely that 14-3-3 is able to react immediately to any misfolding of proteins in the cell, prior to the induction of molecular chaperone protein transcription.

14-3-3's function as a cellular signalling protein is undoubtedly its primary purpose within cells, with the possession of a secondary chaperone role when required under stress conditions. In some instances, the interaction of 14-3-3 with phosphorylated aggregating proteins via the amphipathic binding groove, leads to aggregation enhancement for example Huntington's disease and SCA-1. Intriguingly, modelling of the interaction of 14-3-3ζ with intermediately unfolded ADH suggests that binding via the amphipathic binding groove is blocked during chaperoning, thus diverting 14-3-3ζ away from phospho-protein binding. This molecular adaption may reduce protein aggregation in cells, by recruiting 14-3-3 as a molecular chaperone and simultaneously preventing its interaction with phosphorylated targets which may lead to an enhancement of disease pathology.

8.2 Future Directions

The determination of the dimer interface being the chaperone active site of 14-3-3ζ reveals the potential mechanism of 14-3-3 proteins in neurodegenerative disease. However the roles of 14-3-3 proteins in neurodegenerative disease remain diverse and not well characterised. Therefore further studies into the chaperone action of 14-3-3 must be undertaken.

The dimer interface has been determined to be important for the chaperone action of 14-3-3ζ. To further assess the role of this region of 14-3-3ζ in chaperone activity, future studies involving a forced dimer, which cannot dissociate into a monomer have been undertaken using disulphide bridges introduced into the dimer interface. Examination of the X-ray structure shows that the residues A16 and S58, upon mutation to cysteine residues, have the appropriate distance and angle to form a disulphide bridge (Fig. 8.1). This protein has been expressed in bacteria, but these disulphide bridges do not form natively, with the conditions needing to be refined. This cross-linked protein would be the ideal system to either prove or disprove that the partial dissociation of the dimer interface is crucial for the chaperone ability of 14-3-3ζ. This has advantages over general cross linking (e.g. with glutaraldehyde) as the links between the monomers are specific and any changes in chaperone action can be fully understood.

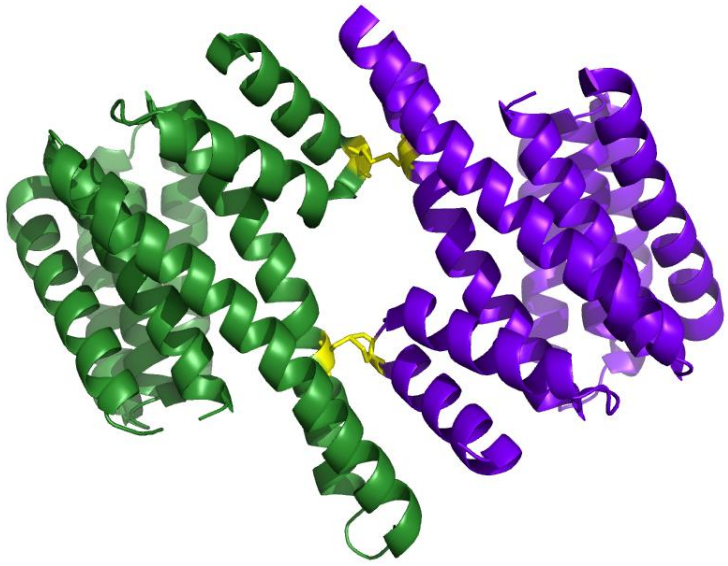

Figure 8.1: The crystal structure of a mutant 14-3-3ζ protein (A16C/S58C) highlighting the disulphide bridges (yellow) across the dimer interface to generate a protein which cannot dissociate from the dimer.

With the partial dissociation of the dimer interface crucial for the chaperone function of 14-3-3ζ, the effect of dimer disruption on the dimer-monomer equilibrium was briefly explored in this thesis. However, this monomer-dimer equilibrium and its importance in chaperone action should be further explored. Subunit exchange of 14-3-3ζ can be monitored by mass spectrometry, by observing the exchange of ^{15}N-labelled and non-labelled 14-3-3ζ protein over time, or alternatively FRET studies via fluorescence labelling of 14-3-3ζ. The effects of altering pH and the presence of clouding agents to mimic cellular crowding as done previously with the molecular chaperones, sHsps can be undertaken using these techniques (87,123). These studies will afford greater information about the monomer-dimer equilibrium and its role in the chaperone ability of 14-3-3ζ.

To further investigate the role of the dimer interface in chaperone action, assays were undertaken with a sphingosine mimetic, #41.14, which showed little effect on the chaperone action of 14-3-3ζ. The precise interaction site of 14-3-3ζ with sphingosine remains unclear. Further investigations (such as NMR spectroscopy, AUC studies, and hydrogen-deuterium exchange with mass spectroscopy analysis) into the nature and site of this interaction and the subsequent disruption would provide greater information about the dimer interface and the role of sphingosine like molecules in the regulation of this region, and its potential role in the chaperone action of 14-3-3ζ. This could be explored by using these sphingosine mimetics in an *in vivo* setting to fully assess the potential of these molecules in the chaperone action of 14-3-3ζ.

The formation of a 14-3-3 dimer is very important for the protein's functionality. However there has been little investigation into the residues important for stabilising this region. To gain more structural information about the interactions essential for the formation and stabilisation of the 14-3-3ζ dimer and the roles of the mutated residues studied in this thesis, additional structural techniques, such as NMR, X-ray crystallography and mass spectrometry should be used. Obtaining X-ray crystal structures of the phospho-mimic, S58D 14-3-3ζ has been attempted, but due to the dimer disruption and the resultant dynamic structure, the crystal structure has not been obtained. However, crystallisation of the other mutant proteins used here has not been attempted. It is unlikely that the triply mutated proteins would yield crystals due to their instability. However the salt bridge mutants (D21N and E89Q) exhibit less dimer disruption and are more likely to yield structures. This analysis would help determine the role of these residues in dimer formation. Native mass spectrometry and

hydrogen-deuterium exchange experiments would also help us to further analyse the dimer disruption caused by these mutations and the residues which are exposed as a result. These techniques would give more information about the residues and interactions important for the formation of 14-3-3ζ's dimeric structure.

Small angle scattering techniques enabled the modelling of a chaperone protein – target protein complex, showing the involvement of the dimer interface. To confirm that this is the likely interaction interface of 14-3-3ζ, small angle scattering experiments should be repeated with other target proteins e.g. α-lactalbumin, reduced insulin. Additionally, NMR spectroscopy experiments should be undertaken of the 14-3-3ζ – aggregating protein complex, to provide some insight to the residues that are involved in the chaperone action of 14-3-3ζ.

All experiments performed in this thesis were against amorphously aggregated target proteins. This model system is a relatively rapid and reliable system for determining the chaperone ability of various proteins. However to undertake a thorough study of the chaperone ability of the 14-3-3ζ proteins used in this thesis, the chaperone activity of the mutated 14-3-3ζ proteins against fibril forming target proteins should be undertaken.

All the 14-3-3 isoforms have been implicated with a neurodegenerative disease, with ζ and ε the most predominant (4). The role of the other 14-3-3 isoforms in disease has not been explored and only the chaperone action of 14-3-3γ has been identified (63). The chaperone ability of the other 14-3-3 isoforms (β, ε, η, σ and τ), and the role of the dimer interface has not been determined. To fully resolve the function of 14-3-3 proteins in neurodegenerative disease, the chaperone abilities of the other isoforms should be investigated.

Even with the discovery of this molecular chaperone functionality, the roles of 14-3-3 proteins in neurodegenerative disease are complex and remain not well understood, with 14-3-3 able to act as both a positive and negative regulator of physiological protein aggregation. Further studies need to be undertaken to fully understand the role that 14-3-3 proteins play in the pathology of these neurodegenerative diseases. Currently, no studies investigating the chaperone action of 14-3-3ζ in a cellular environment have been undertaken. *In vivo* chaperone activity assays have been undertaken with sHsps with both intra- and extracellular fibrillar targets (124). Similar studies should be undertaken with 14-3-3ζ to generate information about how effective 14-3-3ζ is as a molecular chaperone in a cellular

environment, and the species in which 14-3-3 proteins interacts under these conditions. By fully determining the chaperone ability of 14-3-3 proteins in neurodegenerative disease, it can provide further insight into the intricacies of these diseases and lead to the development of the therapeutic tools to treat these conditions.

Appendix A

Biophysical techniques

A.1 Far UV Circular Dichroism Spectroscopy

Far-UV circular dichroism spectroscopy is a major tool for the analysis of the overall secondary structure of proteins. The circular dichroism spectrum is the difference in the extinction coefficients of left-circularly polarised light and right-circularly polarised light, i.e. $\Delta A = A_L - A_R$, as a function of wavelength (125,126). Chiral centres give rise to a difference in the far-UV CD. As all naturally occurring amino acids (with the exception of glycine) contain a chiral centre, the far-UV spectra of proteins in the far-UV regions can be used to characterise proteins. The far-UV CD of proteins is dominated by n-π* and π-π* transitions of amide groups (127). The geometries of the polypeptide influence this transition, resulting in characteristic spectra for each type of secondary structure (Fig. A.1). Thus, deconvolution of far UV CD spectra can be used to assess the composition of secondary structure of a particular protein.

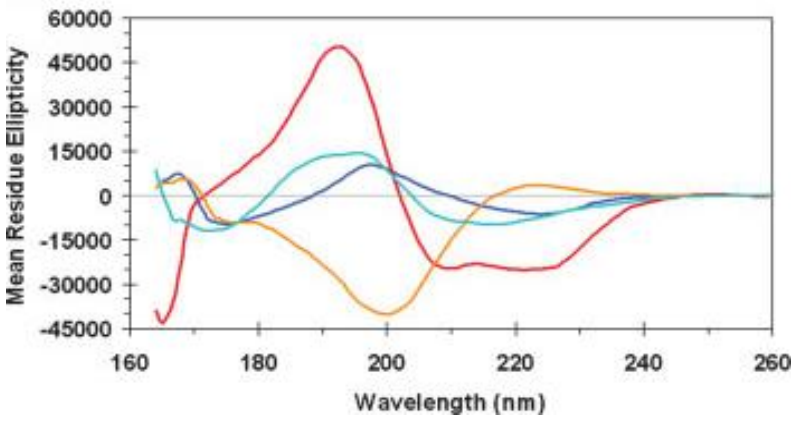

Figure A.1: The far-UV CD spectra of a helical protein myoglobin (red), beta sheet proteins concanavalin A (blue) and beta-lactoglobulin (cyan) and a polyproline rich protein, collagen (orange). Adapted from (127).

In general, α-helical structures give the most accurate results due to their regular, defined structures. Additionally they have very intense CD signals. In contrast, beta-sheet structures tend to more variable, with the potential for both parallel and anti-parallel orientation of adjacent strands, and produce spectra of a lower intensity (127). This can become problematic if a protein contains a large amount of helix with little beta-sheet content, leading to CD spectra in which beta sheet content may be obscured (127).

Unfolding and changes in the overall secondary structure of a protein can be monitored by any changes in the mean residue ellipticity (θ; degrees. cm^2/dmol) of the protein. The main limitation of CD is the relatively low resolution structural data it provides. However, it is a fast, convenient technique compared to X-ray crystallography and NMR. Only a small amount of material is required (0.2-1mg/mL) and, as the technique is non-destructive, the sample can be recovered (126).

A.2 Intrinsic tryptophan fluorescence

Many proteins are intrinsically fluorescent due to the presence of tryptophan, phenylalanine and tyrosine residues. Tryptophan, often found fully or partly buried in the hydrophobic core of many proteins, is the most useful of the three residues. The advantages of tryptophan fluorescence are primarily its environmental sensitivity, in addition to its relatively high quantum yield and extinction coefficient, compared with phenylalanine and tyrosine.

A change in the solvent exposure of the tryptophan leads to shifts in its fluorescence emission wavelength maximum. When buried in the hydrophobic core of a protein with less solvent exposure, the emission wavelength maximum of the tryptophan reduces compared with wavelength value of 360nm for free tryptophan (Fig. A.2A). This is known as a blue shift. If the tryptophan is then released from this hydrophobic core, an increase in the emission wavelength maximum as the tryptophan residue becomes more solvent exposed. This is known as a red shift and can occur when proteins unfold. Often, the intrinsic fluorescence signal of a protein displays a lower intensity than free tryptophan due to quenching effects of adjacent amino acid side chains and peptide bonds. Thus tryptophan fluorescence can be exploited to monitor any structural changes in proteins with a strong tryptophan signature (97).

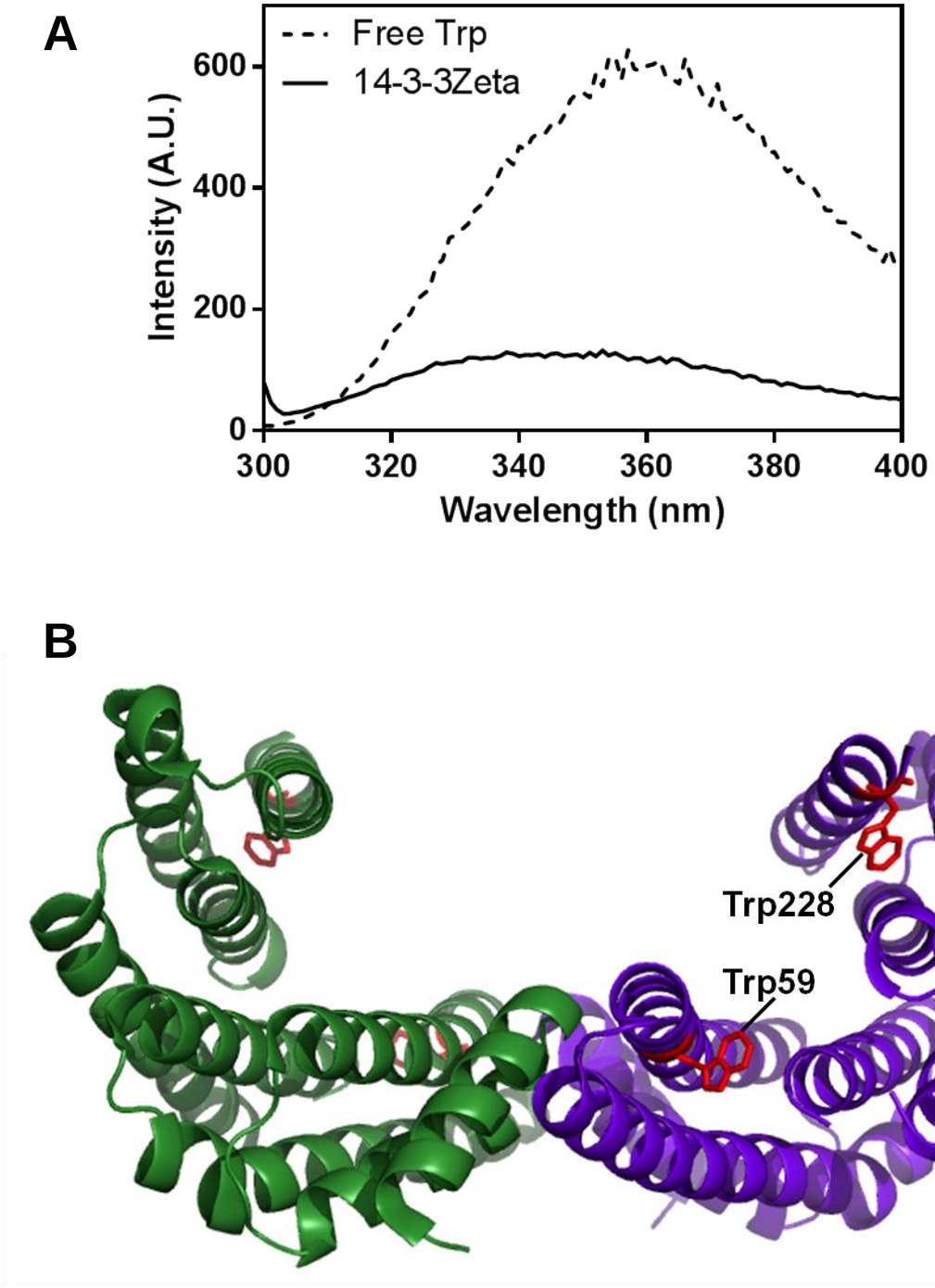

Figure A.2: (A) The fluorescence emission spectra of free Trp (dashed line) and 14-3-3ζ (solid line) when excited at 295nm, showing the resultant blue shift and decrease in intensity, upon burial of the Trp residues in the protein in addition to the quenching effects of the adjacent amino acids. (B) The locality of the two tryptophan residues in the 14-3-3ζ protein are, Trp59 (in helix 3) and Trp228 (helix 9) as indicated.

Each 14-3-3ζ monomer has two tryptophan residues (77); one located in the dimer interface at position 59 and the other near the C-terminal extension at position 228 (Fig. A.2B). Fluorescence studies of 14-3-3γ have revealed that π-π stacking of W233 with Y184 completely quenches the fluorescence of W233 (128). The crystal structure of 14-3-3ζ reveals a similar stacking of W228 and Y179 (Fig. A.3), implying that W59 is likely to be the predominant contributor to the intrinsic fluorescence spectrum of 14-3-3ζ.

It is well known that quenching of the intrinsic tryptophan fluorescence occurs with increasing temperature (129). Proteins unfold with increased temperature, exposing their tryptophan residues and resulting in an increase in fluorescence, which can be used for thermostability studies. With the intrinsic tryptophan fluorescence of 14-3-3ζ there is no observed blue or red shifts observed with increasing temperature. Due to the strong quenching of the structure, solvent exposure results in an increase in the overall fluorescence intensity. We would expect Trp59 to experience the greatest environment change with temperature increase, and as mentioned above, is the major fluorescence contributor for 14-3-3ζ. Therefore any environment changes at Trp59, may not be sufficient to result in a significant shift of the maximum wavelength intensity

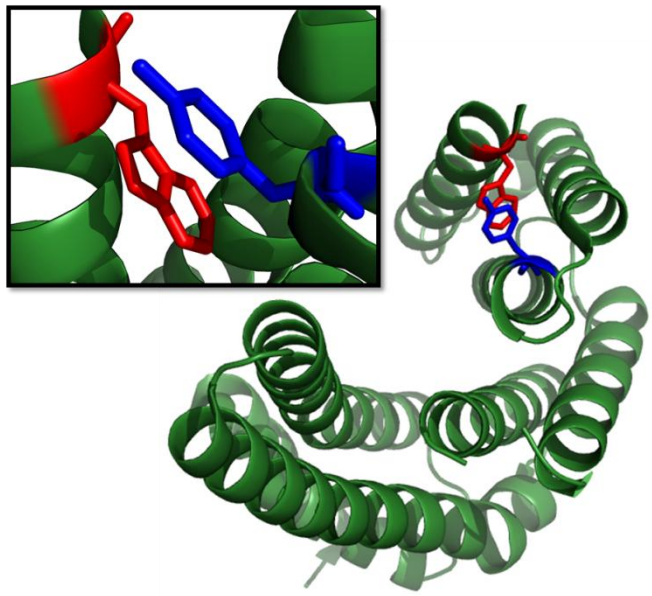

Figure A.3: The π-π stacking of W228 (red) and Y179 (blue) of 14-3-3ζ is equivalent to 14-3-3γ. This interaction potentially quenches the fluorescence of W228.

A.3 Bis-ANS

Fluorescence probes are defined as “compounds which undergo changes in one or more of their fluorescent properties as a result of non-covalent interactions with proteins or other macromolecules” (130). Bis-1-anilino-8-napthalene sulphonate (bis-ANS; Fig. A.4) is one such fluorescent probe which is sensitive to environmental changes, particularly polarity, viscosity and temperature. With regards to interactions with proteins, bis-ANS is particularly sensitive to changes in hydrophobicity. Upon interaction with hydrophobic regions on a protein, the removal from the aqueous solvent results in a blue shift of the maximum wavelength and an increase in fluorescence intensity of bis-ANS (131). In order to probe changes in exposed hydrophobicity, bis-ANS is generally excited at ~385nm with the emission acquired between 400 and 600nm. The maximum emission wavelength is ~500nm.

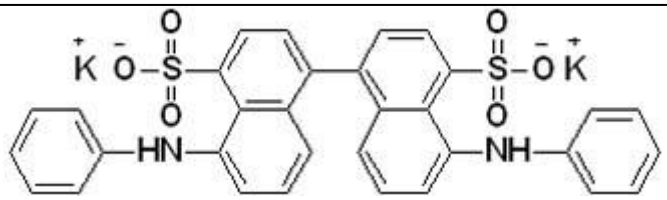

Figure A.4: The chemical structure of Bis-ANS

There is a low accessibility to bis-ANS within the core of the protein, so the binding of the probe is particularly useful for detecting any changes in surface hydrophobicity contained within proteins as a result of unfolding or mutagenesis (131). In the polar, aqueous solvent systems used in the experiments described in this thesis, the quantum yield of bis-ANS is very low. Therefore, any significant increases in bis-ANS fluorescence intensity are due to the interaction with less exposed hydrophobic surfaces, which can protect bis-ANS from significant solvent exposure (132).

In addition to direct excitation, excitation of bis-ANS can also be achieved via tryptophan residues within the protein by Forster resonance energy transfer (FRET). There must be an overlap between the emission spectrum of the donor species and the absorbance spectrum of the acceptor species in order for FRET to occur (79). This criterion is met by the donor tryptophan and accepting bis-ANS. The efficiency of FRET is dependent on the distance between the donor and acceptor molecules. For efficient transfer between the two fluorescent species, a distance of between 1-10nm is required (133). If the distance is greater, then the efficiency of fluorescence transfer is reduced and hence bis-ANS exhibits reduced

fluorescence intensity. Due to this distance relationship, if any fluorescence is observed via FRET excitation, this is likely due to the relatively close proximity of bis-ANS to a tryptophan residue in the protein.

Appendix B

Purity of WT 14-3-3ζ

The purity of WT 14-3-3ζ was assessed using SEC coupled with SDS-PAGE. All protein samples utilised in this thesis exhibited comparable SEC profiles, and were determined to be greater than 95% pure by SDS-PAGE before use (Fig. B.1). Therefore any differences in experimental results are not as a result of impurities present in the protein samples.

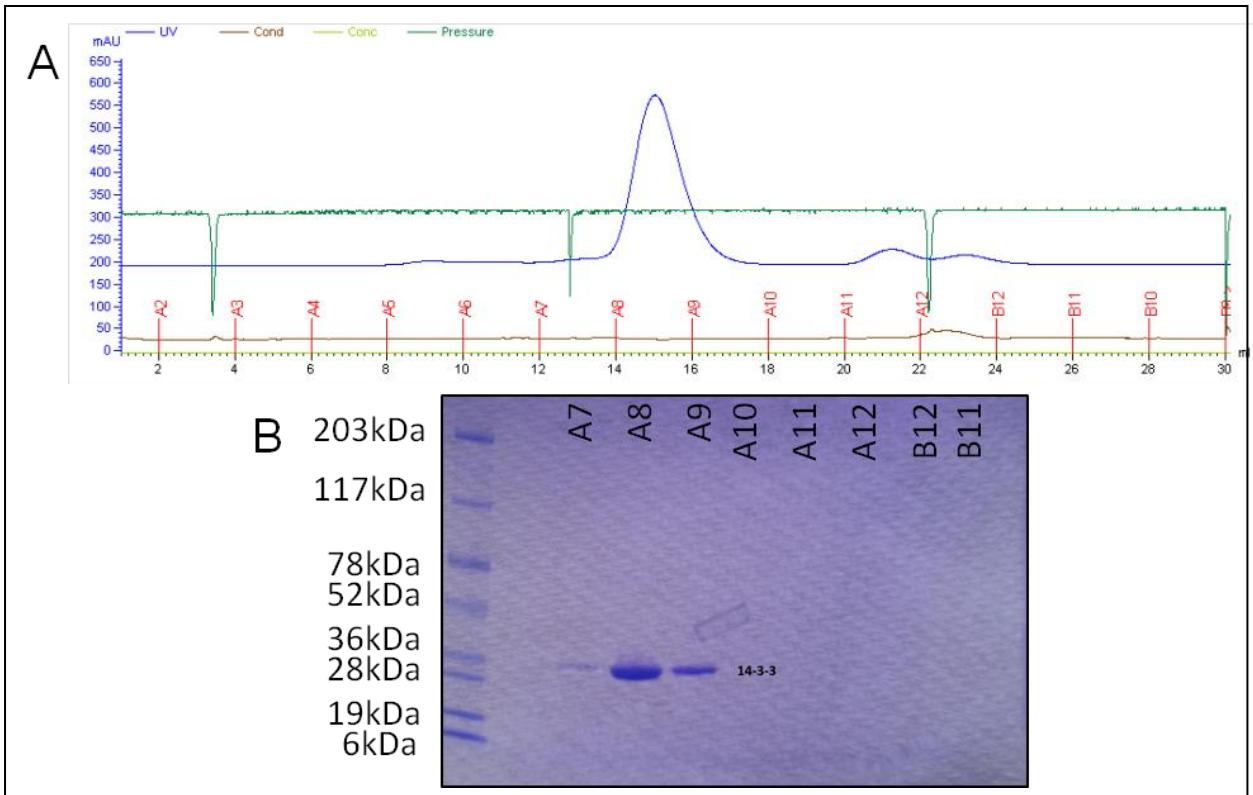

Figure B.1: (A) The FPLC trace of WT 14-3-3ζ (previously purified by Ni-affinity chromatography) after purification by size exclusion chromatography showing one protein peak. (B) SDS-PAGE analysis of the fractions collected via FPLC, confirming that the protein peak after size exclusion chromatography is WT 14-3-3ζ with purity greater than 95%.

References:

1. Gardino, A. K., Smerdon, S. J., and Yaffe, M. B. (2006) Structural determinants of 14-3-3 binding specificities and regulation of subcellular localization of 14-3-3-ligand complexes: a comparison of the X-ray crystal structures of all human 14-3-3 isoforms. *Seminars in Cancer Biology* **16**, 173-182
2. Tzivion, G., and Avruch, J. (2002) 14-3-3 proteins: active cofactors in cellular regulation by serine/threonine phosphorylation. *Journal of Biological Chemistry* **277**, 3061-3064
3. Aitken, A. (2006) 14-3-3 proteins: a historic overview. *Seminars in Cancer Biology* **16**, 162-172
4. Dougherty, M. K., and Morrison, D. K. (2004) Unlocking the code of 14-3-3. *J. Cell Sci.* **117**, 1875-1884
5. Yang, X., Lee, W. H., Sobott, F., Papagrigoriou, E., Robinson, C. V., Grossmann, J. G., Sundstrom, M., Doyle, D. A., and Elkins, J. M. (2006) Structural basis for protein-protein interactions in the 14-3-3 protein family. *Proceedings of the National Academy of Sciences of the United States of America* **103**, 17237-17242
6. Fu, H., Coburn, J., and Collier, R. J. (1993) The eukaryotic host factor that activates Exoenzyme-S of the Pseudomonas-aeruginose is a member of the 14-3-3 protein family. *Proceedings of the National Academy of Sciences of the United States of America* **90**, 2320-2324
7. Hengartner, M. O. (2000) The biochemistry of apoptosis. *Nature* **407**, 770-776
8. Tzivion, G., Gupta, V. S., Kaplun, L., and Balan, V. (2006) 14-3-3 proteins as potential oncogenes. *Seminars in Cancer Biology* **16**, 203-213
9. Morrison, D. K. (2009) The 14-3-3 proteins: integrators of diverse signaling cues that impact cell fate and cancer development. *Trends in cell biology* **19**, 16-23
10. Fu, H. A., Subramanian, R. R., and Masters, S. C. (2000) 14-3-3 proteins: Structure, function, and regulation. *Annu. Rev. Pharmacol. Toxicol.* **40**, 617-647

11. Zeng, Y., and Piwnica-Worms, H. (1999) DNA damage and replication checkpoints in fission yeast require nuclear exclusion of the Cdc25 phosphatase via 14-3-3 binding. *Molecular and Cellular Biology* **19**, 7410-7419
12. Chan, T. A., Hermeking, H., Lengauer, C., Kinzler, K. W., and Vogelstein, B. (1999) 14-3-3 sigma is required to prevent mitotic catastrophe after DNA damage. *Nature* **401**, 616-620
13. Omi, K., Hachiya, N. S., Tanaka, M., Tokunaga, K., and Kaneko, K. (2008) 14-3-3zeta is indispensable for aggregate formation of polyglutamine-expanded huntingtin protein. *Neuroscience letters* **431**, 45-50
14. Yano, M., Nakamuta, S., Wu, X., Okumura, Y., and Kido, H. (2006) A novel function of 14-3-3 protein: 14-3-3zeta is a heat-shock-related molecular chaperone that dissolves thermal-aggregated proteins. *Molecular biology of the cell* **17**, 4769-4779
15. Silhan, J., Obsilova, V., Vecer, J., Herman, P., Sulc, M., Teisinger, J., and Obsil, T. (2004) 14-3-3 protein C-terminal stretch occupies ligand binding groove and is displaced by phosphopeptide binding. *Journal of Biological Chemistry* **279**, 49113-49119
16. Liu, D., Bienkowska, J., Petosa, C., Collier, R. J., Fu, H., and Liddington, R. (1995) Crystal structure of the zeta-isoform of the 14-3-3 protein. *Nature* **376**, 191-194
17. Petosa, C., Masters, S. C., Bankston, L. A., Pohl, J., Wang, B. C., Fu, H. I., and Liddington, R. C. (1998) 14-3-3 zeta binds a phosphorylated Raf peptide and an unphosphorylated peptide via its conserved amphipathic groove. *Journal of Biological Chemistry* **273**, 16305-16310
18. Tzivion, G., Luo, Z. J., and Avruch, J. (1998) A dimeric 14-3-3 protein is an essential cofactor for Raf kinase activity. *Nature* **394**, 88-92
19. Zhang, L. X., Wang, H. N., Liu, D., Liddington, R., and Fu, H. A. (1997) Raf-1 kinase and exoenzyme S interact with 14-3-3 zeta through a common site involving lysine 49. *Journal of Biological Chemistry* **272**, 13717-13724
20. Zhang, L. X., Wang, H. N., Masters, S. C., Wang, B. C., Barbieri, J. T., and Fu, H. A. (1999) Residues of 14-3-3 zeta required for activation of exoenzyme S of Pseudomonas aeruginosa. *Biochemistry* **38**, 12159-12164
21. Wang, H. N., Zhang, L. X., Liddington, R., and Fu, H. I. (1998) Mutations in the hydrophobic surface of an amphipathic groove of 14-3-3 zeta disrupt its interaction with Raf-1 kinase. *Journal of Biological Chemistry* **273**, 16297-16304

22. Haladova, K., Mrazek, H., Jecmen, T., Halada, P., Man, P., Novak, P., Chmelik, J., Obsil, T., and Sulc, M. (2012) The combination of hydrogen/deuterium exchange or chemical cross-linking techniques with mass spectrometry: mapping of human 14-3-3zeta homodimer interface. *Journal of structural biology* **179**, 10-17
23. Messaritou, G., Grammenoudi, S., and Skoulakis, E. M. (2010) Dimerization is essential for 14-3-3zeta stability and function in vivo. *Journal of Biological Chemistry* **285**, 1692-1700
24. Woodcock, J. M., Murphy, J., Stomski, F. C., Berndt, M. C., and Lopez, A. F. (2003) The dimeric versus monomeric status of 14-3-3zeta is controlled by phosphorylation of Ser58 at the dimer interface. *Journal of Biological Chemistry* **278**, 36323-36327
25. Truong, A. B., Masters, S. C., Yang, H., and Fu, H. (2002) Role of the 14-3-3 C-terminal loop in ligand interaction. *Proteins* **49**, 321-325
26. Williams, D. M., Ecroyd, H., Goodwin, K. L., Dai, H., Fu, H., Woodcock, J. M., Zhang, L., and Carver, J. A. (2011) NMR spectroscopy of 14-3-3zeta reveals a flexible C-terminal extension: differentiation of the chaperone and phosphoserine-binding activities of 14-3-3zeta. *Biochem. J.* **437**, 493-503
27. Wang, B. C., Yang, H. Z., Liu, Y. C., Jelinek, T., Zhang, L. X., Ruoslahti, E., and Fu, H. (1999) Isolation of high-affinity peptide antagonists of 14-3-3 proteins by phage display. *Biochemistry* **38**, 12499-12504
28. Australia, A. s. (2013) Key Facts and Statistics 2013. Alzheimer's Australia, Australia
29. Taylor, J. P., Hardy, J., and Fischbeck, K. H. (2002) Biomedicine - Toxic proteins in neurodegenerative disease. *Science* **296**, 1991-1995
30. Hsich, G., Kinney, K., Gibbs, C. J., Lee, K. H., and Harrington, M. G. (1996) The 14-3-3 brain protein in cerebrospinal fluid as a marker for transmissible spongiform encephalopathies. *N. Engl. J. Med.* **335**, 924-930
31. Chiti, F., and Dobson, C. M. (2006) Protein misfolding, functional amyloid, and human disease. in *Annu. Rev. Biochem.*, Annual Reviews, Palo Alto. pp 333-366
32. Treweek, T. M., Morris, A. M., and Carver, J. A. (2003) Intracellular protein unfolding and aggregation: The role of small heat-shock chaperone proteins. *Australian Journal of Chemistry* **56**, 357-367
33. Anfinsen, C. B. (1973) Principles that govern folding of protein chains. *Science* **181**, 223-230

34. Ecroyd, H., and Carver, J. A. (2008) Unraveling the mysteries of protein folding and misfolding. *IUBMB Life* **60**, 769-774

35. Winklhofer, K. F., Tatzelt, J., and Haass, C. (2008) The two faces of protein misfolding: gain- and loss-of-function in neurodegenerative diseases. *Embo J.* **27**, 336-349

36. Ecroyd, H., and Carver, J. A. (2009) Crystallin proteins and amyloid fibrils. *Cellular and Molecular Life Sciences* **66**, 62-81

37. Yoshimura, Y., Lin, Y. X., Yagi, H., Lee, Y. H., Kitayama, H., Sakurai, K., So, M., Ogi, H., Naiki, H., and Goto, Y. (2012) Distinguishing crystal-like amyloid fibrils and glass-like amorphous aggregates from their kinetics of formation. *Proceedings of the National Academy of Sciences of the United States of America* **109**, 14446-14451

38. Jimenez, J. L., Nettleton, E. J., Bouchard, M., Robinson, C. V., Dobson, C. M., and Saibil, H. R. (2002) The protofilament structure of insulin amyloid fibrils. *Proceedings of the National Academy of Sciences of the United States of America* **99**, 9196-9201

39. Carver, J. A., Rekas, A., Thorn, D. C., and Wilson, M. R. (2003) Small heat-shock proteins and clusterin: intra- and extracellular molecular chaperones with a common mechanism of action and function? *IUBMB Life* **55**, 661-668

40. Serpell, L. C., Sunde, M., Benson, M. D., Tennent, G. A., Pepys, M. B., and Fraser, P. E. (2000) The protofilament substructure of amyloid fibrils. *Journal of molecular biology* **300**, 1033-1039

41. Stefani, M., and Dobson, C. M. (2003) Protein aggregation and aggregate toxicity: new insights into protein folding, misfolding diseases and biological evolution. *Journal of molecular medicine* **81**, 678-699

42. Novitskaya, V., Bocharova, O. V., Bronstein, I., and Baskakov, I. V. (2006) Amyloid fibrils of mammalian prion protein are highly toxic to cultured cells and primary neurons. *Journal of Biological Chemistry* **281**, 13828-13836

43. Irvine, G. B., El-Agnaf, O. M., Shankar, G. M., and Walsh, D. M. (2008) Protein aggregation in the brain: the molecular basis for Alzheimer's and Parkinson's diseases. *Molecular medicine* **14**, 451-464

44. Shimada, T., Fournier, A. E., and Yamagata, K. (2013) Neuroprotective Function of 14-3-3 Proteins in Neurodegeneration. *BioMed Research International*, 11

45. Sadik, G., Tanaka, T., Kato, K., Yamamori, H., Nessa, B. N., Morihara, T., and Takeda, M. (2009) Phosphorylation of tau at Ser214 mediates its interaction with 14-3-3 protein: implications for the mechanism of tau aggregation. *J. Neurochem.* **108**, 33-43

46. Wilker, E., and Yaffe, M. B. (2004) 14-3-3 Proteins--a focus on cancer and human disease. *Journal of molecular and cellular cardiology* **37**, 633-642

47. Umahara, T., Uchihara, T., and Iwamoto, T. (2012) Structure-oriented review of 14-3-3 protein isoforms in geriatric neuroscience. *Geriatrics and Gerontology International* **12**, 586-599

48. Kawamoto, Y., Akiguchi, I., Nakamura, S., Honjyo, Y., Shibasaki, H., and Budka, H. (2002) 14-3-3 proteins in Lewy bodies in Parkinson disease and diffuse Lewy body disease brains. *J. Neuropathol. Exp. Neurol.* **61**, 245-253

49. Ostrerova, N., Petrucelli, L., Farrer, M., Mehta, N., Choi, P., Hardy, J., and Wolozin, B. (1999) alpha-Synuclein shares physical and functional homology with 14-3-3 proteins. *J. Neurosci.* **19**, 5782-5791

50. El-Agnaf, O. M. A., and Irvine, G. B. (2001) Aggregation and properties of alpha-synuclein and related proteins. *Journal of Spectroscopy* **15**, 141-150

51. Xu, J., Kao, S. Y., Lee, F. J. S., Song, W. H., Jin, L. W., and Yankner, B. A. (2002) Dopamine-dependent neurotoxicity of alpha-synuclein: A mechanism for selective neurodegeneration in Parkinson disease. *Nat. Med.* **8**, 600-606

52. Chen, H. K., Fernandez-Funez, P., Acevedo, S. F., Lam, Y. C., Kaytor, M. D., Fernandez, M. H., Aitken, A., Skoulakis, E. M. C., Orr, H. T., Botas, J., and Zoghbi, H. Y. (2003) Interaction of Akt-phosphorylated ataxin-1 with 14-3-3 mediates neurodegeneration in spinocerebellar ataxia type 1. *Cell* **113**, 457-468

53. Ellis, R. J. (1997) Do molecular chaperones have to be proteins? *Biochemical and Biophysical Research Communications* **238**, 687-692

54. Hatters, D. M., Lindner, R. A., Carver, J. A., and Howlett, G. J. (2001) The molecular chaperone, alpha-crystallin, inhibits amyloid formation by apolipoprotein C-II. *Journal of Biological Chemistry* **276**, 33755-33761

55. Jolly, C., and Morimoto, R. I. (2000) Role of the heat shock response and molecular chaperones in oncogenesis and cell death. *J. Natl. Cancer Inst.* **92**, 1564-1572

56. Renkawek, K., Voorter, C. E. M., Bosman, G., Vanworkum, F. P. A., and Dejong, W. W. (1994) Expression of alpha-B-crystallin in Alzheimer's Disease. *Acta Neuropathol.* **87**, 155-160

57. Brownell, S. E., Becker, R. A., and Steinman, L. (2012) The protective and therapeutic function of small heat shock proteins in neurological diseases. *Frontiers in Immunology* **3**, 74

58. Kumar, M. S., Kapoor, M., Sinha, S., and Reddy, G. B. (2005) Insights into hydrophobicity and the chaperone-like function of alphaA- and alphaB-crystallins: an isothermal titration calorimetric study. *Journal of Biological Chemistry* **280**, 21726-21730

59. Bloemendal, H., de Jong, W., Jaenicke, R., Lubsen, N. H., Slingsby, C., and Tardieu, A. (2004) Ageing and vision: structure, stability and function of lens crystallins. *Progress in biophysics and molecular biology* **86**, 407-485

60. Dejong, W. W., Leunissen, J. A. M., and Voorter, C. E. M. (1993) Evolution of the alpha-crystallin small heat shock protein family. *Mol. Biol. Evol.* **10**, 103-126

61. Treweek, T. M., Ecroyd, H., Williams, D. M., Meehan, S., Carver, J. A., and Walker, M. J. (2007) Site-directed mutations in the C-terminal extension of human alphaB-crystallin affect chaperone function and block amyloid fibril formation. *PloS one* **2**, e1046

62. Smulders, R. H. P. H., Carver, J. A., Linder, R. A., van Boekel, M. A. M., Bloemendal, H., and de Jong, W. (1996) Immobilization of the C-terminal Extension of Bovine alpha A-Crystallin Reduces Chaperone-like Activity. *Journal of Biological Chemistry* **271**, 29060-29066

63. Chernik, I. S., Seit-Nebi, A. S., Marston, S. B., and Gusev, N. B. (2007) Small heat shock protein Hsp20 (HspB6) as a partner of 14-3-3gamma. *Molecular and Cellular Biology* **295**, 9-17

64. Baxter, H. C., Liu, W. G., Forster, J. L., Aitken, A., and Fraser, J. R. (2002) Immunolocalisation of 14-3-3 isoforms in normal and scrapie-infected murine brain. *Neuroscience* **109**, 5-14

65. Williams, D. M. (2011) *14-3-3z: Structural characterisation and influences on disease related protein aggregation.* PhD, University of Adelaide

66. Sheluho, D., and Ackerman, S. H. (2001) An Accessible Hydrophobic Surface Is a Key Element of the Molecular Chaperone Action of Atp11p. *Journal of Biological Chemistry* **276**, 39945-39949

67. Schuck, P. (2000) Size-distribution analysis of macromolecules by sedimentation velocity ultracentrifugation and Lamm equation modeling. *Biophys. J.* **78**, 1606-1619

68. Schuck, P., Perugini, M. A., Gonzales, N. R., Howlett, G. J., and Schubert, D. (2002) Size-distribution analysis of proteins by analytical ultracentrifugation: Strategies and application to model systems. *Biophys. J.* **82**, 1096-1111

69. Laue, T. M., and Stafford, W. F. (1999) Modern applications of analytical ultracentrifugation. *Annu. Rev. Biophys. Biomolec. Struct.* **28**, 75-100

70. Gilbert, E. P., Schulz, J. C., and Noakes, T. J. (2006) 'Quokka' - the small-angle neutron scattering instrument at OPAL. *Physica B* **385-86**, 1180-1182

71. Svergun, D. I., and Koch, M. H. J. (2003) Small-angle scattering studies of biological macromolecules in solution. *Rep. Prog. Phys.* **66**, 1735-1782

72. Trinklein, N. D., Murray, J. I., Hartman, S. J., Botstein, D., and Myers, R. M. (2004) The role of heat shock transcription factor 1 in the genome-wide regulation of the mammalian heat shock response. *Molecular biology of the cell* **15**, 1254-1261

73. Powell, D. W., Rane, M. J., Joughin, B. A., Kalmukova, R., Hong, J. H., Tidor, B., Dean, W. L., Pierce, W. M., Klein, J. B., Yaffe, M. B., and McLeish, K. R. (2003) Proteomic Identification of 14-3-3 as a Mitogen-Activated Protein Kinase-Activated Protein Kinase 2 Substrate: Role in Dimer Formation and Ligand Binding. *Molecular and Cellular Biology* **23**, 5376-5387

74. Sluchanko, N. N., Chernik, I. S., Seit-Nebi, A. S., Pivovarova, A. V., Levitsky, D. I., and Gusev, N. B. (2008) Effect of mutations mimicking phosphorylation on the structure and properties of human 14-3-3zeta. *Archives of biochemistry and biophysics* **477**, 305-312

75. Yaffe, M. B. (2002) How do 14-3-3 proteins work? - Gatekeeper phosphorylation and the molecular anvil hypothesis. *FEBS letters* **513**, 53-57

76. Masters, S. C., and Fu, H. (2001) 14-3-3 proteins mediate an essential anti-apoptotic signal. *Journal of Biological Chemistry* **276**, 45193-45200

77. Yaffe, M. B., Rittinger, K., Volinia, S., Caron, P. R., Aitken, A., Leffers, H., Gamblin, S. J., Smerdon, S. J., and Cantley, L. C. (1997) The structural basis for 14-3-3 : phosphopeptide binding specificity. *Cell* **91**, 961-971

78. Sluchanko, N. N., Artemova, N. V., Sudnitsyna, M. V., Safenkova, I. V., Antson, A. A., Levitsky, D. I., and Gusev, N. B. (2012) Monomeric 14-3-3zeta has a chaperone-like activity and is stabilized by phosphorylated HspB6. *Biochemistry* **51**, 6127-6138
79. Hawe, A., Poole, R., and Jiskoot, W. (2010) Misconceptions over Forster resonance energy transfer between proteins and ANS/bis-ANS: Direct excitation dominates dye fluorescence. *Anal. Biochem.* **401**, 99-106
80. Sluchanko, N. N., and Gusev, N. B. (2012) Oligomeric structure of 14-3-3 protein: what do we know about monomers? *FEBS letters* **586**, 4249-4256
81. Woodcock, J. M., Ma, Y., Coolen, C., Pham, D., Jones, C., Lopez, A. F., and Pitson, S. M. (2010) Sphingosine and FTY720 directly bind pro-survival 14-3-3 proteins to regulate their function. *Cellular signalling* **22**, 1291-1299
82. Lindner, R. A., Kapur, A., Mariani, M., Titmuss, S. J., and Carver, J. A. (1998) Structural alterations of alpha-crystallin during its chaperone action. *Eur. J. Biochem.* **258**, 170-183
83. Gu, Y. M., Jin, Y. H., Choi, J. K., Baek, K. H., Yeo, C. Y., and Lee, K. Y. (2006) Protein kinase A phosphorylates and regulates dimerization of 14-3-3 epsilon. *FEBS letters* **580**, 305-310
84. Sluchanko, N. N., Roman, S. G., Chebotareva, N. A., and Gusev, N. B. (2014) Chaperone-like activity of monomeric human 14-3-3 zeta on different protein substrates. *Archives of biochemistry and biophysics* **549**, 32-39
85. Shashidharamurthy, R., Koteiche, H. A., Dong, J. H., and McHaourab, H. S. (2005) Mechanism of chaperone function in small heat shock proteins - Dissociation of the Hsp27 oligomer is required for recognition and binding of destabilized T4 lysozyme. *Journal of Biological Chemistry* **280**, 5281-5289
86. Chaudhri, M., Scarabel, M., and Aitken, A. (2003) Mammalian and yeast 14-3-3 isoforms form distinct patterns of dimers in vivo. *Biochemical and Biophysical Research Communications* **300**, 679-685
87. Bova, M. P., Ding, L. L., Horwitz, J., and Fung, B. K. K. (1997) Subunit exchange of alpha A-crystallin. *Journal of Biological Chemistry* **272**, 29511-29517
88. Bova, M. P., McHaourab, H. S., Han, Y., and Fung, B. K. K. (2000) Subunit exchange of small heat shock proteins - Analysis of oligomer formation of alpha A-crystallin and Hsp27 by fluorescence resonance energy transfer and site-directed truncations. *Journal of Biological Chemistry* **275**, 1035-1042

89. Migneault, I., Dartiguenave, C., Bertrand, M. J., and Waldron, K. C. (2004) Glutaraldehyde: behavior in aqueous solution, reaction with proteins, and application to enzyme crosslinking. *Biotechniques* **37**, 790-+

90. Sluchanko, N. N., Sudnitsyna, M. V., Chernik, I. S., Seit-Nebi, A. S., and Gusev, N. B. (2011) Phosphomimicking mutations of human 14-3-3zeta affect its interaction with tau protein and small heat shock protein HspB6. *Archives of biochemistry and biophysics* **506**, 24-34

91. Berkowitz, S. A. (2006) Role of analytical ultracentrifugation in assessing the aggregation of protein biopharmaceuticals. *American Association of Pharmaceutical Scientists* **8**, E590-E605

92. Lebowitz, J., Lewis, M. S., and Schuck, P. (2009) Modern analytical ultracentrifugation in protein science: A tutorial review. *Protein Science* **11**, 2067-2079

93. Pharma, C. (2014) Sedimentation Velocity Analytical Ultracentrifugation (SV-AUC).

94. McRorie, D. K. V., Paul J. Self-Associating Systems in the Analytical Ultracentrifuge. (Coulter, B. ed.

95. Woodcock, J. (2006) Sphingosine and ceramide signalling in apoptosis. *IUBMB Life* **58**, 462-466

96. Kanno, T. a. N., T. (2011) Sphingosine induces apoptosis in hippocampal neurons and astrocytes by activating caspase-3/-9 via a mitochondrial pathway linked to SDK/14-3-3 protein/Bax/Cytochrome C. *Journal of Cellular Physiology* **226**, 9

97. Royer, C. A. (2006) Probing protein folding and conformational transitions with fluorescence. *Chem. Rev.* **106**, 1769-1784

98. Goodwin, K. L. (2010) *The effect of divalent cation, Mg^{2+}; the polyamine, Spermine; the sphingo-lipid, Sphingosine on the molecular chaperone activity of the protein 14-3-3zeta.* B.Sc (Hons), University of Adelaide

99. He, X., Huang, Y., Li, B., Gong, C-X., Schuchman, E. H., . (2010) Deregulation of sphingolipid metabolism in Alzheimer's disease. *Neurobiology of Aging* **31**, 11

100. Di Pardo, A., Amico, E., Favellato, M.., Castrataro, R., Fucile, S., Squitieri, F., Maglione, V. . (2014) FTY720 (fingolimod) is a neuroprotective and disease-modifying agent in cellular and mouse models of Huntington disease. *Human Molecular Genetics* **23**, 15

101. Krueger, S. (1997) SANS provides unique information on the structure and function of biological macromolecules in solution. *Physica B* **241**, 1131-1137
102. Thiyagarajan, P., Henderson, S. J., and Joachimiak, A. (1996) Solution structures of GroEL and its complex with rhodanese from small-angle neutron scattering. *Structure* **4**, 79-88
103. Trewhella, J. (2006) Neutrons reveal how nature uses structural themes and variation in biological regulation. *Physica B* **385-86**, 825-830
104. Timmins, P. A., and Zaccai, G. (1988) Low resolution structures of biological complexes studed by neutron-scattering. *Eur. Biophys. J. Biophys. Lett.* **15**, 257-268
105. Bouchoux, A., Ventureira, J., Gesan-Guiziou, G., Garnier-Lambrouin, F., Qu, P., Pasquier, C., Pezennec, S., Schweins, R., and Cabane, B. (2015) Structural heterogeneity of milk casein micelles: a SANS contrast variation study (vol 11, pg 389, 2015). *Soft Matter* **11**, 806-806
106. Breyton, C., Gabel, F., Lethier, M., Flayhan, A., Durand, G., Jault, J. M., Juillan-Binard, C., Imbert, L., Moulin, M., Ravaud, S., Hartlein, M., and Ebel, C. (2013) Small angle neutron scattering for the study of solubilised membrane proteins. *Eur. Phys. J. E* **36**, 16
107. Curtis, J. E., Nanda, H., Khodadadi, S., Cicerone, M., Lee, H. J., McAuley, A., and Krueger, S. (2012) Small-Angle Neutron Scattering Study of Protein Crowding in Liquid and Solid Phases: Lysozyme in Aqueous Solution, Frozen Solution, and Carbohydrate Powders. *J. Phys. Chem. B* **116**, 9653-9667
108. de Kruif, C. G., Huppertz, T., Urban, V. S., and Petukhov, A. V. (2012) Casein micelles and their internal structure. *Adv. Colloid Interface Sci.* **171**, 36-52
109. Heller, W. T. (2010) Small-angle neutron scattering and contrast variation: a powerful combination for studying biological structures. *Acta Crystallogr. Sect. D-Biol. Crystallogr.* **66**, 1213-1217
110. Krivandin, A. V., Murugova, T. N., Kuklin, A. I., Muranov, K. O., Poliansky, N. B., Aksenov, V. L., and Ostrovsky, M. A. (2010) Study of α-Crystallin Structure by Small Angle Neutron Scattering with Contrast Variation. *Biochemistry (Moscow)* **75**, 1324-1330
111. Trewhella, J. (1997) Insights into biomolecular function from small-angle scattering. *Curr. Opin. Struct. Biol.* **7**, 702-708

112. Konarev, P. V., Volkov, V. V., Sokolova, A. V., Koch, M. H. J., and Svergun, D. I. (2003) PRIMUS: a Windows PC-based system for small-angle scattering data analysis. *J. Appl. Crystallogr.* **36**, 1277-1282

113. Svergun, D. I., and Koch, M. H. J. (2002) Advances in structure analysis using small-angle scattering in solution. *Curr. Opin. Struct. Biol.* **12**, 7

114. Nakanishi, M., and Tsuboi, M. (1978) Rate of increase in fluorescence intensity as caused by deuteration of tryptophan. *Chem. Phys. Lett.* **57**, 262-264

115. Hattori, A., Crespi, H. L., and Katz, J. J. (1965) Effect of side chain deuteration on protein stability. *Biochemistry* **4**, 1213-&

116. Fisher, S. J., and Helliwell, J. R. (2008) An investigation into structural changes due to deuteration. *Acta Crystallographica Section A* **64**, 359-367

117. Liu, X. Y., Hanson, L., Langan, P., and Viola, R. E. (2007) The effect of deuteration on protein structure: a high-resolution comparison of hydrogenous and perdeuterated haloalkane dehalogenase. *Acta Crystallogr. Sect. D-Biol. Crystallogr.* **63**, 1000-1008

118. Li, Z. M., Peng, H., Qin, L., Qi, J., Zuo, X. B., Liu, J. Y., and Zhang, J. T. (2013) Determinants of 14-3-3 sigma Protein Dimerization and Function in Drug and Radiation Resistance. *Journal of Biological Chemistry* **288**, 31447-31457

119. Aswal, V., Chodankar, S., Kohlbrecher, J., Vavrin, R., and Wagh, A. (2009) Small-angle neutron scattering study of protein unfolding and refolding. *Physical Review E* **80**

120. Clarke, M. J., Artero, J. B., Moulin, M., Callow, P., Carver, J. A., Griffiths, P. C., Haertlein, M., Harding, J. J., Meek, K. M., Timmins, P., and Regini, J. W. (2010) Investigation of gammaE-crystallin target protein binding to bovine lens alpha-crystallin by small-angle neutron scattering. *Biochimica et biophysica acta* **1800**, 392-397

121. Sluchanko, N. N., Sudnitsyna, M. V., Seit-Nebi, A. S., Antson, A. A., and Gusev, N. B. (2011) Properties of the monomeric form of human 14-3-3zeta protein and its interaction with tau and HspB6. *Biochemistry* **50**, 9797-9808

122. Han, J., Song, Q. Q., Sun, P., Zhang, J., Wang, X., Song, J., Li, G. Q., Liu, Y. H., Mei, G. Y., Shi, Q., Tian, C., Chen, C., Gao, C., Zhao, B., and Dong, X. P. (2014) Interaction between 14-3-3 beta and PrP influences the dimerization of 14-3-3 and fibrillization of PrP106-126. *Int. J. Biochem. Cell Biol.* **47**, 20-28

123. Ghahghaei, A., Rekas, A., Price, W. E., and Carver, J. A. (2007) The effect of dextran on subunit exchange of the molecular chaperone alphaA-crystallin. *Biochimica et biophysica acta* **1774**, 102-111

124. Outeiro, T. F., Klucken, J., Strathearn, K. E., Liu, F., Nguyen, P., Rochet, J. C., Hyman, B. T., and McLean, P. J. (2006) Small heat shock proteins protect against alpha-synuclein-induced toxicity and aggregation. *Biochemical and Biophysical Research Communications* **351**, 631-638

125. Woody, R. W. (1977) Optical rotatory properties of biopolymers. *J. Polym. Sci. Macromol. Rev.* **12**, 181-320

126. Kelly, S. M., and Price, N. C. (2000) The Use of Circular Dichroism in the Investigation of Protein Structure and Function. *Curr. Protein Pept. Sci.* **1**, 349-384

127. Whitmore, L., and Wallace, B. A. (2008) Protein secondary structure analyses from circular dichroism spectroscopy: methods and reference databases. *Biopolymers* **89**, 392-400

128. Bustad, H. J., Underhaug, J., Halskau, O., and Martinez, A. (2011) The binding of 14-3-3 gamma to membranes studied by intrinsic fluorescence spectroscopy. *FEBS letters* **585**, 1163-1168

129. Bushueva, T. L., Busel, E. P., and Burstein, E. A. (1978) Relationship of thermal quenhing of protein fluorescence to intra-molecular structural mobility. *Biochimica et biophysica acta* **534**, 141-152

130. Edelman, G. M., and McClure, W. O. (1968) Fluorescent probes and the conformation of proteins. *Accounts of Chemical Research* **1**, 65-70

131. Hawe, A., Sutter, M., and Jiskoot, W. (2008) Extrinsic fluorescent dyes as tools for protein characterization. *Pharmaceutical research* **25**, 1487-1499

132. Brand, L., and Gohlke, J. R. (1972) Fluorescence probes for structure. *Annu. Rev. Biochem.* **41**, 843-&

133. Wu, P. G., and Brand, L. (1994) Resonance energy-transfer - Methods and applications. *Anal. Biochem.* **218**, 1-13